UNIVERSITY OF ŽILINA

TRANSCOM 2011

**9-th EUROPEAN CONFERENCE
OF YOUNG RESEARCH AND SCIENTIFIC WORKERS**

PROCEEDINGS

SECTION 6

**MACHINES AND EQUIPMENTS
APPLIED MECHANICS**

ŽILINA June 27 - 29, 2011
SLOVAK REPUBLIC

UNIVERSITY OF ŽILINA

TRANSCOM 2011

9-th EUROPEAN CONFERENCE
OF YOUNG RESEARCH AND SCIENTIFIC WORKERS

under the auspices of

Ing. Eugen Jurzyca
Minister of Education, Science, Research and Sport of the Slovak Republic

&

Prof. Ing. Tatiana Čorejová, PhD.
Rector of the University of Žilina

SECTION 6

**MACHINES AND EQUIPMENTS
APPLIED MECHANICS**

ŽILINA June 27 - 29, 2011
SLOVAK REPUBLIC

TRANSCOM 2011
9-th European conference of young research and scientific workers

TRANSCOM 2011, the 9-th international conference of young European researchers, scientists and educators, aims to establish and expand international contacts and co-operation. The main purpose of the conference is to provide young scientists with an encouraging and stimulating environment in which they present results of their research to the scientific community. TRANSCOM has been organised regularly every other year since 1995. Between 160 and 400 young researchers and scientists participate regularly in the event. The conference is organised for postgraduate students and young research workers up to the age of 35 and their tutors. Young workers are expected to present the results they had achieved.

The conference is organised by the University of Žilina. It is the university with about 13 000 graduate and postgraduate students. The university offers Bachelor, Master and PhD programmes in the fields of transport, telecommunications, forensic engineering, management operations, information systems, in mechanical, civil, electrical, special engineering and in social sciences.

SECTIONS AND SCIENTIFIC COMMITTEE

1. TRANSPORT AND COMMUNICATIONS TECHNOLOGY.
Scientific committee: Černý J. (CZ), Drozdziel P. (PL), Dydkowski G. (PL), Gašparík J. (SK), Havel K. (SK), Janáček J. (SK), Jánošíková Ľ. (SK), Kampf R. (CZ), Kavička A. (CZ), Kazda A. (SK), Novák A. (SK), Palúch S. (SK), Peško Š. (SK), Rievaj V. (SK), Šulgan M. (SK), Volek J. (CZ), Žarnay M. (SK), Žarnay P. (SK)

2. ECONOMICS AND MANAGEMENT.
Scientific committee: Bartošová V. (SK), Blašková M. (SK), Borkowski S. (PL), Březinová O. (CZ), Ďurišová M. (SK), Glebocki K. (PL), Graźulis V. (LT), Hittmár Š. (SK), Hrnčiar M. (SK), Kucharčíková A. (SK), Lyakin A. (RUS), Rostášová M. (SK), Rybakov F. (RUS), Seemann P. (SK), Strenitzerová M. (SK), Tomová A. (SK), Veretennikova B.O (RUS)

3. INFORMATION AND COMMUNICATION TECHNOLOGIES.
Scientific committee: Dado M. (SK), Diviš Z. (CZ), Drozdová M. (SK), Hudec R. (SK), Huotari J, (FIN), Keil R. (DE), Klimo M. (SK), Kolev P. (BG), Kotsopoulos S. (GR), Koudelka O. (A), Kováčiková T. (SK), Madleňák R. (SK), Matiaško K. (SK), Ranc D. (FR), Spalek J. (SK), Vaculík J. (SK), Vaculík M. (SK), Vrček N. (CR), Wieser V. (SK), Zábovský M. (SK)

4. ELECTRIC POWER SYSTEMS. ELECTRICAL AND ELECTRONIC ENGINEERING.
Scientific committee: Altus J. (SK), Blažek V. (DE), Brandstetter P. (ČR), Capolino G. A. (FR), Consoli A. (IT), Čápová K. (SK), Dobrucký B. (SK), Janoušek L. (SK), Luft M. (PL), Rusek S. (ČR), Szkutnik, J. (PL), Špánik P. (SK), Vittek J. (SK)

5. MATERIAL ENGINEERING. MECHANICAL ENGINEERING TECHNOLOGIES.
Scientific committee: Adamczak S. (PL), Bokůvka O. (SK), Dzimko M. (SK), Guagliano M. (I), Kunz L. (CZ), Meško J. (SK), Neslušan M. (SK), Nicoletto G. (I), Palček P. (SK), Skočovský P. (SK), Takács J. (H)

6. MACHINES AND EQUIPMENTS. APPLIED MECHANICS.
Scientific committee: Dekýš V. (SK), Gerlici J. (SK), Chudzikiewicz A. (PL), Jandačka J. (SK), Kalinčák D. (SK), Malenovský E. (CZ), Medvecký Š. (SK), Nemček M. (CZ), Sága M. (SK), Sitarz M. (PL), Szava I. (RO), Zapoměl J. (CZ), Žmindák M. (SK)

7. CIVIL ENGINEERING.
Scientific committee: Bujňák J. (SK), Ferrero A. M. (IT), Garbuz A. (UA), Horváth F. (HU), Ižvolt L. (SK), Melcer J. (SK), Petkova R. (BG), Plášek O. (CZ), Malachova A. (RU), Ungureanu V. (RO)

8. SOCIAL SCIENCES.
Scientific committee: Banáry B. (SK), Cabanová V. (SK), Grecmanová H. (CZ), Hádková M. (CZ), Kráľová Z. (SK), Larry Fast (USA), Lengyelfalusy T. (SK)

9. SECURITY ENGINEERING. FORENSIC ENGINEERING.
Scientific committee: Artamonov S. V. (RU), Burg H. (DE), Dudáček A. (CZ), Horák R. (CZ), Kasanický G. (SK), Klučka J. (SK), Leitner B. (SK), Navrátil L. (CZ), Podbregar I. (SLO), Poledňák P. (SK), Šimák L. (SK), Štofko S. (SK)

ORGANIZING COMMITTEE

CHAIRPERSONS   Čelko Ján, Bokůvka Otakar

EXECUTIVE SECRETARY   Vráblová Helena

MEMBERS   Bača Tomáš, Bačová Katarína, Baďurová Silvia, Belan Juraj, Bomba Lukáš, Brída Peter, Brumerčík František, Gavláková Eva, Hampl Marek, Harušinec Jozef, Horváth Peter, Hrbček Jozef, Jošt Jozef, Kittel Ladislav, Kolla Eduard, Koniar Dušan, Kopas Peter, Lanďák Milan, Lieskovský Anton, Mendrošová Katarína, Mišiaková Kvetoslava, Mokryš Michal, Mrvová Miroslava, Mužíková Karolína, Pácha Matěj, Peterková Andrea, Pilát Peter, Pitor Ján, Raždík Ján, Smetana Milan, Spuchľáková Erika, Šípek Michal, Šramová Veronika, Tengler Jiří, Tkáčová Gabriela, Vaško Alan, Vaško Milan, Vlček Jozef, Vrábel Ján, Vráblová Lucia, Závodská Anna, Zvaríková Katarína, Žiačková Vladimíra

SECTION 6   MACHINES AND EQUIPMENT, APPLIED MECHANICS

REVIEWERS:

Barta Dalibor
Bašťovanský Ronald
Brumerčík František
Dekýš Vladimír
Gerlici Juraj
Grenčík Juraj
Jandačka Jozef
Kalinčák Daniel
Kopas Peter
Kovalčík Andrej
Kukuča Pavol
Lack Tomáš
Lábaj Ján
Lukáč Michal
Malcho Milan
Sága Milan
Toporcer Emil
Vaško Milan
Žmindák Milan

Note:

Authors are responsible for language contents of their papers

CONTENTS

Wheelset and Rail Profiles Transformation

[*]Matúš Bačišin, Tomáš Lack, Juraj Gerlici

[*]University of Žilina, Faculty of Mechanical Engineering, Department of Transport and Handling Technology, Univerzitna 1, 01026 Žilina, Slovakia, {Matus.Bacisin, Tomas.Lack, Juraj.Gerlici}@fstroj.uniza.sk

Abstract. This article discusses the transformation of the wheelset and rail profiles depending on the wheelset lateral position and angle of attack α. Profiles used to transform Cartesian rectangular coordinate system x, y, z in the basic position, then rotated by an angle α about the axis z. The last system in transition coordinate system is normal - tangent.

Keywords: Angle of attack, lateral displacement, wheelset, point of contact, normal, tangent

1. Introduction

The issue of transformation profiles is important as an input for the calculation and analysis of mechanical stress in wheelset and rails contact. Need for the profile transformation is desirable in terms of changing the relative positions of the wheel against rail. Changes are caused by a presupposed wave movement of the wheelset, driving from straight rail to the arc, but also due to other factors, such as wind etc. Specifically, the geometric parameters used as input into the transformation process are: transverse displacement y_p and angle of attack α. The basic computing element is the transformation matrix used in gearing equations between coordinate system. The aim is to achieve expression of profile in the coordinate system normal - tangent in the point of contact.

2. Coordinate systems

Coordinate systems in the process of transformation, we use 3:
x', y', z', 3 – dimensional rectangular coordinate system of the wheel, starting at point $O_{wheel}=(0,0,0)$.
x, y, z, 3 – dimensional rectangular coordinate system of the wheel, starting at point $O_{rail}=(0,0,0)$.
n, t – coordinate system normal – tangent starting at point of the contact between wheel and rail.
The plane created by lines n and t is generally parallel with the plane created by lines y and z.

3. The process of transformation

We have a wheel base coordinate system x', y', z' in this system, we expressed the wheel coordinates: x' = 0, y', z' are dependent on a particular wheel profile. We also have a basic grid rail system x, y, z, in this system, we expressed the rail coordinates: x = 0, y, z are dependent on a particular rail profile. To begin the process of transformation is necessary to know the angle of attack α as well as lateral displacement y_p wheel and rail profiles against each other. At zero lateral displacement y_p and zero angle of attack α are the points O_{rail}, O_{wheel} identical. The coordinate systems are also identical. Generally it is not true. For non-zero angle of attack α is a system x', y', z 'rotated to the system x, y, z about axis z of angle α as shown in Fig. 1.
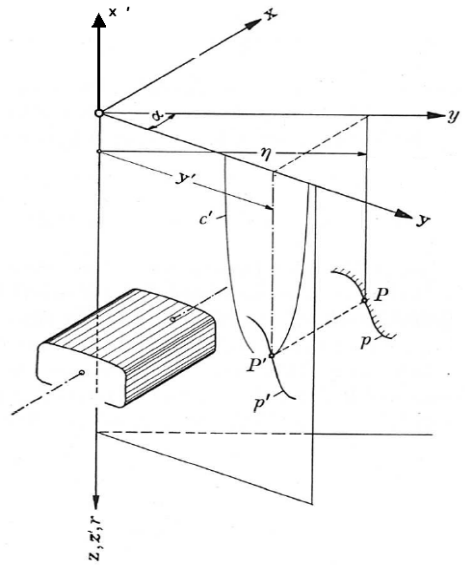
Fig. 1. Mutual rotations of coordinate systems and wheel tracks on the angle of attack α

3.1. Profile projection from the wheel coordinate system to the rail coordinate system

The coordinate system of wheel profile x', y', z ' transformed into a coordinate system of rail x, y, z. Due to the projection of a circle of the profile points to create the ellipse corresponding to each item. The ellipse in profile stands out particularly in the area of the flange. This will create an envelope, which changes the profile, Fig. 2.
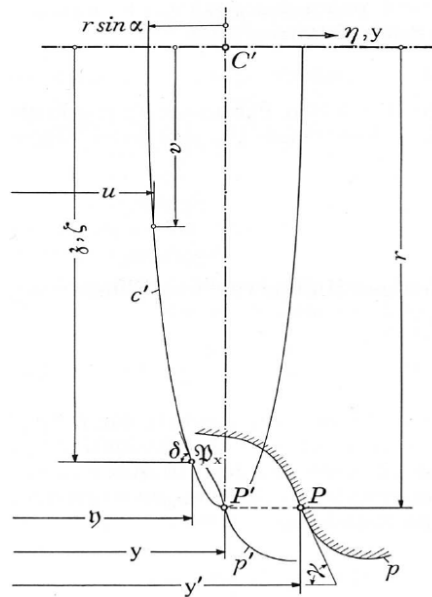
Fig. 2. The envelope of a profile

A profile in the system x, y, z we can get from these relations:

$$y = y'\cos\alpha\cos\varphi - \frac{r}{\cos\alpha}\left(\frac{\sin\varphi\sqrt{1-tg^2\alpha(\cos\varphi tg^2\gamma-\sin^2\varphi)}+tg\gamma\sin^2\alpha\cos^3\varphi}{1+tg^2\alpha\sin^2\varphi}\right), \quad (1)$$

$$z = r - y'\sin\varphi - r\cos\alpha\left(\frac{\sqrt{1-tg^2\alpha(\cos^2\varphi tg^2\gamma-\sin^2\varphi)}+tg\gamma tg\alpha\sin\varphi\cos\varphi}{1+tg^2\alpha\sin^2\varphi}\right), \quad (2)$$

where:
α – angle of attack,

φ – tilting angle of the wheelset,

γ – angle tangent of point in the profile.

3.2. A point of contact finding

The contact point of the profile is obtained taking into account the envelope profile. The point thus obtained we determine the longitudinal displacement of the contact point X in the coordinate system x, y, z.

3.3. Transformation into the wheel coordinate system of wheel x', y', z'

We obtained the distance X of contact point in the coordinate system x, y, z. At the distance X of the coordinate system x, y, z, we compute coordinates of the remaining points on profile. The distance X for each profile point in the system x', y', z' transform to a distance of X' corresponding to each point in the wheel coordinate system x', y', z'. This distance X' is already different for each point. Between the coordinate system x, y, z and x', y', z' we use the transformation matrix **T**:

$$\mathbf{T} = \begin{bmatrix} \cos\alpha & \sin\alpha & 0 \\ -\sin\alpha & \cos\alpha & 0 \\ 0 & 0 & 1 \end{bmatrix}, \tag{3}$$

$$\mathbf{A}*\mathbf{T}^{-1}=\mathbf{B}'' \tag{4}$$

where:

A – matrix of the wheel profil in the x, y, z coordinate system,

α – angle of attack,

γ – angle tangent of point in the profile.

B'' – particularly matrix of the wheel profile in the x', y', z' coordinate system.

We obtained the coordinates in the system x', y', z'. The coordinates z'(i) are identical with coordinates z(i). We change the vertical coordinates z' based on relationship:

$$z'(i) = r - \sqrt{r(i)^2 - x(i)'^2} \tag{5}$$

r(i) – radius on ith point of wheel profile,

r – wheel radius.

x(i)' – horizontal distance of the i–th point in the profile coordinate system x', y', z'.

This recurrent based on relationship (5) we entered in the system of coordinates x, y, z, but already at a distance X. Matrix of coordinates will be called **B'**.

3.4. The transformation of coordinate system to coordinate system normal - tangent

We obtained coordinates in a coordinate system x, y, z at a distance X. Plane acquired translated coordinates parallel to the plane y, z. When we do it we use transformation matrix **Tg:**

$$\mathbf{Tg} = \begin{bmatrix} 1 & 0 & 0 \\ 0 & \cos\gamma & -\sin\gamma \\ 0 & \sin\gamma & \cos\gamma \end{bmatrix}. \tag{6}$$

Solving system of equations:

$$\mathbf{B'}*\mathbf{Tg}^{-1} = \mathbf{N}, \tag{7}$$

where:

B' – profile matrix of coordinates in a x, y, z coordinate system at a distance X,

N – profile matrix of coordinates in the normal - tangent coordinate system.

Multiply the columns of matrix **B', N.**

We obtain the matrix **N** profile in the normal – tangent system (x, n, t).
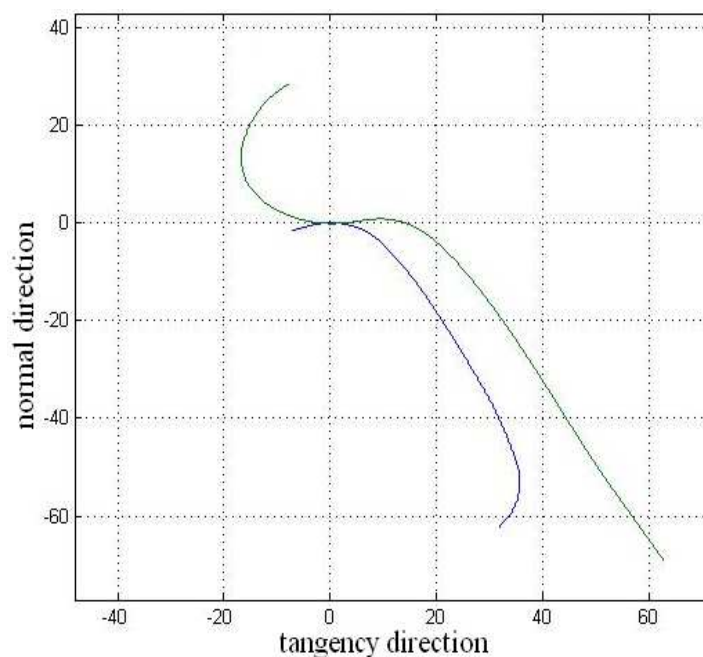
Fig. 3. A shifted contact point sample at an angle of attack α 6.1 ° in the normal - tangent coordinate system at a horizontal distance X = 97 mm. Processed in Matlab using the transprofwheel.m function file

4. Conclusion

Profile transformation takes place in 3 independent steps:
1. Profile determination, taking into account the envelope profile with designated contact point and the horizontal shift X.
2. Transformation points of the profile coordinate system x, y, z coordinate system to x ', y', z' and the acquisition of vertical coordinates z=z'.
3. Transformation points of the profile system x, y, z at a distance X to the normal-tangent.

The resulting transformation profile in coordinates normal - tangent is suitable as an input into the program to calculate the mechanical stress at the contact between rail and wheel.

Acknowledgement

References

[1] BORGEAUD, G. Die *Führung des Fahrzeuges im Geleise und die Vorgänge zwischen Rad unfd Schiene*. SLM Technische Mitteilungen, R. Spies &Co Wien. Juli 1970

[2] IWNICKY, S. *Handbook of Railway Vehicle Dynamics*. CRC Press, Taylor&Francis Group, Boca Raton, 2006

[3] DUKKIPATI, R. V. *Dynamics of a Wheelset on Roller Rig*. *Vehicle System Dynamics, 30*, Swets & Zeitlinger 1998

Hybrid Propulsions and their Use of Rail Transport

[*] Ľuboš Bartík, Daniel Kalinčák

[*] University of Žilina, Faculty of Mechanical Engineering, Department of Transport and Handling Machines, Univerzitna 1, 01026 Žilina, Slovakia, {lubos.bartik, daniel.kalincak}@fstroj.uniza.sk

Abstract. This article deals with hybrid propulsions. It brings up possible solutions of problems with effective use of unused energy in the railway vehicle area. The results of use alternative sources of energy or application of different type of hybrid propulsion are reducing consumption and emissions. This article states existing solutions of hybrid systems with their description and results of measurement which were made.

Keywords: alternative fuels, hybrid propulsion, reduced consumption, fuel cell.

1. Introduction

Today we witness enormous increases in prices of fuel. Further there is also a growing emphasis on reducing emissions arising from their combustion. Therefore it is important to deal with the idea of reducing fuel consumption in transport. Substitution of fossil fuels with alternative fuels (Liquefied Petroleum Gas, Compressed Natural Gas, Ethanol, Methanol, Hydrogen), or extending the use of unconventional energy sources (eg. fuel cells) seems a perspective solution.

Today the alternative fuels are used seldom in operation of traction railcars. It is mainly natural gas, which is among the fossil fuels but its reserves are bigger than those of petroleum. Also in vehicles which use natural gas for its drive it is possible to use biogas of similar composition. But the use of natural gas does not solve problem with greenhouse gases (CO_2). Therefore advanced use of hybrid drives seems to be a good solution to these problems.

2. Hybrid propulsion

Each system using more than one energy source to drive a vehicle is considered to be hybrid propulsion. The most commonly used combination are: internal combustion engine, batteries and electric engine. Drive system with this configuration in the traction railcars allows:

- storage of energy gained by electrodynamic braking and its utilization,
- installation of a primary power source with significantly lower output as in the case the of classic traction drive,
- operation of primary source of energy in optimum regime from the point of view of fuel consumption and emissions,
- shutting off internal combustion engine during standing, auxiliary equipment are powered by energy accumulated in batteries,
- work in closed halls for traction railcars without running internal combustion engine leading to better working conditions.

Application of hybrid propulsion may not be useful for each type of traction railcar. The biggest contribution we can expect from shunting locomotives or urban railcars for passengers with a lot of stops. Therefore it is important for the measurements to analyze the actual operation of the internal combustion engine operating modes, running auxiliary equipment and subsequently to designe the optimal power primary source, necessary capacity and power of batteries. This issue is analysed in publications [1,2,3] etc.

3. Application of hybrid propulsion for traction railcars

3.1. Mitrac Energy Saver (Bombardier)

Measurements of Mitrac Energy Saver has been conducted for four years. The prototype vehicle has been equipped with only one instead of two planned Energy Saver. This allows a direct comparison between a bogie drive with energy storage and bogie drive without energy storage at any time. Mitrac contain UltraCaps with long lifetime and with higher power than batteries. UltraCaps are connected in series so creating one energy unit with ability to store 9 kWh power with 72 % of recoverability [4].
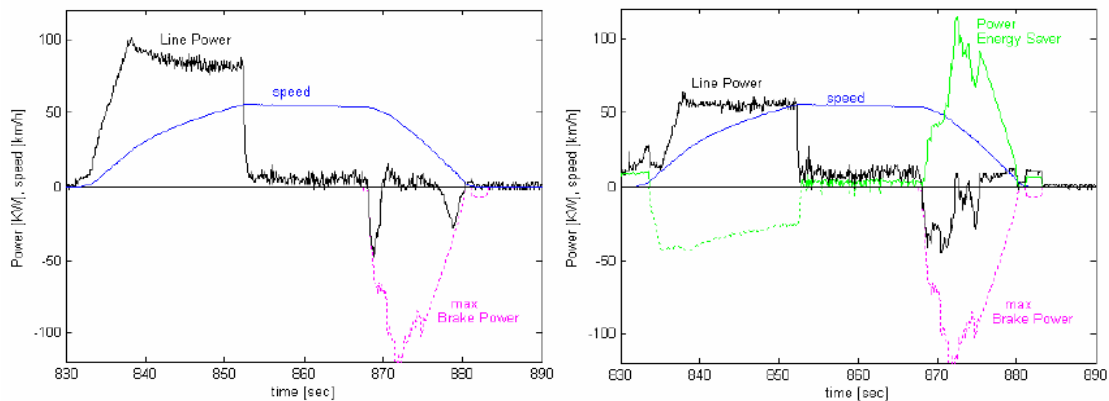
Fig. 1. Left: Power consumption without MITRAC Energy Saver-right: with MITRAC Energy Saver [4]

In **Fig. 1** left side the measured line power consumption of prototype vehicle is shown without Mitrac Energy Saver system. Maximum speed of measurement was 50km/h with maximum power between 80 and 100 kW. The braking energy can only partly be recuperated to the network. In **Fig. 1** right side the line power of the drive with Mitrac Energy Saver is show. The measurements have been done simultaneously on the same track. The power consumption of the vehicle during acceleration is reduced to 55 kW only. During braking nearly all the braking energy can be reused (stored into the energy storage and remaining energy is fed back into the line) [4].

Advantages of Mitrac system [4]:
- reduced energy costs – reduced peak power of all vehicles is equal to the reduction of energy consumption (30 %),
- reduced peak power – and subsequent reduced cost of catenary (substation, trolley line, etc).

3.2. NE train, (Hitachi)

HITACHI, LTD. has been developing hybrid drive systems - aiming to reduce environmental load since 2001. In collaboration with East Japan Railway Company Hitachi constructed a series hybrid drive system - combining a diesel engine and high-energy-density lithium-ion batteries and by mounting this system in a test train called "NE Train." The train body used was a stainless steel body which was the same as series E127 railcars that ran on local lines and powertrain was the same as series E231. In Fig. 2 left is shows the overview of the NE train and overview of energy management and control system on right side.
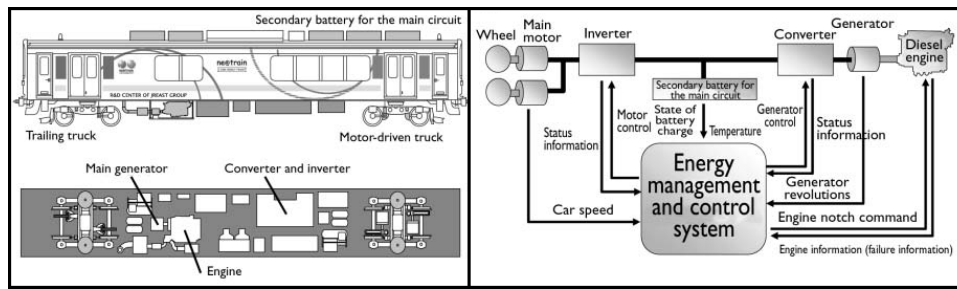
Fig. 2. Left: overview of the NE train, right: overview of the energy management and control system [5]

We do not give detailed description of the principle hybrid systems because the range of this article is limited. The results of tests which were conducted from May to September 2003 on the Nikko, Karasuyama, and Utsunomiya lines are following:

- designed performance is satisfactory (acceleration performance α=2.3 km/h/s [at 35km/h], deceleration performance β> 3.6 km/h/s),
- running with cut-off engine(the car was able to accelerate up to 70 km/h with the use of only the battery),
- the car could run with only the engine when the battery is cut off due to failures,

it was confirmed that the engine stopped when the car stopped at a station after running for more than 5 minutes, and that the engine remained off when the car started again (until it reached approximately 25 km/h).

In **Fig. 3** left we can see results of measurements on line between Nishinasuno and Nozaki. The curve "engine revolution speed" shows the engine running. It is possible to see, that the engine had been stopped when the car was at the station Nishinasuno and started to operate when the car speed reached 25 km/h. After that followed increase engine output from 2N (1700 rpm) to 3N (2100 rpm) when the car speed reached approximately 80 km/h. Further was engine controlled depending on the status of charge of secondary battery. The curve "secondary battery SOC" shows how much energy was stored in batteries when the brake was used to stop the car at Nozaki station.

In Fig. 3 right shows measurement data obtained from the running test conducted between Nikko and Imaichi stations. There is continuous slope of approximately 25‰. The NE train has the "holding braking" function that keeps the car speed under a certain speed level on a download slope. This brake can be controlled in 2 stages. In Stage 1, the battery absorbs regenerative energy. In Stage 2, if the battery charge level reaches a high level, the exhaust brake of the engine consumes the brake energy.
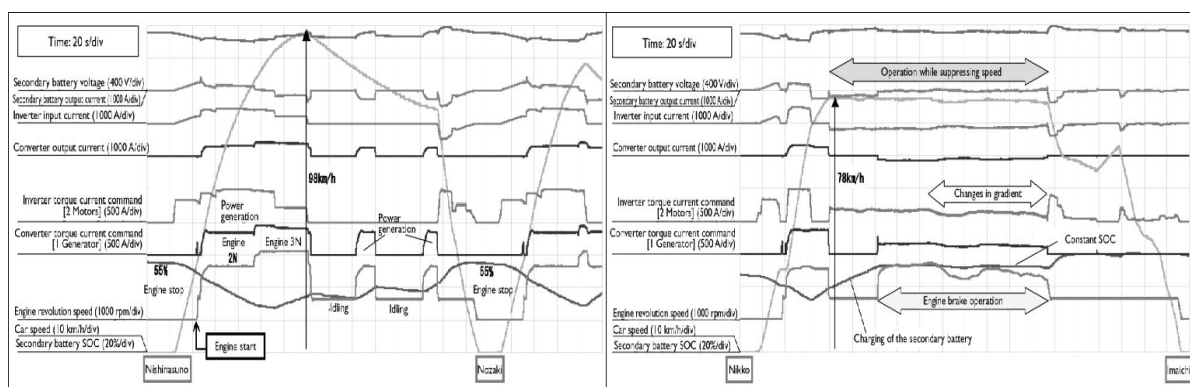
Fig. 3. Left: running test chart (Nishinasuno to Nozaki), right: (Nikko to Imaichi)

According to the simulation, regenerative energy efficiency is of approximately 20 %. In **Fig. 4** is shown comparison between the results of the simulations and the results of running tests conducted. The values were approximately the same.
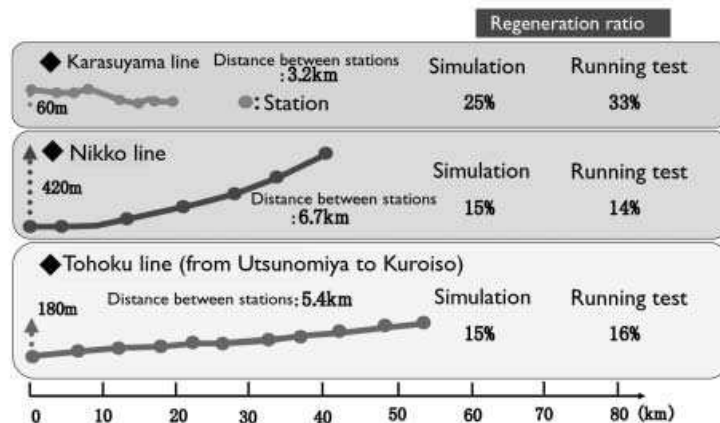
Fig. 4. Comparison of energy regeneration ratio in each line district

4. Conclusion

Examples of hybrid drive systems used in rail transport indicate the possible development direction of these systems in the future. The results which were obtained when testing vehicles with hybrid drive system NE train, showed that hybridization in rail transport has future. Currently are running tests with two testing railcars which contain hybrid drive system, cooperating fuel cell and battery.

References

[1] KALINČÁK, D. *Unconventional traction drive – the way of fuel consumption reduction of motive power units.* In Prace Naukowe „Transport" Nr 1/24/2006. Politechnika Radomska, Wydawnictwo 2006, pp. 76 - 83. ISSN 1230-7823.

[2] KALINČÁK, D., PALKO, P. *Prevádzkové využitie spaľovacích motorov na hnacích koľajových vozidlách a nekonvenčné trakčné pohony.* In Sb. přísp. 4th International Scientific Conference„Challenges in Transport and Communication", Part III, Univerzita Pardubice 2006, pp. 1247 – 1252. ISBN 80-7194-880-2.

[3] KALINČÁK, D., PALKO, P. *Prevádzkové podmienky motorových hnacích vozidiel a hybridné pohony.* In Zb. predn. XVIII. medzinárodnej konferencie „Súčasné problémy v koľajových vozidlách - PRORAIL 2007" Žilina. 19. - 21. 9. 2007. Diel I, pp. 285 - 292. VTS pri ŽU, Žilina 2007. ISBN 978-80-89276-06-6.

[4] STEINER, M., SCHLOTEN, J. *Energy storage on board of DC fed railway vehicles,* Power Electronics Specialists Conference, 2004, PESC 04. 2004 IEEE 35th Annual.

[5] TAKETO, F., NOBUTSUGU, T., MITSUYUKI, O. *Developement of an NE train,* JR EAST Technical Review-No.4, pp. 62 – 70.

[6] http://www.rjcorman.com/railpower.html

Effectivity Analysis of Chosen Numerical Methods for Solution of Mechanical Systems with Uncertain Parameters

[*]Róbert Bednár, Milan Sága

[*] University of Žilina, Faculty of Mechanical Engineering, Department of Applied Mechanics, Univerzitná 1, 010 26 Žilina, Slovakia, {robert.bednar, milan.saga}@fstroj.uniza.sk

Abstract. The paper deals with usability and efficiency problem for the chosen solution methods for mechanical systems with structural uncertainties, which are significantly influencing the analysis results and the analysis itself. In the centre of interest will be the chosen approaches and methods; an application of the chosen approaches is presented - the first one, a simple combination of only inf-values or only sup-values; the second one presents full combination of all inf-sup values; the third one uses the optimizing process as a tool for finding out a inf-sup solution and last one is Monte Carlo technique as a comparison tool.

Keywords: Uncertain structural parameters, MATLAB, Monte Carlo, interval arithmetic.

1. Introduction

Generally, it is possible to say that each engineering problem encounters uncertainties in various forms, e.g. in geometrical parameters, material constants, loads, etc. Many of those uncertainties are based on physical imperfections, the general diversity and complexity of natural phenomena and of course our ignorance or inability to precisely describe characteristics of the investigated problem.

Uncertain parameters appear mostly as random variables and thus are described in the terms of stochastic approach. But without the knowledge of the probability density and the nature of distribution we are forced to use another approach, which could describe the parameters with the mentioned restrains and at the same time contain sufficient information about the character of the uncertainty.

Alternately to the use of probability methods we can use imprecise probabilities [4] and the possibility theory, which involves the theory of interval numbers [2, 3, 5, 6, 7, 8], fuzzy numbers and fuzzy sets [9, 10]. Without the information of the relevance of the data on the interval, we cannot use the fuzzy approach, but are still able to use the interval approach to describe the uncertain parameters, which are considered as unknown but bounded with lower and upper bounds.

Our short study proposes algorithms for modal and spectral interval computations of FE models and their effectivity analysis in view of the input uncertainty degree (2%, 5%, 10%, 20%).

2. Computational methods for interval analysis

If we want to use interval arithmetic approach, an uncertain number is represented by an interval of real numbers [2, 3]. The interval numbers derived from the experimental data or expert knowledge can then take into account the uncertainties in the model parameters, model inputs etc. Complete information about the uncertainties in the model may be included by this technique and one can demonstrate how these uncertainties are processed by the calculation procedure in MATLAB.

During the solving of the particular tasks using the interval arithmetic application on the solution of numerical mathematics and mechanical problems, the problem known as the overestimate effect is encountered. Its elimination is possible only in the case of meeting the

specific assumptions, mainly related to the time efficiency of the computing procedures [3, 4]. Considering uncertain parameters in interval form, some solution approaches already used or proposed by the authors are analyzed [9, 10]. The goal is to present algorithm description and comparison study of the following numerical methods:

- Monte Carlo method (MC) - as a comparison tool,
- a simple combination of only inf-values or only sup-values (COM1),
- a full combination of all inf-sup values (COM2),
- a method which uses an optimisation process as a tool for finding out a inf-sup solution (OPT).

Monte Carlo method (MC) is a time consuming but reliable solution. Various combinations of the uncertain parameter deterministic values are generated and after the subsequent solution in the deterministic sense we obtain a complete set of results processed in an appropriate manner. Infimum and supremum calculation is following

$$\inf\left(F\right)=\min \text{ of all results } F\left(p_i\right), \text{ where } i=1,...,m \text{ and } m\approx 5000\div 100000,$$
$$\sup\left(F\right)=\max \text{ of all results } F\left(p_i\right), \text{ where } i=1,...,m \text{ and } m\approx 5000\div 100000. \tag{1}$$

Solution evaluation in marginal values of interval parameters (COM1) has its physical meaning for many engineering problems. We consider an approach where the extreme output values are obtained by the application of the extreme parameter values on input. That means that the inf-sup is obtained using the deterministic analysis for inf or sup of input uncertain parameters. Inf-sup calculation is

$$\inf\left(F\right)=\min \text{ of } \left[F\left(\underline{p}\right), F\left(\overline{p}\right)\right] \qquad and \qquad \sup\left(F\right)=\max \text{ of } \left[F\left(\underline{p}\right), F\left(\overline{p}\right)\right] \tag{2}$$

Solution evaluation for all marginal values of interval parameters (COM2) which is also based on the set of the deterministic analyses appears as the more suitable one. The marginal interval parameter values are considered again but the inf and sup values are also combined. The method provides satisfying results and can be marked as reliable, even if there is still a doubt about the existence of the extreme solution for the uncertain parameter inner values. Solution for two interval numbers $p_1=\left\langle a_1 \ b_1\right\rangle$ and $p_2=\left\langle a_2 \ b_2\right\rangle$ may be found by this computational way

$$\inf\left(F\right)=\min \text{ of } F\ \left[\left(a_1\ a_2\right),\ F\left(a_1\ b_2\right),\ F\left(b_1\ a_2\right),\ F\left(b_1\ b_2\right)\right],$$
$$\sup\left(F\right)=\max \text{ of } F\ \left[\left(a_1\ a_2\right),\ F\left(a_1\ b_2\right),\ F\left(b_1\ a_2\right),\ F\left(b_1\ b_2\right)\right] \tag{3}$$

The method of the inf and sup solution using the optimization techniques (OPT) is proposed by the authors as an alternative to the first and to the third method. It should eliminate a big amount of analyses in the first method and also eliminates the problem with the possibility of the inf and sup existence inside of the interval parameters for the deterministic values. Computational process for two interval numbers p_1 and p_2 may be found as follows

$$\inf\left(F\right)=F\left(\mathbf{p}_{OPT}\right), \text{ i.e. find } \mathbf{p}_{OPT} \text{ so that } F\left(\mathbf{p}_{OPT}\right)\rightarrow \min,$$
$$\sup\left(F\right)=F\left(\mathbf{p}_{OPT}\right), \text{ i.e. find } \mathbf{p}_{OPT} \text{ so that } F\left(\mathbf{p}_{OPT}\right)\rightarrow \max. \tag{4}$$

3. Solving of truss structure with interval parameters

Considering different uncertain parameters the numerical interval stress-strain study of a three–dimensional truss structure (Fig. 1) was performed.
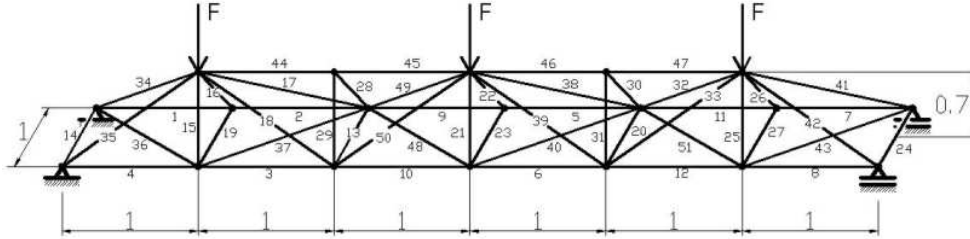
Fig. 1. Analyzed truss structure, dimensions in [m]

As the interval uncertain parameters were the cross-sections of the trusses considered. Because of the computation memory and time demands, fifty one bars have been split into 7 cross-sectional groups. All other parameters were considered as certain.

Certain parameters: $E = 2 \cdot 10^{11}$ Pa, $\mu = 0.3$, $\rho = 7800$ kg$\cdot$m^{-3}, $\delta = 10^{-5}$.

Uncertain parameters: $\mathbf{xf} = [0.02, \, 0.05, \, 0.10, \, 0.20]$,

$A_1 = 3500 \cdot 10^{-6} \cdot (1 + \mathbf{xf}_i) \, m$, $\qquad A_2 = 3000 \cdot 10^{-6} \cdot (1 + \mathbf{xf}_i) \, m$, $\qquad A_3 = 2500 \cdot 10^{-6} \cdot (1 + \mathbf{xf}_i) \, m$,

$A_4 = 2000 \cdot 10^{-6} \cdot (1 + \mathbf{xf}_i) \, m$, $\qquad A_5 = 1800 \cdot 10^{-6} \cdot (1 + \mathbf{xf}_i) \, m$, $\qquad A_6 = 1500 \cdot 10^{-6} \cdot (1 + \mathbf{xf}_i) \, m$,

$A_7 = 1000 \cdot 10^{-6} \cdot (1 + \mathbf{xf}_i) \, m$.
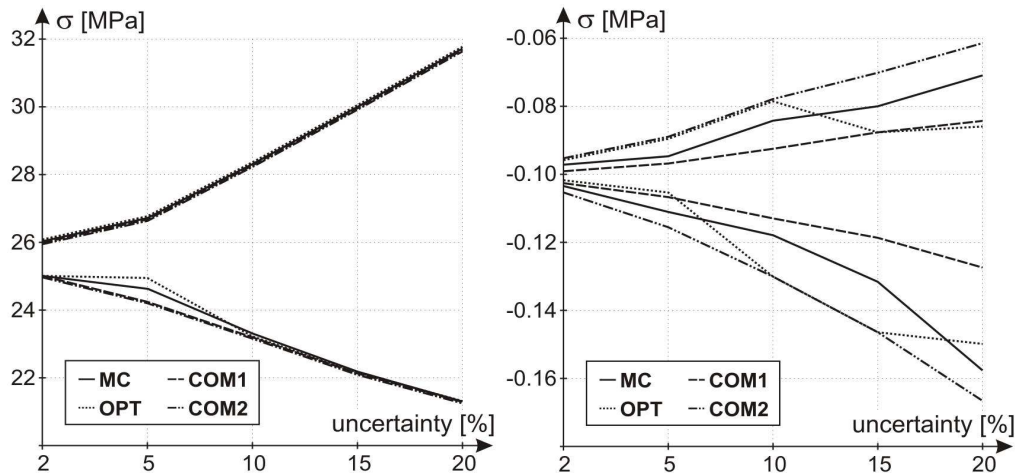
Fig. 2. Stresses solutions on bars No. 5 and 36

Uncertainty	Bar No.	MC	OPT	COM1	COM2
2%	5	< 25.010 26.030 >	< 25.010 26.030 >	< 25.010 26.030 >	< 25.010 26.030 >
	36	< -0.104 -0.097 >	< -0.102 -0.096 >	< -0.103 -0.099 >	< -0.106 -0.096 >
5%	5	< 24.754 26.853 >	< 24.946 26.853 >	< 24.295 26.853 >	< 24.295 26.853 >
	36	< -0.110 -0.095 >	< -0.106 -0.090 >	< -0.107 -0.097 >	< -0.115 -0.090 >
10%	5	< 23.264 28.345 >	< 23.191 28.345 >	< 23.191 28.345 >	< 23.191 28.345 >
	36	< -0.118 -0.085 >	< -0.130 -0.079 >	< -0.113 -0.092 >	< -0.130 -0.079 >
20%	5	< 21.258 31.888 >	< 21.258 31.888 >	< 21.258 31.888 >	< 21.258 31.888 >
	36	< -0.158 -0.071 >	< -0.150 -0.086 >	< -0.127 -0.085 >	< -0.167 -0.062 >

Tab. 1. Stress inf/sup results for the chosen bars [MPa]

4. Conclusion

The paper presents the interval arithmetic application on structural FE analysis. The interval arithmetic provides a new possibility of the examination of quality and reliability of analyzed objects. In the paper authors investigated possibilities of the stress-strain solution of models with interval cross-sectional areas of the truss structure. It shows the solution efficiency for solving problems including uncertain parameters with a various width of the interval.

The analyses results can be summarized as follows:

- COM1 method gives satisfactory results and can be described as reliable for this kind of analyses, although doubt arises in the sense of the existence of extreme solution for inner values of uncertain parameters,
- COM2 method provides decent results, but it is limited due to the exponential growth of the analyses number for complicated problems, once again arises doubt in the sense of existence of extreme solution for inner values of uncertain parameters,
- OPT method provides good results and is suitable for complicated problems because it does not need so many analyses as in the cases of the MC or COM2 methods.

Acknowledgement

References

[1] VAŠKO, M., SÁGA, M., TOTH, Ľ., JAKUBOVIČOVÁ, L. *Short comparison study of the interval arithmetic application and Monte Carlo simulation*, In Computational Mechanics 2003, Nečtiny, Čzech Republic, ISBN 80–7082–999–0, p. 467–474, 2003.

[2] KULPA, Z., POWNUK, A., SKALNA, I. *Analysis of linear mechanical structures with uncertainties by means of interval methods*, Computer Assisted Mechanics and Engineering Sciences, Vol. 5, Poland, pp. 443–477, 1998.

[3] MOORE R., E. *Interval Analysis*. Prentice Hall, Englewood Cliffs, New Jersey, 1966.

[4] NEUMAIER, A. *Interval Methods for Systems of Equations*. Cambridge University Press, Cambridge, 1990.

[5] FORSSÉN, P. *Interval methods I*, **http://www.tdb.uu.se/kurs/optim-mn1/ht01/lectures/lec14_2.pdf**.

[6] ELISHAKOFF, I., DUAN, D. *Application of Mathematical Theory of Interval Analysis to Uncertain Vibrations*, Proc. of NOISE-CON'94, Ft. Lauderdale, Florida, pp. 519-524, 1994.

[7] CHEN, S. H., YANG, X. W. *Interval finite element method for beam structures*, Finite Elem. Anal. Des., 34, p. 75-88, 2000.

[8] ZHANG, H. *Nondeterministic Linear Static Finite Element Analysis*: *An Interval Approach*, School of Civil and Environmental Engineering, Georgia Institute of Technology, 2005.

[9] DEKÝŠ, V., SAPIETOVÁ, A., VAŠKO, M., KOCÚR, R. *Comparison the Results Based on Interval Numbers, Fuzzy Set Method and Probability Approach*, In Annals of the University of Petrosani, Mechanical Engineering, ISSN 1454–9166, vol. 8 (XXXV), p. 11–22, 2006.

[10] VAŠKO, M. *Application of genetic algorithms for solving of mechanical systems with uncertain parameters*. PhD. thesis, Žilina, 2007.

Influence of Impact Hammers on Modal Analysis of Construction

[*]Michal Binda, Tomáš Harčarik
[*]The Technical University of Košice, Faculty of Mechanical Engineering, Department of Applied Mechanics and Mechatronics, Letná 9, 04200 Košice, Slovakia, {michal.binda, tomas.harcarik}@tuke.sk

Abstract. The use of an impact hammer is the simplest and fastest method of inducing construction oscillation. As standard, impact hammers are equipped with sets of exchangeable tips of various firmnesses and heads of various weights, with the use of which it is possible to influence the frequency range and level of inducing force. A comparison of the influence of these exchangeable tips and weights of heads of impact hammers was carried out on a steel frame which served for placement of machinery equipment.
Keywords: Oscillation of mechanical assemblies, experimental modal analysis, impact hammers.

1. Introduction

An oscillating motion is an accompanying event during the operation of almost all machinery equipment. In the majority of cases, it is unwanted. Apart from decreasing the life time and reliability of machinery equipment, in many cases the oscillating motion has an adverse effect upon the quality of the products. Understanding and using methods in dynamic analysis of mechanical assemblies, with which constructors must be familiar, can subsequently allow construction to proceed in a manner to effectively suppress unwanted oscillation and provide peaceful operation of constructions.

2. Experimental modal analysis

Experimental modal analysis is a process of experimental determination of modal parameters (self frequencies, weights, firmnesses, buffering, shape of self oscillations) of linear time invariant systems. Experimental modal analysis is often used for resolving dynamic problems, oscillations and acoustics, which are not resolvable analytically. It includes the theory of modal analysis, an expression of the relationship between measured values as time and frequency relationships and also an estimation of modal parameters on the basis of obtained modal data and their presentation in a suitable format. On the basis of classical oscillation, the theory of modal analysis theoretically explains the existence of self frequencies, buffering coefficients as well as modal shapes for linear systems.

When estimating modal parameters, the majority of current methods require data processed in the form of functions of frequency transfers. A basic task when investigating dynamic properties is to obtain information regarding dynamic properties of mechanical systems from given frequency transfer functions. At present, modern methods of experimental modal analysis are available to determine parameters of a system from measured frequency transfers.

2.1. Measurement methods

There are two methods of measuring oscillations:
- measuring only one parameter (usually the level of echo),
- measuring input and the echo at output.

If the values of generation and echo of the construction are known, the properties of the measured system can be derived from this data. Within this category, there are several approaches

to obtaining the requisite data. The most frequent approach is obtaining data during generation of the construction at one point (within this method, only one line or column of the frequency echo function matrix is measured). There are two modifications of this method:
- SISO (Single Input Single Output) – single input (stimulus), single output (response),
- SIMO (Single Input Multiple Output) – single output, multiple outputs).

Another type of measurement is MIMO (Multiple Input Multiple Output). Generation of construction is implemented at several points.

2.2. Impact hammers

Impact hammers are hammers which are equipped with various additional devices allowing adjustment of the frequency and force of the range of impact effect [1], [3]. An integral part of the hammer is a force converter functioning on the principle of piezoelectrical materials which serve to determine the amplitude of force induced by the strike of the hammer on the construction. The force amplitude is determined by the weight of the hammer head and the speed with which the hammer strikes the construction surface. The frequency range of generation implemented using an impact hammer is determined by the firmness of the material of the hammer head contact surface. The resonance frequency of the hammer head structure is expressed by the formula:

$$f = \sqrt{\frac{contact\,surface\,rigidity}{hammer\,head\,weight}}.$$ (1)

The length of duration of the force effect depends upon firmness (not rigidity) of the impact hammer head contact surface. A firmer head and lower weight of impact hammer causes an increase in frequency ranges.

2.3. PULSE 6

The PULSE 6 measurement system is a universal, practically orientated measurement system for measurement and analysis of sound and oscillation. It provides a platform for a wide range of measurements carried out by a computer designed by Brüel & Kjaer. For adjustment, control and collection of measured data from the measurement device, software supplied with the measurement device is used. The standard supplied software is the type marked 7700. It provides the possibility to adjust analysers, display outputs and control other accessories. Types of analysers and accessories depend upon the installed software.

3. Measurement

A network of points was selected on the steel frame on the basis of an analysis of frame oscillation using the finite element method. For illustration, Tab. 1 shows some self shapes for frequencies.
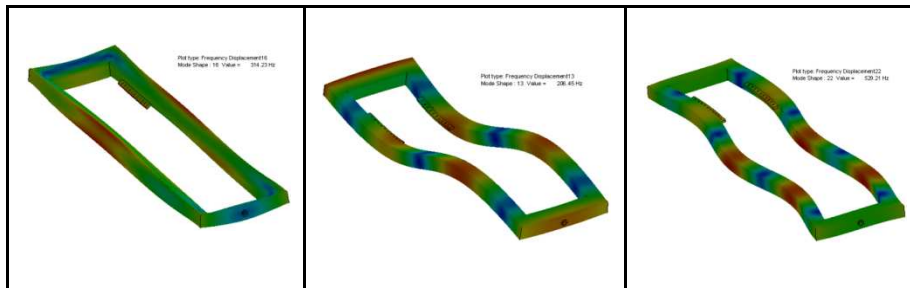
Tab. 1. Self shapes for frequencies

Excitation of a frame was carried out using impact hammers of type 8206 and 8210 from Bruel & Kljaer (Fig. 1).

Fig. 1. Impact hammers type 8206 and 8210

Rubber, plastic and aluminium extensions were used for the tip of the type 8206 impact hammer. A large, type 8210 impact hammer is supplied with four extensions labelled as soft, medium, tough and hard. The measured structure was generated by the impact of the impact hammer in points 1 to 6, whilst the measurement method was gradually repeated using all available impact hammer tips. A triaxial acceleration sensor was placed at reference point A (Fig. 2).
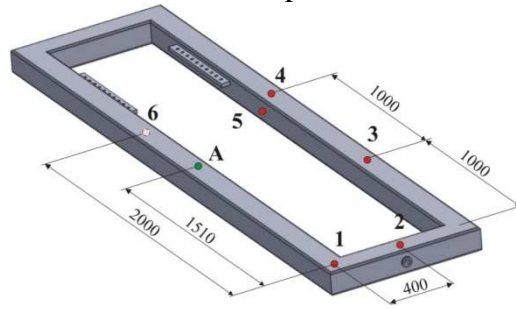
Fig. 2. Positions of reference points

From the obtained data, it is clear that the rigidity of the type 8206 impact hammer tip significantly influenced the shape of time development of generating force (the lower the rigidity of the tip, the wider the impulse and less sharpness of peak of development). The greatness of the generating force also depended upon the rigidity of the tip used. The higher the tip rigidity, less generating force was required to sufficiently oscillate the measured frame.

Impact hammer 8206	Impact hammer tip	Generating force (N)
	rubber	151
	plastic	122
	aluminium	58

Tab. 2. Comparing of excitation forces for type 8206 impact hammer

Type of impact hammer tip	rubber	plastic	aluminium
Shape of generating force developement			

Tab. 3. Generating force development for type 8206 impact hammer

When generating the construction using type 8210 large performance impact hammer, the time developments of generating forces had similar developments as when using type 8206 impact hammer. The width of force impulse depended upon the rigidity of the tip used (the greater the rigidity of the impact hammer tip, the narrower the force impulse). Generating force also depended upon the type (rigidity) of the tip used. When applying the same energy, the greatness of generating power was in line with the level of rigidity of the type 8210 impact hammer tip used.

Impact hammer 8210	Impact hammer tip	Generating force (N)
	soft	1660
	medium	2740
	tough	4600
	hard	5620

Tab. 4. Comparison of generating forces for type 8210 impact hammer

After oscillating the frame using impact force in pre-defined places, the development of accelerations of point A in directions x, y and z were obtained via an acceleration sensor. The shape of individual time dependency was influenced by the greatness of the generating force and the rigidity of the tip used. The measured data was then processed using the PULSE 6 measurement system which resulted in frequency dependence of amplitudes of point A accelerations. When using a type 8206 impact hammer with a rubber tip, there were problems in reading the values of higher self frequencies from the obtained frequency dependence of amplitudes of point A accelerations. The frequency range is influenced by the weight of the impact hammer and the rigidity of the tip used.

Type of impact hammer tip	rubber	Plastic
Frequency dependence of point A in the x direction		
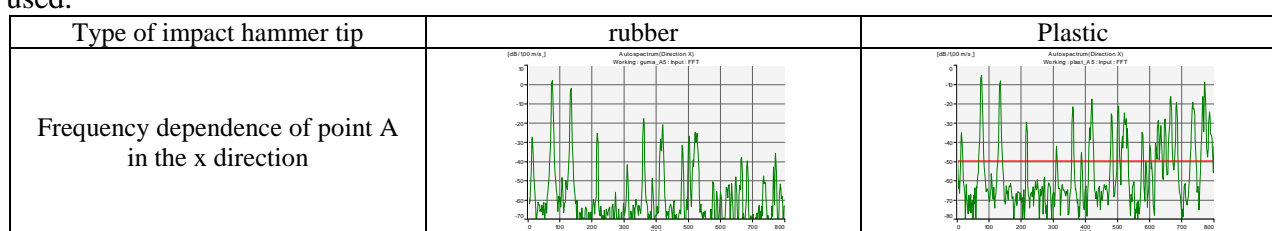
Tab. 5. Frequency dependence of point A acceleration in the x direction when generating a frame in place

4. Conclusion

The frequency range is influenced by the weight of the impact and the rigidity of the tip used. Force amplitude is determined by the weight of the hammer head and the speed with which the hammer strikes the construction surface. A change in the level of impact force can be influenced by a change in size (weight) of hammer head. In case of using a very rigid hammer, input energy will cause a too large frequency range at output whilst part of the frequencies will be outside the range of our required frequency range. The greatest problem connected with the use of impact hammers for generating a construction is ensuring compliance of individual generating effects which is not only related to the same force amplitude induced by a hammer strike but also maintaining the exact position where the hammer comes into contact with the construction surface. It is also very important to avoid a so called double strike. A double strike causes significant problems when processing the signal and influences the measured data. When choosing an impact hammer tip, the fragility of the construction surface and functionality of the measured construction should be taken into account.

Acknowledgements

References

[1] TREBUŇA, F. – ŠIMČÁK, F.: *Príručka experimentálnej mechaniky.* Typopres, Košice, 2007.

[2] BILOŠOVÁ A.: *Experimentální modální analýza*, Spectris Praha spol. s. r.o, Praha, 2001.

[3] CAMERON T.: *Computational and Experimental Modal Analysis of a Clamped-Free Bar.* Mechanical Engineering Applied Physics, MI, 1996

Effectiveness of Machines Utilization for Wood Production

*Stanisław Borkowski, **Krzysztof Mielczarek
*Czestochowa University of Technology, Department of Management,
Institute of Production Engineering, e-mail: bork@zim.pcz.pl
**Czestochowa University of Technology, Faculty of Management, Institute of Production Engineering,
e-mail: k.mielczarek@wp.pl

Abstract. In this article the approach to maintenance of technical objects TPM was introduced. Chosen TPM coefficients were calculated. On the base of TPM coefficients its effectiveness was estimated. Thanks to using PAMCO coefficients the utilization of working time machine was researched. The period of research embraced one year and the object of the analysis was the machine for wood production.

Keywords: TPM, OEE, utilization condition, PAMCO

1. TPM coefficients for circular sawing machine

TPM (Total Productive Maintenance) is an approach to services of technical objects and its equipment. One of the most important aims of introducing TPM is the identification and aspiration for elimination the losses which are caused by uneconomical maintenance of technical objects. These losses concerned: time, speed and the quality. Through elimination these losses it is possible to improve the productivity of plant and equipment [1]. The TPM coefficients are the measuring instruments that are designed for evaluating effectiveness work machine and they are calculated on the base of their performance. They are applying to accessibility in the meaning of active work of machine, utilization in the meaning of planned in percentages loading and the quality of produced by the machine products [2, 3].

Assessment of actual effectiveness of circular sawing machine was carried out in one year period. In the evaluation of maintenance performance, the overall equipment effectiveness (OEE) is the most important and is used as metric to evaluate the manufacturing capability and is a function of equipment availability, performance efficiency and the quality. The OEE coefficient - Overall Equipment Effectiveness is a key standard concerning effectiveness of machines, individual posts, production teams as well as assembly lines used in the TPM program. One of the main aims of the TPM improvement program is to reduce or eliminate Six Major Losses:
- Break down,
- Changeovers,
- Availability loses,
- Speed losses,
- Short stoppages,
- Quality losses.

It allows precisely locating the area which require attention and, in effect, increasing the equipment effectiveness. The OEE factor should be treated as internal unit that allows estimating the improvement or deterioration of the situation while comparing to the situation dating on different period of time on the same production line, device or group of devices [7].

On fig. 1 was introduced average value of the coefficient of exploitation (WE), the performance coefficient (WW), the quality coefficient (WE) and the overall equipment effectiveness (OEE) in one year period.
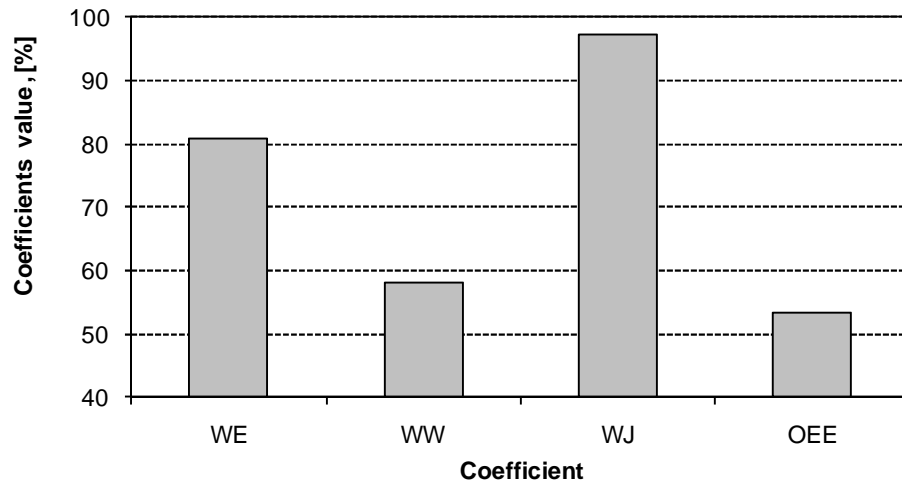
Fig. 1. TPM coefficients value for circular sawing machine in one year period.

For researched circular sawing machine the average result more than 50% means that from machine we can obtain half of products, which can be received in an ideal condition. An 85% OEE is considered as being world class and enterprises should try to reach it. Very often, the OEE factor is much lower. The research indicates that the average OEE coefficient in production companies amounts 60%. On fig. 2 was shown the losses which cause decrease of OEE coefficient for researched circular sawing machine in one year period.
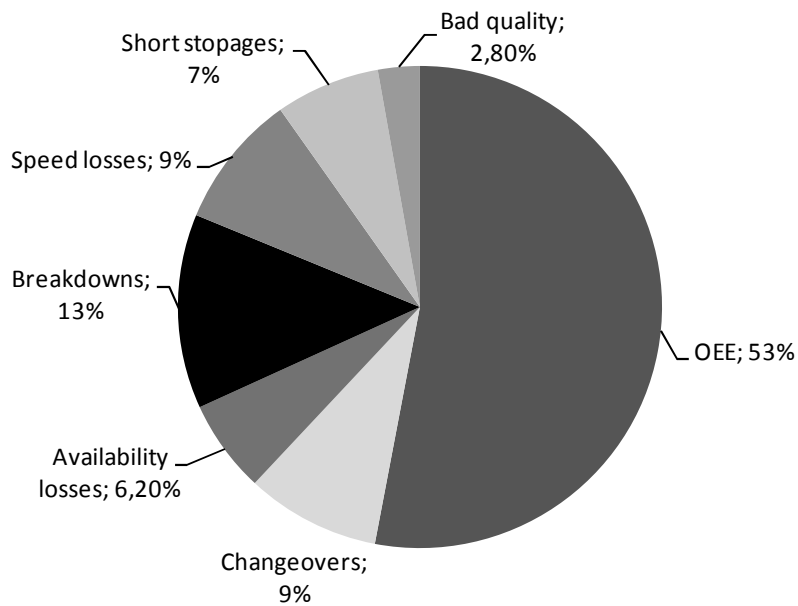
Fig. 2. Distribution of OEE coefficient losses.

For analyzed machine losses caused through breakdowns and changeovers has the main influence on fall of OEE coefficient value. Also the quality losses should be reduced because value 2,8% is considered as too high. Elimination of above-mention losses can contribute to significant increase effectiveness of researched device.

2. Value of PAMCO coefficients for circular sawing machine

The PAMCO method (Plant & Machine Control) is an important tool for evaluation the efficiency of working time machine. According to the PAMCO method time is divided on kinds and individual coefficients are counted using it. On the basis of PAMCO coefficients companies may be accounted for their tasks and target in production, and their results can be compared with other manufacturers and enterprises. In the aim of the presentation the utilization of work time machine and capacity company the time has been divided into several categories, which constitute the basis for calculating their particular fcoefficients and rates, providing the complete and clear picture utilizing the operating time of machines. It is used for evaluation efficiency of machines in different enterprises [4]. Chosen PAMCO coefficients for circular sawing machine were calculated. The value of coefficients PAMCO: Operational Efficiency (OE), Operational Utilization (OU), Production Utilization (PU) and Effective Utilization (EU), were counted from formula introduced in study [1, 5]. For determination PAMCO coefficients date from 12 months were collected. The average values of chosen coefficients were shown on fig. 3.
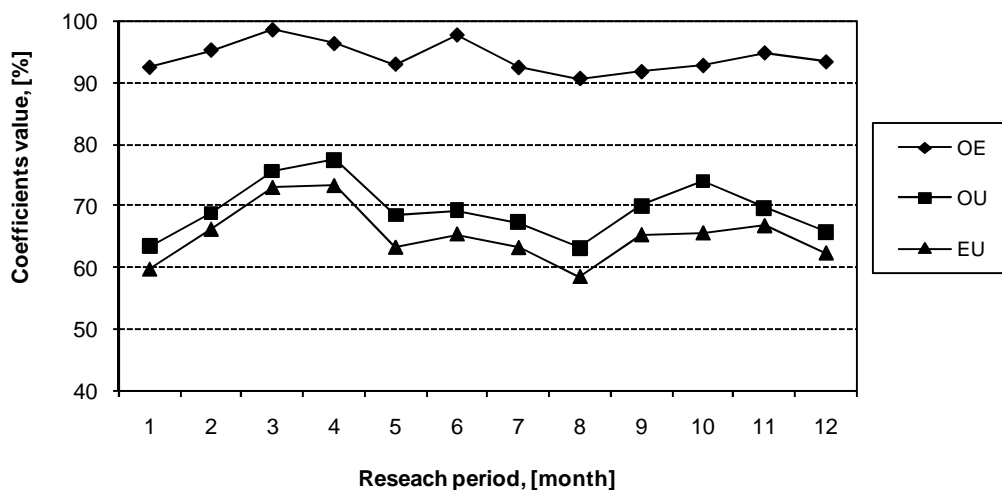
Fig. 3. Value of PAMCO coefficients for circular sawing machine.

From received analysis results that machine is effectively utilized. Shows about it high level of average coefficients PAMCO - Operational Efficiency (OE) oscillated about 95% (optimal value about 91,5%), - Operational Utilization (OU) and Effective Utilization (EU) reached about 70% which nominal value should be more than 50%. These coefficients testify about high utilization of machines working time. It should be shown that level of individual coefficients were subjected significant fluctuations in individual periods. Especially it concerns Operational Utilization (OU) and Effective Utilization (EU). In first four months of the year the value of this individual coefficients was increasing but in following months when the production level was reduced also the coefficients values were smaller.

3. Conclusion

From conducted investigation results that the circular sawing machine is utilized effectively. As a result of the comparison analysis concerning two methods of production equipment effectiveness, that are the TPM and PAMCO coefficients we received different results. The TPM coefficients enable evaluating of device effectiveness with due regard of three components: availability, performance and quality and value of the most important coefficient (OEE) reached value 53% what is considered as an average results. The PAMCO coefficients estimates only the usage scope of (total) device working time while omitting the quality aspect of the device and the most important coefficient Effective Utilization (EU) value 70% means that the machine is utilized in very effective way. The advantage of the OEE factor is full and real perception way on production equipment effectiveness, enabling identifications of main problems within the scope of devices and instruments, what allows to direct improving activities. The advantage of the PAMCO coefficients its universal character, formulating equal comparison criteria. It should be also noticed that machine utilization is not rhythmical. There are ungrounded stoppages, especially not planned. Despite good results, the values of individual coefficients should be constantly monitored. It will allow quickly reacted while wrong effect of working machine will be noticed. Nevertheless, the average value of quality level nearly 3% shows that researched circular sawing machine manufactured a high level of incompatible products.

References

[1] BORKOWSKI, S., SELEJDAK, J., SALAMON, S. *Efektywność eksploatacji maszyn i urządzeń*. Wydawnictwo Wydziału Zarządzania Politechniki Częstochowskiej. Częstochowa 2006.

[2] HRUBEC J., BORKOWSKI S. *Efektywność eksploatacji maszyn i zdolność jakościowa procesu. Efficiency of exploitation machine and capability of process quality*. Instytut Organizacji i Zarządzania w Przemyśle "ORGMASZ". Warszawa 2006.

[3] BORKOWSKI, S., ULEWICZ, R. *Zarządzanie produkcją. Systemy produkcyjne*. Oficyna Wydawnicza „Humanitas". Sosnowiec 2008.

[4] BORKOWSKI S., MIELCZAREK K., SELEJDAK J. *The stability of PAMCO indicators for extrusion machine*. 12th International Scientific Conference. Kvalita a spoľahlivosť technických systémov. Nitra 2007.

[5] BORKOWSKI, S., SELEJDAK, J. *TPM and PAMCO Exploitation factors as quality determinants*. Advanced manufacturing and repair technologies in vehicle industry. 24th International Colloquium. Czech Republic. Svitavy, 2007.

[6] MIELCZAREK, K., BORKOWSKI, S. *Correlation analysis between quality level and TPM coefficients. Chapter 8*. In: *Quality and Production Management in Practice*. BORKOWSKI, S., KOVALENKO, V.S. (red.). Press Association of Universities Russia. Saint Petersburg 2008.

[7] KNOP K., BORKOWSKI S., CZAJA P. 2008. *The Assessment of Efficiency of Jars Filling and Closing Line with the Use of OEE. Chapter 1*. In: *TPM and PAMCO Coefficient as Basis of Estimation of Machines Exploitation Efficiency*. Borkowski S., Kročko V. (red.), Saint Petersburg State Polytechnical University. Saint Petersburg 2008.

Finite Element Implementation of Damage in Composites

[*]Stanislav Danišovič, Milan Žmindák
[*]University of Žilina, Faculty of Mechanical Engineering, Univerzitná 1, 01026 Žilina, Slovakia,
stanislav.danisovic@fstroj.uniza.sk

Abstract. This paper presents numerical modeling of composite damage. The damage model is implemented in ANSYS software for a one dimensional bar element. A return mapping algorithm integration is implemented in conjunction with plane stress element PLANE182. These subroutines should be linked with the ANSYS program beforehand.

Keywords: Finite Element Method, Composite Structures, Damage.

1. Introduction

Composites of the future will offer many advances over those in use today. Composite materials reinforced by fibres are important materials possessing excellent mechanical and also thermal and electro-magnetic properties. Composites with the highest stiffness and strength have continuous (glass, carbon, Kevlar or aramid) fibers embedded in thermoset (polyester or epoxy) matrix. Fibers carry mechanical load, matrix transmits load to the fibers, insures ductility and toughness, and protect the fibers against damage caused by manipulation or surroundings.

Techniques for numerical simulation of the behavior of composites, mostly based on finite element method (FEM), are today becoming routinely used by ever increasing number of design engineers [1,2]. However, the composites failure criteria currently available within most commercial FEM packages suffer from limitations concerning on accuracy, range of application and/or ease of results interpretation. Other effective numerical methods for simulation of composite materials an composite structures are described in [3,4].

This paper presents numerical modeling of composite damage. The damage model is implemented in ANSYS software for a one dimensional bar element. A return mapping algorithm integration is implemented in conjunction with plane stress element PLANE182.

2. Numerical modeling of composite damage

A number of material modelling strategies exist to predict damage in laminated composites, subject to severe static or impulsive loads. Broadly, they can be classified as [5, 6]:

- failure criteria approach (which can be based on the equivalent stress or strain),
- fracture mechanics approach (based on energy release rates),
- plasticity or yield surface approach,
- damage mechanics approach.

Strength-based failure criteria are commonly used with the FEM to predict failure events in composite structures. Numerous classical criteria have been derived to relate internal stresses and experimental measures of material strength to the onset of failure (maximum stress or strain, Hill, Hoffman, Tsai-Wu). These classical criteria implemented in most commercial FE codes are not able to physically capture the failure mode. Some of them cannot deal with materials having a different

strength in tension and compression. The Hashin criteria are briefly reviewed in [7] and improvements are proposed by Puck and Schurmann[8] over Hashin's theories are examined.

However, few criteria can represent several relevant aspects of the failure process of laminated composites, e.g. the increase on apparent shear strength when applying moderate values of transverse compression, or the detrimental effect of the in-plane shear stresses in failure by fibre kinking. The development of a one-dimensional damage mechanics solution involves the definition: 1) a suitable damage variables, 2) an appropriate damage activation function, 3) a convenient damage evaluation.

3. The return mapping algorithm

A return–mapping algorithm is used to solve for variables $\dot{\lambda}, \dot{\delta}, \dot{\mathbf{D}}, \delta, \mathbf{D}$, in numerically approximated form [9]. To implement the return mapping algorithm, expressions for $\partial f / \partial \mathbf{Y}, \partial g / \partial \mathbf{Y}, \partial f / \partial \gamma, \partial \gamma / \partial \delta$ and $\partial \mathbf{Y} / \partial \mathbf{D}$ are needed, where g is the damage activation function, $\mathbf{Y}$ is vector of the thermodynamic forces, f is damage potential function, $\gamma(\delta)$ is the hardening function, δ is the hardening variable, $\mathbf{D}$ is the damage tensor. If we assume $f = g$, the derivative of the potential function and the damage surface with regard to the thermodynamic forces is given by:

$$\frac{\partial g}{\partial Y} = \frac{\partial f}{\partial Y} = \left\{ \begin{array}{c} 0 \\ \dfrac{1}{g}\left(\left(1 - \dfrac{G_{Ic}}{G_{IIc}}\right) \dfrac{1}{4F_{2t}} \sqrt{\dfrac{2E_2}{Y_2}} + \dfrac{G_{Ic}}{G_{IIc}} \dfrac{E_2}{\left(F_{2t}\right)^2}\right) \\ \dfrac{1}{g} G_{12} \end{array} \right\} \tag{1}$$

and the derivative of the damage surface w.r.t the damage hardening function is

$$\frac{\partial g}{\partial \gamma} = \frac{\partial f}{\partial \gamma} = -1 \tag{2}$$

Also, the derivative of the hardening function γ w.r.t. conjugate variable δ is needed

$$\frac{\partial \gamma}{\partial \delta} = \frac{c_1}{c_2} \exp\left(\frac{\delta}{c_2}\right) \tag{3}$$

The derivative of the thermodynamic forces w.r.t. the internal damage variables is

$$\frac{\partial \mathbf{Y}}{\partial \mathbf{D}} = \frac{\partial \mathbf{Y}}{\partial \boldsymbol{\sigma}} : \frac{\partial \boldsymbol{\sigma}}{\partial \mathbf{D}} \tag{4}$$

Furthermore, the derivative of the thermodynamic forces with respect to strain is written as

$$\frac{\partial \mathbf{Y}}{\partial \boldsymbol{\varepsilon}} = \frac{\partial \mathbf{Y}}{\partial \boldsymbol{\sigma}} : \frac{\partial \boldsymbol{\sigma}}{\partial \boldsymbol{\varepsilon}} = \frac{\partial \mathbf{Y}}{\partial \boldsymbol{\sigma}} : \mathbf{C} \tag{5}$$

The following are written in contracted notation and multiplied by the Reuter matrix,

$$\frac{\partial \mathbf{Y}}{\partial \boldsymbol{\sigma}} = \begin{bmatrix} 0 & 0 & 0 \\ \dfrac{-\sigma_2 \nu_{12}}{\left(1 - D_2\right)^2 E_1} & \dfrac{-2\sigma_2}{\left(1 - D_2\right)^3 E_2} & -\dfrac{-\sigma_2 \nu_{12}}{\left(1 - D_2\right)^2 E_1} & 0 \\ 0 & 0 & \dfrac{4\sigma_6}{\left(1 - D_6\right)^3 G_{12}} \end{bmatrix} \tag{6}$$

and

$$\frac{\partial\boldsymbol{\sigma}}{\partial\mathbf{D}} = \begin{bmatrix} 0 & \dfrac{E_2 v_{12}}{1-v_{12}v_{21}}\varepsilon_2 & 0 \\ 0 & \dfrac{E_1 v_{21}}{1-v_{12}v_{21}}\varepsilon_1 - \dfrac{2(1-D_2)^2 v_{12}}{1-v_{12}v_{21}} & 0 \\ 0 & 0 & -8(1-D_6)G_{12}\varepsilon_6 \end{bmatrix} \tag{7}$$

The damage model can be implemented in ANSYS using the USERMAT subroutineusermatps.f, with plane stress element (PLANE 182 or PLANE183) and laminate shells (SHELL181) withIntelVisual FORTRAN Compiler 9.1 for Windows.

4. Numerical examples
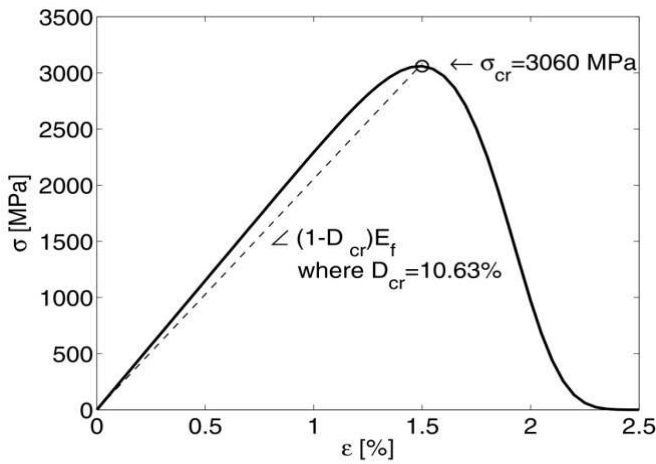
Fig. 1. Fiber tensile damage model response

Example 1

In this example the one-dimensional bar representative of a carbon fiber bundle is implemented in ANSYS using USERMAT subroutine usermat1.f, available in [10]. An one-dimensional bar is represented by a carbon fiber bundle. The nominal stress-strain response is shown a solid line in Fig. 1. Fromfig. 1 we can see that the bundle fails at ε_{cr} = 1.5% andcritical stress value is σ_{cr} = 3060 MPa.

Example 2

In this example the damage model using a return mapping algorithm integration is implemented in ANSYS. This model represents damage caused by transverse tensile stress in-plane shear stress. Compression and longitudinal tension have no effect on damage. Thematerialpropertiesfor AS4/APC2Carbon/PEEK unidirectional prepreg are given in table 1.The model response under only in-plane shear stress is shown in fig. 2.Fromfig. 2 we can see that the bundle fails at ε_{cr} = 3.2%and critical stress value is σ_{cr}= 158MPa.

Fig. 2. Response under in-plane shear stress

E_1 [MPa]	E_2 [MPa]	μ	G_{12}[MPa]	F_{2t} [MPa]	F_6 [MPa]
$131\cdot10^3$	$8.7\cdot10^3$	0.28	$5\cdot10^3$	78	157

Tab. 1. Material propertiesfor AS4/APC2

5. Conclusion

The present work has focused on the development of a failure criteria for laminates made of unidirectional plies under plane stress conditions which has demonstrated to be accurate and to give useful design information, has been implemented into ANSYS release 11, a commercial finite element code. First tested example has been solved a one-dimensional bar by a carbon fiber bundle.

Second tested example has been solved the damage model using a return mapping algorithm integration with the material properties for AS4/APC2 Carbon/PEEK unidirectional prepreg. The obtained results indicate that the existing knowledge on failure mechanisms needs further development.

Acknowledgement

References

[1] De SOUZA NETO, E.A., PERIČ, D., OWEN, D.R.J.*Continuum Modelling and Numerical Simulation of Material Damage at Finite Strains*, Archives of Computational Methods in Engineering, **5**, No 4, 311–384. 1998.

[2] KORMANÍKOVÁ, E., RIECKY, D., ŽMINDÁK, M. *StrengthofCompositeswithShortFibers*. In J. Murín, V. Kutiš, R. Ďuriš, editors, CMAS 2009 Proceedings of International Conference on Computational Modelling and Advanced Simulations. Publishing Slovak TechnicalUniversity, CD ROM, Bratislava, 2009.

[3] KOMPIŠ, V., ŠTIAVNICKÝ, M., ŽMINDÁK, M., MURČÍKOVÁ, Z. *Trefftz Radial Basis Functions*, Computer Assisted Mechanics and Engineering Sciences, 15, Nos. ¾, 239–250, 2008.

[4] ŽMINDÁK, M., NOVÁK, P. *Particles Interactions in Composites reinforced by Fibre and Spherical Inclusions*, Communications, Scientific Letters of the University of Žilina, 2009.

[5] DONADON**,** M,V:,De ALMEIDA, S.F.M., ARBELO, M.A.**,**De FARIA**,** A.R.*A three-dimensional ply failure model for composite structures*, Dept. of Mechanical Engineering, InstitutoTecnologico de Aeronautica – ITA CTA-ITA-IEM, Brazil.2009.

[6] IANNUCI, L., ANKERSEN, J.*An energy based damage model for thin laminated composites*, Composite Science and Technology, **66**, 7-8, 934–951.

[7] DAVILA, C.G., CAMANHO, P.P., ROSE, CH.A. *Failure Criteria for FRP Laminates*, Journal of Composite Materials, **39**, No 4, 2005.

[8] PUCK, A., SHURMANN, H.Failure analysis of FRP laminates by means of physically based phenomenological models, CompositesScience and Technology, 58, No 7,1045–1067, 1998.

[9] BARBERO J.E., *Finite Element Analysis of Composite Materials*, CRC Press, Taylor &FrancisGroup. 2008.

[10]BARBERO, E.J. Web resource, http://www.mae.wvu.edu/barbero/feacm/, 2006.

State of the Art Tools for Railway Vehicles Systems Dynamical Analysis Performance

*Ján Dižo, Juraj Gerlici, Tomáš Lack
*University of Žilina, Faculty of Mechanical Engineering, Department of Transport and Handling Technology, Univerzitná 1, 01026 Žilina, Slovakia, {Jan.Dizo, Juraj.Gerlici, Tomas.Lack}@fstroj.uniza.sk

Abstract. The paper is aimed to the dynamic simulation tools for the rail vehicle running on an actual track simulation. The practical computations performance, contact forces, derailment indexes assessment under various rail head profiles and rails inclinations computational conditions can be executed with the help of some special programme packages. The vehicle parameters correspond commonly to the four-or six axle two or three - bogies wagons or locomotives. The railway wheel tread profiles data can be obtained by the measurement, or from a theoretical specification.

Keywords: multibody system analysis, computer aided simulation, model, railway vehicle and rail model.

1. Introduction

The analysis of mechanical systems (for example the mechanical systems of vehicles) performance is permanently very topical. The vehicle dynamical properties are determined with the help of this analysis during a new vehicle design, or renewal of an older existing vehicle. The Eigen frequencies are characteristic for a vehicle construction [12]. A vehicle mechanical system is excited with various types of loads in the operation and this is the reason why its individual parts oscillate. The aim of a dynamical analysis is not only to judge the influence of an excitation on the mechanical system, but also on the base of that analysis, to propose and to perform the construction changes of a vehicle for the detected negative state elimination or improvement [3].
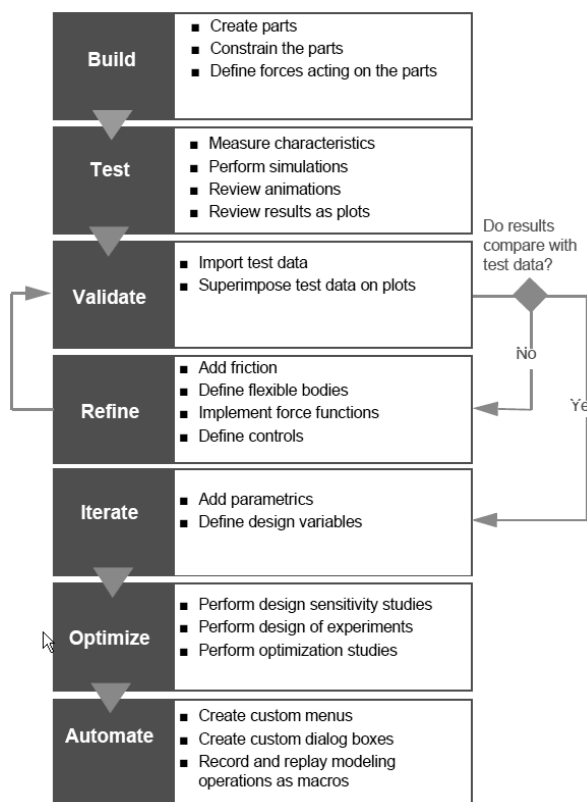
Fig. 1. Steps in Modeling and Simulating

2. Dynamic analysis of rail vehicles

In this chapter are described in sum programs that are most used for problem of modeling dynamics rail vehicles: NUCARS, MEDYNA, ADAMS/Rail, SIMPACK, VAMPIRE, UNIVERSAL MECHANISM and so on [12].

Even through every program have different attributes they were all developed specifically for rail dynamics modeling. Every program includes different methodology, Wheel-rail model, and analysis method and user interface [12].

2.1. NUCARS

In the USA has been developed program NUCARS by the association AAR (Association of American Railroads). He has been widely adopted and has become a standard tool in industry. NUCARS provides a variety of output options that can be used for analysis derailment and dynamic stability analysis. As such, it can be used primarily for dynamic rail vehicles analysis. It simulates dynamic rail vehicles response for individual track conditions. It is capable to predict various rail vehicles response: locomotives, passenger, transit or freight cars on any type of track geometry, including special track work such is turnouts and guardrails. Program is ideal for evaluating and comparing new vehicle designs as well as performing failure analyses such as derailment studies. NUCARS is also used to investigate and improve ride quality. It is used mostly on the American continent, mainly in USA and Canada [3].

2.2. MEDYNA

The program MEDYNA began to develop in the year 1979, when a high-speed transport began to develop by train ICE in Germany. The research institute DFVLR Oberpfaffenhofen and a German company series partook of it development. Program MEDYNA has been develop for a rail vehicles investigation primarily. Motions of a rigid body vehicle are relatively small in respect of a moving included with a vehicle reference system. Therefore MEDYNA is program making use the formalism with a linearized kinematics valid only for small motions [9]. This limiting is equally performance for a single rail track vehicles. Inaccuracy is accruing due to the vehicle length or the train set and due to decrescent radius of a curve. A work with program and a model generation performs in the editor mainly, a graphics possibilities is only for a several graph and diagram types limited. A source code of MEDYNA through FORTRAN is available to a user therefore allows it individual program modifications and extensions [2].

2.3. MSC.ADAMS
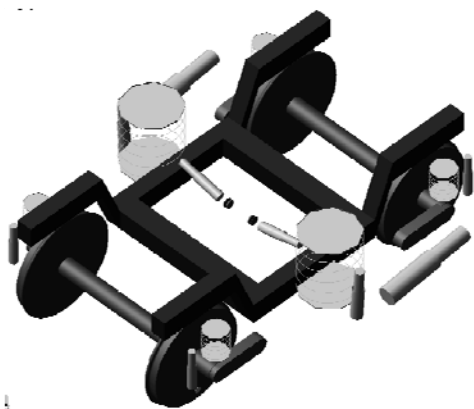
Fig. 2. Railway bogie ERRI wagon created in ADAMS/Rail

The start of the development program ADAMS reach by the year 1977 when the firm Mechanical Dynamics has been establish at the University of Michigan in USA. It has been dealt with the program development and aid. The ADAMS in nonlinear 3D dynamics rigid bodies program what at time provides specialized packages as well as interfaces to another technical and structural programs. The creators of this were centered the most on the application at the automobile industry, but it is use also it other mechanical applications [6]. A model creation performs interactive in the graphics environment and the program allows a very well visualization and animation possibilities. The package for the dynamics rail vehicle analysis, ADAMS/Rail came to be developed in the year 1993 in collaboration with NS Material Engineering (the technical department of the Netherlandish track) and Technical University Delft in Netherlands. The company ArgeCare from Berlin has been taken in with collaboration later. This company assures a program MEDYNA aid. MEDYNA is proposed as the program ADAMS/Rail part. In Fig. 2 is shown the rail bogie ERRI created by program ADAMS/Rail [1].

2.4. SIMPACK

SIMPACK is the package that has been developed in DLR (Deutsches Zentrum für Luft- und Raumfahrt, Oberpfaffenhofen). The program was developed in collaboration with the concern MAN Technologie in the year 1987. SIMPACK is used primarily for automotive, railway and

aerospace industries, engines, wind turbines and power transmission. In every industries is SIMPACK used for design several components and complete system analysis. SIMPACK can also consider any external influences on the system, e. g. ground disturbances and aerodynamic loading [4].
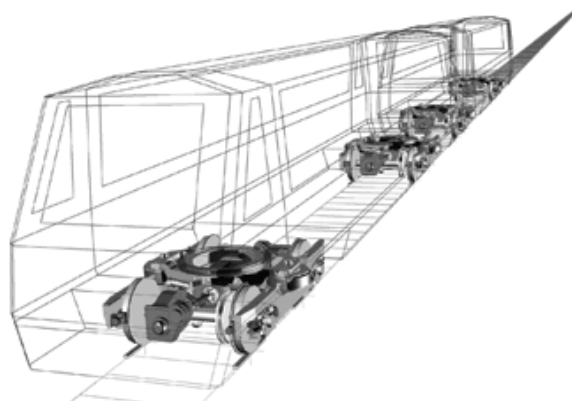
Fig. 3. Trainset model in program SIMPACK

2.5. VAMPIRE

The world development and research center BRR (British Railway Research) has been developed program VAMPIRE. Nowadays this program is distributedby the company AEA Technology Rail. The program is specialized only for a rail vehicles and it utilizes a global coordinate system that moves (as well as refer system in the program MEDYNA) a set speed on a ideal rail track. A model is building in an editor, a graphic input are utilize for a model control and for a visual results [3]. It exceed through an algorithm that allows a very short computational time. This allows a model latterly a vehicles ride at the real time. Additional advantages are jointer elements advisable for a rail vehicles modeling, special filters package and methods for analysis results and a very good documentation [8].

2.6. UNIVERSAL MECHANISM

The other computer modeling dynamic system representative is program UNIVERSAL MECHANISM (UM). It is intended for simulation kinematics and dynamics of planar and spatial mechanical systems. Mechanical systems are described by means of representing them as systems of rigid bodies connected by various kinematical pairs and force elements, so-called multibody systems. Online animation of motion and plots of dynamical performances are available during simulation. There are lots of measurable dynamical performances of mechanical systems: linear and angular coordinates, velocities and accelerations, active forces and moments, reaction forces etc. UM has an advanced postprocessor, which includes linear analysis, statistics, optimization, and export of results. This program is useful tool for the computer-aided modeling of multibody and hybrid systems of various types: aerospace structures, robots, railway vehicles, automobiles, cable systems, etc. UM software includes module for simulation of railway vehicle dynamics: locomotives, freight and passenger wagons, etc. More than 40 modules of various vehicles were created. There are diesel and electric locomotives, passenger cars, freight wagons, railcars, subway wagons and trams[11].

For dynamic analysis rail vehicles and railcar/track interaction are used modules UM Loco, UM Train/Train 3D, UM Rail/Wheel Wear. UM Loco allows the user to create fully parametrized models of vehicles, to calculate the critical speed, analyze 3D dynamics of a vehicle or a train in time domain on straight track or curves with/without irregularities, analyze vehicle Dynamics depending on Wheel and rail profiles, compute natural frequencies and modes as well as root locus, create hybrid rigid-elastic models of vehicles and then estimate stress state and damage sum [11].

3. Conclusion

With the advent of personal computers and fast processors, the use of analytical modeling programs has become less complicated and far more practical for more users. In this paper are described a most widely used computer dynamic analysis tools, mainly rail vehicles. The low cost of computer modeling compared with actual testing is a significant benefit to railcar modeling. Modeling allows a customer to test a new car design without having to build a prototype and tie up the track for testing, therefore increasing productivity through saving valuable time and manpower. The modeling provides equipments for testing such a derailment or jump the tracks also can predict forces and accelerations at various positions throughout the railcar to predict the ride characteristics or to evaluate ideas for improving ride.

Acknowledgement

References

[1] IWNICKY, S. *Handbook of Railway Vehicle Dynamics*. CRC Press, Taylor&Francis Group, Boca Raton, 2006

[2] Dukkipati, R. V., Amyot, J. R.Computer-aided simulation in railway dynamics. Marcel Dekker, New York, USA 1988.

[3] KALINČÁK, D., GERLICI, J., KUKUČA, P., LÁBAJ, J., LACK, T., POLÁCH, O., SÁGA, M. *Dopravný prostriedok – výpočtové metódy*. EDIS Žilina 2005.

[4] LACK, T., GERLICI, J. *Vehicles Dynamical Properties Analysis from the Point of View of Comfort for Passengers*. Archives of Transport. Vol. 19, issue 1-2. Warszawa 2007.

[5] GERLICI, J., LACK, T. *An Analysis of Bumpers and Springs Parameters Influence on the Ride Comfort, (in Slovak). In: Dynamics of Rigid and Deformable Bodies*. Proceedings of V. international conference. Univerzita J. E. Purkyne v Usti nad Labem. Usti nad Labem, 2007.

[6] LACK, T., GERLICI, J. *The Programme System DELTA Exploitation for Numerical Analysis Performances*, (in Slovak). In: 18-th. International Conference "Current Problems in Rail Vehicles - PRORAIL 2007" Proceedings of lectures, Part II. EDIS, Zilina 2007.

[7] LACK, T., GERLICI, J. *Vehicles Dynamical Properties Analysis from the Point of View of Comfort for Passengers*. Archives of Transport. Vol. 19, issue 1-2. Warszawa 2007.

[8] ONDROVÁ, Z., GERLICI, J., LACK, T. *Dynamics properties analysis of rail vehicle when moving*. (In Slovak) Proceedings of the 4-th international conference Dynamics of rigid and deformable bodies. Univerzity of J. E. Purkyně. Ústí nad Labem, 2006.

[9] POLÁCH, O. Railway vehicles dynamics analysis. In: Kalinčák, D. at al.: *Transport mean – computational methods*. Textbook. (In Slovak)University of Žilina. EDIS Zilina 2005.

[10] UZZAL, R. U. A., AHMED, W., RAKHEJA, S. *Dynamic analysis of railway vehicle – track interactions due to Wheel flat with a pitch – plane vehicle model*. Journal of Mechanical Engineering. Vol. ME39, issue 2. Bangladesh 2008.

[11] http://www.umlab.ru/download/marketing/eng/um.pdf

[12] http://scholar.lib.vt.edu/theses/available/etd-62498-1289/unrestricted/chapter1.pdf

Preliminary Design of the RAILBCOT Test Stand

[*]Marek Fusatý, Jozef Harušinec, Juraj Gerlici, Tomáš Lack
[*]University of Žilina, Faculty of Mechanical Engineering, Department of Transport and Handling Technology, Univerzitna 1, 01026 Žilina, Slovakia, {Marek.Fusaty, Jozef.Harusinec, Juraj Gerlici, Tomas.Lack}@fstroj.uniza.sk

Abstract. This paper deals with the design of the test bench RAILBCOT. The device will be used for testing of the railway vehicles' brake components in simulated conditions. Its parameters create the conditions for the realization of tests, which will be certified on the basis of verification testing and measurement validation. The final examination after completion of the implementation of the test bench will be focused on the study of railway wheel profile and brake block wear. This initial design construction is in progress to next modifications, which are based on more efficient arrangement of components, solutions of functional nodes, correction size of components and then reducing the weight. 3D software CATIA V5 R20 was used for this purpose.

Keywords: test stand, brake blocks, wheel profiles modification, rotational rail, computer aided design.

1. Introduction

In recent years the activities in studying properties of brake pairs has been significantly increased in the world. In some countries specialized test equipment is build, on which it is possible to programmatically load wheels, wheelsets, bogies or the whole vehicles. Special area in the test is testing for brake friction conditions analysis.

Braking conditions for testing brakes of rail vehicles are used to test the actual brake assemblies and components under simulated conditions. Therefore they mostly replace expensive braking tests of whole vehicles, which tend to be costly. Much emphasis is placed on studying the behaviour of the friction coefficient and wear. It is therefore necessary to test both parts of the friction pair, e.g. brake blocks and wheel, in conditions simulating the rail operation (speed, contact force, weight of the vehicle on the brake). Conditions can be simulated on dry and wet type of a brake.

Components on the brake bench are tested according to approved international decrees and programmes for comparison tests UIC 541-4 (approval friction testing of brake blocks). The greater part of the UIC brake bench allows to carry out any test prescribed program up to speed of 350 kmh^{-1}.

The issue of the brakes is very extensive and still brings new knowledge, which will be published and gradually put into practice.

1.1. Flywheel test stand UIC

The Department of transport and handling machines (KDMT) Faculty of Mechanical Engineering University of Zilina has installed flywheel brake test bench, which in year 2000 was approved by the institution UIC (Union Internationale des Chemins de fer) in Paris as a universal test bench category D. It is intended for testing brake blocks, brake discs and drums according to UIC 541-3 (disc brake) and UIC 541-4 (Brake blocks). The arrangement of braking bench is on the figure 1.
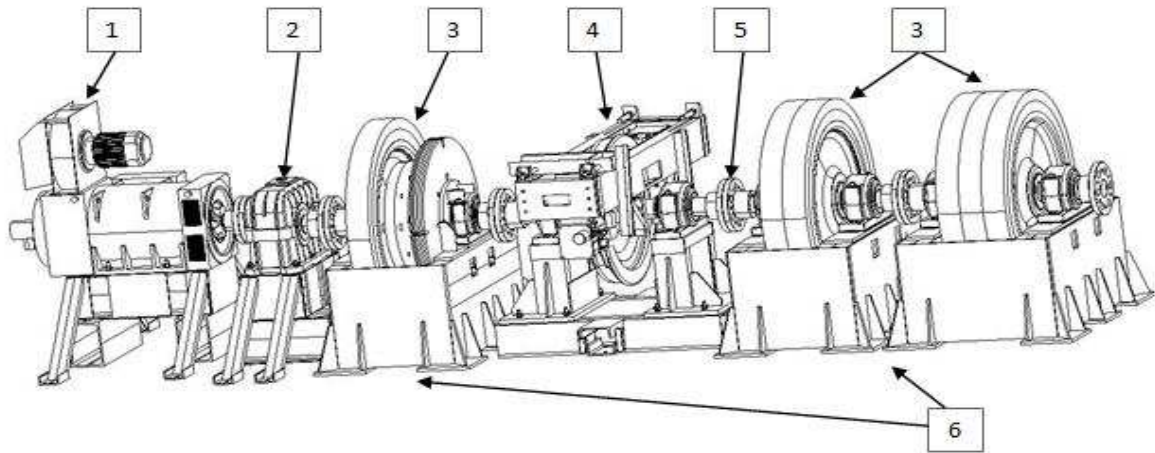
Fig. 1. Scheme of flywheel test brake bench UIC (1- electormotor, 2- gearbox, 3 – system of flywhells, 4 – module for testing brakes, 5- clutch BKN, 6 – base frames)

2. The RAILBCOT Test Stand Preliminary Structural Design

At the Department of Transport and Handling Technology (DMT) a project aimed to the prototype design of the test equipment RAILBCOT for testing brake components of rail vehicles is being solved.

The design conception of the test bench takes into consideration several construction options and adjustments. These designs have to come out of requirements on the constructed device. Therefore it will be necessary to establish a list of requirements, which help us with decision at various variants of conceptions to reach the desired result. Requirements for the function of the test bench are in Table 1.

	Requirements	*Necessity*	*Note*
1	Modular construction	wish	
2	Synchronization functional components	must be	Followed during manufacturing, assembly
2	Control of speed wheelsets	must be	Variability of device
3	Regulation of an axle forces	must be	Variability of device
4	Ease test bench	wish	
5	Easy, quick replacement wheelset	must be	Removing wheelset, assembly
6	Minimum weight, maximum strength the test bench	must be	Selection of semi-finished products with the desired properties
7	Compactness of the test bench	wish	Location in the laboratory
8	Possibility of using commercially available components	wish	Lower price
9	Simulation of drivability of wheelset	must be	Achieving drivability as on the railway
10	Evaluation of wear brake pairs	must be	Main results of measurements
11	Application of load cells, speed, temperature, ...	must be	Main results of measurements
12	Safety	wish	Covers, fencing
13	Other, not specified		

Tab. 1. Requirements for the function of the test brake bench

Unlike the existing flywheel test stand UIC, the new test bench will be operated on the principle of the adhesive and simulated drivability wheelset.

Preliminary structural design of the test bench is in Figure 2.
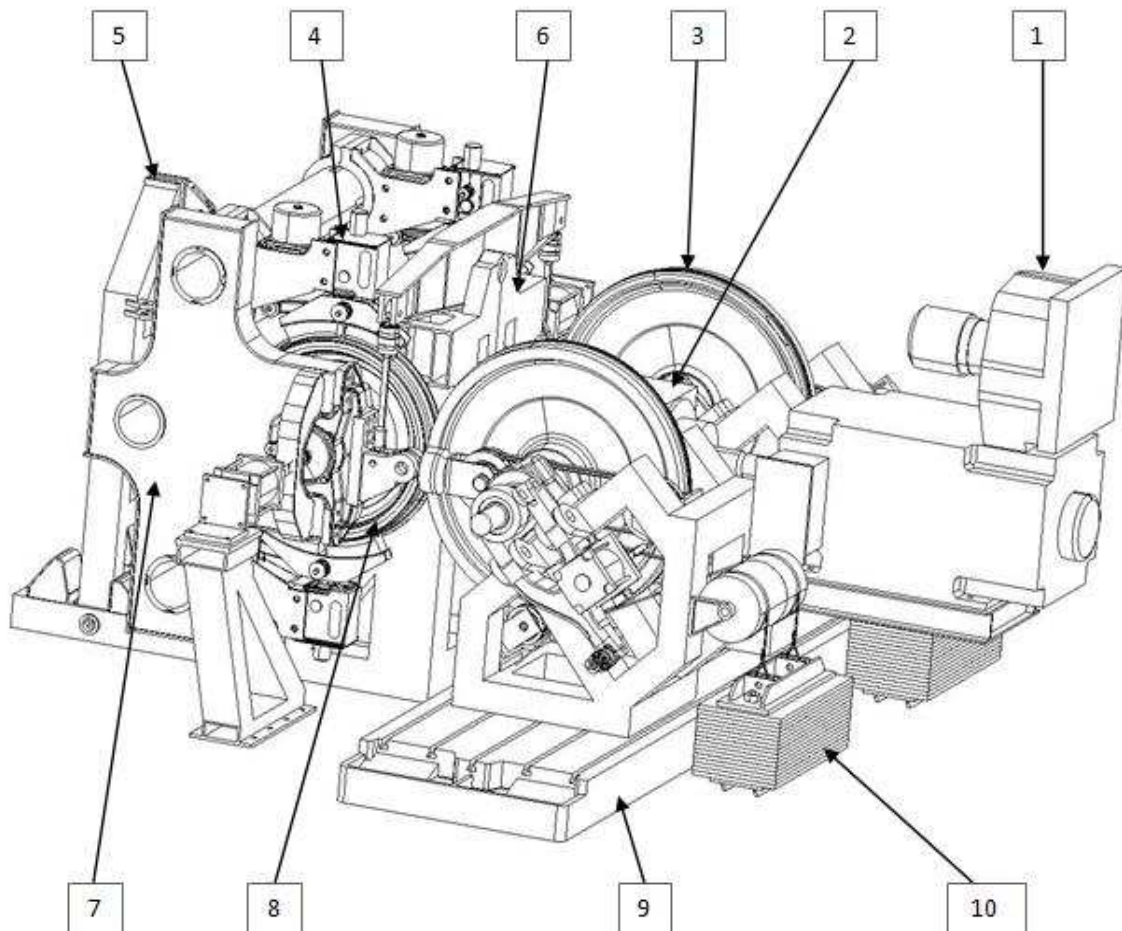
Fig. 2. Scheme of the brake test bench RAILBCOT (1 – electromotor, 2 – gearbox, 3 – rotating rail 4 – brake unit, 5 – rear hinge, 6 – front hinge, 7 – supporting frame, 8 – wheelset, 9 – base, 10 – weight unit)

Alongside design of conception is needed to resolve several of functional nodes, which are necessary for the simulated drivability of wheelset as on the railway.

Such nodes are:
– change of track gauge possibility,
– change of attack angle possibility,
– lateral forces loading solution,
– axle loading solution.

Electromotor (1) through gearbox (2), which has one input and three output shafts will transmit the torque and rotate the rotating rails (3). These ones are mounted in bearing housings which are connected with the frame. The supporting frame (7) will hang on two hinges. Rear hinge (5) is a simpler construction and serves to hold the support frame (7) in the set position. Four brake units (4) are attached to the support frame. Axle boxes are mounted on the wheelsets (8), which are attached with screws to the supporting frame. A pneumatic cylinder creates the necessary axial force. The front hinge (6) is attached with a tilting lever wheelset. By pull rod is connected with axle box - with a supporting frame. A force sensor is placed on pull rod which measures the longitudinal forces emerging during braking. The adapter is attached to the bearing box on which is a force sensor. That is associated with the transfer of rope. Vertical wheel force is inferred weights (10) and each wheel is loaded with one weights. For simulation the passing vehicle of arc are

rotating rails (3) moving off from each other for max. 16 mm. On this change it is used mechanism of transverse displacement a rotating rail, which enables a change gauge of track passing vehicles arc. The test bench is placed on two bases (9).

3. Conclusion

Tests on the brake bench are an integral part of research in the area of characteristics of friction materials. Test bench and tests on them give mainly qualitative comparative values. They have replaced expensive brake tests of whole wagons. This is the reason why it is given so much attention to these devices and to their construction accesses in more countries.

While proposed braking bench gets a final form, it will be necessary to implement many new proposals and modifications. Without using the CAD system and its optimization methods, it would be difficult and time - consuming sizing construction. It follows that deployment of computer technology in conjunction with CAD systems is in many sectors invaluable.

Acknowledgement

References

[1] IWNICKY, S. *Handbook of Railway Vehicle Dynamics*. CRC Press, Taylor&Francis Group, Boca Raton, 2006

[2] GERLICI, J. AND CO.: *RAILBCOT – RAIL Vehicles Brake COmponents Test Stand*, ITMS Code 26220220011. ITMS 26220220011, Project description. Žilina, 2009

[3] HAHN, H., SIEGL, G. *Simulation and experimentelle Verifikation des Rad/Schiene-Rollprüfstands*. Ingenieur-Archiv 57 (1987) 329-384, Springer-Verlag 1987.

[4] ALLOTTA, B. PUGI, L. MALVEZZI, M. BARTOLINI, F. CANGIOLI, F. *A scaled roller test rig for high-speed vehicles*. Vehicle System Dynamics, 48: 1, 3 — 18, DOI: 10.1080/00423111003663576.

[5] UIC. *UIC CODE 541-4 Brakes - Brakes with composite brake blocks – General conditions for certification of composite brake blocks*. UIC, Paris, 2007.

[6] ŘEZNÍČEK, R. CHUDÍK, S. LACK, T. *Test Stand KKVMZ in the International Approval Process*. Proceedings PRORAIL, Žilina, 1999

[7] JASCHINSKI, A., CHOLLET, H., IWNICKI, S. WICKENS, A., VON WÜRZEN, J. *The Application of Roller Rigs to Railway Vehicle Dynamics. Vehicle System Dynamics, 31*, Swets & Zeitlinger 1999

[8] DUKKIPATI, R. V. *Dynamics of a Wheelset on Roller Rig. Vehicle System Dynamics, 30*, Swets & Zeitlinger 1998

Computer Aided Engineering – Application of Finite Element Method in Gear Drive Design Process

[*]Rafał Gołębski

[*]Częstochowa University of Technology, Institute of Machines Technology and Production Automation, Częstochowa Al.Armii Krajowej 21, 42-200 Częstochowa, Poland, e-mail: rafal@itm.pcz.pl

Abstract. The paper presents the FEM model of spur gear with involute outline. 3D assembly drawing gear was built in the environment SolidEdge20. Finite Element Method calculations were made in Workbench12 ANSYS environment, using the module Static structural. Using the tool contact of Ansys 12 Workbench software mating area of gear elements has been obtained. Presented experiment provided us the opportunity to apply advanced computational techniques, FEM in the process of design of whole gear.

Keywords: Spur gear, finite element method, mating area.

1. Introduction

Properly designed and assembled gear should meet the essential criteria for the operation, which mainly include: high durability, steady movement of gear drive components, and low noise emission. In the context of the criteria mentioned above, is not without significance the analysis of mating area of cooperating gear elements. In practice, fairly common method of control is the analysis of mating area during the assembly process of whole gear. In conducting the measurement the surfaces of mating tooth were coated with paint and wheels were turned in the direction of their movement. We are able to observe the results mating areas in adhering to their tooth's surfaces. Analysis of mating area at the design stage of gear gives to the designer a many possibilities to influence to the design assumptions, dynamic modification and therefore their analysis of the different and questionable cases, which in practical verification would be very labour intensive and costly.

2. Gear model – CAD

The model assembly of the gear can be done by using ready-made libraries are available in CAD software, Autodesk Inventor or Solid Edge. Not without significance is selecting the appropriate gear tooth profile. By default, you can use predefined libraries Solid Edge we are dealing with an outline of involute teeth. In the case of significant load -carrying gear and working at high speeds with such a profile seems to be fully justified. In the case of not popular gear model, i.e. circular or cycloid outline it is necessary to manually build and create profile geometry of the wheels cooperating in accordance with the outline drawn. The inclusion in the model of the assembly to engage the correction in the case of Solid Edge requires the designer to redesign the entire model gears manually set the size and type of correction required. For Autodesk Inventor library of ready gear components have the option of placing on the modeling stage gear desired size correction, which in the case of typical design solutions significantly accelerates the work

3. Gear model – CAE

Environment Ansys 12 Workbench is a tool for the new generation, having an intuitive interface, CAD modeling, automatic meshing features, and quick access to modify the model parameters within a single application. The model assembly of the gearbox has been designed in an Solid Edge 20, has been subjected to analysis of helical involute tooth outline. To analyze mating area of gear was used the module Static Structural Analysis. Geometry and orientation of the model was added to the project with a *. IGES files, previously generated in the CAD program, while importing geometry all constraints and dependencies observed during the construction of the deposit model are transferred automatically, so any change and improvement can take place only in the original production environments file. Edit the file in the module "DesignModeler" will not be possible. To the simulation was used tool for analysis of solid bodies contact, - "contact tool".
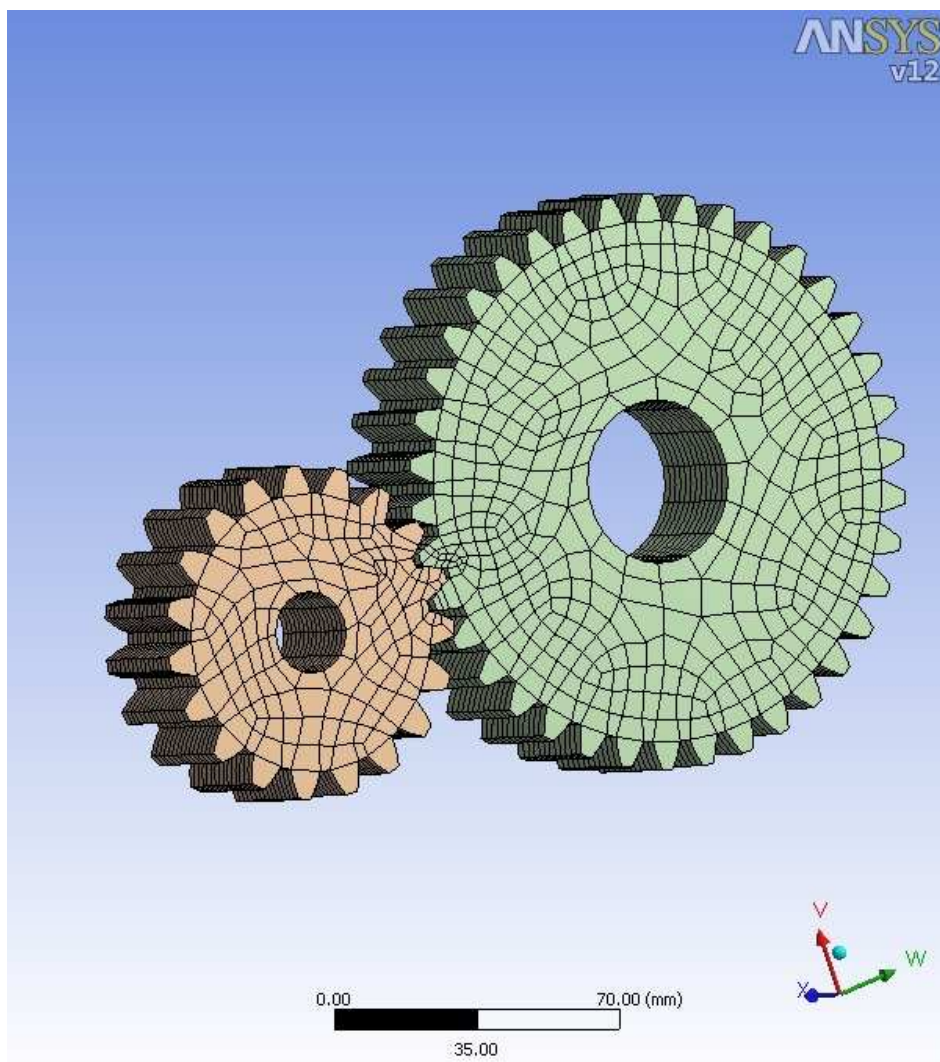
Fig. 1. FEM model of spur gear

To produce the form of pressure on contact surfaces is necessary to load the opposite wheel of torque. Torque can be applied on any surface of the gear, such as a cylindrical hole, or on the flank - Fig.1. Relevant in this case is to define additional local coordinate systems - the function "coordinate system" for the axis of rotation of both wheels, then a torque can be defined as a component for the specified axis coordinate system.

Finite element mesh was generated in the ANSYS Workbench environment, according to the size of the settings as default, also using the "tool contact sizing" was carried out density of the grid in the region of contact of mating surfaces - Fig. 1.

4. Solution

Analysis mating area of gear drive was carried out in the contact area between a pair of teeth from the external tooth contact through the buttresses point to the point of the internal tooth contact Mating area was received in the form of pressure distribution on contact surfaces of teeth. To the module design solutions it is to introduce components "contact tool" for each of gears K1 and K2, and for a common solution to the contact - having both geometries. In the components of "contact tool" project solutions, we can achieve results by adding a bookmark distribution of pressure, "pressure". Fig. 2. presents pressure distribution on the contact surface, shadow area depict proper mating area of gear drive.

Fig. 2. Correct mating area as a pressure distribution on the contact surface

4. Conclusions

Application of FEA in the design engineering allows quick verification of construction in the assumption project, which was to obtain experimental way are often impossible or very time-consuming and costly. For the analysis of mating area cooperating gear we are able to provide exact optimization of gear at the design stage, analysis can be subjected to unusual kinds of shapes of teeth, gears drive can be subjected to the correction at the same time observing the mating area of cooperating wheels

References

[1] OCHEDUSZKO K.*: Koła zębate TIII, Sprawdzanie*, WNT, Warszawa 1972

[2] STOLARSKI T., NAKASONE Y., YOSHIMOTO S., *Engineering analysis with Ansys software*, Elsevier Butterworth-Heinemann, Oxford 2006, UK.

Utilization of High Load Capacity Worm Gear Drive

[*]Rafał Gołębski, Piotr Paszta

*Częstochowa University of Technology, Institute of Machines Technology and Production Automation, Częstochowa Al.Armii Krajowej 21, 42-200 Częstochowa, Poland, e-mail: rafal@itm.pcz.pl, paszta@itm.pcz.pl

Abstract. The paper presents the analysis of utilization of high load capacity worm gear drive which was a component of excavator. The excavator, equipped with worm gear drive high capacity transmission was use as a model for analytical investigation. Calculation of durability of overlapping with largest influence parameters of overlapping in work was shown. Finally the calculation of efficiency of worm gear drive was made and in the graphs was presented in the function of influence of others parameters.

Keywords: worm gear drive, worm, worm wheel.

1. Introduction

Worm gear drives have very different uses, and can be found in many devices ranging from household appliances to complex industrial machinery. High-power transmissions are used as a component in the mechanism of driving of excavator. Mechanism of drive elements of excavators is equipped with worm gears of large sizes and strengths, which can carry working under variable load for many years. Worm gear has a compact design that the relatively small size allows you to realize significant ratios, allowing decreasing the weight of the machine. As you can see the designers have solved the issues of design and construction parameters matching worm gear drive, allowing implementing of movement of these huge machines a reliable manner as possible.

For the analysis of essential performance parameters of gear drive has been used as an example a worm gear drive – fig.1. with following parameters: rated power P = 200kW, axial module m = 20 mm, axis distance a = 510mm, gear ratio i = 14.

Fig. 1. High power transmission worm gear drive - motoreducer

2. Permissible load of worm gear drive

Worm gear with defined parameters and a specified dimensional accuracy of its elements - the worm and worm wheel, and correctly assembled can transmit the specified load, which quite often in the literature and industrial practice is referred to as the limit load gear [1]. At the limit load capacity and durability of the worm gear affects a very large number of factors and to clarify the boundaries of one or two factors on the robustness of the structure of worm gear drive would be abuse. Nevertheless, the thesis according to which the limiting load of gear drive may be the result of a single factor, is justified and is dictated by the needs of counteract to various forms of untimely wear.

Worm gear calculation tests are used to determine the safety factor and comparing it with the rate of acceptable factors. For this purpose is to determine the theoretical values of worm gear transmission efficiency, limit the time of utilization of worm gear or as a consequence of the duration of the reliability of the calculated in an amount of mating cycles of worm and worm wheel. In the operating conditions may occur quite often to premature wear of the worm gear teeth and actually tighten up their tooth will be determined the allowable operating time of transmission of whole worm gear. The experiment will determine the acceptable analytical lifetime of worm gear and the relationship effect on this parameter size and distance of the axis of worm and worm wheel. Calculation of the boundary of abrasive wear of teeth worm wheel also allows different empirical relationship:

$$S_{wm} = \frac{s \cdot \sigma_{hm} \cdot a \cdot N_L}{E_{max}} \qquad (1)$$

Where:
s – parameter of the slipping distance
σ_{hm} – average stress in the contact area
a – axis distance
N_L – number of cycles
E_{max} - reduced value of elastic modulus

Abrasive wear of the teeth calculated by dependence [1] will take place after a certain period of time, assuming that the working conditions of the transmission in no way deviate from the optimum there must be understood as proper lubrication, without overloading the transmission and with the correct assembly of gear drive components - worm and worm wheel. In the next stage of computation allowable work time of worm gear will be specified.

$$L_h = \frac{N_L \cdot i_{rz}}{60 \cdot n} \qquad (2)$$

N_L – number of cycles
i_{rz} – gear ratio
n – rotational speed of worm
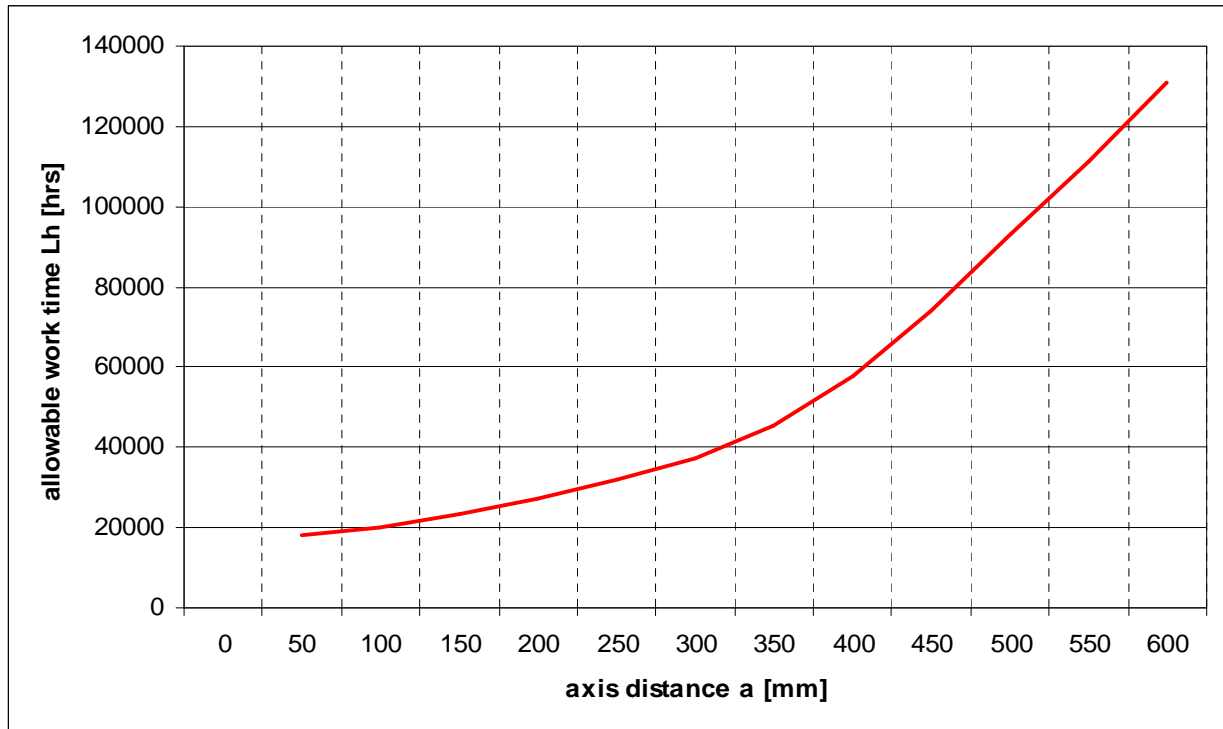
Fig. 2. Allowable work time of worm gear drive

Factor having the greatest impact on the value of the results of the calculations is the distance axis of worm and worm wheel – fig.2. For the gear with the axis distance a= 510 mm, allowable work time about 100 000 hours of continuous work has been calculated. This quantity is more than 3 times larger than in the case of standard extent size of gears – for example with axis distance a=150 mm.

3. Total ideal efficiency

The efficiency of the worm gear drive working as a reducer is the ratio of effective work derived by the worm gear shaft to work supplied to the shaft of the worm [1]. The loss of efficiency of worm gears mainly is associated with slipping and replacing the mechanical energy into heat but we should also take into account losses in the bearings, seals, and idle losses. The most important parameter determining the efficiency is the angle of height of the helix – fig.3. The formula for determining the total theoretical efficiency, with consideration of losses in the gearbox takes a form:

$$\eta_{ca^3} := \frac{P_{zn}}{P_{zn} + P_V}$$

(3)

Pzn – analytical efficiency without mechanical losses
Pv – loses factor (includes loses: thermal, frictional)
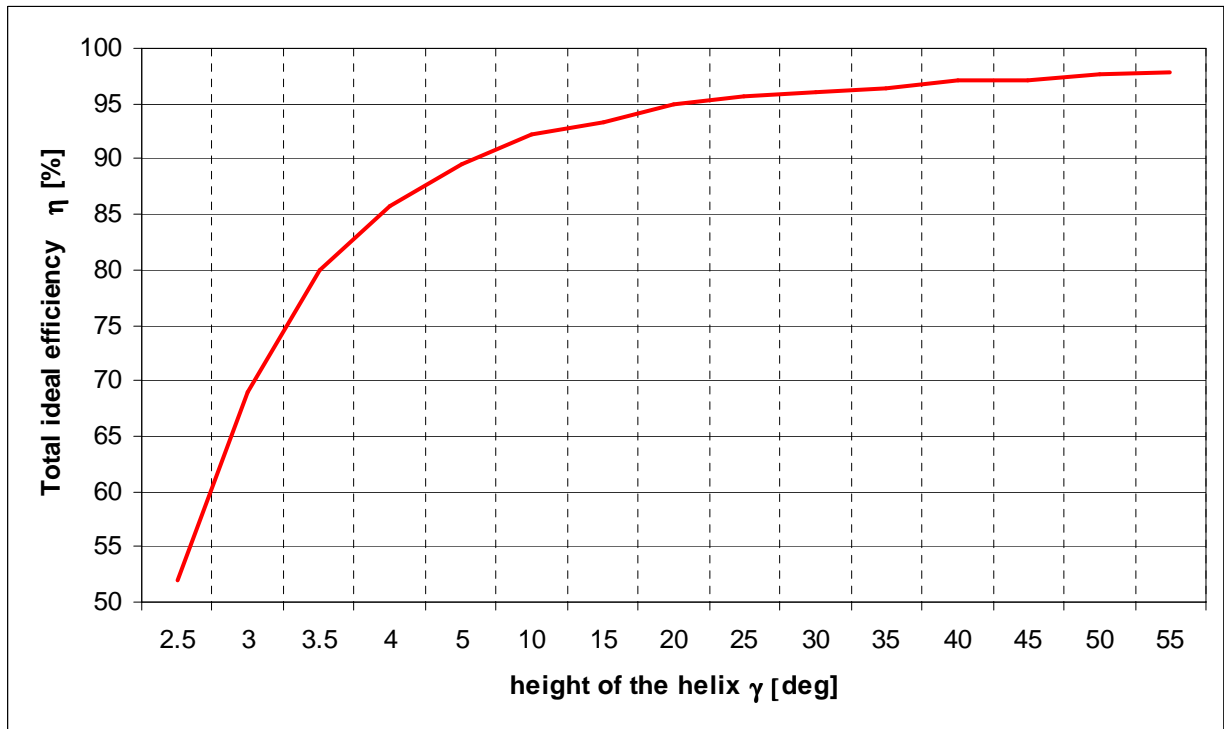
Fig. 3. Total efficiency of worm gear drive shown as a function of height of the helix.

4. Conclusions

To achieve high efficiency and reliability of work, the worm gear drive must be designed on the basis of computer aided calculation, this enables incorporate a complicated load distribution in gear drive, and we can include to calculations other important factors as a slip speed, and factor of definition of type of work – continuous or intermittent. In the case of very large drives evaluation and research are very difficult because these gears often work the intermittent cycle and with very high and variable worm wheel burdens, which determination in the practice are not possible. Opportunity to compare the actual state of the mathematical description allows refining applied mathematical relationships and in the future may enable the creation of virtual gear drives with completely predictable parameters from the utilization aspect of work.

References

[1] MARCINIAK M.: *Obciążalność zazębienia przekładni ślimakowych.* Wydawnictwo Politechniki Łódzkiej, Łódź 2004 r.
[2] OCHĘDUSZKO K.*: Koła zębate, sprawdzanie*. Wydawnictwa Naukowo- Techniczne, Warszawa 1972 r.

Experimental Production of Wood Pellets with Additives

[*]Michal Holubčík, Radovan Nosek, Jozef Jandačka

[*]University of Zilina, Faculty of Mechanical Engineering, Department of power engineering, Univerzitna 8215/1, 01026 Žilina, Slovakia, {michal.holubcik, radovan.nosek, jozef.jandacka}@fstroj.uniza.sk

Abstract: In this work are described the possibilities for improving efficiency of wood pellets production. The introductory part shortly analyze the properties of wood pellets, combustion and production of pollutants when combusted it. The production process of wood pellets is simply described in the next part. The main task of this work is to introduce efficiency pelleting lines and cost reduction of the wood pellets production as fuel with a focus on the effects of adding additives. The results of experimental measurements and properties of wood pellets with different additives are presented in the final part.

Keywords: wood pellets, additives, efficiency, pellet mill

1. Introduction

The aim of this work is to increase production efficiency and properties of wood pellets by addition of additives. This paper contains information about wood pellets properties, the process of manufacturing wood pellets, use of equipment with a focus on the principle of the individual species pellet mills. It is pointed out, what happens during the pelleting process and problems that may occur in this process. The main objective is to find out the influence of additives to the efficiency of production and properties of wood pellets.

2. Production of wood pellets

Wood pellets are producing from by – product of wood processing – wood sawdust. Wood pellets are made by pressing wood materials at high pressure and temperature, i.e. pelleting process. Production of wood pellets has following procedure (see Fig. 1.):

- Pretreatment of raw material (separation (heavy particle and magnetic separator), crushing)
- Drying
- Pelleting
- Cooling
- Storage and transporting
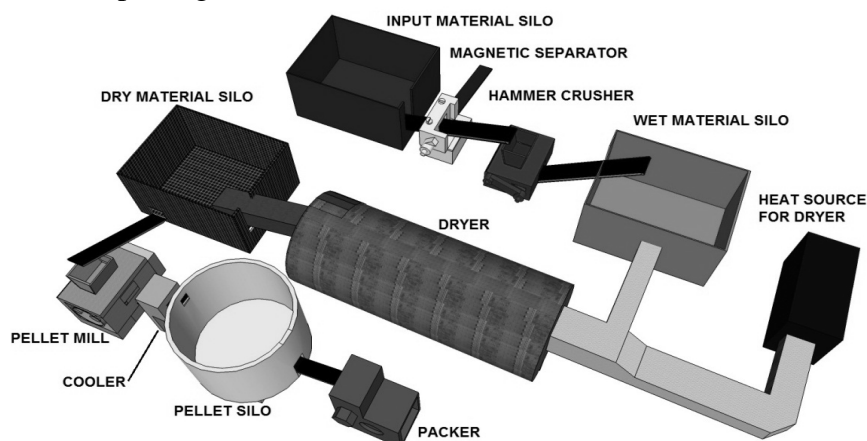
Fig. 1. Scheme of pelletizing line

2.1. Pelleting

Pelleting is the most important operation, which takes place in the pellet mills. In this process is done the compaction of raw wood material itself. Wood is pushed through the holes and this increases the temperature in the facility for 90-110 °C. At this temperature will start to release binder contained in the wood (lignin), which holds pellet in due form.

3. Experimental production of wood pellets with the addition of additives

3.1. Used additives

The fuels produced from biomass must meet certain energy, environmental and economic criteria. The forthcoming European Union standard would allow the content of additives up to 5 percent. Manufacturers produce wood pellets without any additives according to established standards. Disuse of additives is mainly due to the fact that this area has not been adequately studied and it is therefore necessary to carry out such experiments. The effect of specific additives in the wood pellets before the experiment can only be assumed. Additives affect the pelleting process, the properties of pellets and combustion of wood pellets.

The additives are added to a substance in order to improve some of its properties. Usually in practice happens that with the improving characteristics occur new deficiencies. It is necessary to analyze effects of additives on pellets properties for each experiment. In the experiments were used following types of additives:

Motor oil - is suitable for lubrication, sealing, protecting and sediment from corrosion, easy to mix with fuel, but especially given the high burn hydrogen production with the lowest emissions. It is expected that the use of oil will reduce friction when pushing material through the holes in the matrix, which would reduce the electric power of pellet mill and wear of functional components. Reducing energy intensity pellet mill will increase the efficiency of production of wood pellets.

Vegetable oil - this oil should have the same effects as motor oil. Using vegetable oil is expected to increase the calorific value of pellets, as the low calorific value of the oil is higher (37.1 MJ.kg-1), compared to the value of clean wood pellets.

Cornstarch - the use of this additive should increase resistance to abrasion of pellets; pellets should have a smoother surface, better hardness and thus the overall quality.

Dolomite - the addition of dolomite to pelleting process should reduce the production of SO2 during the combustion of wood pellets.

Sodium carbonate - is used as a means of creating an alkaline environment.

Urea - it is expected to reduce the low calorific value and an increase in density, marked change in moisture content and strength of wood pellets is not expected.

In this work were produced wood pellets with varying amount of additives in comparison with pellets free of additive (see Table 1).

Pellets with additives	Amount of additives [%]
Wood pellets - Reference sample	Without additives
Motor oil	0,5 ; 1
Vegetable oil	0,5 ; 2 ; 5
Cornstarch	0,5 ; 1 ; 2
Dolomite	0,5 ; 1 ; 2
Sodium carbonate	0,5 ; 1
Urea	0,5 ; 1

Tab. 1. Amount of used additives for production of wood pellets

3.2. Experimental production

Each material has different qualities and characteristics. Therefore each material will behave differently in the pellet mill based on its moisture, density and binding qualities. Below is what a material should behave like, and what to target for. If the raw material has the correct qualities for making a pellet, you should see the following things happen (see Fig. 2.).

A. The material first enters the pellet mill and comes into contact with the pressing roller.
B. Some of the material will be compressed under the roller through the die holes.
C. Represents the material carpet that lies between the die and pressing roller. As more material is added to the pellet mill the pressing roller adds this to the carpet. The roller therefore compresses the bottom of the carpet through the die.
D. Represents the compression of the material through the die. If the material has the correct qualities heat and pressure will be produced due to friction, as the material is compressed through the die.
E. With sufficient friction, heat and pressure a shiny dense pellet will emerge. Once this pellet cools it will dry and become hard, this is then ready for use.
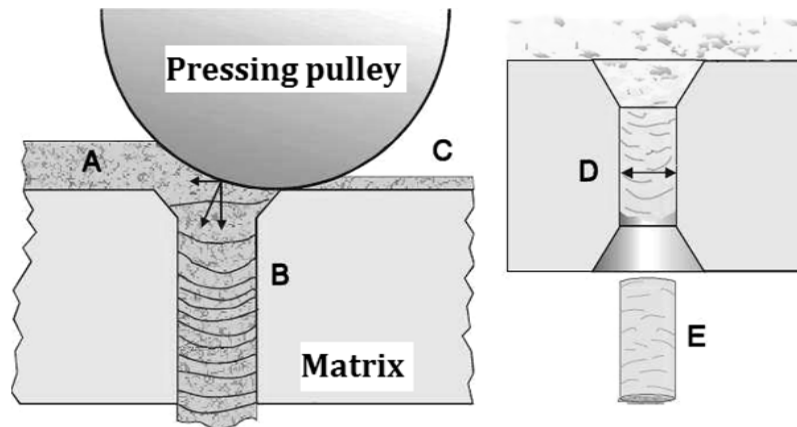
Fig. 2. Pellet machine process with the correct properties starting material (PELHEAT)

3.3. Production procedure

Input material was dry wood shavings from pine wood, supplied by an external company. In tested material was found to be a low moisture content (8-9%). That moisture of input material is inadequate and needed to be increased to about 10-20%. Experiments revealed that the optimum moisture content of sawdust is 15-16%. To achieve optimum moisture content of material was necessary to add the right amount of moisture. Therefore, for 1 kg of dry sawdust was added approximately 60 to 70 grams of water.

Fig. 3. Experimental pellet mill

Subsequently, the additive was mixed with sawdust, in order to achieve desired amount of raw input material. Then the sawdust was mixed with additive to the nearest 0.1 g, in order to achieve desired amount of raw input material. Thus prepared a total of 7 samples with additive were further pressed to pellets in the pellet mill (see Fig. 3.).

4. Analysis of results

4.1. Effect of additives on the input power of pellet mill

The input power of engine is an important factor influencing the energy intensity pelletizing lines. The additives affect the friction generated in the matrix of pellet mill, thereby is changing the input power of engine. Effect of additives on the input power is shown in the table 2.

Sample	Input power [W]
Motor oil	3792
Vegetable oil	3830
Dolomite	3830
Cornstarch	3868
Reference sample	3907
Sodium carbonate	4060
Urea	4098

Tab. 2. Effect of additives on the input power

The lowest input power has been achieved in the case of pellets with motor oil. Significant increase of input power and friction in the matrix was found in the production of wood pellets with the addition of urea and sodium carbonate. Presumption of reducing input power by using cornstarch have not been found, this value is slightly increased.

4.2. Effect of additives on the pellets proporties

To determine the effect of additives on properties of wood pellets are necessary experimental measurements. Experimentally observed properties are moisture content, density, bulk density, lower calorific value, quality and lower flow temperature of wood pellets.

5. Conclusion

More test and experiments are necessary in order to improve parameters of wood pellets. The measured results indicate that pellets with sodium carbonate have higher flow temperature in comparison with reference sample. This can lead to reduction of slagging and fouling in the plant. In the rest of the samples were measured lower flow temperatures in comparison with reference sample.

Acknowledgement

References

[1] ALAKANGAS, E. & PAJU, P. (2002). *Wood pellets in Finland – technology, economy, and market.* Technical research centre of Finland Jyväskyla.

[2] DZURENDA L.: *Combustion of wood and bark* I.-2005, Editorship TU in Zvolen, Slovakia, ISBN 80-228-1555-1

[3] JANDACKA, J., & MALCHO, M. (2007). *Biomass as energy source*. Zilina, Slovakia: Editorship GEORG.

[4] PELHEAT – *Biomass Pellet Production Guide* (http://www.pelheat.com)

[5] ZIDEK, L. (2006). *Vykurovanie drevnymi peletami*, BIOMASA, zdruzenie pravnickych osob, Povazská Bystrica.

Testing of Railway Brake Blocks

*Jozef Hriňák, Rudolf Řezníček, Marek Fusatý

*University of Žilina, Faculty of Mechanical Engineering, Department of Transport and Handling Machines, Univerzitná 1, 010 26 Žilina, Slovakia, {jozef.hrinak, rudolf.reznicek, marek.fusaty}@fstroj.uniza.sk

Abstract. This paper describes different types of railway brake blocks and problems that may arise at their homologation and implementation into the service. It points out on the possibility of change of cast iron braking blocks for the composite blocks, to reduce noise level produced mainly during the braking of freight wagons in rail transport. Next, the paper describes a flywheel brake bench and presents some results obtained during testing of various brake blocks.

Keywords: Brake blocks, brake test bench, coefficient of friction, composite materials.

1. Introduction

Reducing and suppression of noise in railway transport is still very important subject. These problems are solved by all areas which are active in railway transport. Whether it is construction and designing new railway lines where the noise is increasing in an existing environment, or a reconstruction and renovation of present railway lines which are not oriented only to reaching higher speeds of trains but also to reduce a level of noise in railway transport. The most effective way to reduce noise in railway transport is reducing noise directly on a source. Researches showed that the noise is not created only at braking but also at a movement of a train. Noise during the movement is created by roughness and unevenness of a wheel and a rail. Unevenness on the tread of wheel is created mainly by deposit from cast iron brake blocks. During intense breaking, material of the brake block is melted and attached on the tread of the wheel.

Noise reducing during braking of goods wagons is possible only by replacing cast iron brake blocks for composite brake blocks. This solution is not so easy, because it is necessary to solve some technical problems in this area.

- Alternative product must guarantee desired friction coefficient and keep specified braking distances as cast iron brake blocks.
- Train set that is braking with different braking blocks must not generate disallowed pressures in direction of the movement or other effects which are undesired during the braking.
- Because by braking plenty of heat is created and composite brake blocks are not able to lead away so much heat as cast iron brake blocks, the wheels are more heat stressed.
- Alternative product must be economically attractive and operating costs must not overrun operating expenses of cast iron brake blocks.

2. Present state

Brake blocks which can replace iron cast brake blocks are divided into the three categories according to value of the friction coefficient (K, L, LL). Brake blocks from the category K have the higher friction coefficient that is why application of these brake blocks is limited only for new or reconstructed wagons with redesigned braking system. Brake blocks from the category L have the lower friction coefficient as from the category K but the friction coefficient is higher compared with the friction coefficient of cast iron brake blocks. That is the reason, which does not allow replacing cast iron brake blocks throughout range. Equivalent replace for iron cast brake blocks are brake

blocks from the category LL. These brake blocks have the similar friction coefficient as cast iron brake blocks.

Composite brake blocks are compounding of a polymeric matrix and fillers. Fillers are mainly metallic and oxide dusts. Fillers are added in order to increase heat conductivity of brake blocks. These types of brake blocks are divided by compound and thermal treatment into organic and metal-ceramic (sintered with the matrix of copper or ferrum).

Before using of a new type of composite brake blocks, the approval process according to the norm UIC 541-4 have to be performed. The basic requirements for the geometric dimensions, mechanical, physical and chemical properties as well as requirements for the coefficients of friction are prescribed in this norm. There is also described the procedure of tests, which consists of two parts. The tests start by testing of brake blocks on with UIC approved brake bench accordance with testing programs defined in this norm. The second part of the tests runs on vehicles during 12 months long continuous railway operation. It is checked in assessing long-term tests:
- the wear of brake blocks and wheels,
- the emergence of metallic inclusions in the brake blocks,
- the possible deposit of organic composite blocks on the wheels, which can reduce the electrical conductivity between the wheel tread and rail. [4]

3. Specification of brake bench test results

In following text composition of UIC railway flywheel brake bench placed in Department of transport and handling machines (KDMT), Faculty of Mechanical Engineering, is described.
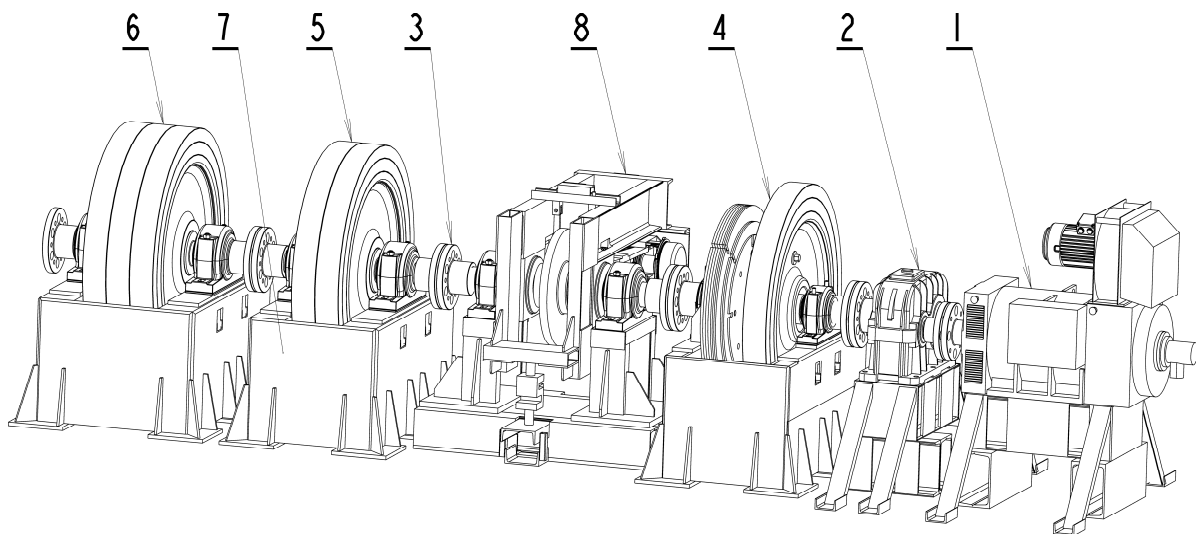
Fig. 1. The scheme of UIC flywheel test brake bench of KDMT

Pos. 1   Elektromotor (P = 265 kW, P_{max} = 400 kW, n = 3200 1/min)

Pos. 2   Gearbox (gearing ratio i = 1,5 , resp. i = 1,72, i = 2,5 and i = 4)

Pos. 3   Clutch BKN

Pos. 4   Flywheel 400 kgm^2 = 280 + 120 kgm^2 (2x5+3x10+4x15) (Base inertia mass 20 kgm^2)

Pos. 5   Flywheel 600 kgm^2

Pos. 6   Flywheel 900 kgm^2

Pos. 7   Base frame

Pos. 8   Disc brake or wheel brake

This brake bench is approved by UIC since the year 2000. It serves for the homologation tests, certification of the properties of brake blocks and brake pads of disc brakes and for measurement of real friction coefficients and heat stress of individual parts of railway brake. Various other tests are also made by customer requirements. In following figures 2 – 3 values of mean friction coefficients

for brake blocks COSID 810 and JURID 777 measured on UIC brake bench of KDMT are described.
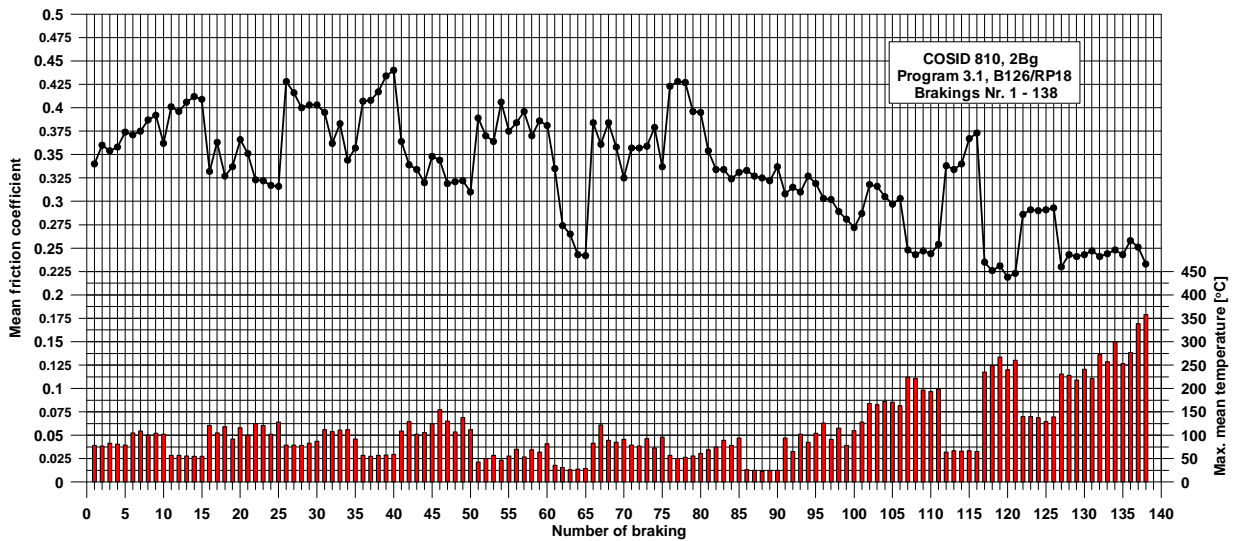
Fig. 2. Values of mean friction coefficients for brake blocks COSID 810 of type K [1]
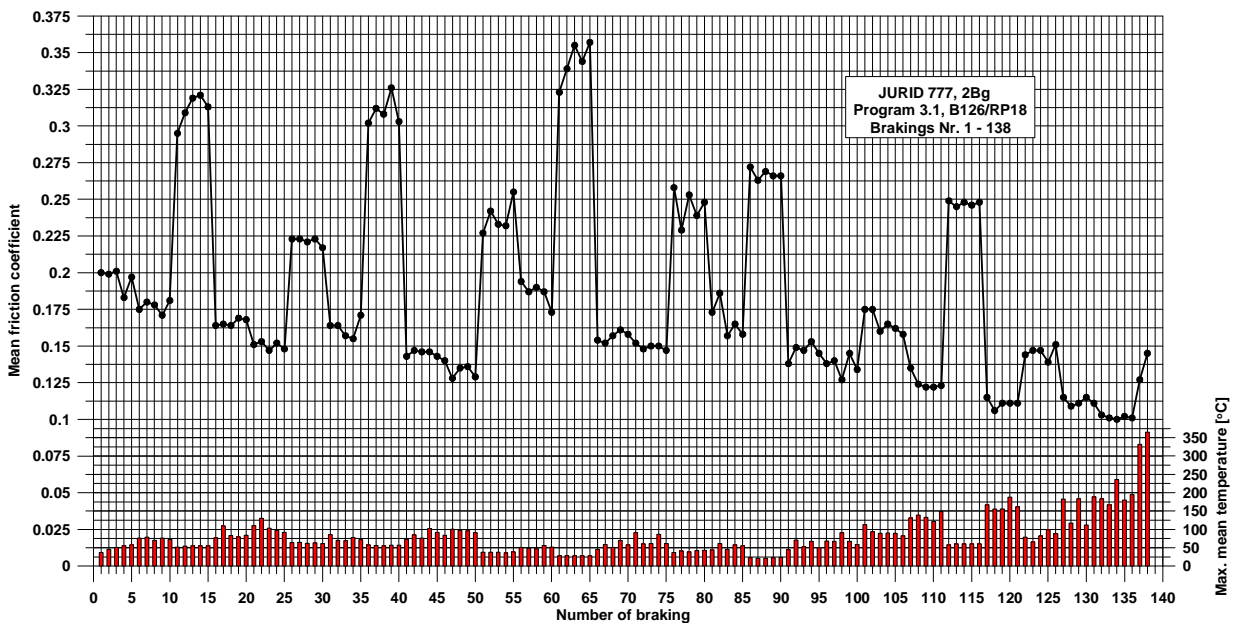
Fig. 3. Values of mean friction coefficients for brake blocks JURID 777 of type LL [2]

4. Conclusion

The graphs show that the middle friction coefficient is more stable at the brake blocks type K than at the type LL. Its value is not so velocity and contact force dependent as it is seen on pictures 2 and 3, for example by braking No.15 an 16. Both brakings are from the velocity of 120 km/h and the difference is only in contact force. The contact force of 8 kN is for the braking No.15 and the contact force of 19 kN is for the braking No. 16. The friction coefficient differences in this two cases of braking are for the brake blocks type K approximately 0,078 and for the blocks type LL circa 0,15.

The maximum mean temperature obtained from three thermocouples, which were evenly distributed 9mm under the wheel tread were also monitored at the tests. This value shows with what temperature the rail wheel is stressed, because of the comparatively smaller heat removal due to lower thermal conduction of composite materials at braking comparison to cast iron blocks.

References

[1] ŘEZNÍČEK, R. *ÜBERPRÜFUNG DES BREMSPRÜFSTANDES VON ZSSK NACH DEM BERICHT B1126/RP 18 MIT DER BREMSSOHLE COSID 810*. Berichtnummer KDMT : P-102-0004a/09, October 2009.

[2] ŘEZNÍČEK, R. *ÜBERPRÜFUNG DES BREMSPRÜFSTANDES VON ZSSK NACH DEM BERICHT B 126/RP 18 MIT DER BREMSSOHLE JURID 777*. Berichtnummer KDMT : P-102-0004b/09, October 2009

[3] *UIC Code 541-4, OR, Brakes – Brakes with composite brake blocks – General condition for certification of composite brake blocks*, 4th edition , January 2010, UIC Paris

[4] HRIŇÁK, J., ŘEZNIČEK, R., KALINČÁK, D. *Operation and verification of composite brakes BLOCKS*. VII International Scientific and Practical Conference of Students and young scientists "Trans-Mech-Art-Chem", Moscow, May 2010

The Theoretical Background of the New Method for Adaptive Identification of Random Excited Structures

[*]Veronika Chladná, Bohuš Leitner

[*]University of Žilina, Faculty of Special Engineering, Department of Technical Sciences and Informatics, 1.mája 32, 01026 Žilina, Slovakia, {Veronika.Chladna, Bohus.Leitner}@fsi.uniza.sk

Abstract. The paper deals with the possibilities of using mathematical apparatus of a stochastic time series for stochastic systems identification and modelling, especially mechanical ones. Its purpose is to briefly characterize fundamental terms and equations of mathematical apparatus of time series and to show some possibilities of developed identification strategy for identification of two simple model structures - 3 DOF system and very simple beam structure.

Keywords: Time Series, Autoregressive Models, Algorithm of Adaptive Identification, Stochastically Loaded Parts.

1. Introduction

There are two commonly used methods for mechanical dynamic systems identification. The first of them, based on the drawing of structure, is the dynamic version of Finite Element Method. The second one is an experimental method based on determination of transmission response and mode shapes of structure using digital Fourier analyzer..

2. Mathematical Formulation of Problem and Its Background

By the experimental identification by means of digital Fourier analyzer there are two essential steps involved in the determination of the modal parameters and mode shapes.

The starting point of the analysis technique relies on the estimation of spectra and subsequent determination of corresponding transfer functions. In the second step the measured transfer functions are used to extract the necessary modal information. Anticipating mostly the stochastic nature of mechanical dynamic system's excitation and response, time series methods and Data Dependent Systems (DDS) [1] approach seems to be very suitable and effective in the area of dynamic modelling too.

There are two theoretical areas concerning the above mentioned problems. The first is a classic approach to the vibrations of mechanical dynamic systems. It is well known, that in case of n-degree of freedom systems they are represented by system of ordinary differential equations of second order in matrix form as:

$$\mathbf{M}\ddot{\mathbf{x}} + \mathbf{B}\dot{\mathbf{x}} + \mathbf{K}\mathbf{x} = \mathbf{F}(t) \qquad (1)$$

where $\mathbf{M}$, $\mathbf{B}$ and $\mathbf{K}$ are $\underline{n}$ x $\underline{n}$ mass, damping and stiffness matrices, $\ddot{\mathbf{x}}, \dot{\mathbf{x}}, \mathbf{x}$ and $\mathbf{F}(t)$ n–dimensional column vectors of accelerations, velocities, displacements and force respectively. For the type of solution of this system are essential the eigen-values of left-side of matrix equation, which are usually, obtained as complex numbers. The real parts of them have physical meaning as damping ratios and imaginary parts are natural frequencies.

The second theoretical area of theme is theory of stochastic processes. It was shown in [1], that any continuous system could be represented (in a scalar case) as differential equation in form [1, 2]

$$\left(D^n + \alpha_{n-1}D^{n-1} + \alpha_{n-2}D^{n-2} + ... + \alpha_1 D^1 + \alpha_0\right). X(t) =$$
$$= \left(\beta_m D^m + \beta_{m-1}D^{m-1} + ... + \beta_1 D^1\right). Z(t) \qquad (2)$$

for which holds $E[Z(t)] = 0$ and $E[Z(t).Z(t-n)] = \delta(n).\sigma_Z$, where $\underline{n}$, $\underline{m}$ indicate the order of the model, $D = d/dt$ is the differential operator, $Z(t)$ is white noise, E denotes the expectation operator, $\delta(n)$ is the Diracs delta function and α's and β's are model parameters.

When such system is sampled at uniform interval Δt, differential equation (2) becomes a difference equation

$$X_t - a_1.X_{t-1} - a_2.X_{t-2} - ... - a_n.X_{t-n} = \varepsilon_t - b_1.\varepsilon_{t-1} - ... - b_{n-1}.\varepsilon_{t-n+1} \qquad (3)$$

for which holds $E(\varepsilon_t) = 0$ and $E(\varepsilon_t.\varepsilon_{t-n}) = \delta_k.\sigma_e^2$. Values X_t, X_{t-1}, X_{t-2}, ... are values of process, a's and b's are parameters of the model, ε_t, ε_{t-1}, ε_{t-2}, ..., ε_{t-n+1} are residuals, E denotes the expectation operator and δ_k is Kronecker delta function,. Such a model is called *Autoregressive Moving Average* of order (n, n-1) – ARMA (n,n-1).

It is obvious that parameters of continuous and discrete model of the same process must be functionally related. The simplest way to express this relationship is by using roots μ_i and λ_i of characteristic equations of formula (2) or (3). The relationships then takes form as

$$\lambda_i = e^{\mu_i \Delta t} \quad \text{or} \quad \mu_i = \frac{1}{\Delta t} \ln \lambda_i \qquad (4)$$

In case of multivariate systems (mechanical dynamic systems) the **Vector Autoregressive Moving Average – VARMA model** is obtained in form [3]:

$$\mathbf{A_0}.\mathbf{X_t} - \mathbf{A_1}.\mathbf{X_{t-1}} - ... - \mathbf{A_n}.\mathbf{X_{t-n}} = \boldsymbol{\varepsilon_t} - \mathbf{D_1}.\boldsymbol{\varepsilon_{t-1}} - ... - \mathbf{D_{n-1}}.\boldsymbol{\varepsilon_{t-1}} \qquad (5)$$

respectively in form

$$(\mathbf{A_0} - \mathbf{A_1}.\mathbf{B}^1 - \mathbf{A_2}.\mathbf{B}^2 - ... - \mathbf{A_n}.\mathbf{B}^n).\mathbf{X_t} =$$
$$= (1 - \mathbf{D_1}.\mathbf{B}^1 - \mathbf{D_2}.\mathbf{B}^2 - ... - \mathbf{D_{n-1}}.\mathbf{B}^{n-1}).\boldsymbol{\varepsilon_t}$$

which can fully express the relationships in structure during its vibrations and where $\mathbf{X_t}$ and $\boldsymbol{\varepsilon_t}$ are vectors of measurements and white noise series, $\mathbf{A_i}$ and $\mathbf{D_i}$ are matrices of system parameters, $\mathbf{B}$ is vector of back shift operators, $\boldsymbol{\sigma_\varepsilon^2}$ is matrix of dispersion and reciprocal correlation's and δ_k is Kronecker delta function. If one analyses a mechanical dynamic system with a numerical technique and its vibrations and exciting forces measure in uniform sampling intervals Δt, it is possible to develop discrete models to describe the relationship between output (vibration) and input (exciting forces) after Fig. 1.
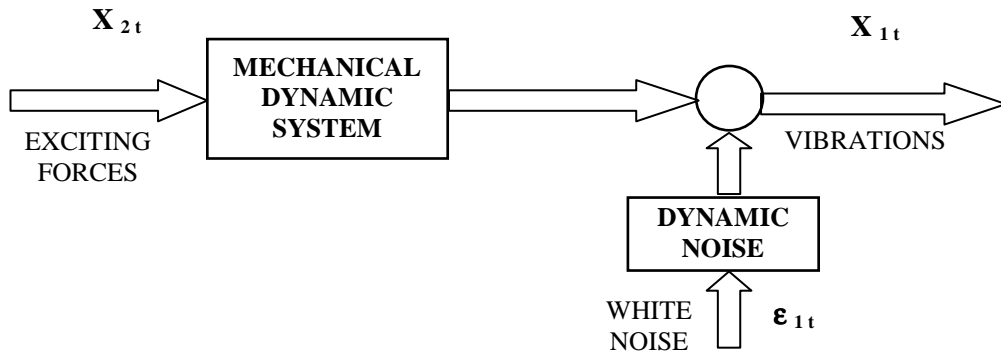
Fig. 1. Block scheme of mechanical system dynamics

Dynamics of the mechanical system and dynamics of noise is represented by a discrete transfer function. Supposing non-existence of feed back between vibrations of structure can be expressed in its excitation (which hold for structures tests) one gets a resulting model of structure dynamics in form [3]

$$\left(1 - a_{111}.B - a_{112}.B^2 - ... - a_{11n}.B^n \right).X_{1t} = \left(a_{120} + a_{121}.B + ... + a_{12n}.B^n \right).$$
$$.X_{2t} + \left(1 - b_{111}.B - b_{112}.B^2 - ... - b_{11(n-1)}.B^{(n-1)} \right).\varepsilon_{1t} \quad (6)$$

where attached assumptions shown in formula (5).

3. The Results of Identification for Two Simple Models

Procedure of statistically adequate models is getting concentrated in principle of output signals substituting (using non-linear least square method) with models of gradually increasing order until the decreased sum of squares becomes statistically non-significant on a chosen level of significance. Physical meaning of such a procedure is in that we are trying to substitute the system with a model with the lowest number of statistically significant modes of vibrations [4].

During this procedure, each increase of model order by two introduces (a further degree of freedom). If its contribution in not significant, the former model is taken as statistically adequate. In detail is involved strategy described in [2]. The theoretically correct approach mentioned in [1] and fully developed in [2].

As the examples of this procedure are the results of identification of two simple models – 3 DOF system (Fig. 2, Tab. 1, Tab. 2) and very simple beam structure (Fig. 3, Tab. 3).
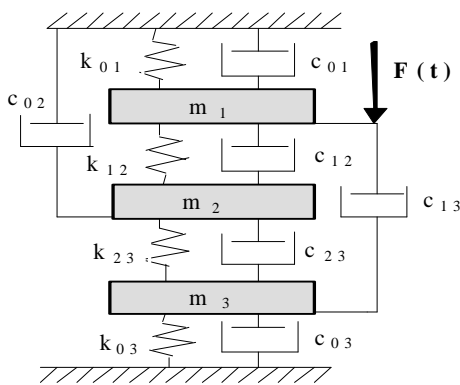
Fig. 2. Three Degrees of Freedom System   **Fig. 3.** FEM Model (Beam Elements)
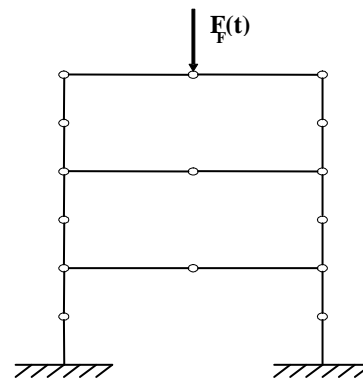
X	A1	A2	A3	A4	A5	A6
X1t	1.5820	-2.8093	2.5325	-2.5329	1.2516	-0.7089
X2t	1.3915	-2.4370	2.0704	-2.1175	-0.9362	-0.5819
X3t	1.5859	-2.8081	2.4854	-2.4907	1.2183	-0.7271

Tab. 1. Summary of Identified Parameters of ARMA model

		1st Mode		2nd Mode		3rd Mode	
		n_1(Hz)	1	n_2(Hz)	2	n_3(Hz)	3
ARMA	X_{1t}	1.2958	0.04701	1.9647	0.06908	2.7945	0.02754
	X_{2t}	1.2926	0.03468	2.1071	0.13760	2.8203	0.03408
	X_{3t}	1.2941	0.03069	1.9788	0.04885	2.8152	0.04163
Real values		1.2926	0.05289	2.0621	0.06664	2.8297	0.05945

Tab. 2. Summary of Identified Parameters of 3 DOF system

	1st Mode	2nd Mode	3rd Mode	4th Mode	5th Mode	6th Mode
FEM	8.406	25.873	42.439	103.935	126.626	126.626
ARMA	8.523	26.037	42.238	Non-sign.	Non-sign.	Non-sign.

Tab. 3. Natural Frequencies of Beam Structure

Above-mentioned procedure of identification using non-linear least square method and F-test of statistical adequacy is theoretically correct but very tedious and slow, therefore not suitable for on-line identification. For this purpose a new algorithm based on theory of adaptive and learning systems was developed and successfully tested in [2].

Once having the ARMA parameters of dynamic model determined, the procedure of dynamic performance of structure simulation is very simple. One has to start with generation of random residual εt, which are supposed to be normally distributed with zero mean and $\sigma\varepsilon$ determined from residual sum of squares of the model. The step-wise procedure looks like.

1.	Generate ε_1,	$X_1 = \varepsilon_1$,
2.	Generate ε_2,	$X_2 = a_1.X_1 + \varepsilon_2 - b_1. \varepsilon_2$,
3.	Generate ε_3,	$X_3 = a_1.X_2 + a_2.X_1 + \varepsilon_3 - b_1. \varepsilon_2 - b_2. \varepsilon_1$,
....	....	....
(n+1)	Generate ε_{n+1},	$X_{n+1} = a_1. X_n + a_2. X_{n-1} +...+ a_n. X_1 + \varepsilon_{n+1} - b_1. \varepsilon_n -...- b_{n-1}. \varepsilon_2$
(k>n+1)	Generate ε_k,	$X_k = a_1.X_{k-1} + a_2.X_{k-2} +...+ a_n.X_{k-n} + \varepsilon_k - b_1. \varepsilon_{k-1} -...- b_{k-1}. \varepsilon_{k-n+1}$

The way of simulation of vector (multivariate) system is more complex but essentially the same [2].

4. Conclusion

It introduces problems were proposed and verified in a frame of grant research *VEGA #9/0430/09 named „Stochastic Methods of Identification of Mechanical Structures Dynamic Systems"* where some possible applications of the proposed identification procedure were investigated. Advantage of ARMA models utilization is in fact that their parameters can one obtains directly from adequate models without necessity of transfer function determination.

Further, any subjective judgment is eliminated because the tests of statistical adequacy are strictly defined. Results of further problems using proposed procedure by dynamic analysis and identification of modal characteristics of mechanical systems showed a relatively good agreement between theoretical and identified values.

From presented facts one can develop that above shown assumptions and theoretical starting points are correct and developed procedure can reduce number of calculation in an expressive way and improve efficiency of mechanical structures dynamic calculation.

References

[1] MÁCA, J. *Identifikácia a modelovanie dynamických systémov*. [Monograph]. Military faculty, University of transport and communications, Žilina 1991

[2] LEITNER, B., URÍČEK, J. *A Method for Adaptive Identification of Stochastically Loaded parts of Mechanical Systems*. In: Proceedings of the 3.rd international multi-conference on engineering and technological innovation IMETI 2010. Orlando, Florida, USA: Vol. II., p. 174-179. ISBN 978-1-936338-03-0.

[3] LEITNER, B. *A new approach to identification and modelling of machines dynamic systems behaviour*. In: Proceedings of the 14th international conference Transport means 2010. Kaunas University of Technology, Kaunas, Lithuania. 2010. p. 17-20, ISSN 1822-296X.

[4] Michaelides P. G., FASSOIS, S. D. *Stochastic Identification of Uncertain Structural Dynamics via a Random Coefficient Model Approach*. Proceedings of the USD 2010 International Conference on Uncertainty in Structural Dynamics, pp. 5305-5318, Leuven, Belgium, 2010.

Thermal Conductivity of Rocks and Geothermal Heat

[*]Michaela Chovancová, Milan Malcho

[*]University of Žilina, Faculty of Mechanical Engineering, Department of Power Engineering, Univerzitná 2, 01026 Žilina, Slovakia, {milan.malcho, michaela.chovancova}@fstroj.uniza.sk

Abstract. The article deals with the thermal conductivity of rocks as an important parameter for quantifying the potential heat of the rocks. Describes the design of the experimental device for measuring thermal conductivity and measuring procedure. They will be measure samples of rocks from deep borehole to be used for obtaining *low-potential energy*. Thermal conductivity of ground will be input value for the simulation of heat flows in the borehole using CFD methods.

Keywords: thermal conductivity, ground, deck method of measuring thermal conductivity.

1. Introduction

Exploitation of renewable energy is the main trend of 21st century field of energy. Earth's heat is one of the most attractive alternative energy source. Thermal conductivity of rocks is one of the main monitored physical quantities in the use of earth heat. It is the physical parameters characterizing ability of rock to conduct a heat. Because rock is inhomogeneous three-phase system has other features vast block of rock, the other part lying between the major cracks and different from it the obtained drilling core. Thermal conductivity of rocks depends on the petrographic type, density, porosity and moisture (decreases with increasing porosity and increases with greater water content) and its spatial arrangement. It has a large variance and is different in any direction. Its detection is important for considerations and model calculations of temperature location in the earth's crust and it has from rock parameters cardinal importance for the dimensioning of the heat input of heat pumps. Also it has a significant influence on the depth of the borehole, because the thermal conductivity is higher, the borehole can be shorter.

Thermal conductivity λ				
rock	$Wm^{-1}K^{-1}$		ground	$Wm^{-1}K^{-1}$
	from	to		
basalt	1,70	1,70	dry ground	0,30
granite	1,90	4,00	dry coarse sand	0,20
calcite	0,80	3,00	dry clay	0,14
loam	0,40	1,20	wet ground	1,90
sand	0,30	1,20	by water saturate sand	1,72
runite	2,90	2,90	by water saturate loam	0,88

Tab. 1. Typical values of the coefficient of thermal conductivity for the selected type of rock

2. Design device on measuring thermal conductivity of rocks

One method for determining the thermal conductivity is a stationary method of plate and on its principle is designed and constructed measuring device. It is an electrically heated circular aluminum plate with a diameter of 200mm, which includes two spiral reel from special resistance cables. One is located in the centre of plates and has a temperature t_1. Its performance is equal to the heat flow that enters the soil. The second spiral is located at borders of the plate and is heated to the temperature t_1 and its task is to eliminate the marginal effect of temperature field.

This means that heat flows escaping into isolation will not significantly adversely affect the measurement. Resistance wires are connected to a dual DC laboratory power supply of electricity, which is continuously adjustable output voltage or output current continuously adjustable.

To the entire aluminum plate from the top and bottom is placed measured sample rocks on the total area S, the total thickness is 100 mm. The sample must have the whole length of the same thickness and parallel surfaces. In order to ensure constant temperature t_2 on the outside of the rock, the thermoplates are placed there. Thermoplates are aluminum plates with the diameter 200mm, which have loaded the capillary tubes with outer diameter 4mm. In capillaries with the aid of circulation thermostat flows cooling water by over constantly temperature t_2.

To obtain accurate temperature values on surface electric plate on either side glued foil thermometers to measure temperatures t_1 and to detect temperature t_2 stick foil thermometers on the inner surface thermoplate. The entire device is isolated from surroundings with ISOVER polystyrene EPS 50 thickness 100 mm.
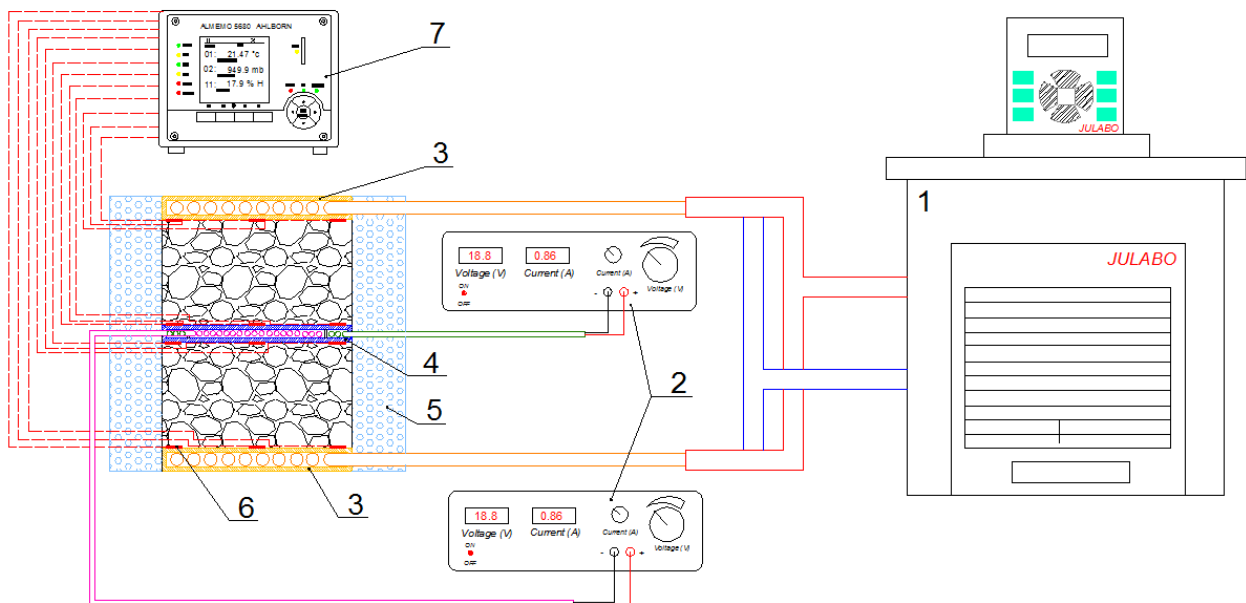
Fig. 1. Scheme device for measuring thermal conductivity of rocks,1) circulation thermostat Julabo, 2) laboratory sources on direct current, 3) thermoplates, 4) electrically heated aluminum plate, 5) isolation isover EPS50, 6) foil thermometers, 7) central measuring station

3. Calculation thermal conductivity

To determine thermal flow in the rock is needed calculate electric power of spirals. The value of voltage and current were read from laboratory DC source. These date were used for calculation of direct current power in following equation

$$P = U.I \ [W]. \tag{1}$$

Heat flow, which is transported into the soil is equal to the electrical power and spirals can be determined from Fourier law

$$\dot{Q} = \frac{\lambda(t_1 - t_2).S}{2l} \ [W]. \tag{2}$$

All required attributes can be measured, so that thermal conductivity is then determined from the simple regard expression from equation (1.2)

$$\lambda = \frac{\dot{Q}.2l}{(t_1 - t_2).S} \ [W.m^{-1}.K^{-1}]. \tag{3}$$
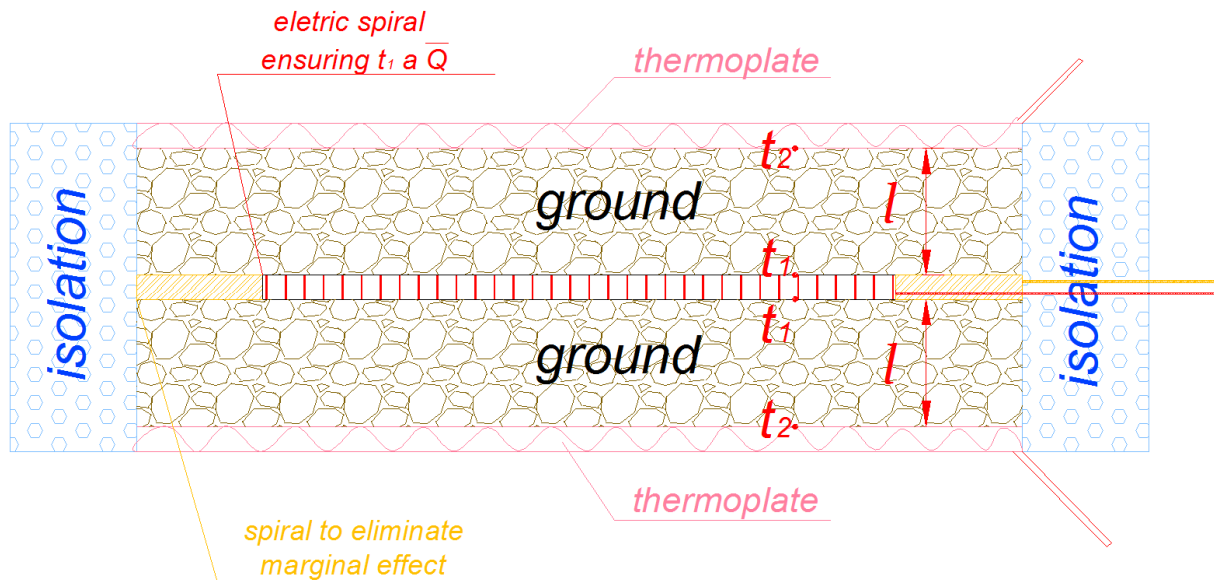
Fig. 2. Arrangement of heater surfaces and heated surface of stationary method of plate to determining thermal conductivity

4. Conclusion

The objective of measurement was to determine the thermal conductivity of rock cores for obtaining low-potential heat from rocks. Measured results will be used for the simulation of heat flows in the borehole. We are interested in how they affect efficiency heat pump life and well recharge in the summer of solar thermal solar panels.

The aim is to assess whether it is effectively charge borehole in summer. The second objective of measurement will determine the impact of moisture, porosity and density of rocks on its thermal conductivity.

Acknowledgement

References

[1] BAEHR, H. D., STEPHAN, K. 2006. *Heat and mass transfer*. Berlin: Springer, 2006. 688s. ISBN 3-540-63695-1.

[2] SAZIMA, M. a kol. 1989. *Sdílení tepla*. Praha: STNL – Nakladatelství technické literatúry, 1989. 592s. ISBN 80-03–00675–9.

[3] SIDEROVÁ, M., WITTENBERGER, G. 2006. *Stabilita systému využiatia tepelnej energie Zeme*. In Acta Montanistica Slovaca. 2006, roč. 11, mimoriadne č. 1, s. 158-161.

[4] HARSH, G., SUKANTA, R. 2007. *Geothermal energy: An alternative resource for the 21st century*. Amsterdam: Elsevier, 2007. s. 279. ISBN-13: 978-0-444-52875-9.

[5] RYBÁR, P. 1996. *Zemské zdroje, ich využitie a ochrana*. In Acta Montanistica Slovaca. 1996, roč. 1, č. 2, s. 117-130.

[6] LENHARD, R., JANDAČKA J., JAKUBSKÝ, M. 2010. *Zariadenia na simuláciu transformácie nízkopotenciálneho geotermálneho tepla na teplo vhodné pre vykurovanie*; XVII. Medzinárodná vedecká konferencia: Aplikácia experimentálnych a numerických metód v mechanike tekutín a energetike; 28.-30.4.2010; str. 185; ISBN 978-80-554-0189-8.

Description of the Turbocharger Garrett GT 1749V Lubrication System

[*]Marek Idzior, Maciej Bieliński, Tomasz Borowczyk, Wojciech Karpiuk
*Poznan University of Technology, 60-968 Poznań, Poland,
{marek.idzior, wojciech.karpiuk}@put.poznan.pl,
{maciej.bielinski, tomasz.borowczyk}@doctorate.put.poznan.pl

Abstract. This article provides an overview of the construction of the turbocharger Garrett GT 1749V. Particular attention was paid to the description of the design and operation of the bearing system.

Keywords: Turbocharger, construction, combustion engine.

1. Introduction

Description of the turbocharger is a general form. Located in order to facilitate the understanding of issues relating to damage arising Garrett GT turbocharger 1749V. Description of the construction of the turbocharger focuses on presenting the structure of the bearing system. Descriptions of the structure housing the turbine and compressor have been missed.

This article is an introduction to the article: "Influence of non elimination causes of turbocharger failure Garret 1749V for further exploitation of the new component", by Marek Idzior, Maciej Bieliński, Tomasz Borowczyk, Wojciech Karpiuk publicated in a Transcom – Zilina 2011 conference.

2. Constructional features of the Garrett GT turbocharger 1749V

Described turbocharger is built according to modern standards in force in this type of structures. We are focused on the fall of the turbocharger compressor, turbine and part of the central body. Air compression takes place in a rotating compressor, the centrifugal (axial – radial) of the twisted blades. Compressor wheel is made of aluminum alloy. Exhaust gases expansion occurs in the turbine centripetal turbine (radial – axial). The turbine wheel is made of high alloy steel, is connected to the shaft of the turbocharger. Compressor and turbine rotor with the shaft is shown in Figure 1.
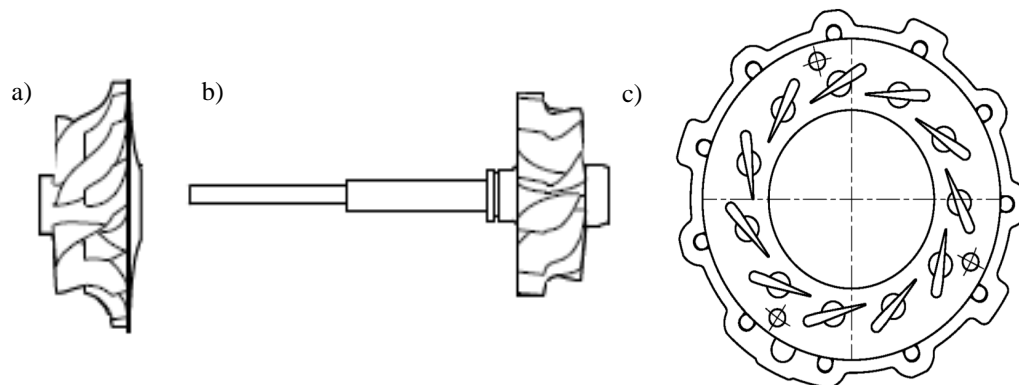
Fig. 1. Selected elements of Garrett turbochargers 1749V: a) compressor wheel, b) shaft turbine rotor, c) set of blades control ring [1]

Turbocharger shaft is journalled by bearings: sleeve bearings and thrust bearing. Spreads bearings oil is supplied to the turbocharger from engine oil main. Oil is supplied to the bearings in two points, hollow channels inside the body (Fig. 2). Radial forces from the reaction of exhaust gases are transferred the turbine rotor, and reaction force from the intake air are transferred the compressor rotor. Bearings bushing are shown in Figure 2. Bearings bushing are a sleeve bearing made of bronze alloy, cooperating with the turbocharger shaft extension.
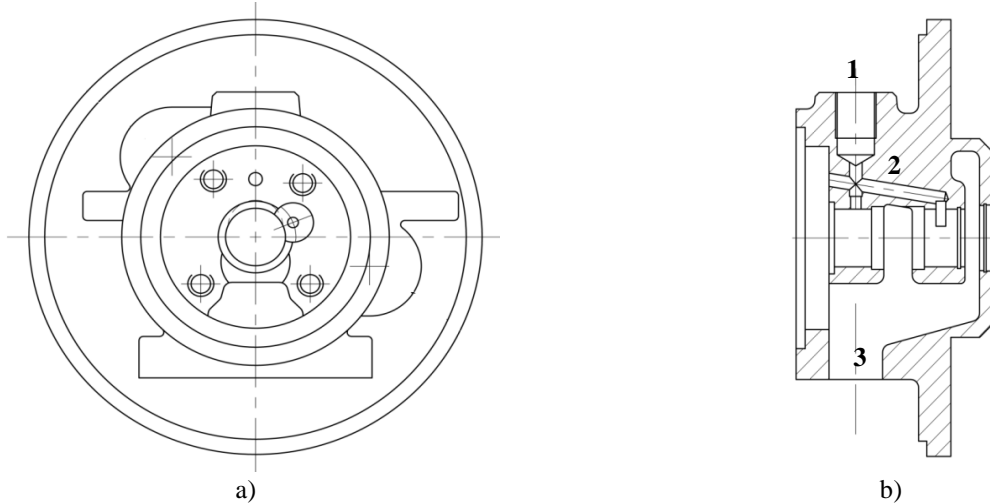
Fig. 2. Garrett turbocharger center housing 1749V: a) general view, b) cross-sections: 1-flow of oil, 2-channel hollow oil, 3-drain oil [1]

To the contact zone with pin bushings bearings, the oil is supplied through the holes located on the periphery of the sleeve. Two grooves on the circumference of the pan cause that collects in them ensure continuity of oil in the bearing oil film. The oil pan comes out with two holes top and bottom (Fig. 3b). Oil flowing bottom hole is supplied directly to the volume in control ring body the turbocharger, in which he collects. Opening the oil flows on the surface of the outer sleeve while receiving heat from the walls. Acetabulum is protected against rotation wedge, round whose axis is mounted in the control ring body middle (Fig. 3c).
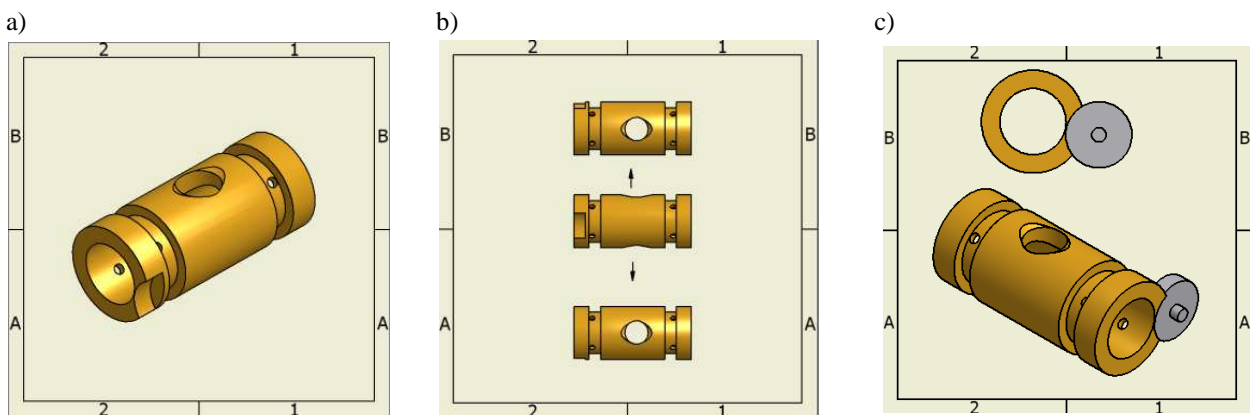
Fig. 3. Radial slide bearing bushing: a) general view, b) top and bottom hole trailing oil, c) method to determine position relative to the body bearings acetabular

Longitudinal sliding bearing is composed of a shield made of bronze alloy, both sides cooperating with steel pins, which rotate together the rotor. Longitudinal sliding bearing is show in Figure 4. Oil to the friction zone is fed inside the hollow bore shield bearing the channel flows created by selecting the surface. Arbors bearings are pressed against the blade axial resultant force coming from the turbine exhaust gases and compressed air in the compressor.

Axial force on the turbine shaft is transmitted to the front surface of the shaft neck, and from the compressor rotor cylindrical surface of the compressor. The fact that the stem moves the load bearings surface of the blade determines the resultant force: axial component side of the turbine and

compressor. At a fixed rotor speed and acceleration is greater than the resultant force on the turbine, while during deceleration, on the side of the compressor.

Turbocharger rotor seal is achieved by two seal rings. From the side of the turbine is mounted in a ring groove on the shaft (it is possible to rotation) and the central control ring body (mounted on a permanent basis). In addition to the ring on the shaft from the turbine is made of one piece labyrinth seal.

From the side of the compressor seal ring is seated in a groove made in the stem thrust bearing (pivot mounted) and the lower part of the compressor housing (permanent). The individual elements of the longitudinal bearing turbochargers are presented on Figure 4b. Deposit with a part of the rotor shaft and the seals are shown on the Figure 4c.
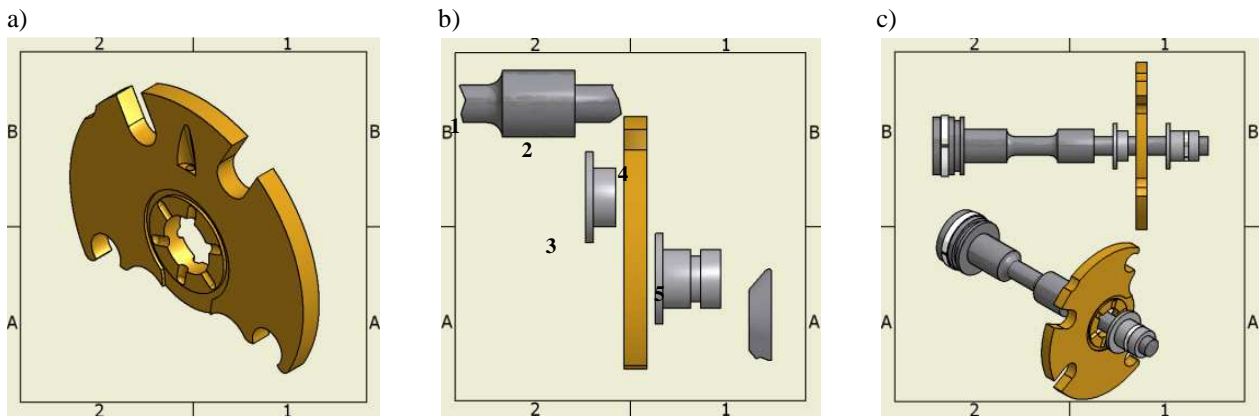
Fig. 4. Longitudinal sliding bearing: a) disc bearings, b) the elements of bearings:
1-pin shaft, 2-spindle bearings of the turbine, 3-disc bearings, 4-pin on the side of the compressor, five-helical part of the compressor rotor, c) view of the assembled bearing assembly

3. Conclusion

Turbocharger ensures the correct operation of sliding bearings of the rotor. This function is achieved by transverse and longitudinal bearing. The bearing system is closely connected with the lubrication system. Turbocharger rotor lubrication system has two basic functions, lubricates and cools the moving parts. Lubricating oil come from the bus engine oil. From a structural point of view, this is not insignificant. However, this impact was due to by maintenance.

References

[1] www.melett.com/turbo_parts_catalogue 03.2011

Influence of non Elimination Causes of Turbocharger Failure Garret 1749V for Further Exploitation of the New Component

*Marek Idzior, Maciej Bieliński, Tomasz Borowczyk, Wojciech Karpiuk
*Poznan University of Technology, 60-968 Poznań, Poland,
{marek.idzior, wojciech.karpiuk}@put.poznan.pl,
{maciej.bielinski, tomasz.borowczyk}@doctorate.put.poznan.pl

Abstract. In this article had described a case of damage caused by non-removal of a turbocharger primary cause of failure. The effects within the turbocharger bearing system have been described. Description have been supported a detailed photographic documentation using a microscope. Discussions on the causes of failure have been conducted.

Keywords: Turbocharger, combustion engine, maintenance, damage.

1. Introduction

This article is based on research material - turbochargers removed from the vehicles operating under real conditions. The study was carried out in establishments involved in regeneration and repair of turbochargers for internal combustion engines. There was analyzed Garrett turbocharger business model 1749V. Observation was carried out using Motic SMZ-168 microscope, which was equipped with digital video camera Motic 2000. The paper presents the construction and principle of operation of the turbocharger. Damage caused by the incursion to a foreign body on the compressor rotor was analyzed.

This publication is limited to the analysis of damage caused by the lack of suitable turbocharger lubricating oil parameters. Descriptions of the structure and working principle have been missed. Damage in the turbocharger has been resulted from the failure to comply with the necessary service actions, which is removing the causes of damage. Contaminated in oil have not been removed. Failing to remove the primary causes of damage, causes rapid destruction in the new turbocharger. This occurrence is commonly noticed in practice.

2. Description of damage to the turbocharger bearings in place as a result of momentary interruption in the supply of lubricating oil.

Turbocharger bearing system is shown in Figure 1. It consists of a set of slide bearings, journal bearings and thrust bearing. Turbocharger bearing system is shown in Figure 1. It consists of a set of bearings, the transverse and longitudinal. Bearing sleeve is made of an alloy of bronze, cooperating with the valve shaft with a chrome steel. Grease is the oil from the bus engine. Disc thrust bearing is also made of an alloy of bronze, cooperating with two pins. Oil is supplied to the bearings through the holes radially arranged next to the circumference of the sleeve (4 per side). The middle hole is used for oil draining and receiving heat from the friction zone. To the thrust bearing oil is fed from the body by a single duct made in the disc. Oil is drained by canals on the surface of the disc. Oil from the transverse and longitudinal bearing gets to the middle area of the body of a turbocharger, which continued for drainage orifices reaches the sump of the engine.
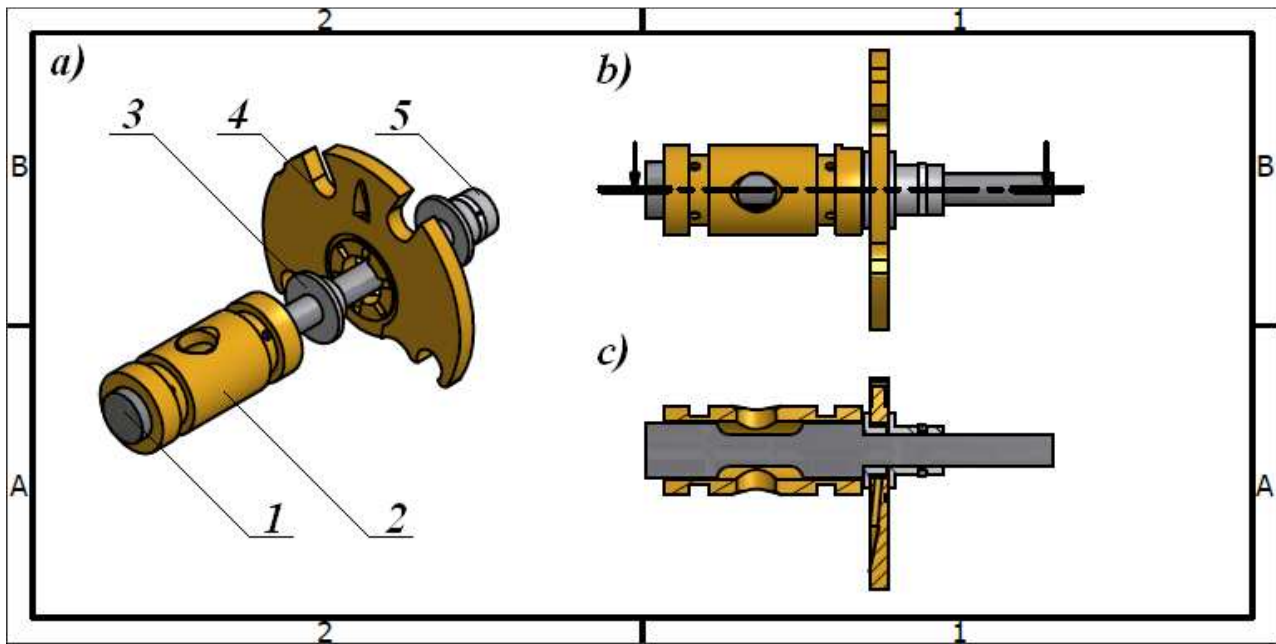
Fig. 1. Construction of a turbocharger bearing system: a) isometric view 1 - shaft, 2 – journal bearing bush, 3, 5 – bearings pin, 4 – journal bearing disc, b) view of submission, c) cross-section view

In the described turbocharger, oil was contaminated by the hard inclusions such as burnt oil in the conduits or the origin of metallic foreign bodies. Impurified oil splashed into the zone of cooperation pairs of friction bearings causes abrasive surface. Abrasion occurs due to implantation in hard-contamination of one of them. This causes furrowed and microcutting contrasurface. This event is compounded by the high speed rotor and an insufficient quantity of oil in areas of friction. Abrasive wear the disc around thrust bearing shown in Figure 2a. and the new bearing surface in Figure 2b.

a)

b)
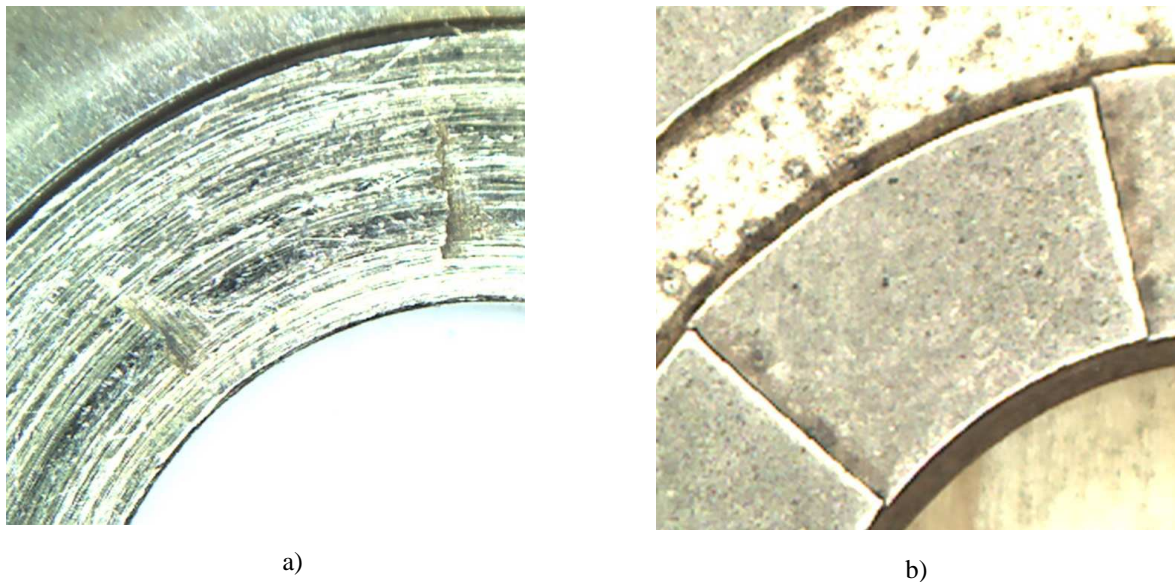
Fig. 2. Thrust bearing disc: a) damaged area, b) new surface (magnification 10x)

As a result of adverse events, bearing, by modifying geometrical parameters did not attended its function. Distortion of these parameters resulted in the presence of the turbocharger shaft axial clearance, which contributed to increased stress in the sealing rings and, consequently, break the ring on the side of the turbine. Ringless results in a decrease of oil pressure in bearings, and penetration of it into the exhaust system. The pressure drop of oil worsens the conditions in the

bearing lubrication, and the ability to create a film of oil. In this case, the liquid friction becomes to mixed friction.

Because of this, and the fact that the contaminated oil, mechanical wear has been cooperating with the pivot shaft bearing section. It was observed deep sulcus and grooves on its surface (Fig. 3).

a)

b)
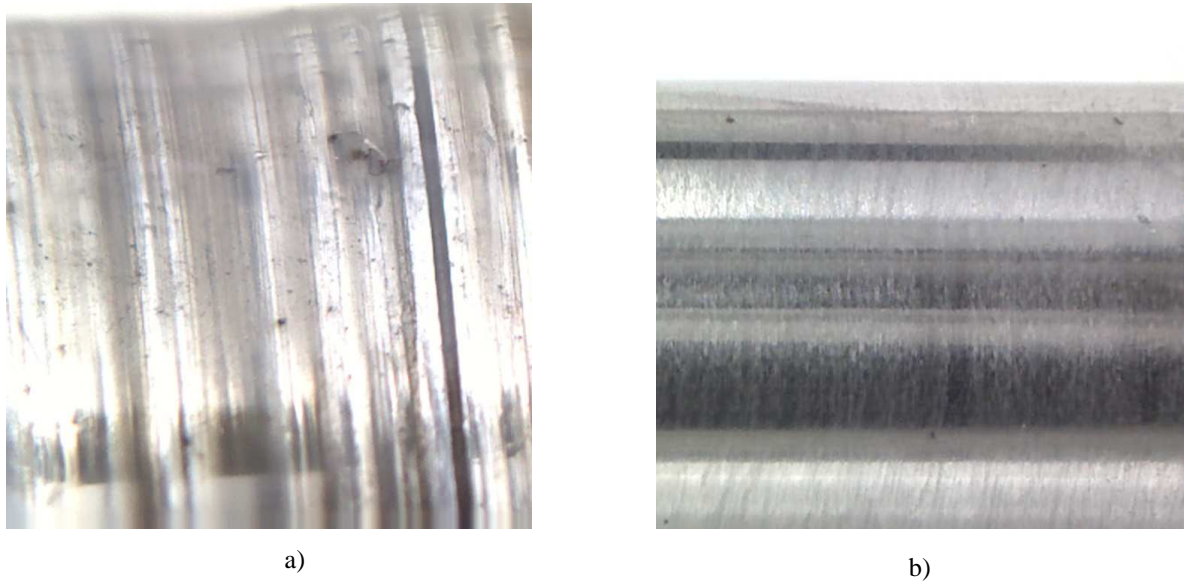
Fig. 3. Turbine shaft: a) lateral sulcus and grooves, b) new shaft surface (magnification 20x)

Destruction within the journals shaft and bearings components, also affect the emergence of negative vibrations shaft of the turbocharger. Vibrations of small amplitude but high frequency (f ≈ 3 kHz), the destruction process in these areas increase. The adverse effect of vibration can be observed on the outer surface of the thrust bearing. Because the nominal sleeve remains stationary relative to the body, in this connection, there is a fritting event. Destructive mechanism of this process is the simultaneous influence of adhesion, grafting intensive oxidation.

a)

b)

Fig. 4. Thrust bearing bush: a) outside surface (magnification 20x), b) new bearing bush (magnification 3x)

This intense oxidation is caused by increased activity of the surface layer as a result of contact stress and strain [2]. The effect of fretting on the surface of the thrust bearing is shown in Figure 4, which confirms the oscillation compressor – shaft – turbine.

The increasing amplitude of vibration, with unchanged frequency led to an increase in stress in the shaft turbocharger and its bursting. As a result, the team has been destroyed, damaging the rotor blades of the turbine and compressor.

a)   b)

Fig. 5. The broken shaft: a) magnification 2x, b) magnification 10x

3. Conclusion

This failure analysis shows that during replacement of used turbochargers for a new, should be removed cause of the damage. If this step is neglected or damaged causes diagnosis will be incorrect turbocharger component failure is repeated. In the current case before the next turbocharger replacement would replace the turbo engine oil and filter. In addition, consideration should be given to the patency of the channel inlet and outlet of the turbocharger oil or prophylactically replaced.

References

[1] IDZIOR M, BIELIŃSKI M, BOROWCZYK T.: *Analiza uszkodzeń turbosprężarki Garrett GT 1749V w rzeczywistych warunkach eksploatacji.* Szczyrk 2011.

[2] LAWROWSKI Z.: *Tribologia. Tarcie, zużywanie i smarowanie,* Wrocław, Oficyna Wydawnicza Politechniki Wrocławskiej 2008.

[3] Materiały zebrane z praktyki rzeczoznawczej autorów.

[4] Turbocharger Technician's Guide, Detroit/Michigan, Detroit Diesel Corporation 1994.

Reduction of Torque Variability in Two-Cylinder in-Line Engines

[*]Antoni Iskra

[*]Poznan University of Technology, Faculty of Machines and Transportation, Department of Internal Combustion Engines, Piotrowo 3, 60-965 Poznan, Poland, antoni.iskra@put.poznan.pl

Abstract. 2-cylinder in-line engines are considered as characterized by high torque instability and high external inertia forces. This paper presents possibilities of improvement in torque stability and eventually rotational speed by elimination of the 2nd order harmonic from engine total torque. A graph has been presented which illustrates explicitly an improvement in stability of the tangential force generated by a 2-cylinder engine if the 2nd harmonic component was balanced. Attention has been paid to the present day possibilities of the 2nd order harmonic elimination by its balancing with an electrical machine of hybrid drive.

Keywords: Run irregularity, torque variability, two-cylinder engines.

1. Introduction

There is a general belief that high torque instability and high external inertial forces are characteristic features of two-cylinder in-line engines. This opinion is entitled for as case of simple constructions devoid of systems reducing such inconveniences. When the top priority is a low cost of production generally the measures improving the dynamics of 2-cylinder engines are not applied. The engine of FIAT 126p car produced in Poland for decades could be the right example. However, the 2-cylinder engine arouses interest also in drives for which the overall cost is a minor decision factor. A good example for such a situation is the engine of BMW – F800S motorcycle [1]. On this engine a balancing mass has been applied of kinematics explained in Fig. 1 presenting the engine crank system.
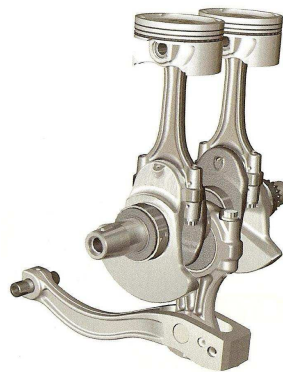
Fig. 1. The crank system of the BMW F800S motorcycle engine

With a certain approximation a swinging mass connected to additional connecting rod directed opposite to regular connecting rods offers a possibility of balancing forces both of 1st and 2nd order. Consequently, the engine of crank mechanism presented in Fig. 1 does not generate external forces. A unit of this type does not generate external torque as well and the only phenomenon producing vibrations is a variable torque transmitted to the power receiver via engine shaft. Unfortunately, the variability of torque is far more intensive than in engines of higher number of cylinders.

2. Torque transmitted to power receiver via engine shaft

The variable torque transmitted to the power receiver produces torsional vibrations of engine crankshaft and this was the reason why constructors tried to minimize the variability of torque resulting from gas and inertia forces from the very beginning of engine history. The simplest way is the increase in cylinder number and keeping the angle interval between ignitions constant. Such assumption leads to the course of torque presented in Fig. 2 as the specific tangential force.
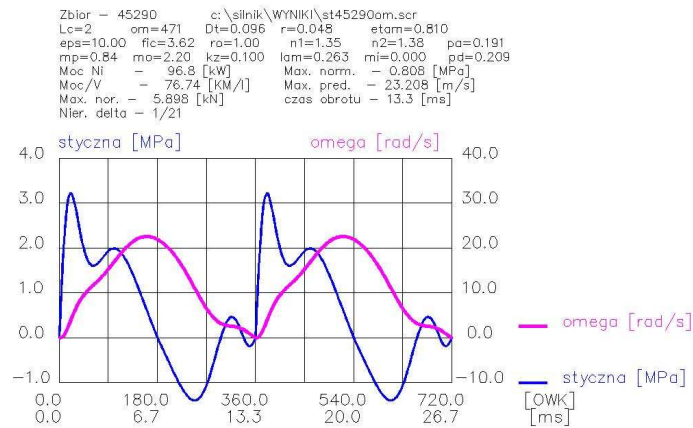
Fig. 2. Course of specific tangential force – thin blue line, and shaft momentary angular speed – thick magenta line; 2-cylinder, 4-stroke in-line engine 90% load at nominal speed 4500 [rpm] – 471 [rad/s]

The variable tangential force causes about 5% of angular velocity fluctuations presented with magenta line in Fig. 2. Such high fluctuations in angular velocity mean the speed irregularity level δ_2 equal to 1/21. If the assumed swept volume 1390 ccm was distributed into four cylinders the speed fluctuations would be much lower. Fig. 3 presents engine parameters as in Fig. 2 but for a 4-cylinder in-line engine.
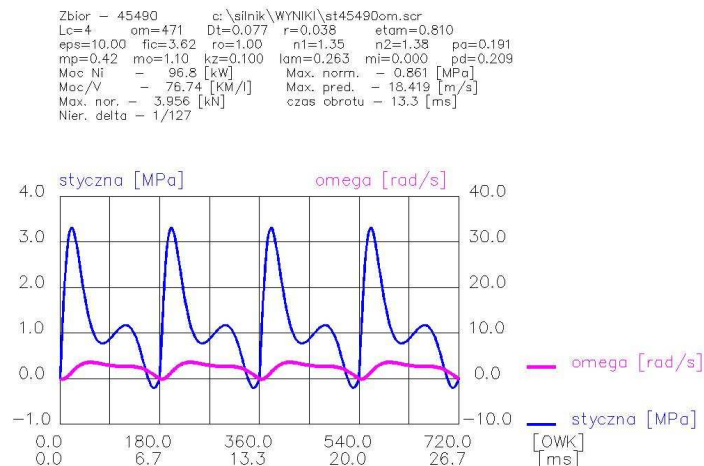
Fig. 3. Course of specific tangential force – thin blue line, and shaft momentary angular speed – thick magenta line; 4-cylinder, 4-stroke in-line engine 90% load at nominal speed 4500 [rpm] – 471 [rad/s]

Calculations of speed irregularity level for a 4-cylinder engine have been carried out reducing proportionally masses and dimensions: linear, areal and volumetric. Masses were reduced double fold (proportionally to the reduction in cylinder volume) while the linear dimensions were reduced in ratio to the cube root of cylinder volume and the cube root of volume change elevated to the

76

square has been applied in case of area. The flywheel inertia was not changed which should be done on a real 2-cylinder engine and was justified for illustration of differences in torque stability of 2 – and 4-cylinder engines. The carried out analyses proved that the 4-cylinder engine generates torque five fold more stable than the 2-cylinder engine. More precise relation between speed irregularity level of analyzed engines is $\delta_2/\delta_4 = 127/21$.New Roman is recommended font. There are type sizes specified in Tab. 1. The usage of particular styles will be described in detail in particular situations.

3. Improvement of the run irregularity level by removing the 2nd order harmonic

The course of tangential force from Fig. 2 one can present as a sum of harmonics of which one of the 2nd order was marked magenta in Fig. 4.
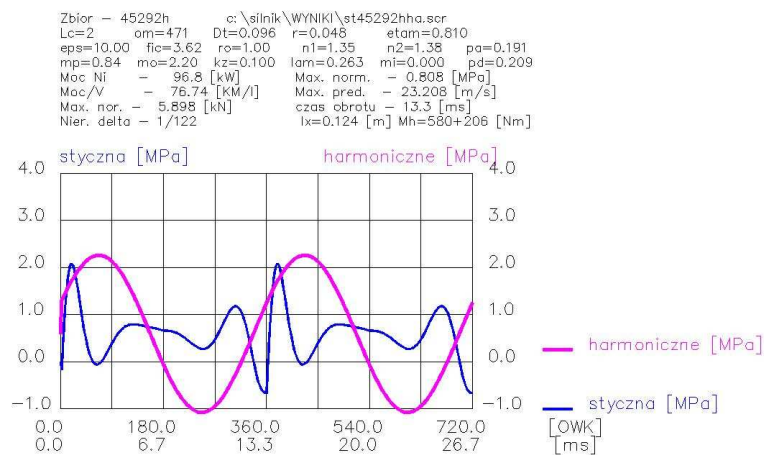
Fig. 4. The course of 2nd order harmonic – magenta line – set apart from the course of tangential force presented in Fig. 2, and the course of corrected tangential force – thin blue line

If the values constituting the course of 2nd order harmonic were taken away from the tangential force, one would obtain the corrected course of tangential force as the blue line in Fig. 4. Elimination of 2nd order harmonic improves manifold the δ_2 speed irregularity level of 2-cylinder engine and makes this level similar to the one of 4-cylinder engine, i.e. 1/122 and 1/127 respectively.

4. Possibilities of generation of variable counter moment to 2nd harmonic

In practice there are various methods of harmonic moment generation. Since this moment does not require a delivery of energy to the system, one can assume that the proposed action would not deteriorate engine efficiency. One of the ways the harmonic moment can be generated is coupling engine shaft to an electrical machine. Nowadays such combinations are met in so called hybrid drives. However, in the case of 2-cylinder engine the value of torque harmonic of 2nd order becomes a problem. As seen in Fig. 4 the amplitude of 2nd order harmonic of tangential force is 17 MPa, which corresponds to the amplitude of, torque 580 Nm. Such a value exceeds 2.5 fold an average torque generated by engine at analyzed conditions. In contemporary hybrid drives both mechanical and current permissible loads do not allow for generation of so extreme parameters. On the other hand it should be highlighted that a very rapid progress can be noticed in the construction of more powerful electrical machines purposed for application in hybrid drives. It is very probable that in near future 2-cylinder IC engine coupled with electrical machine will become a real challenge for a 4-cylinder engine.

5. Conclusion

Possible construction of a 2-cylinder engine of torque stability corresponding to the stability of 4-cylinder engine allows to obtain a unit far better than 4-cylinder in-line engine universally applied as a drive of passenger car today. 2-cylinder engine of the same volume as 4-cylinder demonstrates numerous advantages like:

–   A smaller surface to volume ratio of combustion chamber,
–   A smaller total surface of friction, which concerns cylinders, main and crank bearings and others,
–   A lower cost of manufacturing thanks to a smaller number of engine parts,
–   A more compact construction, which would be particularly advantageous in hybrid, drives because it allows housing an electrical machine under the hood.

Undoubtedly, the justification of the last thesis can be seen as external view of the BMW F800S engine presented at the beginning of the paper [1].
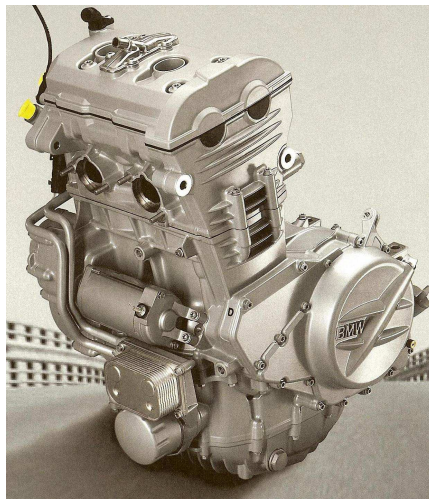
Fig. 5. External view of the BMW F800S 2-cylinder engine

References

[1] GUMPESBERGE, M., LANDERL, Ch., MIRITSC, J., MOSUMUE, E., MUELLER, P., OHRENBERG G. *Der Antrieb der neuen BNW F 800*. MTZ 06/2006.

Identification of the Combustion Engine Resistance to Motion Torque Components

[*]Antoni Iskra, Maciej Babiak, Jarosław Kałużny
[*]Poznan University of Technology, Faculty of Working Machines and Transportation, Institute of Combustion Engines and Transportation, ul. Piotrowo 3, 60-965 Poznan, Poland
{Antoni.Iskra, Maciej.Babiak, Jarosław.Kaluzny}@put.poznan.pl

Abstract. Identification of the combustion engine resistance to motion is necessary in every investigations aimed at limiting the frictional losses. In spite of many attempts of measuring the frictional resistance components there still are no functional test beds that would allow to take measure of frictional force or frictional torque in particular assembly. Most often the mean value of the torque for one or even two full revolutions of the crankshaft is determined. From many regards it is more convenient to determine the resistance to motion torque of the combustion engine with external drive but the torque from external drive is unfortunately disturbed by torsional vibration. There is at least theoretical possibility of separation the torque generated by vibration from the raw measuring signal. In the paper obtained results and selected problems of those separations are presented.

Keywords: internal combustion engine, coupling torque, harmonic components, proper vibration of the crankshaft

1. Introduction

Identification of the combustion engine resistance to motion is necessary in every investigations aimed at limiting the frictional losses. In spite of many attempts of measuring the frictional resistance components there still are no functional test beds that would allow to take measure of frictional force or frictional torque in particular assembly. Usually the value of coupling torque of the engine with the power receiver is the basic measurement during the combustion engine investigations. Most often the mean value of the torque for one or even two full revolutions of the crankshaft is determined. The test bench equipped with torque sensor is shown on fig. 1.
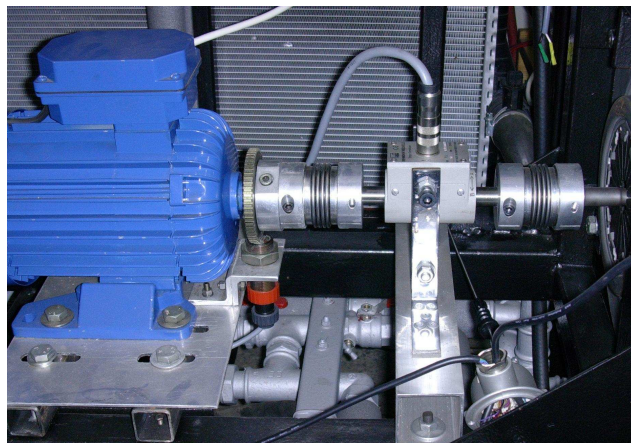
Fig. 1.   The test bed of the two cylinder passenger car combustion engine equipped with the measurement set for the instantaneous torque values

The resistance to motion of the combustion engine occurs during rotation of the crankshaft no matter if the engine is in normal operation or if it revolved by the external engine. From many regards it is more convenient to determine the resistance to motion torque of the combustion engine

with external drive. The torque from external drive is unfortunately disturbed by torsional vibration because the rotor of driving engine creates the vibratory assembly with the tested engine crankshaft. From this reason torque sensor placed between the rotor and the crankshaft measures the torque which is the sum of resistance to motion torque of investigated engine and the torque generated by vibration. The frequency of the torque generated by vibration in longer period of time usually is not exactly the multiplicity of driving engine rotational frequency, so there is at least theoretical possibility of separation the torque generated by vibration. In the paper obtained results and selected problems of those separations are presented.

2. Torque transmited from the driving engine shaft to the crankshaft of investigated combustion engine

On figure 2 with the thickest green line the course of torque is presented. It was measured on the test bed at 3000 rpm.
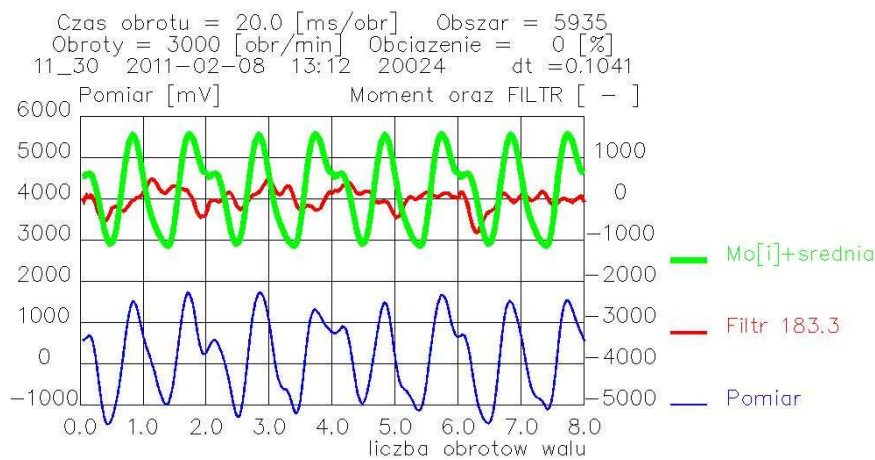
Fig. 2. The course of torque measured with the torque sensor – the thinness blue line, torque obtained after excluding harmonic components which are the multiplicity of the 720 degrees working cycle – the thickest green line, the sum of harmonic components excluded from the measured signal – red average thickness line

It can be noticed that the course of measured signal is not repeatable in the following working cycles. From the work character of the piston engine results the periodicity formation of resistance to motion components. These components are mainly: the resistance of compression, resistance of inertia, frictional resistance. As a result the coupling torque of the drive with the engine on the test bed shown on fig. 1 should repeat in cycles of two revolutions of the crankshaft. The only component of coupling torque which frequency is different from the shaft revolutions frequency is the frequency of various proper vibration forms. Theoretically it is possible that the frequency of one of the forms is close to the shaft rotational speed but this phenomenon is simple to detect.

From described regularity results that harmonic different from the multiplication of shaft revolutions frequency can be excluded. As a result of described operation the course of torque was obtained and is pointed out on fig. 2 with the thickest green line. Additionally with the red line the course of excluded harmonic components summary is presented.

3. Comparison of revised resistance to move torque with calculated torque of the investigated engine

Making the statistic course of the resistance to move torque is a typical operation connected with designing the new engine. Despite omitting the shaft proper vibration the statistic course of torque allows to estimate energetic characteristics of the new engine but such course is little useful in strength calculations. However to evaluate the obtained course of revised resistance to move

torque which is shown on fig. 2 a comparison with calculated statistic course shown on fig. 3 was made.
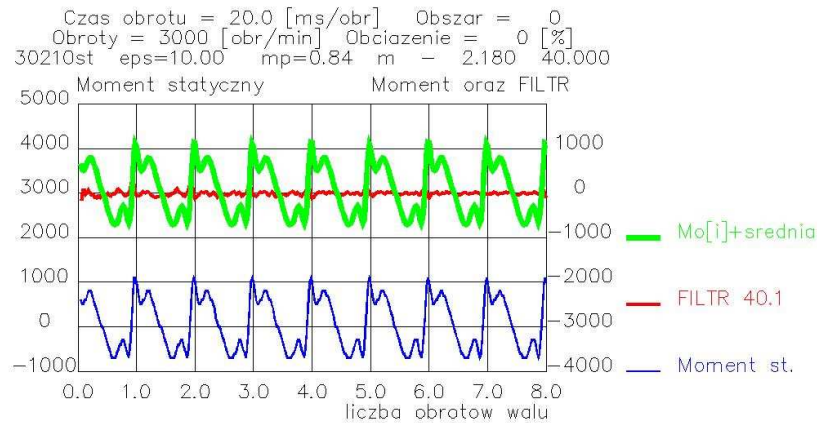
Fig. 3. The course of statistic torque obtained with use of computer simulation – the thinness blue line, The course of torque obtained after excluding harmonic components which are the multiplicity of the 720 degrees working cycle – the thickest green line, the sum of harmonic components excluded from the measured signal – red average thickness line

As it can be noticed there are some distinctions between character of modified measured course (fig. 2) and character of simulated course (fig. 3). It mainly concerns the repeatability of courses. The measured signal repeats every two revolution and simulated signal repeats every one revolution. Because courses apply to the two cylinder four stroke engine the repeatability of statistic course is obvious. But results of revised measurements do not confirm apparent evident computer simulation results. It could be connected with greater torsional deflection of the crank more distant from the torque sensor.

4. The influence of engine speed accuracy at excluding proper vibration components from the measured signal

Presented method of revising measured signal of the coupling torque is saddle with many errors. The main problem is the precise determination of the periodical torque components frequencies which become from the engine function and not from the proper vibration. To determine how does the engine speed measurement error influence at the obtained revised signal the analogous to presented on fig. 2 analysis was made but with incorrectly assumed engine speed at 2900 rpm instead of 3000 rpm. Obtained revised course is presented on fig. 4
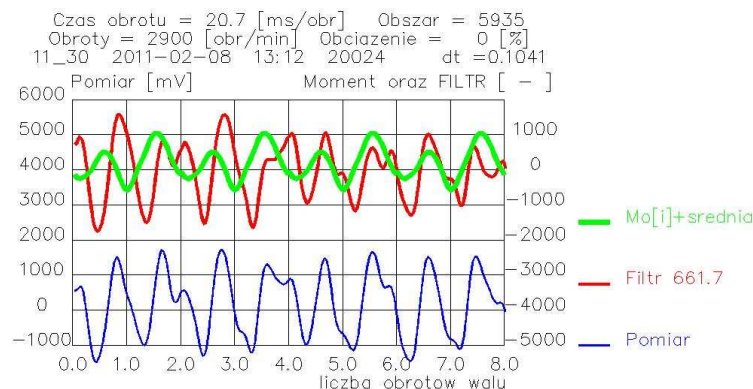
Fig. 4. The torque course from torque sensor – the thinness blue line, The course of torque obtained after excluding harmonic components which are the multiplicity of the 720 degrees working cycle – the thickest green line, the sum of harmonic components excluded from the measured signal – red average thickness line. The assumed engine speed is 3 % less than the actual engine speed

It is easy to notice that if rotational speed is 3 % less than the actual engine speed the revised course differs from both actual engine speed revised course (fig. 2) and the course obtained with use of computer simulations (fig. 3).

Only if the actual engine speed dispersion is less than 0,5 % from the assumed for revising it basically does not influence at the correctness of realized revising (fig. 5).
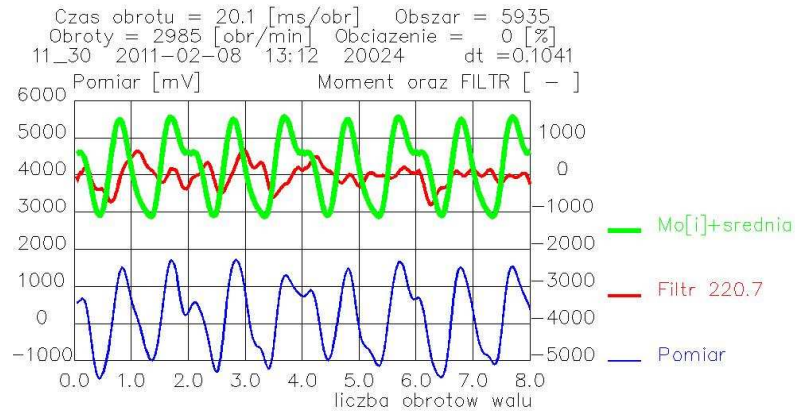
Fig. 5. The torque course from torque sensor – the thinness blue line, the course of torque obtained after excluding harmonic components which are the multiplicity of the 720 degrees working cycle – the thickest green line, the sum of harmonic components excluded from the measured signal – red average thickness line. The assumed engine speed is 0,5 % less than the actual engine speed

5. Conclusion

The presented method of revising the measured resistance to motion torque of the combustion engine is necessary to determine instantaneous torque values for example to evaluate the internal friction in the combustion engine. In this method precise maintain of the engine speed is required. It is recommended that the engine speed is specified with accuracy not less than 0,5 %.

References

[1] ISKRA, A. *Dynamika mechanizmów tłokowych silników spalinowych*. Wydawnictwo PP. Poznań 1995.

Geothermal Heat Transport in Laboratory Models

[*]Michal Jakubský, Richard Lenhard, Stanislav Gavlas, Milan Malcho
[*]University of Žilina, Mechanical Engineering, Department of EnergyTechnology, Univerzitna 2, 010 01 Žilina, Slovakia, {michal.jakubsky, richard.lenhard, stanislav.gavlas, milan.malcho} @fstroj.uniza.sk

Abstract. In the call OPVaV-2008/2.2/01-SORO Operational Programme for Research and Development - Transfer of knowledge and technology from research and development into practice (ITMS-26220220057), whose strategic objective is "Device to use low-potential geothermal heat without forced circulation of heat carrier a deep borehole, near the Zilina University realized two deep wells (150 m). The purpose of these wells is their connection to the available technology and the need for continued use of Žilina University. Simultaneously with the realization of this goal, he made a prototype device to gain low-potential geothermal energy in the comparative test-drilling in the indoor laboratory.

Keywords: low-potential geothermal energy, ground exchanger, simulator of transport geothermal heat

1. Obtaining of the Earth Heat

Nature of geothermal energy must be sought in the Earth's core. It's actually store inside the Earth, which arises from the decay heat of radioactive substances with long-lived. Geothermal energy is due to the temperature difference between upper and deeper zones, through radiation, convection and conduction moves to the Earth's surface [1]. Despite the fact that the earth's core heat escapes through cracks in rocks geothermal energy is considered as an alternative energy source because limitless potential for us. This energy is able to meet our worldwide consumption and its annual increase.

Heat that is stored in the ground, thus geothermal heat is used almost always indirectly (except hot couple that operate directly on the turbine blades). We receive it in the heat exchanger (eg natural collector) and by-circuit and heat transfer of the substance thus obtained heat is transported to the evaporator heat pump

Heat exchangers are devices that are built into the geothermal heat exchange stations and place them in the heat transfer process under the laws of thermodynamics, that is from warmer - the primary substance of heat transfer (geothermal water) into the cooler - the secondary heat transfer substance. Heat exchanger the polyethylene pipe (earth collectors) is considered as a heat exchanges too to store into a ditch.

1.1. Vertical collector-Earth Probe

The most effective type of ground collector is vertical collector, which is stored in a borehole. Drilling depths up to 150 m (approximately 10kW pulse heat pump) is placed near the buildings, at least 10 m apart. Number of wells is designed with respect to the heated object. In the case of new buildings is possible to place such a bore and directly below it. The actual drilling must be preceded by a hydrogeological survey. In the above-mentioned temperature is constant at depths from 8 to 12 °C which allows the heat pump to work efficiently and continuously. Such a heat pump works with an annual average heating factor 3 to 3.5. Heat transfer between the heat pump and the ground is usually secured with brine (antifreeze concentrate, water and frost-based glycol) which flows in tubes stored in the borehole. Work is part of the primary circuit of the probe. The probe is inserted into the hole and surrounding area is filled suspension (bentonite). Thus achieves a better heat transfer and prevents contamination of groundwater. After pouring a suspension of the probe has not pulled out or in case of repairs. Therefore, we use special materials (PE 100), which are

intended to wells and have high mechanical strength against possible engraving in introducing the probe into the borehole.

Fig. 1. Vertical earth heat exchanger with a probe and a load introduced into the borehole

2. Simulation of transport geothermal heat

Before the construction of a laboratory model we had to design a structure which would allow comparison of the two interiors and technology at the same time as closely as possible emulate the processes performed in boreholes located in the University Campus. Then we choose the appropriate components and suggest ways how to involve the simulator. The main objective was therefore to devise and implement a system with forced circulation of heat carrier, and without forced circulation heat carrier for the use of low-potential geothermal heat from geothermal simulator transport of heat.

Fig. 2. Device applied to the laboratory "boring"

Equipment using forced circulation heat carrier will respond in the construction to an equipment currently used to transport heat from deep borehole using heat pipes. The second device without the use of forced circulation heat carrier will be based on the use of U tubes for the transport of heat from deep borehole with different working substances (CO_2, NH_3). The aim of this project is to design and verify an appropriate heat pipe design, with different content of a substance, and all equipment for transport of heat from the geothermal well to heat sink. Based on

available knowledge of heat transfer, construction of boreholes and geological composition of rocks as well as the geothermal gradient was prepared engineering design simulator.

The device allows us to measure the flow of heat from the rocks into the heat pump circuit and experimentally determine the parameters of contact vaporization of the heat pipe and rocks. Simulator for low-potential heat transport through the phase of transition in the vaporization and condensation of the tube at temperatures below 0 °C to develop research activities in the verified production technology heat pipe suitable for the use of terrestrial heat at low temperature in a laboratory environment. Individual components of research facilities enable thermal kinetic parameters of transport of heat from rocks to heat the vehicle model. The device allows realistic modeling of heat flow from the rock into the heat transfer fluid.

2.1. Purpose of equipment

- Earnings low potential GE disused way through gravitational U tube without forced circulation of the carrier.
- Comparison of the effectiveness and weaknesses of the new technology of proven technology (vertical heat exchanger with forced circulation of the carrier).
- To carry out experimental measurements on low-potential geothermal heat simulator.
- Analyze the measured results.

3. Construction

The device is assembled from a few simple components. PVC pipe diameter D = 500 mm and length 5 m surrounding a hole in a cylindrical shape. This outer tube is slid PVC pipe with a diameter of 200 mm and the same length. This is a very hole in which they are located heat pipes (device 1) or U tube (device 2). With ring space is filled with wet sand, whose thermal conductivity is 1.63 Wm⁻¹ K-¹. The area around the heat pipe (200 mm), representing itself and the well is filled with bentonite.

Fig. 3.   Installing a heat exchanger system to "pipe in pipe" heated by electric cables

After the outer circumference of pipe (500 mm) is wound in a spiral-shaped incandescent power cord with 10 watts / m. Cable diameter is 6 mm and 10 mm spacing. Heater borehole simulator is divided into 3 sections. Incandescent cable is insulated with aluminum foil. Heating power cables is so geared towards the well and is prevented by external temperatures. Glow cables are in our case the Earth's heat that is accumulating in wet sand (rocks) and subtracted using the U pipe or heat pipes. With properly spaced thermocouples over height (5m) and average (0.5 m) equipment to obtain data on heat transfer from the periphery of the borehole (glow cable) towards the center hole (heat pipes).
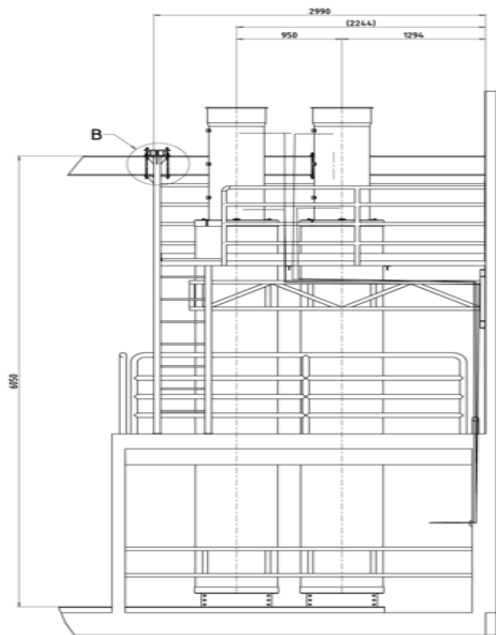
Fig. 4. From project to realization

4. Conclusion

Device to simulate low-potential geothermal energy transformation into heat suitable for heating allows your designing mimic processes in deep wells. By examining these processes in laboratory conditions to obtain knowledge on the best heat transfer fluids, exercise, heat transfer, conduction of rocks etc. Final task is to compare the two technologies using this device.

Acknowledgement

References

[1] PETRAŠ, D. 2009. *Nízkoteplotné vykurovanie a obnoviteľné zdroje energie*. Bratislava: Jaga,2009. 216 s. ISBN 80-07-00031-5

[2] LENHARD, R., JANDAČKA, J., JAKUBSKÝ, M. *Zariadenia na simuláciu transformácie nízkopotenciálneho geotermálneho tepla na teplo vhodné pre vykurovanie*, Zborník prednášok zo17.medzinárodnej vedeckej konferencie Aplikácia experimentálnych a numerických metód v mechanike tekutín, Žilina: EDIS, 2010. 185 s. ISBN 978-80-554-0189-8.

[3] LENHARD, R.., JAKUBSKY, M., NEMEC, P. *Device for simulation of transfer geothermal heat with forced and without forced circulation of heat carrier*, Fourth Global Conference on PCO 2010, Kuching – Sarawak - Malaysia 2010, ISBN 978-983-44483-32.

Measurement of Emissions in Domestic Boiler

[*]Jana Jurkechová, Radovan Nosek, Jozef Jandačka

[*]University of Žilina, Faculty of Mechanical Engineering, Department of Power Engineering, Univerzitná 1, 010 26 Žilina, Slovakia, {jana.jurkechova, radovan.nosek, jozef.jandacka}@fstroj.uniza.sk

Abstract. The paper presents an analysis measurements of emission in domestic boiler. As a heat source was used pellet boiler with a heat power equal to 18 kW. The boiler is designed to burn wood pellets with a diameter of 6 to 10 mm. Boiler was connected to the chimney where were carried out measurement of emissions. The gas analyzer was used for measurement of following emissions - O_2, CO_2, CO, SO_2, NO_x. The whole process was controlled automatically from the control system. Tests were performed at different times of feeding and standing period. From the measurements were found optimal operating conditions of the boiler.

Keywords: biomass, emissions, boiler, heat output

1. Introduction

Biomass consists of plant materials and animal origin. It can be used not only for heat, but also to generate electricity in combustion devices.

The pellet is the name of granule circular cross section with a diameter of about 6-8 mm and a length of 10-30 mm. Pellets are made only from waste materials such as sawdust, wood shavings, without any chemical additives. They have low ash content (0,5 to 1%), low water content (10%) and high calorific value (about 18 MJ/kg). One of the pellets advantage is CO_2 neutral production, which means that their combustion arises only so much CO_2, how much plants can consume during the growth of the atmosphere during photosynthesis. Combustion of pellets is the ecological heating, since they does not contain chemical artificial binding materials, sulphur, halogens or heavy metals.

Emissions from combustion of biomass are the principal source of environmental pollution. Quality of combustion in small boilers is mostly affected by the temperature of combustion, the supply of atmospheric moisture, fuel moisture and the technology used. In biomass combustion escape into the atmosphere these pollutants: CO_2, CO, SO_2, NO_2 and NO. Globally, the most carbon dioxide that causes greenhouse effect and global warming impact. From an ecological point of view have a significant negative impact of nitrogen oxides and hydrocarbons evaporated, which is under the influence of solar radiation involved in the formation of photochemical smog.

2. Experimental setup

Experimental measurements have been performed in domestic boilers for combustion of wood pellets with heat power equal to 18 kW. Boiler is used mainly for heating of houses. In boiler were burned wood pellets. Boiler was placed on weight that is used to measure fuel consumption. Measurements in the boiler have been done for 90 minutes. Optimal conditions and power control are designed electronically controlled fuel supply and air supply with electronically controlled fan, depending on the user-defined parameters required by the heating and hot water.

The scheme of experimental setup is shown in Figure 1. The experimental device consists of heating and cooling circuit. Circuit are separated by a heat exchanger.
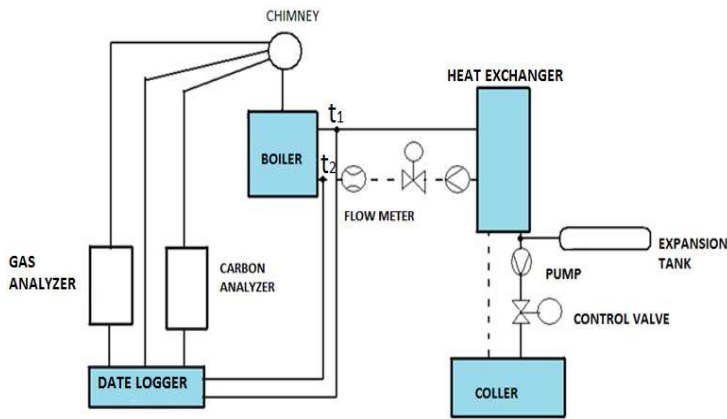
Fig. 1. The measurement setup
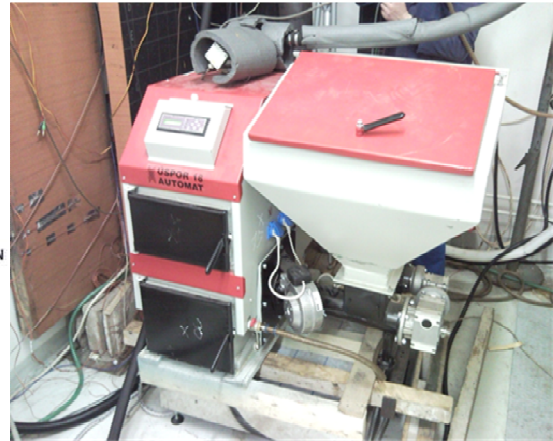
Fig. 2. Automatic pellet boiler

3. Measurements of the boiler

Tests were performed at constant time of standing and feeding pellets. The first series of measurements was carried out at constant time-standing pellet 25 seconds (time of burning pellets in the burner) and changed the times of feeding pellets - 9, 12, 15, 18 seconds (the time at which the pellets are conveyed from the reservoir to the burner). The first test was conducted at a nominal heating capacity of 18kW boiler. At rated thermal output, the boiler is operated so that the smooth running of its potential. The second series of measurements was carried out at constant time of feeding pellets - 18 seconds and changed the times of standing-25, 28, 31, 34 seconds. During the measurements were analyzed emissions by analyzer and recorded by the measuring unit. Data logger was connected to a computer, which recorded all the measured variables. All continuously measured variables were determined at intervals of 20 seconds.

4. Results of experimental measurements

During the measurements are watching content in flue gas emissions and also the heat output depending on the fuel metering. The highest heat power was achieved at the operating mode 18/25 seconds (feeding/standing). The progressive decreasing of the feeding period resulted in reduction of the boiler power.
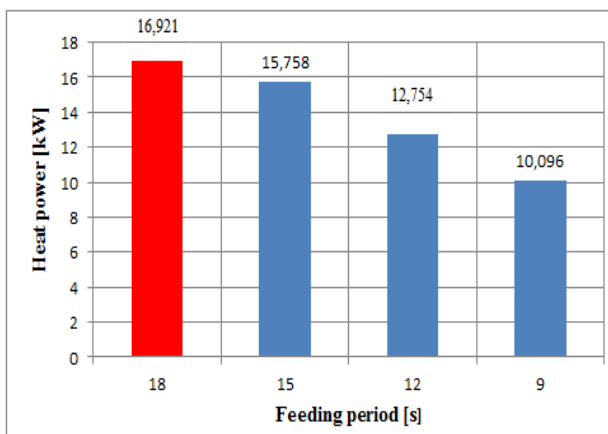
Fig. 3. Comparison of heat power for different operating modes
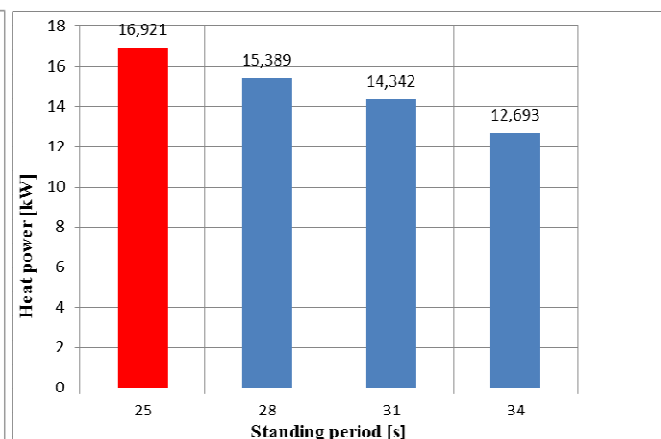
Fig. 4. Comparison of heat power for operating modes

On the Fig. 4. is shown course of performance of the boiler at constant time of feeding pellets, 18 seconds. The highest heat power was achieved at the operating mode 18/25 seconds (feeding/standing). The progressive shortening of the standing period resulted in reduction of the

boiler power. The following figures present emission concentrations at various settings of the boiler.

The largest concentrations of emissions have been reported in settings 18-25. From the measurements it was found that shortening the times of feeding pellets resulted in reduction of CO and CO_2. In measurements were recorded low concentrations of SO_2 and NO_x.
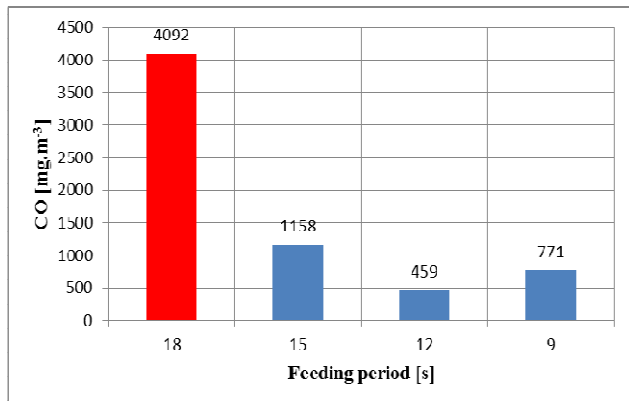
Fig. 5. Average values CO for constant time standing period
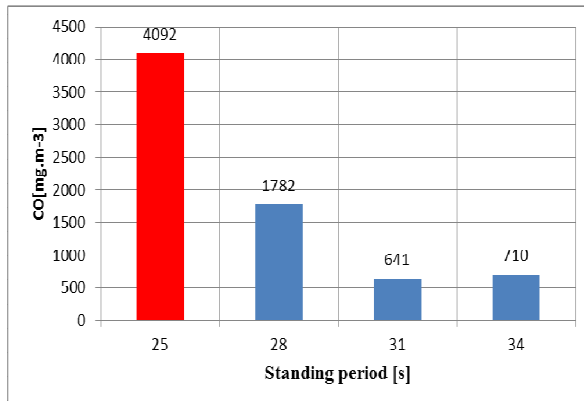
Fig. 6. Average values CO for constant time of feeding period
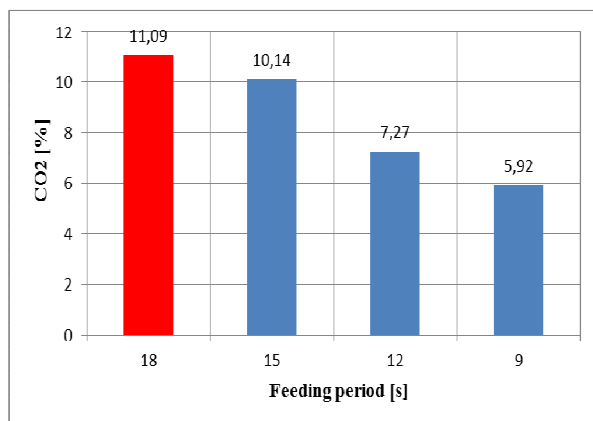
Fig. 7. Average values CO_2 for constant time of standing period
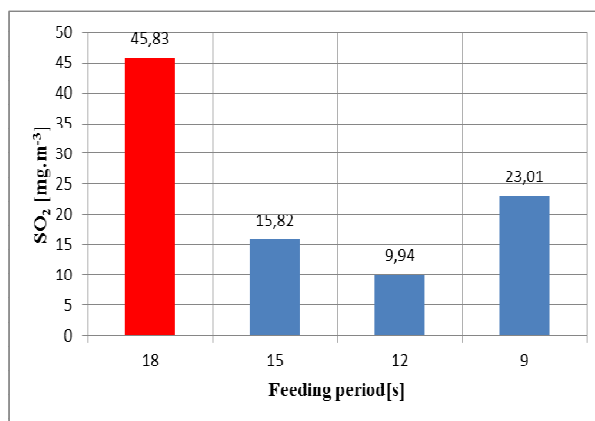
Fig. 8. Average values SO_2 for constant time of standing period
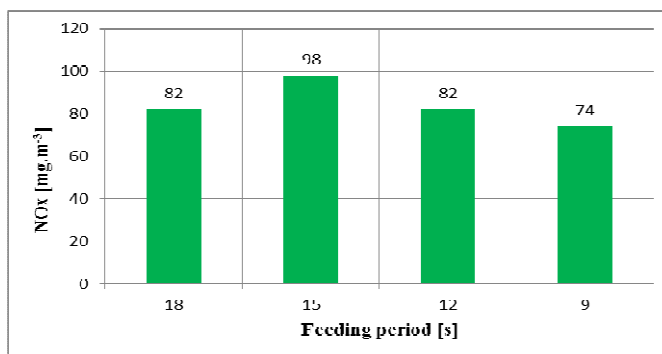
Fig. 8. Average values NO_x for constant time of standing period

5. Conclusion

The measurements was found that the impact of fuel metering has a significant influence on the performance and emission parameters of the heat source. In this work was proposed the method for measurement of boiler for combustion of wood pellets with a nominal heat output of 18kW. As a fuel were used pellets with high heating value and provide automatic operation of the boiler. The boiler was automatically controlled during the measurements. For complete combustion of biomass is necessary to provide enough air, a sufficiently high temperature, proper humidity and enough time to burn fuel. The basic pollutants whose concentrations were measured in the flue gas are CO_2, CO, NO_x, SO_2, O_2.

Acknowledgment

References

[1] JURKECHOVÁ, J.: *Vplyv dávkovania paliva na výkonové a emisné parametre zdroja tepla.* Diplomová práca 2010, Katedra energetickej techniky, Žilinská univerzita v Žiline

[2] DZURENDA, L. *Spaľovanie dreva a kôry.* vydanie I.-2005. Vydavateľstvo TU vo Zvolene. 2005. 124 s. ISBN 80-228-1555-1

[3] JANDAČKA, J. – MALCHO, M. *Biomasa ako zdroj energie.* Juraj Štefúň – GEORG, Žilina, máj 2007, 78 s. ISBN 978-80-969161-4-6

[4] MIKULÍK, M. – JANDAČKA, J. *Postupy správneho vykurovania.* Jozef Bulejčík, Mojš. 2009. 128 s. ISBN 978-80-969595-7-0

[5] VITÁZEK, I. – TIROL, J. – HAVELKA, J. *Analýza spalín pri spaľovaní biomasy.* In : Strojárstvo (Mechanical Engineering Journal), 2009, mimoriadne vydanie, jún, s. 394-297. ISSN 1335-2938

[6] Norma STN EN 303-5: *Vykurovacie kotly na tuhé palivá dodávané ručne a automaticky, s menovitým výkonom do 300kW.* časť 5.

Reduction of Diesel Engine Emissions

[*]Martin Kadák, Peter Tučník, Vladimír Hlavňa
[*]University of Žilina, Faculty of Mechanical Engineering, Department of automobile technology,
Univerzitná 2, 01026 Žilina, Slovakia, {martin.kadak, peter.tucnik, vladimir.hlavna}@fstroj.uniza.sk

Abstract. The paper deals with diesel engine emissions in exhaust with the focus on the nitrogen oxide. The paper highlights some of the methods of NO_X reduction with the focus on verification methods of the temperature reduction of the charging medium. The paper shows a basic scheme of measuring the engine bench by creation of extremely low temperature of charging air. Cooling of charging air is ensured through the double-degree cooling. According to scheme there were designed two intercoolers. Simulations of these two intercoolers are instrumental to state estimation of measuring the low temperatures of charging air. The simulation results show, that the change of coolant temperature is possible, charging air temperature changes in the desired values. The low temperatures are allowed to obtain experimental of information on the development of NO_X.

Keywords: intercooler, simulation, charge air flow, nitrogen oxides, emissions.

1. Introduction

Emissions of diesel engine in comparison with emissions of gasoline engine have certain differences. Emissions have differences in concentrations in exhaust gas and in chemical composition, too. The reasons for differences are based on different way of preparation and mechanism of ignition. At the beginning of combustion process of diesel engine is carried by the ignition of the appropriate fuel concentration with the air influenced by compression heat. Combustion in diesel engine occurs in lean mixtures. Mixture is in minimal contact with the wall, which suppresses quenched effect of the wall, therefore diesel engines have considerably lower content of the products of incomplete combustion CO and unburned hydrocarbons CH in the exhaust gases, than in the gasoline engines. In the exhaust gases are also included particular matter. On the formation of particular matter has the greatest impact the last combustion phase. The problem of diesel engines is the content of NO_X and unburned (revised) hydrocarbons adsorbed by the carbon particles. In the analysis of fraction of particular matter captured on a filter are the unburned fuel and oil quantity called soluble organic fraction (SOF-soluble organic fraction). Leave emissions limits for exhaust gas combustions engine for vehicles of category N is shown in the Tab.1.

	ROK	CO $g.kW^{-1}h^{-1}$	HC $g.kW^{-1}h^{-1}$	NO_X $g.kW^{-1}h^{-1}$	PM $g.kW^{-1}h^{-1}$
Euro I	1992	4.5	1.1	8.0	0.36
Euro II	1996	4.0	1.1	7.0	0.25
Euro III	1998	2.1	0.66	5.0	0.10
Euro IV	2005	1.5	0.46	3.5	0.02
Euro V	2008	1.5	0.46	2.0	0.02
Euro VI	2013	1.5	0.13	0.4	0.01

Tab. 1. EU Emission Standards for HD Diesel Engine source : http://www.dieselnet.com/standards/eu/hd.php

In the performance of diesel engines emission limits of is one of the most important problem of implementation levels of nitrogen oxides (NO_x).

2. Reduction of NO_X content in the exhaust gases

Methods of reducing NO_x are divided into two basic categories: the primary methods, consisting in the suppression of NO_x during combustion and secondary methods, consisting in the subsequent removal of NO_x from exhaust gas.

2.1. Primary methods of reduction NO_X in the exhaust

Primary methods of reduction NO_X use the knowledge of their creation. From the analysis of NO_X results is clear that during the combustion process can reduce the NO_X formation by three main ways: by reduction of the combustion temperature, by reduction of the O_2 concentration in the flame and by reduction of the residence time of reactants in areas with favourable conditions for NO_X formation. Generally, in practice it doesn't use just one method separately, but in their combination. It is used to control the amount of combustion air, to edit design of combustion chamber, to exhaust gas recirculation, to flame cooling and the fuel escalation.

2.2. Secondary methods to reduce NO_X in the exhaust

Secondary methods reduce the quantity of NOX in the exhaust gas. There are several methods, but the most commonly are used the selective non-catalytic reduction (SNCR) and the Selective Catalytic Reduction (SCR). The other methods using to reduction of NOX in the exhaust gases can be given active deNOX system, CRT (Continuosly Regenerating Trap) system and non-thermal plasma.

3. The parameter impact of extremely low temperatures charging air on the gaseous emissions

On the department of automobile technology FME University of Žilina the problematic of gaseous emission engines is actively solved. Currently, we are engaged by the research of the influence of charging air extremely low temperature on the gaseous emissions and the other parameters of the diesel engine. Reduction of the charging air temperature reduces the temperature of working medium at the beginning of the cycle. It can be assumed, that by the reduction of the temperature of working media, at the beginning of the working cycle occur (for constant conditions) in a reduction in temperature throughout the work cycle. Reducing temperature of working cycles will influence the maximum combustion temperature, which determine the formation of nitrogen oxides.

For the purpose of experimental verification of the impact of extremely low temperatures charging medium on the gaseous emissions and other parameters of the engine is built the specifically test bench (Fig.1) with double-degree cooling of the charging air in the series.

The first degree of cooling the charging is provided by the heat exchanger constructions air-air, the cooling air flow provides for a variable fan powered by the crankshaft. The second stage of charge cooling is designed as heat exchanger of type air-liquid. A forced circulation of cooling fluid is provided by circulator pump, which is included into cooling circuit with a special mixing tang on the ensure of extremely low temperatures.
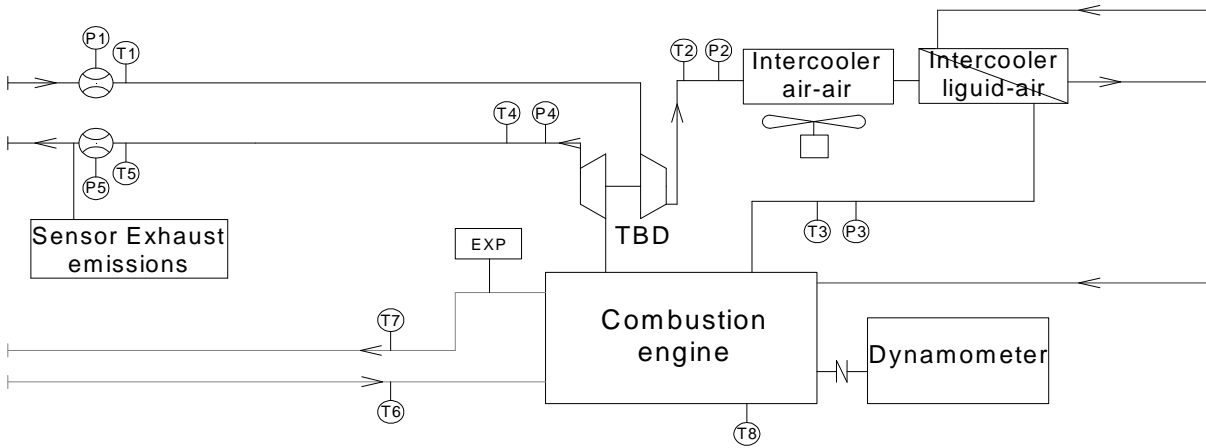
Fig. 1. Basic wiring diagram test bench

3.1. Proposal of parameters intercoolers

The calculation of the first degree of intercooler is assumes the charging air Intel temperature is 100°C.The charging air pressure behind the blower has the value of 170 000 Pa. Air mass flow rate has the value of 820 kg.h^{-1}. Cooling air mass flow rate is 1 992 kg.h^{-1} at 20°C. The intercooler surface of heat transfer from the side of charging air the value of 1.9055 m^2. The intercooler surface of heat transfer from the side of cooling air the value is 4.32 m^2. The used value of head transfer coefficient on the side of charging air has the value α_L=78 W.m^{-2}K^{-1}. For the cooling air heat transfer coefficient was used value of α_L=78 W.m^{-2}K^{-1}. The values for het capacity are 1 005 J.kg^{-1}.K^{-1}. Resultant heat transfer coefficient for the first intercooler calculated according the formula (1) has the value α_L=54 W.m^{-2}K^{-1}. The outlet temperature of charge air calculated according the formula (2) is 45.5 °C and the outlet temperature of cooling air calculated according the formula (3) is 42.4 °C.

$$k = \frac{1}{\dfrac{1}{\alpha_L} + \dfrac{S_L}{S_w} \cdot \dfrac{1}{\alpha_w}} \tag{1}$$

$$t_s = t_{d2} - \Delta t_L = t_{d2} - (t_{d2} - t_{w1}) \cdot \frac{1 - e^{\left[-\left(1 - \frac{W_d}{W_w}\right)\frac{k \cdot S_L}{W_D}\right]}}{1 - \dfrac{W_D}{W_w} e^{\left[-\left(1 - \frac{W_d}{W_w}\right)\frac{k \cdot S_L}{W_D}\right]}} \tag{2}$$

$$t_{w2} = (t_{w1} + \Delta t_w) = t_{d2} + (t_{d2} - t_{w1}) \cdot \frac{W_D}{W_w} \cdot \frac{1 - e^{\left[-\left(1 - \frac{W_d}{W_w}\right)\frac{k \cdot S_L}{W_D}\right]}}{1 - \dfrac{W_D}{W_w} \cdot e^{\left[-\left(1 - \frac{W_d}{W_w}\right)\frac{k \cdot S_L}{W_D}\right]}} \tag{3}$$

The calculation of the second degree follows the calculation of the first degree. Coolant mass flow rate is 3600 kg.h^{-1}. The intercooler surface of heat transfer from the side of cooling air has the value of 3 m^2. The intercooler surface of heat transfer from the side of coolant has the value of 0.99 m^2. The value of head transfer coefficient on the side of coolant has the value α_L=78 W.m^{-2}K^{-1}. The value for het capacity is 4 186 J.kg^{-1}.K^{-1}. Resultant heat transfer coefficient for the second intercooler is calculated according the formula (1), it has the value α_L=75 W.m^{-2}K^{-1}. The charging air outlet temperature and coolant outlet temperature dependency on the coolant inlet temperature is demonstrated in the Tab. 2.

Coolant inlet temperature (°C)	Air charge outlet temperature (°C)	Coolant outlet temperature (°C)
20	29.57	20.87
17.5	28.01	18.46
15	26.44	16.04
12.5	24.88	13.63
10	23.32	11.21
7.5	21.76	8.80
5	20.20	6.38
2.5	18.63	3.97
0	17.07	1.55

Tab. 2. Charge air outlet temperature and coolant outlet temperature dependency on the coolant inlet temperature

4. Conclusion

The paper deals with the numerical simulation of temperature reduction of charging air using double-degree cooling. The simulation is used to verification of application possibilities of the proposed to double-degree cooling, with purpose to achieve the required temperature of charging air.

From the cooling simulation results it can be seen that by using of temperature t_{w1}=0°C in the scheme a minimum temperature of charging air t_{min}=17.07°C can be achieved. The simulation shows that by an appropriate change of coolant temperature can be modified the charging air temperature in the range from t_{min}= 17.07 °C to t_{max}= 29.57 °C. The achievement of the required charging air temperatures allows the verification of simulation impact of temperature on the NO_X formation, which was published in [1].

Acknowledgement

References

[1] HLAVŇA, V., KADÁK, M., MRUK, A. *NOx and extremely low temperatures of charging*. In: Journal of KONES -Powertrain and transport, Vol.17, No. 3, Warsaw 2010, ISSN 1231-4005;

[2] TOPORCER, E., KOVALČIK, A., TUČNIK, P. *Intercooler for extremely low temperatures of charging*. In: Journal of KONES -Powertrain and transport, Vol.17, No. 3, Warsaw 2010, ISSN 1231-4005;

[3] KOVALČIK, A. *Pressure and flow measurement in a nonconventional energetic system*, In proceedings of international conference "TRANSCOM 2009", ISBN 978-80-554-0031-0, proceedings, Section 6, EDIS – Publishing house of University of Žilina 2009.

[4] HUDÁK, A., BARTA, D. *Analýza prúdenia chladiaceho media v okolí valca motora Z8004C. In: Hydraulika a pneumatika: časopis pre hydrauliku, pneumatiku a automatizačnú techniku*, ISSN 1335-5171, vol. 7, No. 1-2, 2005, p.52-54.

Use the Fireplace Insert for Heating Hot Water

*Katarína Kaduchová, Milan Malcho, Richard Lenhard, Stanislav Gavlas
*University of Žilina, Faculty of Mechanical Engineering, Department of Power engineering, Univerzitna 1, 010 26 Žilina, Slovakia, {katarina.kaduchova, milan.malcho, richard.lenhard, stanislav.gavlas}@fstroj.uniza.sk

Abstract. The paper deals problems with heating of hot water in small biomass heat sources. In the development of local furnace small power for burning wood in currently based on the energy policy of the European Union, with particular emphasis on the efficiency of combustion equipment and low exhaust emissions. In recent years there has been, in the context of significant growth in all prices energy, increased interest in the possibility to use fireplace inserts as a local heat source. Reduced consumption leads to heat that is beginning to use the fireplace with a heat exchanger for hot water.

Keywords: Fireplaces insert, hot water, biomass, heat exchanger

1. Introduction

Combustion devices are devices in which the combustion of solid, liquid and gaseous fuels, there is a conversion of chemically bound energy in the fuel into heat, which is then used for heating or hot water.

Combustion devices can be divided into two main groups, namely:

- central (transmit heat released by burning heat transfer fluid (water, oil). Heat transfer fluid is then heated each room, rooms, etc.).
- local (used for space heating, in which they are located. The basic types of structures include stoves, open and closed fireplaces, fireplace inserts. They are used in most cases, as additional sources of heat).

2. The principle activities of the fireplace inserts

Fireplace inserts are finished furnace with adjustable air supply, with glass doors and direct outlet burnt gas in the chimney. They stand in a room alone, or may be incorporated into sheath the fireplace. Part of the heat produced from the fireplace insert is transmitted by radiation, mainly through the glass doors and part of the convection air heating.

Fig. 1. Fireplace inserts

Fireplace inserts are made either as a grate or without grid and material the fireplace inserts is either steel or cast iron. For heating smaller spaces such as huts, respectively smaller spaces can be

used fireplace inserts with built-in hot-water heat exchanger, which heats the heating water. Then some of the heat used to warm air heating especially the space in which the fireplace and some heat is used for hot water heating adjacent rooms with heaters.

3. Heating hot of water

Heating hot of water in small source for combustion of biomass is performed by hot-water heat exchanger. Hot water heat exchangers are usually welded from sheet pressed piece, or pipe and are integrated into the fireplace, while allowing additional heating by water systems heating. The heat exchangers are most commonly placed between the fireplace and flue of fireplace, or in the second shell of fireplace. Hot water may be directly connected to the heating system, or may accumulate to storage for later use.

3.1. Hot water heat exchanger placed in the fireplace inserts

This method is most used in the manufacture of the fireplace inserts. The system is based on that heat exchangers are the rear side, or deflector, and by combustion is walls heated of the furnace, which then heats water which passes through exchanger. Hot water heat exchangers are also mounted in the fireplace, but still as part of a fireplace insert. It is appropriate reason that strong cooling of the fire and there may be more efficient burning of wood, and thus also to greater efficiency.

Fig. 2. Hot water heat exchanger placed in the fireplace insert.

3.2. Hot water heat exchanger of the fireplace inserts

In this case, hot water heat exchanger mounted in the hearth, or to the flue tile liner. The advantage of this arrangement is that the exchanger does not affect the burning in the fireplace, while the residual heat is utilized to the outgoing to chimney. Used to several ways to transfer heat from the flue gas to heating water. Efficiency transport heat can be achieved by appropriate arrangement of heat transfer surface area, or an appropriate ribbing their surfaces.

Fig. 3. Hot water heat exchanger of the fireplace insert.

3.3. Fireplace insert with externally attached hot-water heat exchanger

External hot water heat exchanger can be connected to refer to any fireplace insert. Normally, hot water heat exchangers are available with an output of 10 kW. The system operates on the basis of heat removed from the fireplace insert to a special, heat-resistant fan and blown into the heat exchanger. Copper coil exchanger, in which the water is heated by hot air and circulating pump transports water back into the system. This system has the great advantage of the possible connections more active and effective regulatory and measurement techniques. Another advantage is the possibility of hot-water heat exchanger container and transported to prioritize, or more heat radiators, floor heating or heat water**.**

3.4. Heating of hot water in small heat sources to biomass using heat pipes

Another way to use the fireplace insert for heating hot water is using heat pipe. Heat pipes are hermetically of sealed tubes, suitably filled with working medium, such is antifreeze, water, and alcohol. Heat pipes are installed one end of the up chimney, which not affect the combustion in fireplace and it is utilized outgoing heat up the chimney fireplace insert. The other end of the heat pipe is embedded as a fired heat exchanger to heat hot water tank, where it releases its heat.
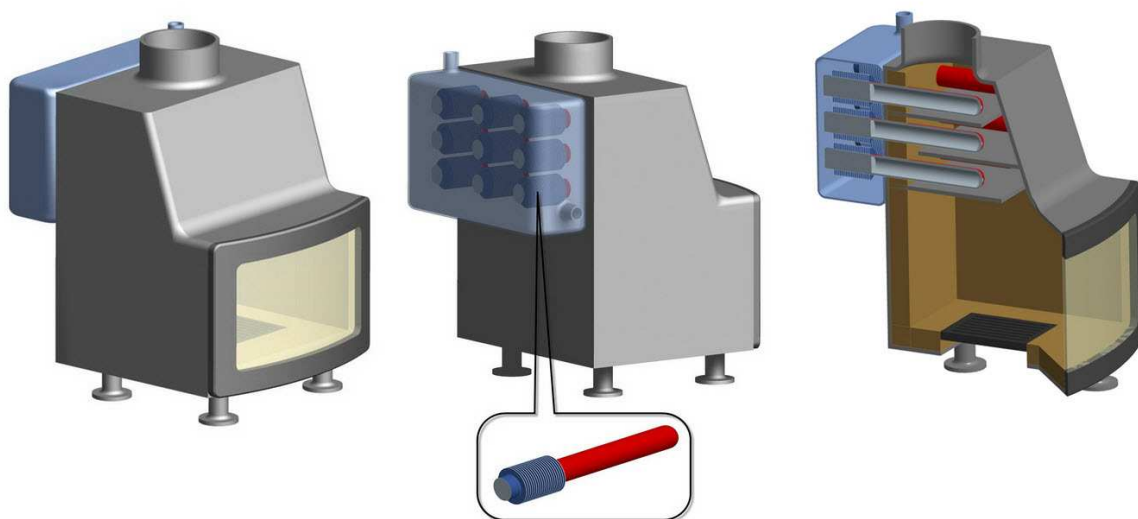
Fig. 4. Fireplace insert with heat pipes

Principle of heat pipe

Heat pipe through the burnt gas at one side is heated, it causes the end of the heating side tube will start working medium in heat pipe evaporate. Subsequently, the steam passes through the tube to the cold end, which is embedded in a hot water heating tank, here condensed prior back into liquid and gravity flow goes back to the warm end, where it evaporates again. This raises the circulation of working medium associated with the transfer of heat to the temperature difference.

In this method of heating hot water will consider capillary heat pipes. As a working medium will be used antifreeze, water, or alcohol. Appropriateness of working medium will detected experimentally.

Acknowledgement

References

[1] JANDAČKA, J., MALCHO, M., MIKULÍK, M. *Technológie pre prípravu a energetické využitie biomasy.* 2007, ISBN 978-80-969595-3-2.

[2] MIKULÍK, M. *Technológie pre kachľové pece*. 2009, ISBN 978-80-969595-6-3.

[3] JANDAČKA, J., PAPUČÍK, Š., KAPJOR, A., LENHARD, R. *Kombinované zdroje tepla na spaľovanie biomasy.* 18. Medzinárodná konferencia Vykurovanie 2010.

[4] NEMEC, P., ČAJA, A., LENHARD, R. Influence working position of heat pipe on their thermal performance, Experimental fluid mechanics 2010, ročník 4, rok 2010,Technicka Univerzita v Liberci 2010, ISBN 978-80-7372-670-6.

[5] NOSEK, R., – JANDAČKA, J. – SZLEK, A. *Simulation of coal combustion process in small boiler*, Fourth Global Conference on Power Control and Optimalization, ročník 4, rok 2010, číslo 1, ISBN 978/983-44483-32.

[6] JANDAČKA, J. – NOSEK, R. – PAPUČÍK, Š. – CHABADOVÁ, J. *Vplyv dávkovania paliva na tvorbu emisií a tepelný výkon domáceho kotla*, SGGW,ročník 24 rok 2010 číslo 73, str. 265, ISSN 1989-5912

[7] PETERSON, G.P. *An introduction to heat pipes: modeling, testing, and applications*. 1994, ISBM 0-471-30512-X.

[8] www.stavebnik.sk

[9] www.krby-kama.cz/sk

[10]www.krby-kachle.etrh.net

[11]http://mijori.sk/

Extreme Combustion Engine Downsizing in Middle Class Vehicles in the Ecological, Economical and Technical Aspects

*Jarosław Kałużny, Jarosław Markowski, Maciej Babiak
*Poznan University of Technology, Faculty of Working Machines and TRANSPORT,
Piotrowo 3, 60-965 Poznan, Poland, {Jaroslaw.Kaluzny, Jaroslaw.Markowski,
Maciej.Babiak}@put.poznan.pl

Abstract. The technological advancement in the production of construction materials, fuels, oils and advancement in the machine construction only adds to the continuous improvement of combustion engines. This development aims at a reduction of the exhaust emissions, reduction of fuel consumption while still ensuring high level of performance (engine parameters) and reliability under different operating conditions. Currently the most discussed issue is the reduction of exhaust emissions and fuel consumption. One of the trends in this matter is seeking new engine design solutions. The paper presents one of the concepts of development of piston combustion engines aiming at far reaching downsizing.

Keywords: emission, supercharged SI engines, downsizing.

1. Introduction

Growing transport needs cause the exploitation of fossil fuels to grow, thus adding to the global emissions to the atmosphere. A combustion engine is the moist widespread powertrain used in transport and its wide application results from such features as: a advantageous ratio of mass to power output, reliable operation, adaptability to different applications and access to wide infrastructure necessary for the engine proper operation. These features have caused that intense search for new sources of propulsion has failed to provide a wide application for any of the alternatives. What is more an objective analysis of the achievements indicates that the combustion engine is still to remain the most widespread source of propulsion for at least the next two decades. The operation of combustion engines is connected with limitations as well - they currently result from growing global environment pollution. In the context of the ecology of engines a particular role is played by the emission of carbon dioxide that grows proportionally to the consumption of fuel. The fuel consumption grows continuously along the growth of the popularity of TRANSPORT. The idea behind the here presented engine concept is the motivation to come up with rational solutions (applicable on a wide scale at limited costs) that would contribute to the efficient reduction of carbon dioxide and fuel consumption in engines used in road transport. In the authors' opinion the most successful method of the reduction of fuel consumption and the exhaust emission is downsizing.

2. The concept of extreme downsizing in a middle class vehicle

Downsizing is a reduction of the engine displacement while maintaining its maximum power output and an improvement of the course of the maximum torque as a function of engine speed. The above listed objectives can be completed through engine supercharging. This is the most efficient way of increasing the maximum value of the mean effective pressure. Engines designed in such a way have a high torque at low engine speeds and that is why in traction applications they are at least equal to the traditional solutions and in many cases they outrank them.

The reduction of the fuel consumption in engines designed in line with the idea of downsizing does not result from the improvement of the efficiency in the whole area determined by the operating conditions. Combustion engines for vehicle applications have been manufactured and perfected for over 100 years and we need to assume that their current level of advancement results from the current level of technology and in such a situation any growth of the overall efficiency is practically impossible. Downsizing reduces the fuel consumption through the change of the operating conditions of the engine. In order to provide equivalent tractive conditions the engine designed in line with the idea of downsizing must operate under higher load- higher against its reduced displacement through mean effective pressure.

The authors see a potential in the development of gasoline engines in the aspect of downsizing. Automotive manufacturers introduce gasoline engines of direct fuel injection and twin charging– an example here may be the TSI engine by Volkswagen – yet, these are usually engine of high power output, designed to be fitted in a relatively small group of vehicles. The TSI engine proves that the supercharging of a gasoline engine and obtaining the maximum values of the mean effective pressure exceeding 2 MPa is possible while maintaining the costs of the construction within rational boundaries. The TSI engine due to its high power output is not suitable for the most popular middle class vehicles.

The authors deem downsizing as extremely suitable, both in terms of ecology and economy in designing two cylinder gasoline engines of the maximum power output of 70 kW for the application in the most popular middle class vehicles.

In serially manufactured European vehicles a two-cylinder engine (with few exceptions) has not been used for decades. The production of two cylinder engines in Europe was seized in the after-war period. They were replaced with larger four cylinder ones. At the then level of technological advancement this policy was entirely understood due to low unit power outputs of the engines. From this historical times superficial judgments remained that two cylinder engines are not suitable for use in vehicles due to a lack of even operation and body vibrations caused by poor balancing of the piston crank assembly. The development of technology can now easily compensate these imperfections by the application of a dual or triple mass flywheel or an electric machine located in the place of the flywheel and additional balancing shafts, not to mention the use of boxer type piston configuration [3]. In the authors' opinion it is worth attempting to verify the already well-rooted convictions, in this case entirely out of date due to technological advancement.

To sum up, the issues that need solution in supercharged two cylinder gasoline engines as a source of propulsion we can divide into the following groups:
1. thermal loads of the engine resulting from the supercharging and high values of mean effective pressures,
2. mechanical loads resulting from supercharging,
3. limitations of supercharging resulting from knocking while still maintaining a relatively high compression ratio conditioning the engine efficiency,
4. exhaust emissions, nitric oxides in particular,
5. lack of torque evenness (in two cylinder engines),
6. engine vibrations resulting from poor balancing of the piston crank assembly.

The authors are sure that the solution of all the listed issues is possible and that it is justified to take action in this matter. In the case of thermal loads the existing analysis of motorcycle engine solutions can be of assistance. Motorcycle engines have high unit power outputs exceeding 200 KM/dm^3. Figures 1 and 2 show an example of a design of a two-cylinder engine that, if supercharged and modified in design, could be fitted in a vehicle.

Fig. 1. Two cylinder Rotax-BMW engine, of displacement of 0,798 dm3 and unit power output of 80 kW/dm^3, used in BMW motorcycles [2]

Fig. 2. Piston crank assembly in the Rotax-BMW engine [2]

3. Development potential resulting from the specificity of a two cylinder engine design

The application of a two cylinder engine as a source of propulsion does necessitate solving numerous issues but at the same time creates new possibilities of development and applications of the technical solutions, whose implementation in classic four cylinder engines is difficult. Naturally, particularly attractive become those solutions that could contribute to an additional redecution of the fuel consumption. The following concepts we can list here: crankshaft support on roller bearing, variable compression ratio and pulse charging.

The problem of the application of roller bearings as crankshaft bearings was an object of a wide scale research project by FEV. The presented reports and publications [4] indicate a possibility of obtaining a much higher engine mechanical efficiency, which results from a high (30%) share of the crankshaft in the total engine friction losses. The said investigation by FEV did not lead to general application of the crankshaft roller bearings. One of the significant hurdles was the need to use divided bearings for crankshafts of four cylinder engines that were the object of the research. A V-type or boxer type two-cylinder engine has only two bearings located at both ends of the crankshaft, which solves the problem of the fitting of bearing that have undivided ball tracks.

The support of a short and rigid crankshaft on only two bearings also creates the possibility of using mechanisms controlling variable crankshaft axis, which enables varying of the compression ratio. Variable compression ratio is a highly desired feature in engines where supercharging was applied as a method of reduction of fuel consumption. A variety of solutions related to variable compression ratio (crankshaft position against the cylinders and cylinder head) have been analyzed in detail in [1, 4].

Pulse charging allows better use of the energy of the exhaust gases, which is a very valuable property in the aspect of improvement of the engine–supercharger operation [5]. A better exploitation of the energy of the exhaust gases may allow a wider cross section of the turbine intake while maintaining good conditions of operation of the engine–turbocharger assembly under dynamic engine load and low engine speeds. This feature is extremely valuable in highly supercharged traction engines. In the case of a two-cylinder engine there is a possibility of separate exhaust feed from two cylinders to the divided turbine intake, which would fully use the advantages of pulse charging.

4. Conclusions

In recent years the research and development works on gasoline engines have been very intense. Such a situation is related to the possibility of application of simple aftertreatment systems that in a relatively economical way lead to more environment friendly powertrains. The issue still to be solved is the engine low overall efficiency that is directly related to the fuel consumption as opposed to a diesel engine. Currently out of the European vehicle manufacturers only FIAT decided to manufacture two cylinder engines for their vehicles – their engines are developed according to the latest downsizing technology. The said engine has a straight cylinder configuration, is turbocharged and is fitted with a balancing shaft. This is the first step towards extreme downsizing of a gasoline combustion engine. The discussion presented in this paper indicates that it is purposeful to apply two cylinder V-type engines in middle class vehicles and because of their multiple advantages they may constitute a final solution.

References

[1] BOLLIG, Ch., HABERMANN, K., SCHWADERLAPP, M., YAPICI, K. *Variable Verdichtung, Ein Weg zur effizienten Hochaufladung*. MTZ 12/2001

[2] GUMPESBERGER, M., LANDERL Ch., MIRITSCH, J., MOSMÜLLER, E., MÜLLER, P., OHRNBERGER, G. *Der Antrieb der neuen BMW F 800*. MTZ 6/2006

[3] ISKRA, A., KAŁUŻNY, J., BABIAK, M. *Możliwości poprawy stopnia nierównomierności biegu 3-cylindrowego silnika spalinowego w układach hybrydowych*. Konmot-Autoprogres 2008

[4] MERKISZ, J., MARKOWSKI, J., KAŁUŻNY, J., MĄDRY, J. *Analiza możliwości poprawy parametrów eksploatacyjnych silnika spalinowego przez zmianę stopnia sprężania i ciśnienia doładowania*. VI Ogólnopolskie Sympozjum Naukowe Doładowanie Silników Spalinowych, 2008

[5] WISŁOCKI, K: *Systemy doładowania szybkoobrotowych silników spalinowych*; WKŁ, 1991

Analysis of Transport Properties of Gravitational Heat Pipes with Using a Different Type and Quantity of Filling

[*]Zuzana Kolková, Alexander Čaja, Milan Malcho
[*]University of Žilina, Faculty of Mechanical Engineering, Department of Power Engineering, Univerzitná 1, 010 26 Žilina, Slovakia, {zuzana.kolkova, alexander.caja, milan.malcho}@fstroj.uniza.sk

Abstract. Using the heat pipe allows the use of waste heat and its removal from the place of origin to the colder environment. Heat pipes work on the thermosyphon principle. While maintaining a small temperature difference to transfer large heat output. Heat transfer is ensured in the process of evaporating in the vaporization part, condensation in the condensing section and a return of the condensate into vaporization part. Heat pipes may be filled with different working substances, whose choice depends primarily on the temperature range of cooling and compatibility with the tube material. Gravitational heat pipes are mainly used in vertical position with the condensing portion located above the vaporization part.

This article analyzes the influence of the type of working substance and its amount on heat output gravitational heat pipes. Parameters necessary to evaluate the performance of heat pipes have been obtained using the experimental device.

Keywords: heat, heat pipe, heat transfer.

1. Introduction

Heat pipe is a simple and ingenious system, which serves to transfer heat output while maintaining a small temperature difference. The use of heat pipes allows for example the use of waste heat and its removal from the place of the heating system. Heat pipes allow solving the tasks related to the desired increase in performance, reducing size and weight of the rising demands for life and operational reliability of electrical equipment.

The heat pipes have various dimensions and shapes according to using and construction of device for which are assigned. The material selection to heat pipe is affected by temperature conditions for which is heat pipe assigned, whether ultra-low or ultra-high temperatures. Every cooling medium used as filling in heat pipes has various chemical and physical properties.

It is also important what amount of substances is used in the investigation of transmission properties of heat pipes. Too little fluid can lead to complete evaporation of excess liquid and can cause flooding of the heat pipe.

2. Production of gravitational heat pipes

Mechanical preparation of production gravitational heat pipe is mainly in the preparation of individual parts of the tube. Sheath of the tube is from a copper tube (in our case the length of 500 mm internal diameter and 13mm external diameter 15mm), filling capillary and sealing components of the heat pipe (Fig. 1.).

This method of implementation was applied to all heat pipes. After filling of desired amount of water and ethyl alcohol (10ml, 15ml, 20ml and 25ml) using a rotary pump to drain the air from the heat pipe. After some time the pressure reached 3kPa (Fig. 2.).

Heat pipes filled with ethyl alcohol (10ml, 15ml, 20ml and 25ml) is required for pumping immersed in a cooling bath. Ethyl alcohol boils at low temperatures. Without cooling, there is boiling and subsequent evaporation of the working substance from the tube. Cooling of the tube was

secured with liquid nitrogen. Filling capillary is closed after pumping air by special pliers. This process prevents the re-intake of air.
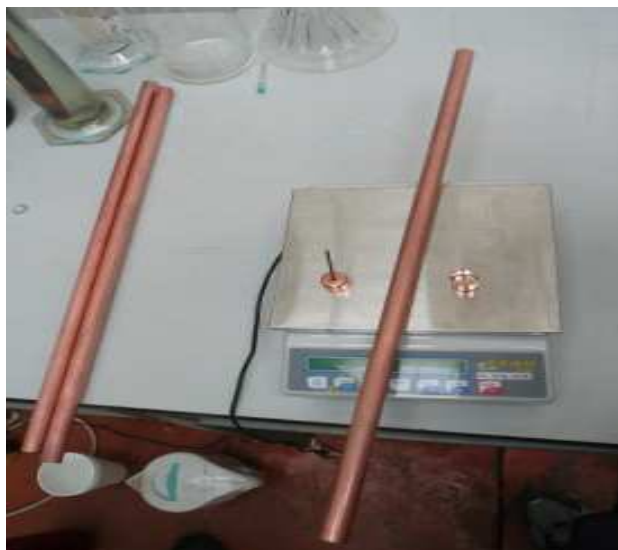
Fig. 1. Different parts of the gravitational heat pipe

Fig. 2. Pumping air through a rotary pump

3. Proposal for a method for measuring the cooling power of gravitational heat pipes

Thermal power transferred heat pipe is measured by the involvement of the picture No. 3. Spiral from copper capillary is wound to the gravitational condensation of the heat pipe contact surfaces of the condenser tube be coated conductive paste to improve heat transfer. In measuring the heat pipes in a vertical position. Vaporization part of the heat pipe is submerged in a container with water heated thermostat (MLW U 15) at 70 ° C. Condensation section with wound spiral and adiabatic part they are insulated over the space of thermostat in polystyrene container to avoid condensation of environmental influences. Input down part of spiral is connected to a water from cooling thermostat (Julabo MODEL SE) at 10° C.

The water passes by spiral across the condenser coil around the part and goes through the ultrasonic flow back into the cooling thermostat. On input and output part of the coil are connected temperature sensors NiCr-Ni, which record a change of temperature of coolant medium. Other thermometers of type Pt100 are in an thermostat to provide heating and cooling and one thermometer reads ambient temperature. Coolant flow rate is measured by ultrasonic flow KAMSTRUP TYPE 66C22A1372. All thermometers and ultrasonic flow meter are connected to the input of measuring units AHLBORN ALMEMO 5690-2 (Fig.4.). The control panel transmits information using special software to personal computer in the form of a Microsoft Excel spreadsheet.

Fig. 3. Connection cooler to flow thermostat

Fig. 4. Experimental measuring device

4. Evaluation of the measured variables

The survey was carried on gravitational heat pipes in a vertical position Water and ethyl alcohol were used to determine transmission characteristics of different capacity cartridges (10ml, 15ml, 20ml and 25ml). Mass flow of cooling water was maintained at 21 liters / hour. Calculation of the temperature difference of cooling water that flows through the coil of copper capillary, scanned on entry and exit of the helix is calculated according to equation (1) in the form

$$\Delta \overline{t_i} = \overline{t_0} - \overline{t_p}. \tag{1}$$

Where:

$\Delta \overline{t_i}$ – the difference of middle temperatures the cooling water in fixed state[°C],

$\overline{t_0}$ – the middle value of output temperature the cooling water [°C],

$\overline{t_p}$ – the middle value of input temperature the cooling water [°C].

The calculation of middle heat pipe power value from measuring values is determined by the formula (2):

$$\overline{Q} = \overset{\bullet}{m}.c_p.\Delta \overline{t_i}. \tag{2}$$

Where:

$\overline{Q}$ – the middle power value in fixed state [W],

$\overset{\bullet}{m},$ – mass flow rate of cooling water [kg/s],

c_p – the specific heat capacity on constant pressure [J/kg.K],

$\Delta \overline{t_i}$ – the difference of middle cooling water temperatures in fixed state [°C].

By analyzing the quantity of filling it was found that the best transmission properties of the heat pipe filled with water volume 15 ml. It is the most effective by heat pipes filled with ethyl alcohol to use volume 20 ml. The water showed better properties by assessing of the type of filling. However, it is not suitable for use in operating temperatures below freezing. Ethyl alcohol is suitable for outdoor use, thus freezing too. Its transmission characteristics are compared with water, a little worse, because it has less heat capacity and latent heat. Comparative graph was created from the transferred heat output (Fig. 5).
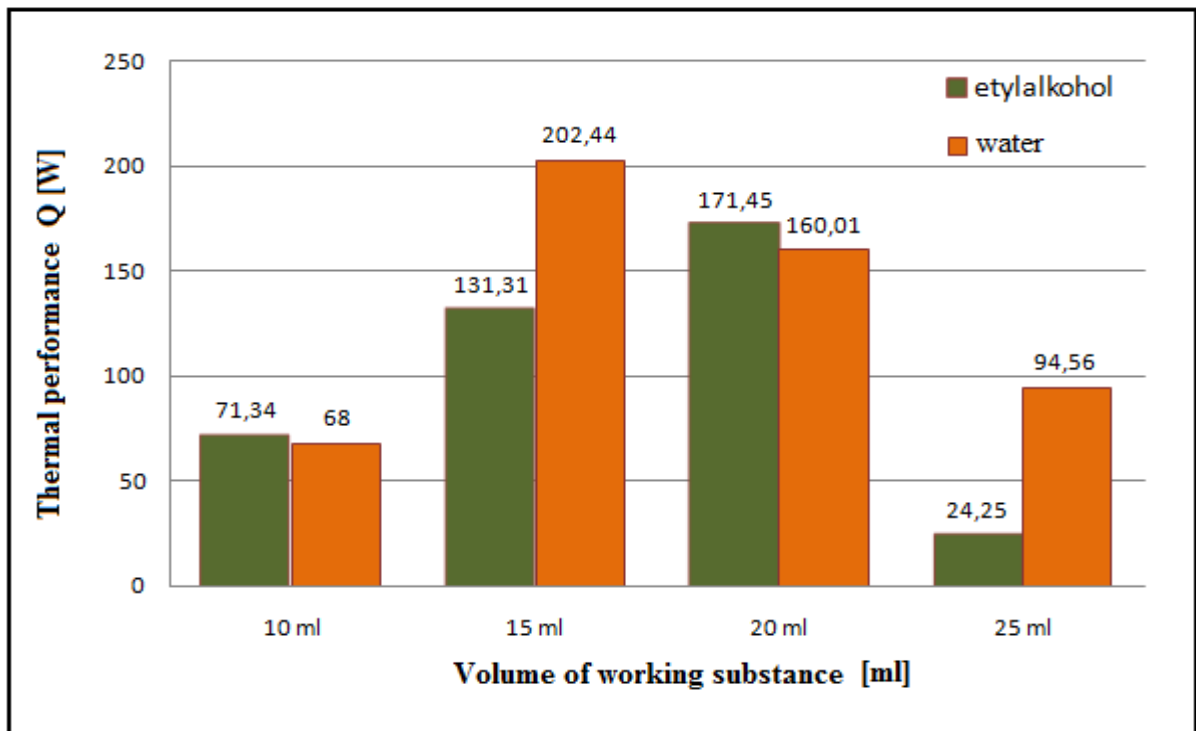
Fig. 5. Comparison between the size of the transferred heat flux heat pipe with two working substances

5. Conclusion

Applied calorimetric method of calculating the thermal power transmitted heat pipe enables you to locate a suitable amount of filling the heat pipe as well as quantify the heat output in the desired range of temperatures. Designed experimental device makes easy to vary the boiling temperature in the heated heat pipe and coolant temperature in the condensing section. At the proposed facility can be tested heat pipes of other geometrical parameters too.

Acknowledgment

References

[1] KOLKOVÁ, Z.: *Vplyv množstva a druhu náplne tepelnej trubice na jej prenosové vlastnosti*, Diplomová práca 2010, Katedra energetickej techniky, Žilinská univerzita v Žiline

[2] HLAVAČKA V., POLÁŠEK F., ŠTULC P., ZBOŘIL V.1990: *Tepelné trubice v elektrotechnice*, SNTL – nakladatelství technické literatury, Praha 1990

[3] REAY, D., KEW, P. 2006. *Heat Pipes Theory, Desing and Applications*. UK: Fifth Edition. 2006. ISBN-13: 978-0-7506-6754-8

[4] ČAJA, A. – NEMEC, P. – JANDAČKA, J. 2009. *Vplyv množstva a druhu náplne tepelnej trubice na odvod tepla*. In Mechanical Engineering journal. Stojárenstvo. ISSN 1335-2938, 2009, s. 22-23

[5] NEMEC, P. – ČAJA, A. – LENHARD, R.: *Thermal performance measurement of heat pipe*, In Book of Abstract on Fourth Global Conference on PCO 2 – 4 Decembre 2010, Kuching – Sarawak–Malaysia, str. 14, ISBN 978-983-44483-32.

[6] VITÁZEK, I.: *Teplotechnika a hydrotechnika*. (2. nezmenené vydanie). Nitra: Vydavateľstvo SPU, 2008, 104 s.

Dry Ice Blasting Technology

[*]Marián Kollár, Peter Zvolenský

[*]University of Žilina, Mechanical Engineering Faculty , Department of Transport and Handling Technology, Univerzitna 2, 01026 Žilina, Slovakia, {marian.kollar, peter.zvolensky}@fstroj.uniza.sk

Abstract. This paper discusses dry ice blasting technology which can be used for cleaning different surfaces. It describes the characteristics of technology, phase and its advantages compared with other technologies. Dry ice blasting technology is in Slovakia still little used.

Keywords: Blasting, Dry ice, Carbon dioxide.

1. Blasting with dry ice, CRYOCLEAN

Dry ice is conventional name for solid form of carbon dioxide. Dry ice sublimates, thus varies from solid-state to gaseous without passing on liquid state by normal atmospheric pressure. Sublimation temperature is -78,5 °C

One of the possibilities of use of dry ice in industry is cleaning. Small particles of dry ice are blown with compressed air against surface to be purified. By this way it is possible to remove residuals on industrial installations, ink, adhesives, oil, color, mold and rubber. This technology is alternative for sandblasting, hot steam cleaning, pressurized water, solvents, because the environmental burden is very low.

Properties of dry ice:
– It is a natural refrigerant with high cooling power,
– It is odorless and hygienic,
– It does not contain pathogens,
– It is bacteriostatic and displaces oxygen in the air,
– It does not melt, does not leave wet imprints and does not damage goods or its packing. [5]

1.1. Dry ice blasting has three phases

Kinetic – when granules (pellets) of dry ice, driven by flow of compressed air, are hitting at speed of sound on surface, they break and release contaminants from purified surface. [1,2]

Thermal – due to its low temperature (-79 °C) it causes on impact on purified material by local undercooling. Due to different expansion coefficients of base material and coating it causes tension that facilitates removal of impurities from the surface. [1,2]

Sublimation – on hit of dry ice pellets it occurs simultaneously their instantaneous sublimation, i.e. the transition from a solid state to the gas phase. At the same time there is approximately 700-fold increase of the volume of gas phase and this „explosive" effect separates contaminant from cleaned surface [1, 2].
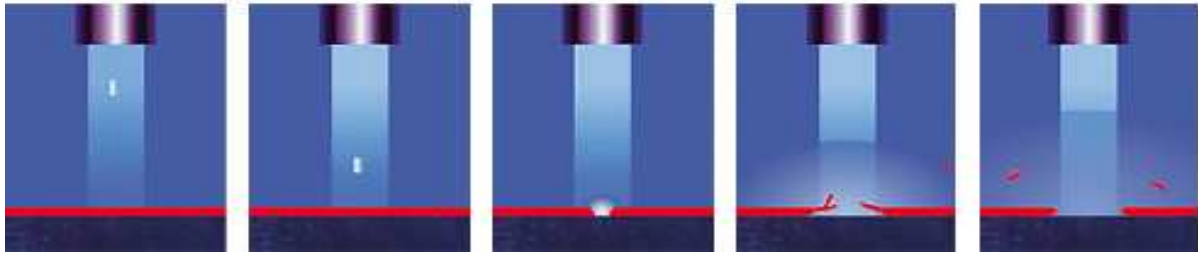
Fig. 1. Principle of dry ice blasting [3]

1.2. Benefits of Dry Ice Blasting

The process of dry cleaning

Dry ice blasting is pure dry process. Dry ice pellets are of CO_2 and they immediately evaporate by contact with the cleaned surface.

No waste

Technology treatment does not produce secondary waste. After cleaning the removed residues are simply swept or vacuum cleaned.

Ecologic

Dry ice blasting system is ecological technology. No leakage of toxic substances occurs and there is no use of support chemicals. It save costs associated with the additional removal of other abrasive media, (sand, slag, soda and the like.), or solvents.

Non-aggressive

Dry ice blasting is non-abrasive. Cleaned surfaces remain undamaged, what can't be achieved by cleaning with steel brush, scrapers or other pressure cleaning (sandblasting, blasting slag, metallic materials and the like.

It enhances the quality of production

Dry ice blasting allows maintaining clean tools and equipment during the manufacturing process, without complicated disassembly or costly equipment downtime. It provides a proven cost reduction.

Quickly and efficiently

The combination of quick cleaning and wide range of application nozzles, allows for effective cleaning also difficult to access parts. There are no remains of cleaning material. It is not necessary to dismantle the cleaned equipment; it is cleaned on the spot. The total time required for the cleaning process, is thus significantly reduced.

Reducing costs

Shortening the machinery downtime. Improving the production quality. Cleaning on site without complex dismantling. It reduces the cost for cleaning and maintenance, replaces expensive and environmentally harmful chemicals and solvents.

Dry ice blasting is appreciated especially by services, where it is not possible to use other, conventional cleaning methods, as solvents or abrasive materials. Abrasive material – dry ice, simply evaporates.

The method is suitable for removing various contaminants such as different sediment, adhesives, carbon deposits, grease, dust, bitumen's, paints and the like. Dry ice is inert and

therefore it is very suitable for cleaning in environments with high hygiene requirements as food or pharmaceutical industry [1, 2].

2. What is needed to use technology
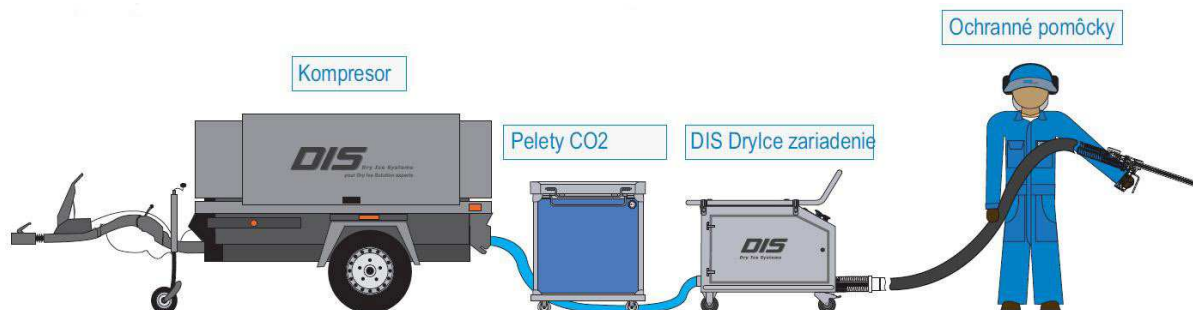
Fíg. 2. Set-up of equipment for dry-ice blasting

Compressor
From $1,5m^3$/ minimum quantity supplied, pressure 6 Bar, stationary or mobile.

Dry ice pellets
Produced in DIS Pelletier or from supplier of industrial gases. Cooler for storage of dry ice pellets.

System DIS Dry Ice
Device for spraying dry ice DIS Dry Ice.

Protective Equipment
Earmuffs, goggles, industrial protective clothing, sufficient fresh air. Fig. 2 [1, 2].

3. Conclusion

Dry ice blasting is a method, which finds very wide range of applications in various industries. It is suitable for cleaning hard to reach parts of machinery and technology units, which are still installed in production. Cleaning does not require dismantling of technological units or disposal of secondary contamination. Impurities are removed after cleaning by vacuum cleaner or are swept. Abrasive material, dry ice, simply evaporates. The blasting is ideal for maintenance of production machinery and facilities where access is difficult. The technology is environmental friendly and hygienic.

References

[1] http://www.icetech.sk/www. Icetech.sk/uvod.html
[2] http://www.ictech.sk/index.php?id=1uvod
[3] http://www.coldjet.com/en/information/what-is-dry-ice-blasting.php

Flow Modeling in an Evaporator of a Nonconventional Energetic System

[*]Andrej Kovalčík, Emil Toporcer, Vladimír Hlavňa
[*]University of Žilina in Žilina, Faculty of Mechanical Engineering, Department of Automotive Technology, Univerzitná 1, 01026 Žilina, Slovakia, {andrej.kovalcik, emil.toporcer, vladimir.hlavna}@fstroj.uniza.sk

Abstract. An alternative medium (lithium bromide liquid) flows in a cooling jacket of a combustion engine of a nonconventional energetic unit. The paper deals with a modeling of flow of a cooling medium in an evaporator, which is a part of a cooling absorption system.

Keywords: nonconventional energetic unit, flow modeling, evaporator, cooling medium, combustion engine.

1. Introduction

A nonconventional combustion engine is a part of a nonconventional energetic system (see Fig. 1). An engine cooling liquid is replaced by mixture of the lithium bromide liquid with water. The solved energetic system is defined in area of trigeneration systems. The mentioned system is a source of electric energy, cold and heat.
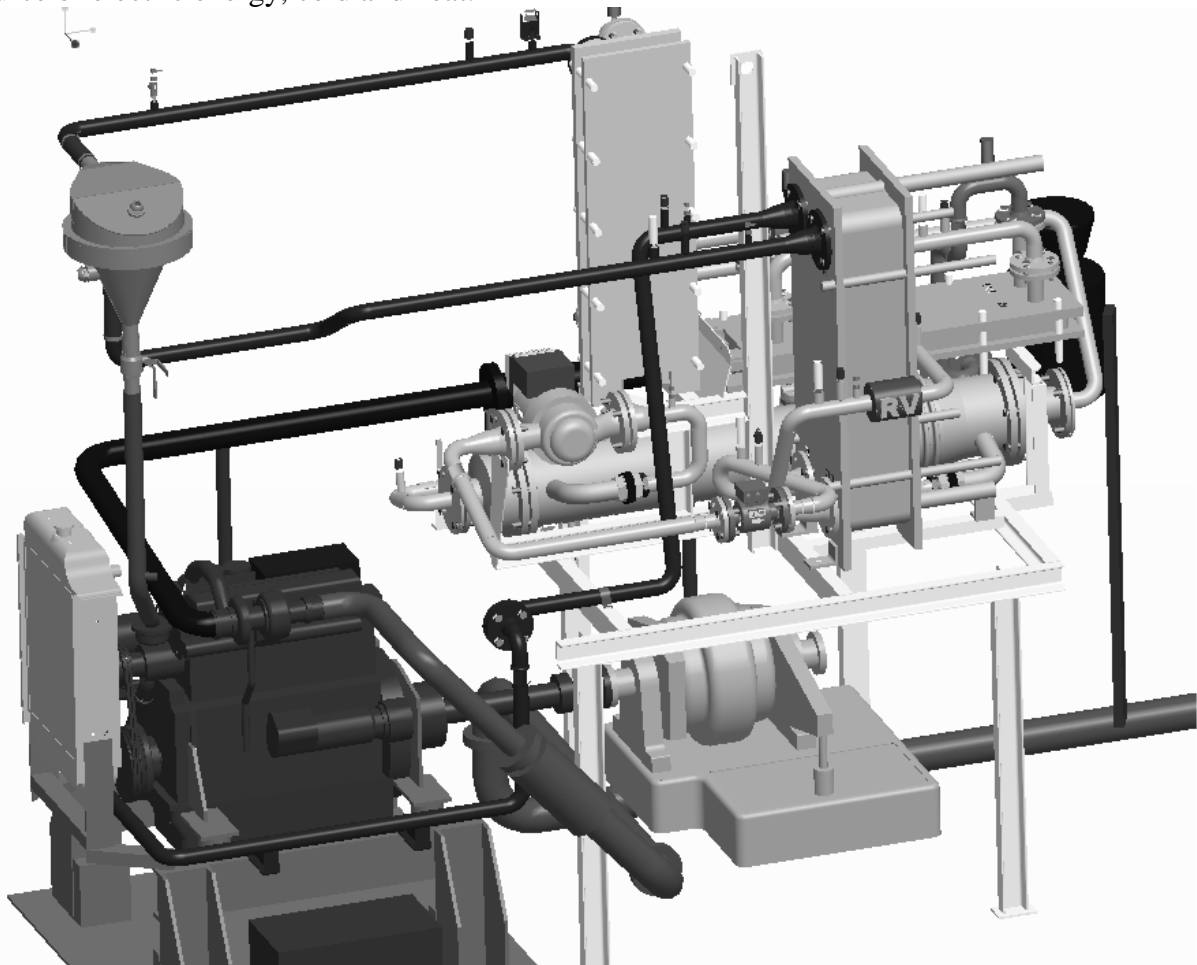
Fig. 1. CAD (Computer Aided Design) model of the nonconventional energetic system

2. Definition of the Model and the Flow Simulation

The space geometrical model corresponding to the geometry of the original evaporator is created in the CAD (Computer Aided Design) software ProEngineer WildFire 2. One half of the evaporator is created because of the decrease in the demand on the computational means. This CAD model is then imported into the preprocessor Gambit. The imported model is repaired and a suitable mesh is then created. The last step is the definition of the types of boundary conditions. The resulting computational mesh consists of about 455 000 elements and is illustrated in the Fig. 2.

The created computational mesh is imported into the CFD (Computational Fluid Dynamics) code Fluent. The boundary conditions are specified by their specific values. The time step has the value of 0.001 s. The RNG k-ε turbulent model is used for the mathematical model.
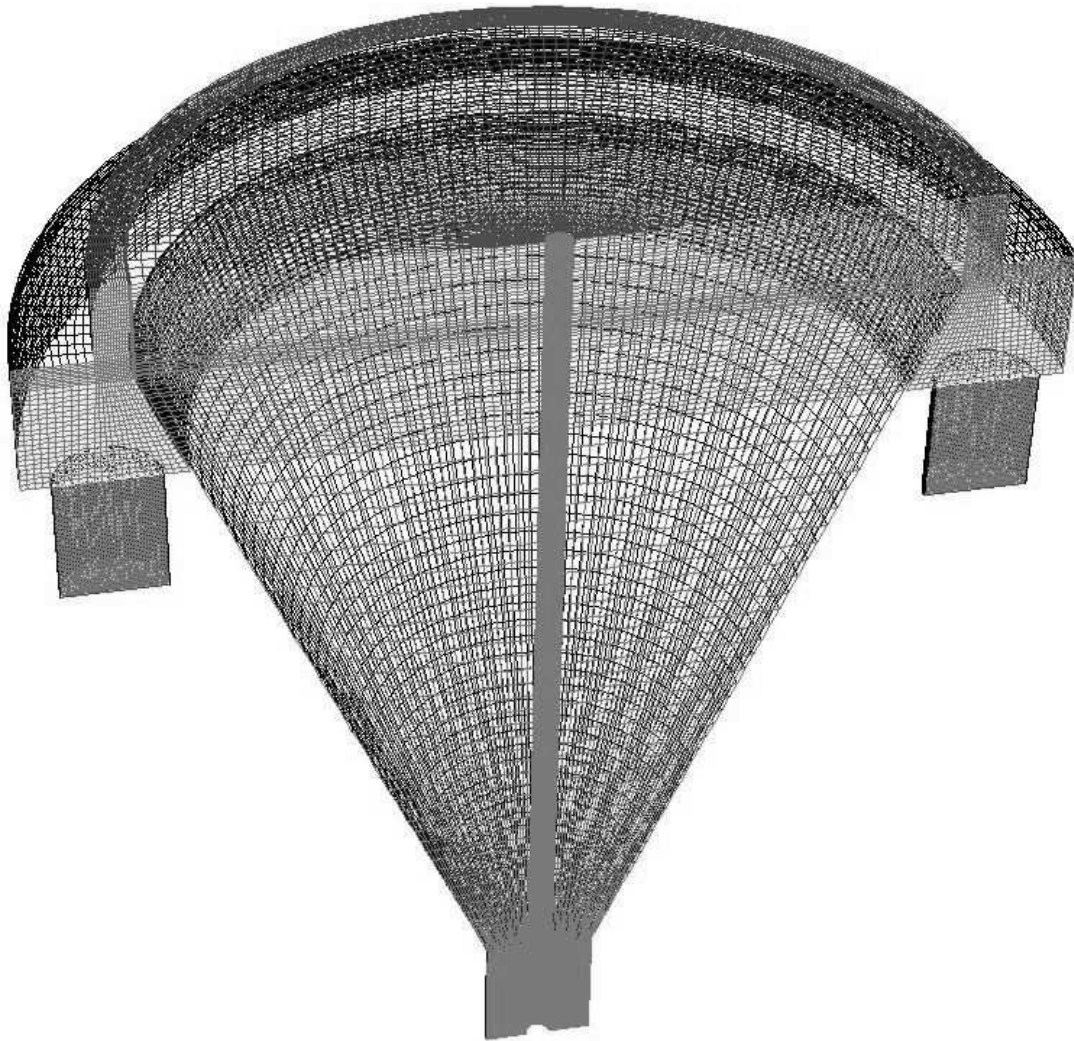
Fig. 2. The computational mesh of the evaporator

3. Achieved Results

The filling of the evaporator ring by the cooling medium is shown in Fig. 3, 4 and 5. The off-take is able to take away all the needed amount from the evaporator. The simulation shows that the lithium bromide liquid starts to pour through the edge of the evaporator cone in the time of about 2.5 s after the initiation of the calculation. The starting cooling liquid level has the value of 1 cm under the edge of the evaporator cone. The value of 1 cm is used because of the decrease in the computational time.

Fig. 3.   Coolant level in the evaporator in the time of 2.5 s
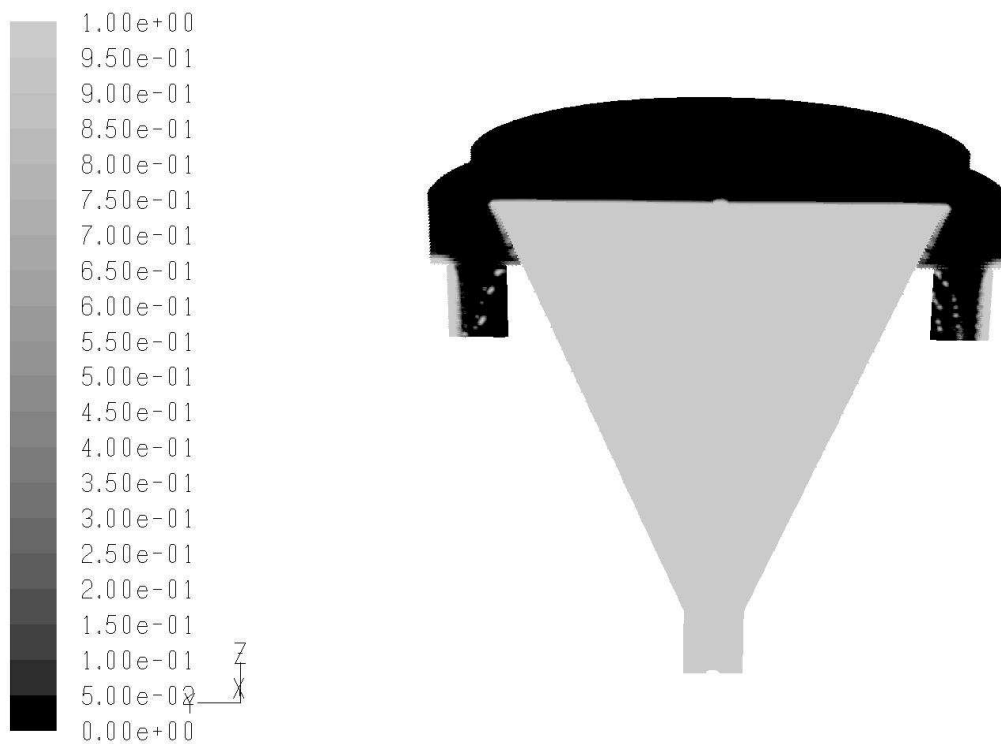
Contours of Volume fraction (libr)   (Time=5.0000e+00)   Mar 10, 2009

Fig. 4.   Flow in the evaporator in the time of 5 s

Contours of Volume fraction (libr)   (Time=2.5000e+01)   Mar 10, 2009
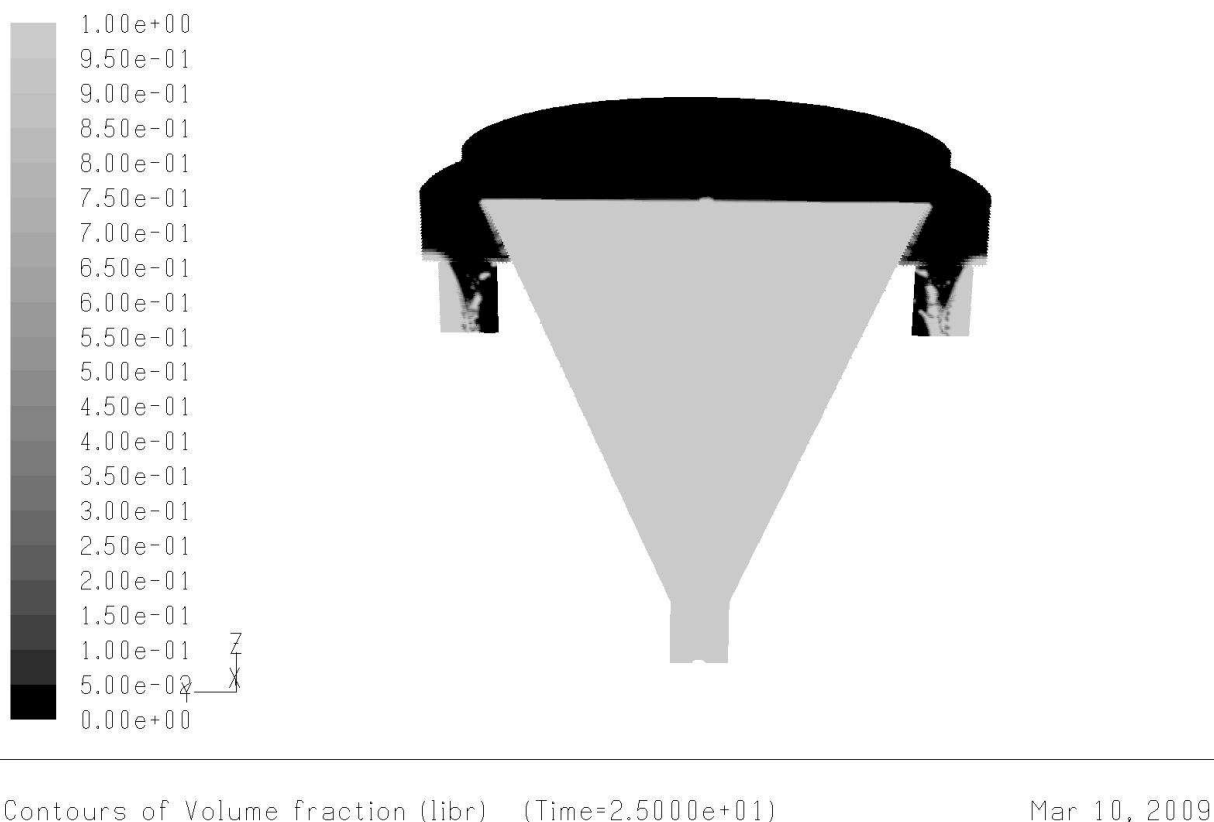
Fig. 5. Flow in the evaporator in the time of 25 s

4. Conclusion

The simulation shows that the cooling medium starts to pour through the edge of the evaporator cone in the time of about 2.5 s after the simulation starts. In the presented Figs. 4 and 5 it can be seen that the off-take is able to take away the needed amount of cooling liquid from the evaporator.

Acknowledgement

References

[1] HUDÁK, A., BARTA, D. *Analýza prúdenia chladiaceho media v okolí valca motora Z8004C*. In: Hydraulika a pneumatika: časopis pre hydrauliku, pneumatiku a automatizačnú techniku, ISSN 1335-5171, vol. 7, No. 1-2, 2005, p.52-54.

[2] KONDEPUD, D. *Modern Thermodynamics*. John Wiley and Sons, 1998.

[3] LABUDA, R., ISTENÍK, R. *Vplyv dynamiky zmeny režimu spaľovacieho motora na jeho prevádzkové veličiny*. In proceedings of the international conference KOKA 2005, ISBN 80-01-03293-0, CTU Prague, Prague, 2005, p.173-178.

[4] LÁBAJ, J., BARTA, D. *Unsteady flow simulation and combustion of the ethanol in diesel engines*. In: Communications, ISSN 1335-4205, Vol. 8, No. 2, 2006, pp. 27-37.

Measurement of Particulate Matter of Combustion Engine

[*]Jozef Krakovský, Vladimír Hlavňa, Andrej Kovalčík

[*]University of Žilina, Faculty of Mechanical Engineering, Department of automotive technology, Univerzitna 1, 01026 Žilina, Slovakia, {j.krakovsky, v.hlavna, a.kovalcik}@fstroj.uniza.sk

Abstract. The production of engine emissions is negative effect of the combustion process of fuel-air mixture in combustion chamber. The variety of reasons of production emissions are quality of combustion, combustion velocity and chemical facilities of fuel-air mixture. Subsequently the amount of emissions is needed monitor and analyze. The correct monitoring and analyzing of harmful pollutants enable to reduce of impact on the living environment. The paper deals with the method of analyze of particular matter in the engine exhaust emission of diesel engine.

1. Production of emissions

The emissions accrue from the combustion process of fuel-air mixture in engine cylinder. Quantity and part of emission-particles is depended on chemical fuel composition and combustion process. Fig.1 shows the percentage part of exhaust emissions in combustion gas.

Fuel ($C_nH_mO_l$) + Air (O_2N_2...)

⇩

Burning

⇩

Exhaust emissions				
CO_2 + H_2O + N_2 + O_2	CO	HC	NO_X	PM
↓ ↓ ↓ ↓	↓	↓	↓	↓
<15% <10% <72% <1%	<1%	<0,5%	<0,5%	<0,5%
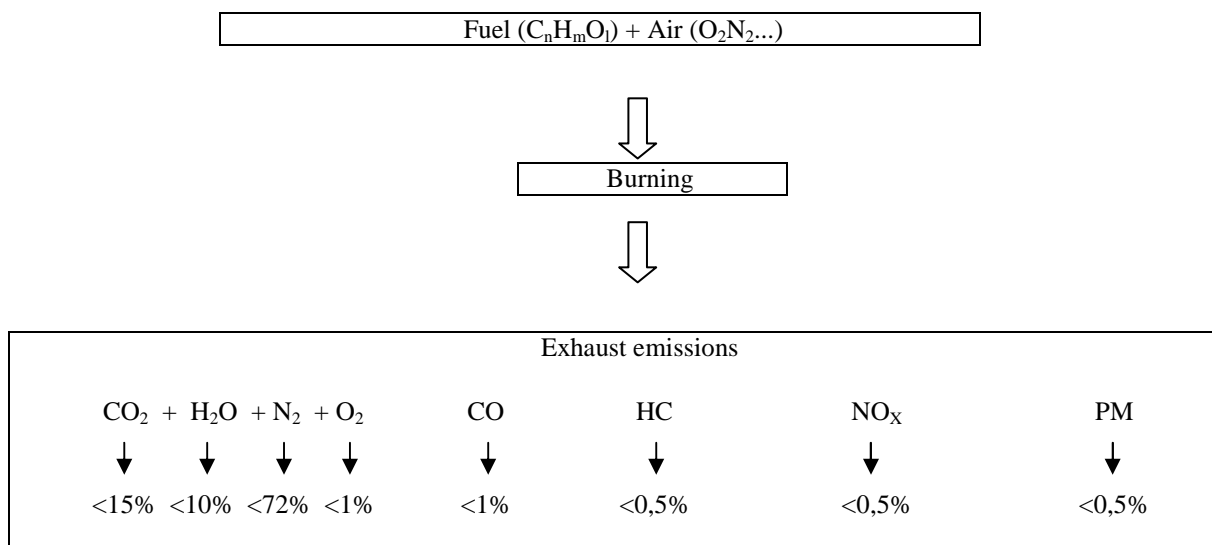
Fig. 1. Percentage part of exhaust emissions

2. Particulate matter and soot

By analysis of exhaust there are obtained information about the exhausts physical and chemical properties. On Fig.2 we can see that the percentage of particulate matter of exhaust gases is about 0,5%. Particulate matters are defined as all elements which are retained on the precisely defined filter during measurement. The greatest part of particulate matters consists of soot and hydrocarbons.

2.1. Soot

Soot is the product of incomplete combustion process. It arises due lack of air in combustion space of the engine. The favorable circumstances for soot formation are long injection time and thermal decomposition of fuel [1]. Sources of the soot creation are fuel and oil. Soot belongs to the group of not burned residues of gaseous and liquid fuels. These solids are made in gas phase and they cause yellow luminous flame. This is happening if the used fuel is diesel. Soot underlying smoke of the diesel combustion engines.

Smoke is defined as coloring of the exhaust gas. The smoke is measured in HSU (hartridge smoke units): $0 \div 100$ or in absolute unites absorption coefficient m^{-1}: $0 \div \infty$. Measuring of smoke of the combustion engines is necessary to do in order to not crossing the emission limits. Smoke, as an idea, was associated only for the diesel engines but with the coming a new EURO norm number 5, it has began to concern for the petrol combustion engines with direct-injection gasoline, too.

3. Measuring of the particulate matter

In defining the physical character of the particulate matter is the main emphasis for weight, dimensions and shape given. Chemical character of the particular matter is not analyzed, because of high difficulty and low relevance [2]. The amount of the particulate matter is measured by several methods. There are:
- gravimetric method,
- optical method,
- photo-acoustic method,
- frequency method,
- laser anemometry,
- method of the measuring of pressure on the filter.

From the previous options of the measurement methods is the gravimetric method most used.

3.1. Gravimetric method

The principle of the gravimetric method is weighing of precisely defined filters. Filters are weighted before and after a measurement. Difference of filter's weights is equal to weight of the particular matters. Before and after the measurement filters must be stabilized in the special chamber shows on Fig. 2.

Humidity and temperature are maintained on the same value in this chamber. The special filters must be stabilized at least for 8 hour in this chamber. The humidity is maintained about $30 \div 60\%$. The temperature is maintained between $20 \div 30$ºC. Stabilization is necessary to do in order to guarantee the same options before and after sampling. Possibly changing conditions would have negative consequences to measurement accuracy, because weighed mass is very low.

Fig. 2. Special weighing chamber

The measurement takes place on precisely declared points of the selected technical characteristics. Also the manipulation with filters must be with special tools only. If it is necessary to take filters after the measurement to another place, we can take them only in Petri dishes or in a special removable disc shows on Fig. 3. This is necessary to do in order to maintain the same humidity of the filters.

Fig. 3. Special removable disc with filters

During the measurement process pass specified quantity of the exhaust gas through the filters. Crossing gas through the filters is exhaust gas filtered and the particular matters are captured by the filter. Fixed part of the exhaust is transported from the exhaust tract to isokinetic probe where it is diluted with clean air. This action is necessary to do because of reduce temperature of the mixture of exhaust gas and clean air. The temperature on the filters not exceed 52ºC in order to not destruction them. The whole process is getting on within narrow limits of parameters like a exhaust flow, clean air flow, humidity, pressure and especially of the temperature.

4. Conclusion

Smoke of the diesel combustion engine is negative reality of the current status of the traffic. Gravimetric method, like one of the several methods for analyzing amount of the particular matters, is difficult process. During the processes of gravimetric method it is necessary to observe a lot of measuring practices with maximum accuracy. Early and accuracy analysis of particular matters creation can help to avoid the negative consequences of the environment.

References

[1] LÁBAJ, J.: *Spaľovanie a plameň*. Book center in Žilina, 2002

[2] MERKISZ, J.: *Emisja czastek stalych przes silniki spalinowe o zaplonie samoczynnym*. Editorship of University Politechniki Poznanskiej, 1997

Robotics and Automation Systems Applied on the Modern Battlefield

[*]Jakub Kulpa

[*]Kielce University of Technology, Department of Mechatronics and Machine Building,
Tysiąclecia Państwa Polskiego 7, 25-314 Kielce, Poland, jakub-kulpa@wp.pl

Abstract. Partly autonomous robotic combat systems are increasingly used on the modern battlefield. These are used to eliminate the human factor during hazardous activities, fulfill the roles of observation and combat. Through the uses of modern automation systems, weapon becomes much more precise. The paper presents selected examples of automated systems for combat.

Keywords: robotics, automation, control, robot, weapon.

1. Introduction

Ideally, robot soldiers would be able to achieve the same military goals a human group could manage. They'll have to be autonomous and able to identify targets, distinguish between friendly and enemy forces, engage the enemy and interact with others in ways beyond simply firing a weapon. Right now, most robots [1] are controlled remotely by a human being at a command station, though some robots have limited autonomy and can get from point A to point B with minimal supervision. For a robot army to be an effective fighting force, it would be best if individual robots could assess situations and make decisions without relying on human input.

The Army continues to work with government agencies like NASA, universities and corporations to push for more research into achieving this goal [2]. Part of the Future Combat Systems Program is the Autonomous Navigation System (ANS) project. ANS's goal is to create a modular navigation system that technicians can install in all unmanned and manned ground vehicles. The system will include navigation sensors, global positioning systems (GPS), inertial navigation systems (INS), perception sensors and collision detection software.

The robots are divided into four categories:

- Unmanned Aerial Vehicles (UAV) designed for surveillance and reconnaissance missions;
- Small Unmanned Ground Vehicles (UGV) that can enter hazardous areas and gather information without risking the lives of soldiers;
- Multifunctional Utility/Logistics and Equipment (MULE) vehicles designed to provide combat support in conflict situations;
- Armed Robotic Vehicles (ARV) that weigh 9.3 tons and can either carry powerful weapons platforms or sophisticated surveillance equipment.

2. Selected examples of applied robotics systems on the modern battlefield

2.1. SWORD robot

Most popular of automated machine that are on army equipment is a SWORD Robot. The full name is Special Weapons Observation Reconnaissance Detection System. Robot was designed by Bob Quinn and it is a composed of weapon system mounted on unmanned   standard Talon chassis designed by Foster-Miller which is mostly used by sappers.

There are a many different weapons which can be mounted on the SWORDS; M16 rifle, 5.56 mm SAW M249, 7.62 mm M240 machine gun, 0.50 cal M82 Barrett rifle, a six barreled 40 mm grenade launcher or quad 66 mm M202A1 FLASH incendiary weapon.

Those robots are created to replace a soldier or to help them in difficult actions. Some of these jobs, such as getting rid of bombs or walking through minefields, have the potential to save many human lives.

Fig. 1. SWORD robot model

Sword robots are controlled by human [3]. It is used to increase a distance between the soldiers and enemy force. The soldiers can participation in the action, without of risk to be killed.

The first stage of the project was to design a chassis which give possibility to move on different grounds like rocks, sands, snows and event under the water. Robot is equipped with 5 cameras. One is behind the scope and gives possibility to aim to the target. Second one is on the top and it can be rotated in 360 °, next one is on the left side it is wide angle camera with zoom. The next two are erected on front and back of robot. The robot is controlled via a handheld console.

2.2. The Starstreak High Velocity Missile

The Starstreak High Velocity Missile (HVM) system is a close range surface to air missile (SAM), which has the capability to engage lightly armored land vehicles although the missile's main strengths is when combating air targets. The missile is a laser-beam riding system, one of its kind, which, because of its particularly precise laser control and rapid duration of flight, can overcome a mixture of threats, together with airborne targets such as Unmanned Aerial Vehicles (UAVs) and helicopters, added to exterior targets, stationary systems or stands.

Fig. 2. HVM rocket

Once the missile is at a harmless distance from the operator, the second phase rocket motor will fire. As the second phase is used up, the three dart sub-munitions are out. Each dart is made up of a revolving fore-body with two canard fins connected to a non-revolving back installation including four fins. In addition, the back installation contains the electronic components that direct the missile device. The missiles are controlled (for the indication of the direction) by two laser beams into a 2D matrix by the target seeking element. The laser is adjusted in relation to its situation in the anticipated medium. Such adjustment is identified by each of the sub-munitions.

2.3. Unmanned aerial vehicle- Predator

The Predator is an unmanned aerial vehicle (UAV) used primarily by the United States Air Force (USAF) and Central Intelligence Agency (CIA) for surveillance and reconnaissance missions. Initially conceived in the early 1990s for reconnaissance and forward observation roles, the Predator is equipped with cameras and other sensors but has been modified and upgraded to carry and fire two AGM-114 Hellfire missiles or other munitions.

The Predator and sensors are managed from the ground station via a C-band line-of-sight data link or a satellite data link for beyond-line-of-sight operations. The crew in the ground control station is a pilot and two sensor operators. The aircraft is equipped with the AN/AAS-52 Multi-spectral Targeting System, a color nose camera (generally used by the pilot for flight control), a variable aperture day-TV camera, and a variable aperture infrared camera (for low light/night). At the beginning, Predators were equipped with synthetic aperture radar for looking through smoke, clouds or haze, but it was removed to reduce weight. The cameras produce full motion video and the synthetic aperture radar produced still frame radar images. There is sufficient bandwidth on the data link for two video sources to be used at one time, but only one video source from the sensor ball can be used at any time due to design limitations. Either the daylight variable aperture or the infrared electro-optical sensor may be operated simultaneously with the synthetic aperture radar, if equipped.

Fig. 3.   Unmanned aerial vehicle – Predator

The newest Predators models are equipped with a laser designator that allows the pilot to identify targets for other aircraft and even provide the laser-guidance for manned aircraft. The system can be deployed for worldwide operations. The Predator aircraft can be disassembled and loaded into a container for travel. The ground control system and PPSL are transportable in a C-130 Hercules (or larger) transport aircraft. The Predator can operate on a 1,524 meters by 23 meters hard surface runway with clear line-of-sight to the ground data terminal antenna. The antenna provides line-of-sight communications for takeoff and landing.

2.4. Powered exoskeletons

Humans have long used armor as an artificial exoskeleton for protection, especially in combat. Exoskeletal machines (also called powered exoskeletons) are also starting to be used for medical and industrial purposes, while powered human exoskeletons are a feature of science fiction writing, but are currently moving into prototype stage.

A powered exoskeleton, also known as powered armor is a powered mobile machine consisting primarily of an exoskeleton-like framework worn by a person and a power supply that supplies at least part of the activation-energy for limb movement. Exoskeletons are created to help and protect the user. They could be applied, for example, to assist and protect soldiers or construction workers,

or to aid the survival of human in other hazardous environments [4]. A wide medical market exists in the future of prosthetics to provide mobility assistance for aged and infirm people. Other possibilities include rescue work, such as in collapsed buildings, in which the device might allow a rescue worker to lift heavy components, while parallel protecting the worker from falling rubble.

Fig. 4. XOS 2 Raytheona exoskeleton

Engineers also want to apply exoskeletons in the army. It can be used to help soldiers in difficult tasks, such as loading rocket or carrying heavy equipment. XOS 2 Raytheona exoskeleton gives many new possibilities to human like extra strength and stamina. But the main problem which has to be solved is a power supply.

3. Conclusion

There are many possibilities of applying the new fields of automatics and robotics on the modern battlefield. The idea is to replace humans by intelligent machines and use them in place where the human don't have access. It is possible to send a robot like SWORD to recognize the situation which can eliminate the human factor. Combat robot designing is quite difficult and very expensive. For this moment it is impossible to create autonomous robot which can recognize who is ally or enemy. Event when we create this kind of machine there is a risk related with eventual software or hardware errors which can be dangerous for operator. A hard problem to solve is the power source. For example the exoskeletons can work only when supplied with power cable. Military robots must undergo rigorous testing for eliminate potential errors and problems during missions. Rapid development of robotic warfare brings us closer to futuristic battles carried out by the intelligent machines.

References

[1] MORECKI. A, KNAPCZYK, J. *Podstawy robotyki.* Warszawa. WNT, 1999.

[2] MISZALSKI, W. *Inteligentne roboty wojskowe.*Warszawa: Instytut Logistyki Wojskowej Akademii Technicznej, 2001.

[3] SPONG, M, VIDYASAGAR, M. *Dynamika i sterowanie robotów*. WNT, 1997.

[4] GREENMEIER, L. *Real-Life Iron Man: A Robotic Suit That Magnifies Human Strength*., Scientific American,2008

[5] Website materials

Running Variability of Low Loaded SI Engine with High EGR Rates

[*]Ľubomír Miklánek
[*]Czech Technical University, Faculty of Mechanical Engineering, Technicka 6, 166 07 Prague, Czech Republic, {lubomir.miklanek}@fs.cvut.cz

Abstract. Content of this article is description of experimental investigation of running variability changes of a spark ignition (SI) engine in a low load by uncooled recirculated exhaust gas (EGR) delivery into the intake. Changes in running variability of the low loaded SI engine were investigated in the framework of the research of possibilities for engine efficiency increasing by decreasing of pumping work during the charge exchange. Examined engine was four stroke, naturally aspirated and natural gas fuelled with stoichiometric concept. Pumping work was decreased by EGR delivery. Significant decrease of pumping work was obtained only under very high EGR rate conditions. However, the running variability was significantly increased under the same very high EGR rate conditions.

Keywords: Running variability, SI Engine efficiency, low engine load, EGR.

1. Introduction

It is generally known, that the SI engine efficiency in the low load is very small, [1]. Internal combustion (IC) engine in a vehicle is working in the low load about 50% and more of the whole operating time, especially in urban traffic. That is why, the engine efficiency in the low (part) load is very important. Just small increase of engine efficiency may have a significant effect on fuel combustion and thereby CO_2 emissions especially in urban traffic. That is the reason for continuation of research of possibilities for low loaded SI engine efficiency increasing at the author's workplace.

In this research, the pumping work decrease by uncooled EGR delivery into the intake was investigated. Decrease of pumping work by various EGR rates is shown in Fig. 1.
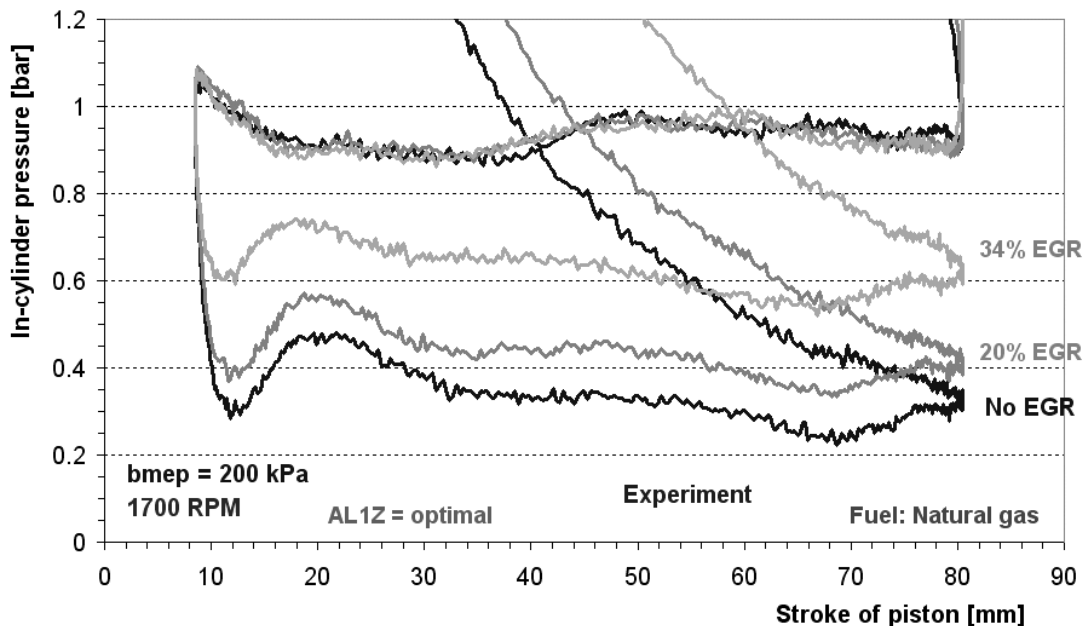

Fig. 1. Change of in-cylinder pressure patterns of SI engine during the charge exchange by various uncooled EGR rates, 1700 RPM, bmep=200 kPa.

In-cylinder pressure patterns in the low-pressure part of working cycle of low loaded SI engine are shown in Fig. 1. As visible, the work for charge exchange is decreased with increase of EGR delivered into the engine intake. Significant decrease of work for charge exchange appears only under high EGR rate conditions. Patterns, shown in Fig. 1, were acquired during the steady-state dynamometer tests at naturally aspirated and natural gas fuelled SI engine Skoda 781 with stoichiometric concept. More about the experiments and data evaluation is described in [2].

The question is how the running variability of SI engine will be changed under mentioned very high uncooled EGR rate conditions. Similar experimental research was already carried out at another workplace, see [3], however without running variability investigation.

2. Data Acquisition for Running Variability Investigation

To investigate the running variability of SI engine under conditions of very high EGR rate (over 20%), the experiments described below were carried out with appropriate data acquisition. Scheme of the appropriate data acquisition for running variability investigation is shown in Fig. 2.
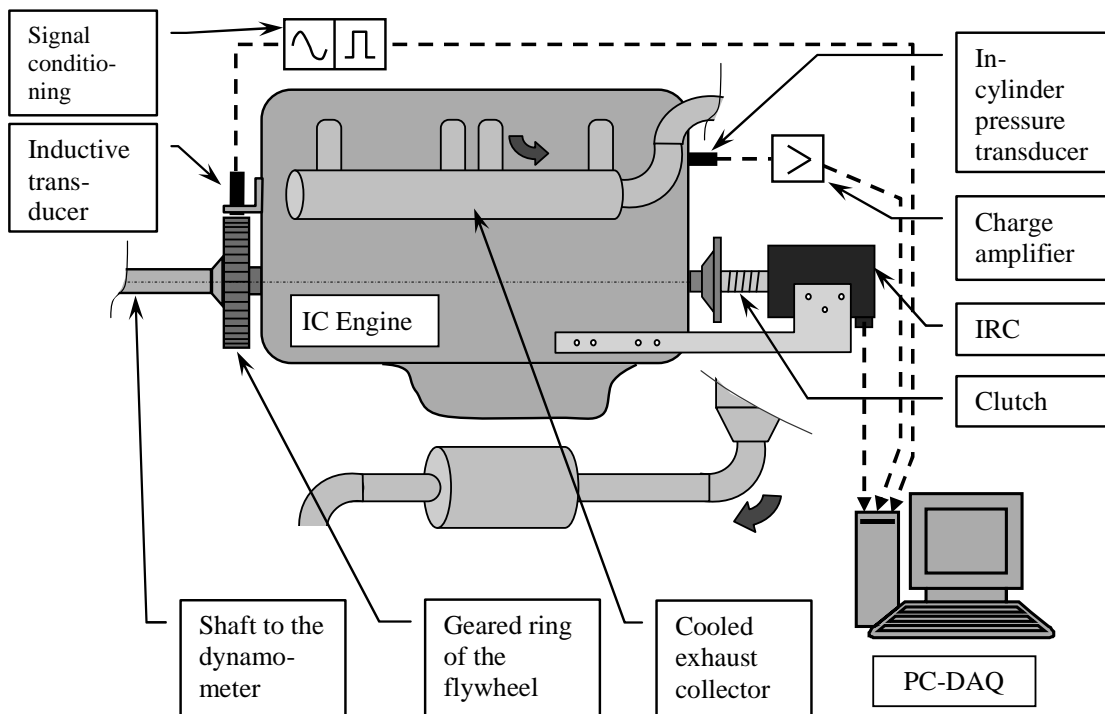
Fig. 2. Scheme of the data acquisition usable for running variability investigation of the tested SI engine.

As it is visible in Fig. 2, data for running variability evaluation were sensed using inductive transducer at the flywheel side of the engine crankshaft. The teeth of geared ring of the flywheel (124 teeth) were used for pulses generation in inductive transducer.

At the pulley side, the incremental rotary encoder (IRC) was placed. IRC was coupled with crankshaft due to a clutch.

Pulses from inductive transducer had to be conditioned to TTL standard and then were sensed using a counter card with very high clock tick frequency (50 MHz), [4]. However, IRC was applied for sampling the in-cylinder pressure data acquisition. In-cylinder pressure data acquisition was in progress simultaneously with data acquisition for running variability evaluation.

Engine speed was chosen at value 1700 RPM during the experiments. Loading of the engine was chosen at the value of brake mean effective pressure (bmep) 200 kPa, which was about 23% of the maximal load of the tested engine.

3. Data Evaluation, Results

A special software, developed at author's workplace, [5], was used for evaluation of recorded data both of in-cylinder pressure patterns and running variability. Because recorded patterns of instantaneous speed from applied sensor were interfered with undesired frequencies, a filtration using Fourier analysis was used. Fourier series for periodic function upon [6] is defined:

$$f(t) = B_0 + \sum_{n=1}^{\infty} A_n \, sin(\, n\omega t\,) + \sum_{n=1}^{\infty} B_n \, cos(\, n\omega t\,) \qquad (1)$$

where:

A_n, B_n:	coefficients of Fourier series;	n:	harmonic (integral) number,
t:	time;	ω:	angular frequency.

Consecutive, the final patterns of measured instantaneous crankshaft speed were made by choosing selected harmonic components using Inverse Fourier Transformation (IFT) with goal to suppress undesired interference. These conditioned patterns of measured instantaneous crankshaft speed are shown in Fig. 3 together with calculated patterns from in-cylinder pressure data in case of NO EGR. In this way, it is possible to compare the instantaneous crankshaft speed calculated from combustion progress (assumed it is the same in all cylinders) to measured patterns.
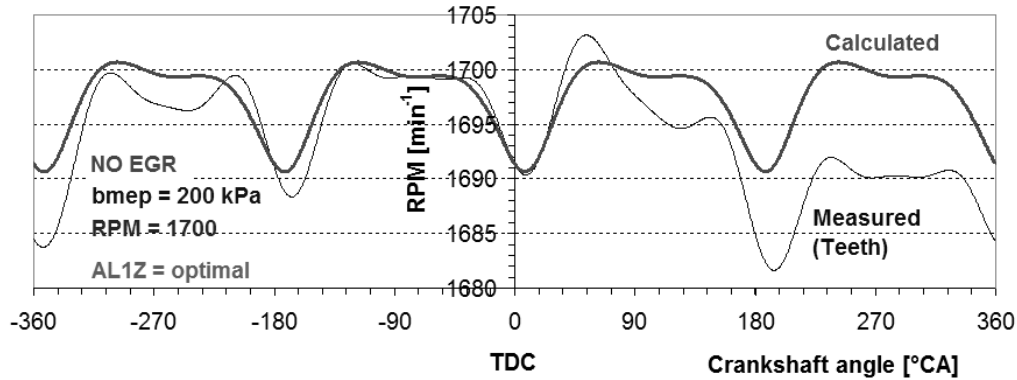

Fig. 3. Measured and calculated patterns of instantaneous crankshaft speed in case without EGR delivery.
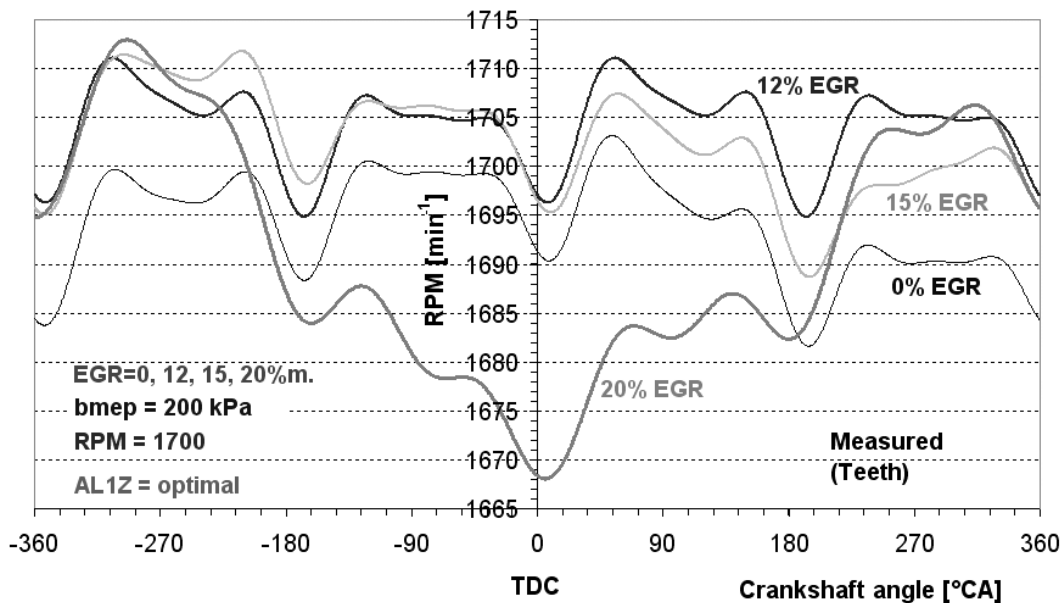

Fig. 4. Measured patterns of instantaneous crankshaft speed in case of EGR rate up to 20%m.

Measured (and conditioned using IFT) patterns of the instantaneous crankshaft speed of tested engine in the case of uncooled EGR rate from 0 to 20 % (by mass) are shown in Fig. 4. As it is visible, the running variability of engine is changed negligible up to the EGR rate of 15 %. However, running variability is increased with EGR rate increasing at the value of 20%.

In Fig. 5, we can recognize the further increase of running variability of engine with uncooled EGR rate increasing.
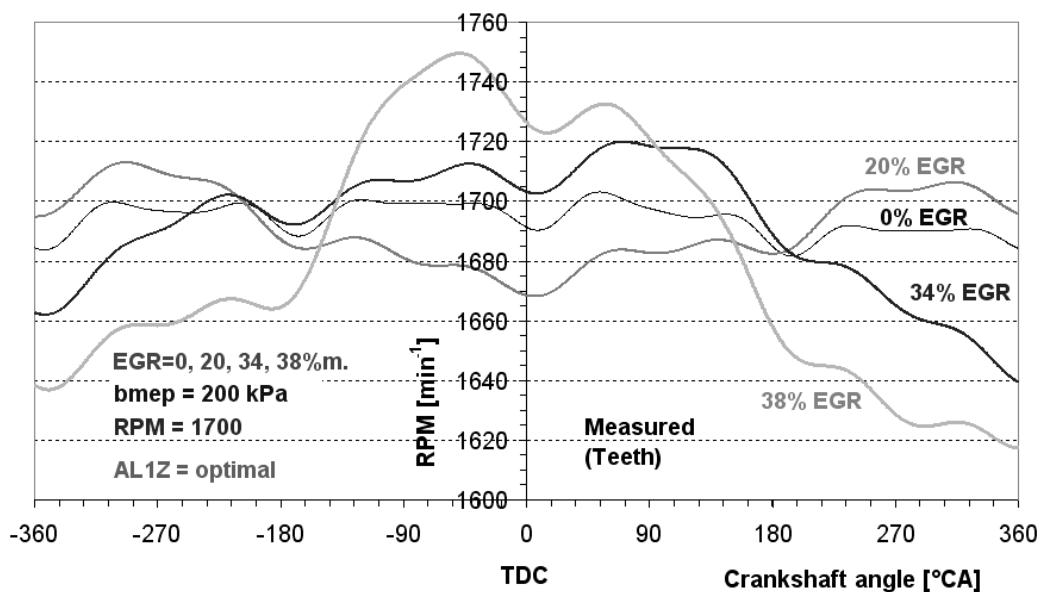
Fig. 5. Measured patterns of instantaneous crankshaft speed in case of EGR rate from 20 up to 38%m.

4. Conclusion

Running variability investigation of low load tested engine under condition of very high uncooled EGR rate was carried out. Acquired data were conditioned using Inverse Fourier Transformation. Based on the results, the running variability is significantly increased over EGR rate of 20% (by mass). It is caused by combustion deterioration in consequence of very high content of inert gas in combusted mixture. In order to improve the combustion progress it could be apply e.g.: plasma discharge, more spark plugs in cylinder, etc.

Acknowledgement

References

[1] KUTLAR, A., O., ARSLAN, H., CALIK, T., A. *Methods to improve efficiency of four stroke spark ignition engines at part load.* Elsevier Ltd., 2005.

[2] MIKLÁNEK, Ľ.: *Working cycle changes by EGR delivery into intake of SI engine in a low load.* MECCA, Vol. 8, No. 3 + 4, , pp. 35-39, ISSN 1214-0821, CTU in Prague, 2010.

[3] BREHOB, D., D., AMLEE, D. R. *Effects of inlet air heating and EGR on thermal efficiency of a SI engine at part load.* SAE Paper 901713, SAE Int. Warrendale, 1990.

[4] NOVÁK, J. *Data Acquisition Card for Time-Record.* Department of Measurement, CTU in Prague, 2009.

[5] TAKÁTS M. *INTEC – software for evaluation of in-cylinder pressure record.* Josef Božek Research Center Code Library, CTU in Prague, 2006.

[6] KUFNER, A., KADLEC, J. *Fourierovy řady*, Academia 1969.

Energy Intensity Analysis of City Hybrid Vehicle Using the Driving Simulation

[*]Martin Mruzek, Dalibor Barta, Pavol Kukuča
[*]University of Zilina, Faculty of Mechanical Engineering, Department of automobile technology,
Univerzitna 1, 01026 Žilina, Slovakia, {martin.mruzek, dalibor.barta, pavol.kukuca}@fstroj.uniza.sk

Abstract. This document describes the analysis of energy problems of hybrid drive for urban traffic. Introductory section deals with the division and the concept of hybrid vehicles. The next section provides an energy intensity analysis using the driving simulation by modified urban driving cycle by NEDC and by real driving the vehicle in a city. The comparison of the average power necessary for vehicles with different parameters is in the last part of this paper.

Keywords: hybrid drive, driving simulation, energy intensity

1. Introduction

Constantly tightening emission limits for vehicles and decreasing of oil reserves lead to the more effective use of energy. Alternative fuels, improving combustion engines, the use of hybrid technology or vehicles with pure electric propulsion are the part of this problem solution. It is also an effort to use the energy which would be wasted otherwise, for example kinetic energy during braking.

2. Hybrid drive

Vehicle hybrid drive means the combination of two or more power sources. The most common combination in automotive industry is the use of internal combustion engine and electric motor. The advantages of both systems can be used by appropriate combination of internal combustion engine and electric motor. This leads to fuel savings and to corresponding reduction of air pollutants in the exhaust gases.

Division according to the share in using the secondary power source:

Microhybrid – is a stop - start system, which requires much stronger starter and vehicle battery.

Mildhybrid – except of the stop – start system and recuperation energy system this system can support internal combustion engine by small electric motor, if it is necessary.

Fullhybrid – it is possible to drive vehicle with internal combustion engine and with the use electric motor only.

Plug-in hybrid – vehicle battery can be recharged from the public electricity network.

2.1. Configuration of hybrid drive

Serial hybrid

Serial hybrid is powered as well as electric vehicle purely by electro motor. Internal combustion engine serves as the drive of the generator, the source of the electricity. Internal combustion engine can be operated in a very narrow revolutions range, or in one revolution mode. This eliminates wasteful areas of the working characteristics such as idling, or the lower partial load range. The engine can be set to the optimal operating range with maximum efficiency. The disadvantage of a serial hybrid is the multiple energy conversion.
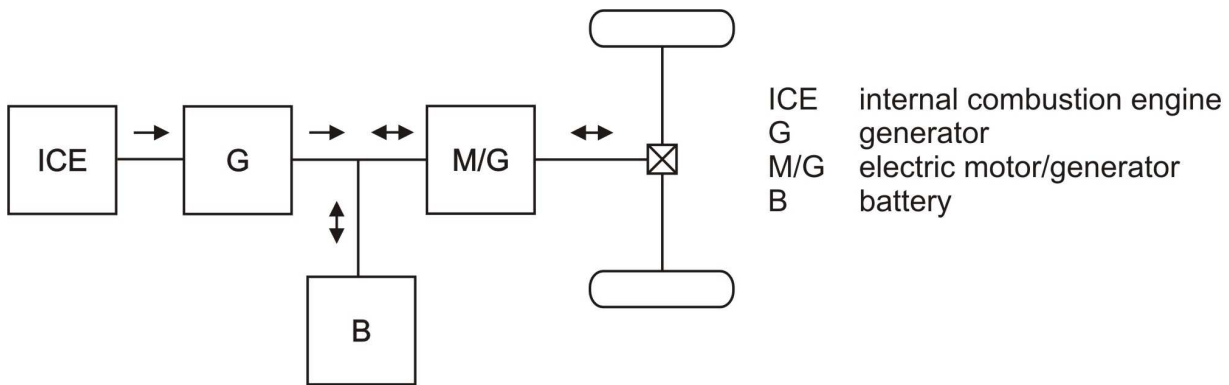
ICE	internal combustion engine
G	generator
M/G	electric motor/generator
B	battery

Fig. 1. Serial hybrid

Parallel hybrid

The parallel hybrid has a direct mechanical connection between the internal combustion engine and the wheels, much like conventional vehicle. The conventional type gear box is shared for electrically-driven branch, too. At this configuration, it is sufficient to change the speed of an electric motor in relation to the internal combustion engine only in the appropriate range.
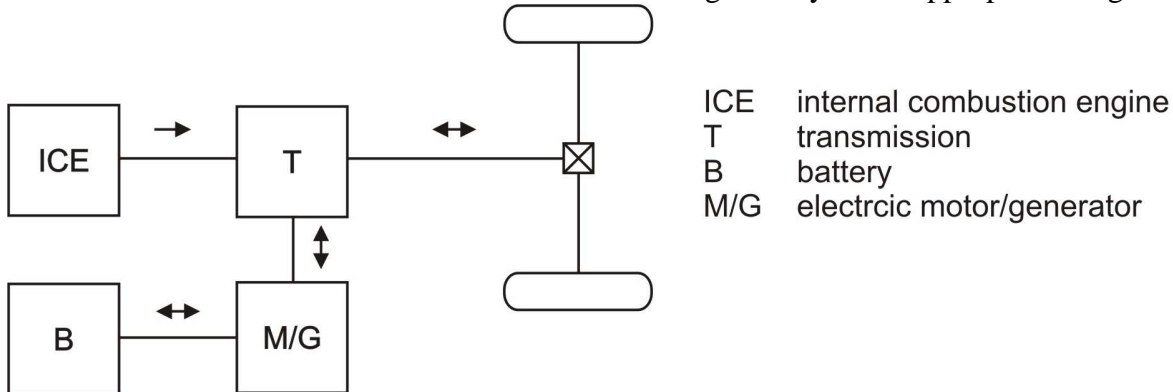

ICE	internal combustion engine
T	transmission
B	battery
M/G	electrcic motor/generator

Fig. 2. Parallel hybrid

Serial/parallel hybrid

Combination of serial and parallel configuration can eliminate the disadvantages of both systems. Its equipment with internal combustion engine, electric motors, transmission components, clutch, overrunning clutch or brakes can be various. For example, it can be a serial hybrid with an interconnection clutch between internal combustion engine and wheels. The branch performance can be done mechanically by differential or electrically.

3. Energy intensity of the hybrid drive

When designing the components and power management of hybrid we can start from the driving simulation of the vehicle. Based on the driving simulation we can determine the size of energy that would be otherwise wasted and thereby also dimension the components of the hybrid drive. The philosophy of a hybrid drive is that the vehicle drive doesn't work constantly on maximum power, the power peaks can be supported by energy accumulator and unused energy can be accumulated. That means that we can use an internal combustion engine with lower performance. The aim of the driving simulation is to determine the average power needed for the vehicle drive.

We could use the urban part of the NEDC cycle which is used to measure of fuel consumption like a driving simulation. This cycle consists of a series of accelerations, consistent drivings, braking and stopping. Maximum speed in this cycle is 50 km.h^{-1} and the average speed is 19 km.h^{-1}. Because this cycle is simple for our using, it doesn't contain the climbing resistance, is insufficient for design of the hybrid drive. We can use two ways to achieve the optimal reason. One possibility

is to adjust the urban NEDC cycle by supplementing the resistance of the climb. We can also make the driving simulation using the real driving in the city traffic, which seems to be better alternative. The simulation was created using the measured values of acceleration, speed, distance and climb on chosen routes. The measurement of distance, speed and acceleration was made with contactless measuring device based on the Doppler phenomenon and with GPS data logger in order to determine the climb. The measurement was made on conventional vehicle. Consequently we determine the driving resistance of the vehicle and set its performance requirements. The particular simulation was measured in the city with the population of 311,650 and the area of 214 km^2. The population density is 1,500 inhabitants per km^2. The total distance is 12 km. The maximum climb value was 8,8% and the value of maximum descent was 10,2%.

Fig. 3. Elevation profile of real driving simulation
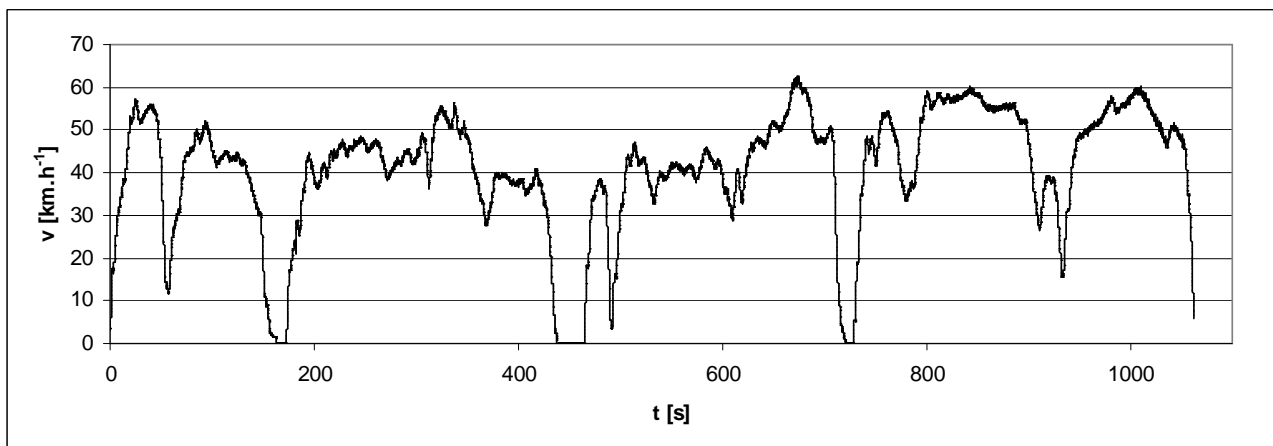
Fig. 4. Real urban driving profile

We use the parameters of small city vehicle to compare the both cycles under consideration. The parameters of the vehicle are: weight of the vehicle of 300 kg, frontal area of 1,3 m^2, aerodynamic drag coefficient c_x of 0,35, coefficient of the rotating parts of 1,1. Resulting value of the average power according to modified NEDC urban cycle is 1,24 kW and according to the real simulation is 1,48 kW.
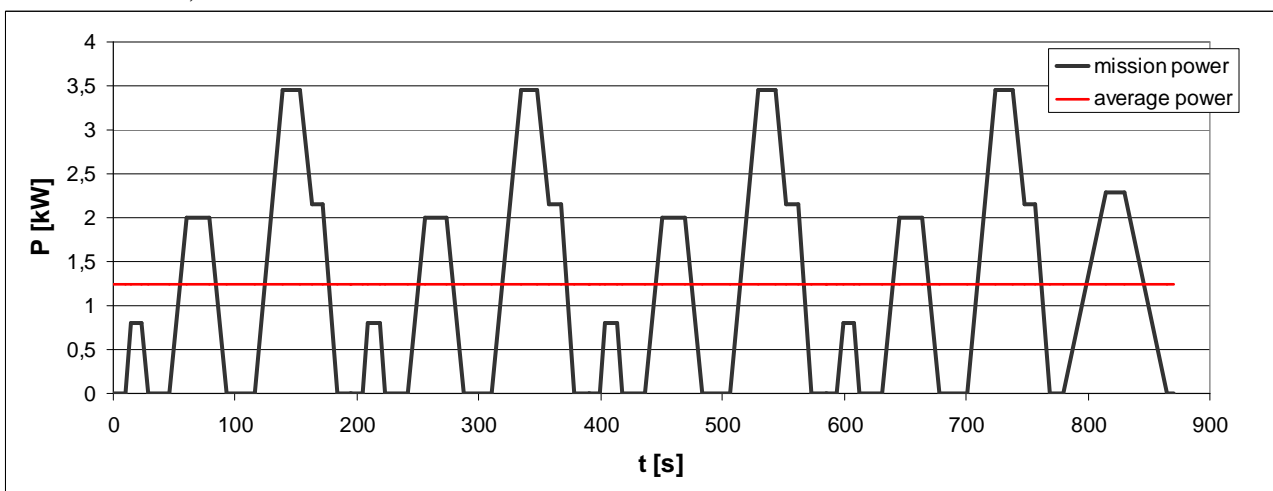
Fig. 5. Modified NEDC urban cycle for small city vehicle
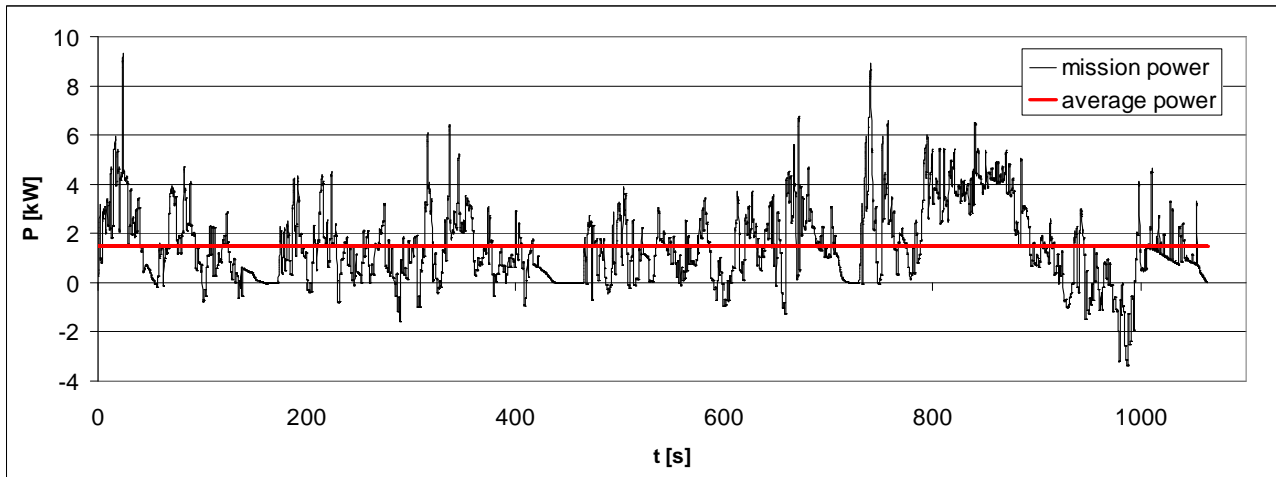
Fig. 6. Real driving simulation for small city vehicle

The comparison of energy intensity for vehicles with different parameters like average power, highest required power PMAX and the highest possible power for the recovery Pmrek is stated in Table 1.1. The results show that the vehicles with larger mass are more energy-consuming, but they can acquire more of unused energy. Vehicle of the mass of 1600 kg could theoretically acquire and use the 21,32 kW, while the vehicle of the mass of 300 kg only 3,37 kW. It must be remarked that the acquisition and storage of recovered energy is difficult. When using the battery as energy storage the maximum recharge current is limited, therefore it is not possible to accumulate all of the energy.

| m [kg]	300	800	1100	1350	1600
S_x [m^2]	1,3	2	2,4	2,5	2,7
c_x [-]	0,35	0,35	0,33	0,31	0,34
λ [-]	1,1	1,25	1,5	1,6	1,6
$P_{average}$ [kW]	1,48	3,53	5,11	6,26	7,42
P_{MAX} [kW]	9,33	25,26	37,99	46,15	56,83
P_{mrek} [kW]	3,37	10,12	14,3	17,98	21,32

Tab. 1. Vehicle comparison

4. Conclusion

One measurement is not enough to build the corresponding simulation. It is necessary to include various routes in cities with different number of population to the simulation. Driving in the city center with higher number of crossroads, the need for frequent stopping and with multi-track roads connecting the various city districts, should be appropriately distributed. We must also take into consideration the factor of the traffic operation level, which is different in rush hours and during the weekends.

Acknowledgement

References

[1] Vlk, F. *Alternativní pohony motorových vozidel*. 1. vydání. Brno, ISBN 80-239-1602-5

Using Evolutionary Algorithms and Bodner–Partom Model to Determine the Properties of Material

[*]Viera Nohajová, Jozef Bocko

[*]Technical University in Košice, Faculty of Mechanical Engineering, Department of Applied Mechanics and Mechatronics, Letná 9, 042 00 Košice, Slovakia, {viera.marcinova, jozef.bocko}@tuke.sk

Abstract. This paper presents the Bodner-Partom model and evolutionary algorithms to simulate the stress-strain relationship of standard tension test and to identify several constants describing the behavior of common elasto-viscoplastic material. The results depend on the different settings of evolutionary algorithm. This work is focused to determine the most appropriate settings of evolutionary algorithm to obtain the best results for Bodner-Partom model.

Keywords: Plasticity, Bodner-Partom model, evolutionary algorithms.

1. Introduction

Sometimes we face technical problems, which are hard to solve experimentally. If the experimental identification of several material parameters is too complicated and expensive, we could use some numerical model to describe the behavior of these materials. The behavior of viscoplastic material is precisely described by Bodner-Partom model. The identification of parameters of Bodner-Partom model was implemented by evolutionary algorithm. The material parameters are determined from standard experimental data from tension test.

2. Basic information about the Bodner-Partom model

The Bodner-Partom model is a set of constitutive equations for elastic-viscoplastic strain-hardening homogeneous isotropic material, which do not use the yield criterion to separate the elastic area from the inelastic one. This model can be used for small deformations and the whole load and release history. The viscoplastic constitutive laws are formulated by differential equations based on different material parameters. The Bodner-Partom model uses 8 constants to determine the strain rate, kinematic hardening and isotropic hardening.

The Bodner-Partom model is based on the assumption that the total deformation rate consists of elastic and inelastic components.

$$\dot{\varepsilon}_{ij} = \dot{\varepsilon}_{ij}^{e} + \dot{\varepsilon}_{ij}^{p} , \tag{1}$$

where $\dot{\varepsilon}_{ij}^{e}$ is the elastic strain rate and $\dot{\varepsilon}_{ij}^{p}$ is the plastic strain rate.

The elastic strain rate $\dot{\varepsilon}_{ij}^{e}$ is obtained from elastic stress-strain relation

$$\dot{\varepsilon}_{ij}^{e} = \frac{\dot{\sigma}_{ij}}{E} , \tag{2}$$

where E represents the Young's modulus.

The plastic strain rate $\dot{\varepsilon}_{ij}^p$ is formulated as

$$\dot{\varepsilon}_{ij}^p = D_0 \exp\left[-\frac{1}{2}\left(\frac{Z^2}{\sigma_{ef}^2}\right)^n\right]\frac{\sqrt{3}\,s_{ij}}{\sigma_{ef}}, \tag{3}$$

where D_0 is the assumed maximum plastic strain rate, Z is the total hardening variable, σ_{ef} represents the effective stress and s_{ij} is the deviatoric stress. This is the general kinetic equation.

The basic equations of unified elastic-viscoplastic theory are kinetic equation and evolution equations for isotropic and directional hardening.

The special forms of general kinetic equation for uniaxial stress σ_{11} and simple shear $\dot{\gamma}_{12}^p$ are

$$\dot{\varepsilon}_{11}^p = \frac{2}{\sqrt{3}}\left(\frac{\sigma_{11}}{|\sigma_{11}|}\right)D_0 \exp\left[-\frac{1}{2}\left(\frac{Z}{\sigma_{11}}\right)^{2n}\right],$$

$$\frac{1}{2}\dot{\gamma}_{12}^p = D_0\left(\frac{\tau_{12}}{|\tau_{12}|}\right)\exp\left[-\frac{1}{2}\left(\frac{Z}{\sqrt{3}\,\tau_{12}}\right)^{2n}\right]. \tag{4}$$

The total hardening Z consists of isotropic Z^I and directional Z^S hardening

$$Z = Z^I + Z^S. \tag{5}$$

Isotropic hardening is formulated by expression

$$Z^I = Z_1 - (Z_1 - Z_0)\exp(-m_1 W_p), \tag{6}$$

where Z_1 is the maximum value of isotropic hardening, Z_0 is the initial value of isotropic hardening, m_1 is the rate of isotropic hardening, W_p is the accumulated plastic work.

Directional hardening is expressed by equation

$$Z^S = \beta_{ij}\,u_{ij}, \tag{7}$$

where β_{ij} is a directional hardening variable and u_{ij} is a direction of stress.

The material constants, that are needed to formulate the uniaxial stress-strain relation are E, D_0, n, Z_0, Z_1, m_1. The general shape of stress-strain curve in the inelastic domain is obtained by hardening rate m_1 and by ratio of the maximum to initial value of isotropic hardening $\frac{Z_1}{Z_0}$. The particular curve can be obtained by Z_0, that is additionally determined for a given n, with D_0 initially set. Different combinations of n and Z_0 can be determined for particular values of m_1 and $\frac{Z_1}{Z_0}$ from the equations (4) and (6).

3. Introduction to basics of evolutionary algorithms

Evolutionary algorithms are part of sub-symbolic artificial intelligence and they are inspired by processes of natural evolution. They are used as a problem solving methods by minimizing error and maximizing of an attribute of individual in a population of solutions, which is called fitness. The typical parts of evolutionary algorithms are:
- Initialization: creating a first population of individuals
- Selection: chooses the best parents of new individuals for crossover

- Crossover: producing new individuals from two or more parents
- Mutation: random changing of the individuals when solution finding goes to a dead end
- Termination condition: tells the algorithm when to stop.

As the evolutionary algorithms are well known approach of solution finding, we won't describe them here more in general, but rather focus on their application in our case. For more information please refer to literature mentioned in references at the end.

4. Determination of material constants

The parameters are determined from test data of standard tension tests for the Bodner-Partom model. The common homogeneous isotropic elasto-viscoplastic strain-hardening material was used for experiment. The material parameters are determined by minimizing the difference between the experimental data and curves simulated numerically. To find the best correlation between experimental and numerical curve we used the evolutionary algorithms. The function of the corresponding optimization problem has a form

$$f(c_1,...,c_N) = \sum_{k=1}^{K}\left\{\sum_{i=1}^{M}\left[\sigma_{k,i}^{\exp} - \sigma_{k,i}^{num}(c_1,...,c_N)\right]^2\right\} \rightarrow \min , \qquad (8)$$

where $c_1,...,c_N$ are N material constants, that are determined, K is the number of experimental curves, with that we have. M is the number of points represented in stress-strain relations. $\sigma_{k,i}^{\exp}$ is the experimental stress value in the i-th point related to the corresponding strain at the strain rate k. $\sigma_{k,i}^{num}$ is the numerical stress value, that is calculated at the corresponding strain.

For the fitness calculation of an individual the following equation is used:

$$fitness(c_1,...,c_N) = \frac{1}{\left[1 + f(c_1,...,c_N)\right]}, \qquad (9)$$

where the chromosome of an individual is a set of N material constants $c_1,...,c_N$. The stress-strain curve is simulated numerically and the fitness of each individual is calculated, where the values of $c_1,...,c_N$ are applied. The lower the fitness value is, the higher is the suitability of the individual for the crossover. The chromosome of an individual consists of the combination of these parameters: E, D_0, n, Z_0, Z_1, m_1, Z_3, m_2.

Points of stress-strain diagram obtained by EA are compared with points of stress strain curve experimentally obtained. EA minimizes the error between the experimental and numerical points. The solutions obtained from EA provide the parameters of Bodner–Partom model that we are looking for.

The focus of this work was to find the best parameters of evolutionary algorithms, which lead to the best constants of Bodner–Partom model. Different settings of evolutionary algorithms influence the quality of output results. It is a necessary to determine the best settings of algorithm to obtain good results. The number of individual in one generation, duration of the algorithm run, selection methods, crossover methods, the number of elite individuals were changed in algorithm. The error calculated as the numerical difference between the curve obtained from the tension test at common conditions and the curve created by evolutionary algorithm was monitored. The following picture shows the best results. There were 24 individuals in generation, the maximum number of generations was 300, the remainder method of selection and scattered method of crossover were used and the number of elite individuals was 8, i.e. 33,33 %.
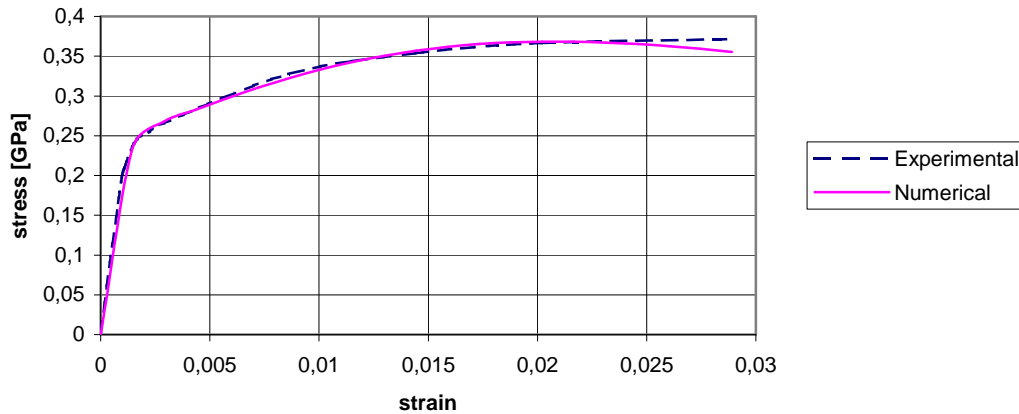
Fig. 1. Stress-strain curve with the most suitable parameters.

The program was running 177 second and the error was 0,0588. The most adequate constant for Bodner-Partom model obtained by evolutionary algorithm are: Young´s modulus E = 161,83 GPa, assumed maximum plastic strain rate $D_0 = 171\ 410\ 000,0$ 1/s, controls rate sensitivity n = 1,0333, initial value of isotropic hardening $Z_0 = 1,817$ GPa, maximum value of isotropic hardening $Z_1 = 9,537$ GPa, controls rate of isotropic hardening $m_1 = -11,505$ 1/GPa, maximum value of directional hardening $Z_3 = 1,5691$ GPa, controls rate of directional hardening $m_2 = 254,06$ 1/GPa.

5. Conclusion

For the identification of several material constants some numerical model can be used to describe the behavior of that material. The parameter determination is more convenient this way compared to experimental methods, which are more complicated than numerical ones. To find the appropriate material constants for measured tension curve when using a numerical model the evolutionary algorithms can be used. The quality of results depends on the different settings of evolutionary algorithms. The best results were obtained using 24 individuals in generation, the maximum number of generations was 300, remainder method of selection and scattered method of crossover were used and the number of elite individuals was 8, i.e. 33,33 % in evolutionary algorithm. The program was running 177 seconds and the reached error was 0,0588.

Acknowledgement

References

[1] BODNER, S. R. *Unified Plasticity for Engineering Applications*. New York: Kluwer Academic/Plenum Publishers, 2002.

[2] PYRZ, M. *Parameters Identification of Viscoplastic Models Using Evolutionary Algorithms*. XXI ICTAM, Warsaw. 2004.

[3] MACH, M. *Evolučné algoritmy: Prvky a principy*. Košice: Elfa. 2009.

Test Stands for Railway Brakes and Their Parts Testing Utilization

[*]Ján Paluch, Juraj Gerlici, Tomáš Lack
[*]University of Žilina, Faculty of Mechanical Engineering, Department of Transport and Handling Technology, Univerzitna 1, 01026 Žilina, Slovakia, {Jan.Paluch, Juraj Gerlici, Tomas.Lack}@fstroj.uniza.sk

Abstract. This paper deals with brake tests, which can be made directly in the operation or in the testing laboratories. The UIC 541-3 and the UIC 541-4 standards solve this field theoretically. The paper is aimed at nowadays brake test benches used in Europe, too. The article deals in more detail with the "UIC flywheel brake test stand" with its design and software equipment. This test bench is utilized for testing properties of braking materials prototypes. The software called "LaGer", developed by the Department of Transport and Handling Technology staff is used for data acquisition and data assessment. This is a part of this brake test stand, too.

Keywords: brake, brake tests, the UIC standards, homologation of test benches, flywheel test stand, test stand control software.

1. Introduction

Brakes are among the most important parts of each railway vehicle from the point of view concerning quality and safety of railroad operation. They are often mentioned especially in accordance to building corridor's railway lines and increasing of running speed where are higher requirements for braking equipment, too.

The actual braking tests can be performed directly in traffic or in testing laboratories. Measurements in traffic, called "the test lines", are based on putting a wagon to the specific train and its uncoupling from the measuring train set in the test section (in Slovakia the test sections are Senec - Sládkovičovo, Poprad - Svit, Haniska pri Košiciach - Košice). Measurements in testing laboratories are performed on testing facilities called "the testing rings" or "the testing benches" in conditions simulating the real railway traffic (in Slovakia there's one UIC bench stand by the company ZSSK Slovakia in Žilina).

2. Nowadays known brake test benches

The braking test benches of the railway's companies and producer's of brake blocks and brake lining serve testing brake assemblies and their elements in conditions, which are simulated the reality and they replaced too expensive break tests on real "test lines". It goes about:
- homologation friction tests of brake linings and brake blocks according to UIC 541-3 and UIC 541-4 standards,
- preliminary verification tests of brake linings prototypes and brake blocks prototypes,
- tests on durability of braking shoes, linings, disc and track wheels.

The most significant parameters are the friction coefficient and wear. Therefore it's necessary to test two pairs of friction couple (brake disc with lining or railway wheel with shoe) in conditions simulating real traffic – e.g. vehicle velocity, contact pressure, wagon weight falls on the brake, drag braking, road loan simulation, dry braking, braking during rain or during snow. According to aspect of measurement accuracy it's necessary to ensure the achievement of equal values of the test results comparing the same type of products from a particular producer. The UIC (Union Internationale des Chemins de Fer) test benches are homologated by expert's workgroup ERRI B

126.3, where the mechanical and instrumentation layout with equipment of a particular test bench is controlled.

Currently in Europe there are at least twenty test benches, eight of them are the accredited (homologated) UIC test benches.

2.1. Producer's test benches

The producer's test benches didn't pass the approval (certification) progress by the UIC organization and they aren't homologated by UIC. Among the leading producers of brake linings and brake blocks belong companies: "Becorit", "Bremskerl", "Honeywell Bremsbelag", "Knorr - Bremse systeme" from Germany, "Flertex", "Faiveley Transport" from France, "TMD Friction", "General Mogul" from United Kingdom, "CoFren" from Italy and "Icer" from Spain.

These companies also own their test benches called as "the dyno machines".

2.2. UIC homologated test benches

The nowadays existing and homologated test benches (stands) by the UIC organization belong the test benches of railway companies: DB (Deutsche Bahn) in Minden, SNCF (Société Nationale des Chemins de fer Francais) in Vitry, FS (Ferrovie dello Stato) in Firenze, PKP (Polskie Koleje Państwowe) in Warsaw, CFR (Caile Fera Romane) in Bucuresti, ČD (České Dráhy) in Prague, ZSSK Slovakia (Železničná spoločnosť Slovensko) in Žilina.

3. The UIC flywheel test stand in Slovakia

The UIC flywheel test stand (approved for ZSSK company) in Slovakia is homologated brake stand by the UIC organization, which is situated at the University of Žilina, Faculty of Mechanical Engineering, Department of Transport and Handling Technology. In 2000 it was taken to homologation progress by the UIC SVA ERRI B 126 workgroup and was homologated as a universal test bench of "D" category.

Test bench			ŽSSK Slovakia
Place			Žilina
Maximal size of test piece		[mm]	Ø1400 x 300
Main shaft	Maximal power	[kW]	400
	Maximal rotation speed for i= 1,5 (i = 1,72;, i = 4)	[rpm]	2100, (1850, 800)
	Maximal braking moment	[kNm]	25
	Number of bearings	[pcs]	4, 6, 8
Moment of inertia	Electronic flywheel mass simulation allows to add		1100, (1300, 3000)
	I_0 (basis fixed rotation inertia mass)		20
	I_1 (flywheel mass detachable)		5 (2x)
	I_2 (flywheel mass detachable)		10 (3x)
	I_3 (flywheel mass detachable)	[kg.m^2]	15 (4x)
	I_4 (flywheel mass detachable)		280
	I_5 (flywheel mass detachable)		600
	I_6 (flywheel mass detachable)		900
	I_{MAX}		1900 (4900)

Tab. 1. Main parameters of the ZSSK Slovakia test bench.

3.1. Construction of flywheel test bench ZSSK Slovakia

Basic elements of this bench are the engine, set of flywheel masses, brake stations for testing disk brakes and block brakes, air ventilation equipment, water spraying equipment, systems for managing service and evaluation of measured data.
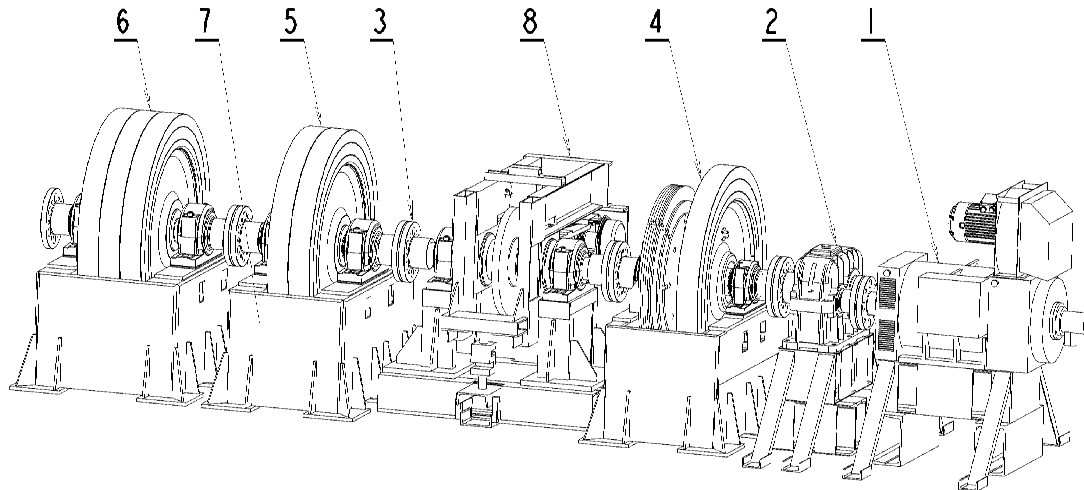
Fig. 1. UIC flywheel test bench 1 - D. C. electric motor, 2 - gearbox, 3 - electromagnetic disengaging clutch, 4 - flywheel with adjustable moment of inertia, 5 and 6 - flywheels, 7 – base frame, 8- disc brake test group

The engine consists of D.C. electric motor with separate excitation - type SB280LN8B, which is controlled by 4-quadrant thyristor converter with a reverse. The gearbox is connected with electric motor through a clutch and its gear ratios are i = 1,5 / 1,72 / 4. Nominal torque moment this electric motor is 1592 Nm with nominal power 265 kW, with the possibility of overloading up to 50% from 20 to 60 seconds. Maximum rotation speed of electric motor is 3200 rpm with maximum torque moment is about 800 Nm. This maximum rotation speed allows this brake with gear ratio i = 1,5 to reach the maximum rotation speed of break shaft until 2100 rpm and then to reach maximum speed of 350 km.h^{-1} for medium worn wheel's diameter 890 mm. With using gearbox with gear ratio i = 4 it's possible to reach the maximum velocity about190 km.h^{-1} for wheel diameter 1250 mm.

Other elements on test bench are three flywheels balanced in company ABB Brno. Total mass moment of inertia of the first smallest flywheel is 400 kgm^2 (it consists of one switchable flywheel with moment of inertia 280 kgm^2 and ten pieces of small flywheel masses detachable with total moment of inertia of 100 kgm^2, which are associated with a pressured bearing disc with moment of inertia of 20 kgm^2 to the shaft). The second flywheel has moment of inertia 600 kgm^2 and the third flywheel has the mass moment of inertia 900 kgm^2.

Brake stations are used for testing brake linings and discs (disc brake) or for testing brake shoes and track vehicles wheels (block brake). On each stand it's used a pneumatic brake cylinder with diameter 8 or 10 inches.

3.2. Test stand control software

The Test stand bench is equipped with the program system named LaGer. We can say that program system LaGer is the software tool for interactive design of programs (application forms) for continuous monitoring of measured places, automated measurement, recording of measured data, data assessment, controlling of experiments, data exports in the formats suitable to continue in processing with CSV and TXT formats, graphical presentations with WMF export, measure protocol processing and printing. The program system is based on the philosophy of the open component system. With advantage the Component Works (National Instruments), the ActiveX components set for data acquisition, numerical analysis, computations and data presentation can be implemented. The program contains the Designer that allows on-line editing of the application form. All activities are done during the program run. We can say that under editing of application form we understand the creation of new instances of the registered components, their removal, settings of the published properties and assigning the methods for processing of the published

events of these components. Setting of the published properties and events of the components is guarantied by „Object inspector" of the Designer.

Setting of the component properties influences the behavior of the component and in the visual components the appearance and the location too. By assigning of the method to the given event of the component, we can guarantee the processing of the event by assigned method.
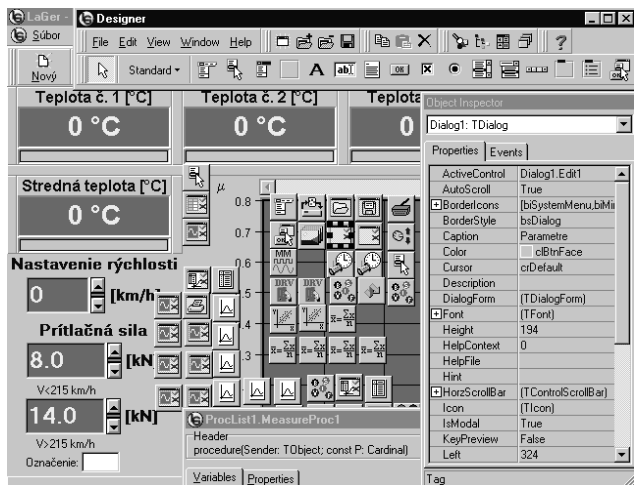

Fig. 2. The screen of application form in the program LaGer in the regime of active Designer

4. Conclusion

The research and the development of new friction materials on purpose of reducing tread wear, noise and vibration are performed nowadays and also the elimination of impacts on nature and the environment are carried out. The result of these activities should be an introduction of most suitable friction material into using in real conditions. The best known and the most commonly worldwide used braking systems are the system of block brakes and the system of disc brakes.

Acknowledgement

References

[1] HAHN, H., SIEGL, G. *Simulation and experimentelle Verifikation des Rad/Schiene-Rollprüfstands.* Ingenieur-Archiv 57 (1987) 329-384, Springer-Verlag 1987.

[2] GERLICI, J. AND CO.: *RAILBCOT – RAIL Vehicles Brake COmponents Test Stand*, ITMS Code 26220220011. ITMS 26220220011, Project description. Žilina, 2009.

[3] ALLOTTA, B. PUGI, L. MALVEZZI, M. BARTOLINI, F. CANGIOLI, F. *A scaled roller test rig for high-speed vehicles.* Vehicle System Dynamics, 48: 1, 3 — 18, DOI: 10.1080/00423111003663576.

[4] UIC. *UIC CODE 541-4 Brakes - Brakes with composite brake blocks – General conditions for certification of composite brake blocks.* UIC, Paris, 2007.

[5] ŘEZNÍČEK, R. CHUDÍK, S. LACK, T. *Test Stand KKVMZ in the International Approval Process.* Proceedings PRORAIL, Žilina, 1999

[6] JASCHINSKI, A., CHOLLET, H., IWNICKI, S. WICKENS, A., VON WÜRZEN, J. *The Application of Roller Rigs to Railway Vehicle Dynamics. Vehicle System Dynamics, 31*, Swets & Zeitlinger 1999

[7] DUKKIPATI, R. V. *Dynamics of a Wheelset on Roller Rig. Vehicle System Dynamics, 30*, Swets & Zeitlinger 199

[8] GERLICI, J. – LACK, T.: *Program System LaGer.* Scientific Papers of the University of Pardubice, Series B, The Jan Perner Transport Faculty 5 (1999), ISSN: 1211-6610, ISBN: 80-7194-283-9. pp. 19-28, Univerzita Pardubice 2000.

[9] LACK, T. – GERLICI, J. *Automated measure system on the accredited test stand of Slovak Railways.* PRORAIL 2003" pp. 47-54, EDIS, ISBN 80-968823-7-6, Žilina 2003.

Designing a Lightweight Milling Machine Using SolidWorks Software

*Piotr Paszta

*Częstochowa University of Technology, Institute of Machines Technology and Production Automation, 42-200 Częstochowa, Al. Armii Krajowej 21, Poland, paszta@itm.pcz.pl

Abstract. The paper presents the sequence of designing a lightweight numerically controlled milling machine using SolidWorks software. Then the machine was made in accordance with the design and implementation meets the structural assumptions. By using the transparent box-design all structural and kinematics systems are well visible. The machine is fully functional, is used for learning the fundamentals of programming. Cutting machine is used for teaching purposes.

Keywords: Milling machine, SolidWorks.

1. Introduction

In the last years reveals a very rapid development of computer-controlled cutting machine, spurred by the manufacturers of electronic components, cutting tools, control systems as well as leading manufacturers machines. Processing machines are more and more common to use and available, and users put their growing technological requirements and utility forcing designers to continuously and manufacturers increasingly better solutions to design, control and operation.

The rapid growth of numerically controlled machines can be seen in the industry, as well as in smaller companies where often is modernized conventional machines by using independent engines and equipped with computer numerical control.

High availability of ready-made components and parts makes it possible to build machines from the basics, they are applicable to the needs of education, training machine operators as well as purely numerical modeling a hobby or strictly professional. With many advantages of numerically controlled cutting machines (such as the ability to increase production flexibility, high reproducibility of geometrical objects, short times of processing, high dimensional accuracy), they are more common use.

Currently functioning a lot terms referring the same machine, universally function names such as milling plotter, plotter, CNC engraving and milling machine CNC. Very often some of these terms are used to describe the same machine.The plotter is a computer peripheral device, constructed on the basis of the table, which is used for large flat surfaces having even a few dozen square meters, it can cut out shapes and patterns, as well as draw engraved, often it is widely used in graphic design, advertising industry, for modeling of reliefs. Work performed on these machines often overlap with the work implemented at milling machines.

Computer-controlled milling machine, however, puts greater requirements on the usually, the rigidity and precision machining, productivity tools and application-driven spindles with power from a few kW offering a rough cutting. They are now mainly versatile machines for surface treatment of shaped and flat and new construction are increasingly alternatively with the the spindle equipped in measuring heads, water jet cutting or laser cutting. Milling engraving machines are lightweight milling machines and are equipped with high reaching speeds electrospindles of tens of thousands revolutions per minute, this gives the possibility of using carbide tools with diameters of less than one mm, and the use of high speed machining HSM.

2. Description Of Milling Machines Description Of Milling Machines

The article described the construction of a model of teaching lightweight milling engraving machines with movable gate (Fig. 1). It was created in the work leaded in the Częstochowa University of Technology Institute of Machines Technology and Production Automation [3].

Components have a total functionality and thanks to using twisted-box design with a transparent PMMA are well visible. Milling with the scope of the working space of X: 290mm Y: 420mm Z: 100mm allows performing machining of medium size in the materials to be milled and especially non-ferrous metals, plastics, wood, MDF boards and laminates. All axes are driven by stepper motors, transmission to trapezoidal screw follows through the claw coupling, in addition, each axle has also enabling erasing backlash nut on the bolt. Milling engraving machines resolution is 0.01 mm. Drives feeds are now important components of of numerically controlled machines. This puts them more and more demanding, because to a large extent determine the machining depends on their positioning accuracy, repeatability, speed and acceleration of movement. Drives feeds are now important components of of numerically controlled machines. This puts them more and more demanding, because to a large extent determine the machining depends on their positioning accuracy, repeatability, speed and acceleration of movement.

The machine is equipped with High-speed spindle power of 500W. It is powered by a single phase mains voltage, and the design allows for easy transport and launching in any room. For the control can be used any computer with an installed and properly configured control program, for example, ArtSoft Mach3's.
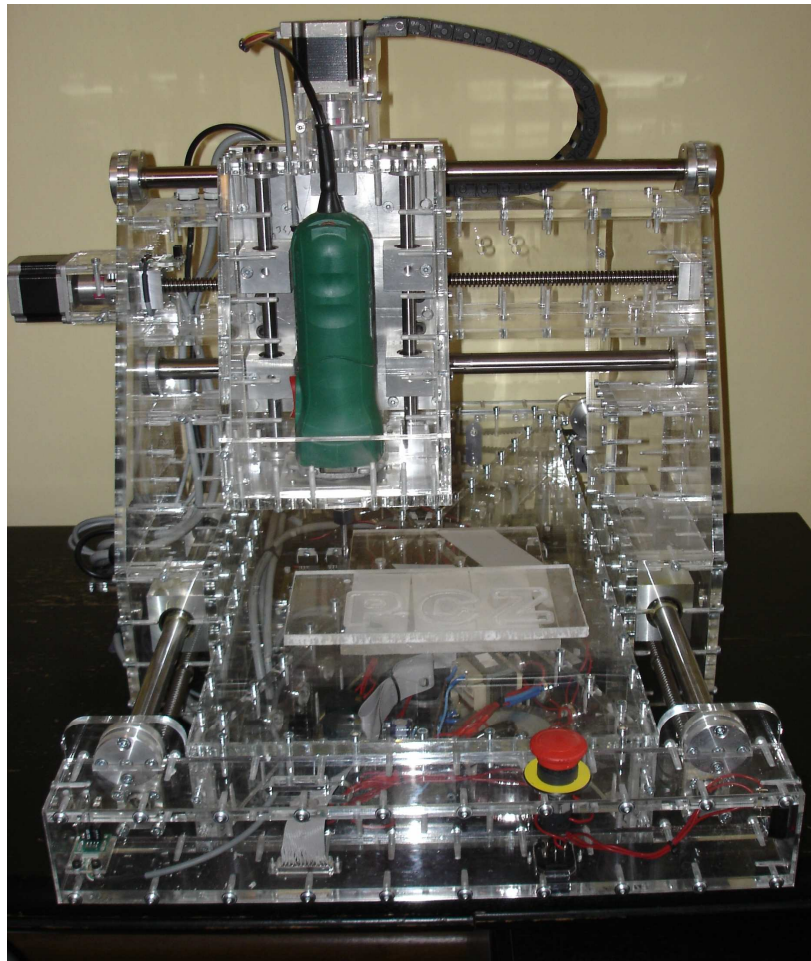

Fig. 1. View of the milling machine.

Virtual milling machines project was executed using specialized software, SolidWorks Dassault Systèmes SolidWorks Corp. (Fig. 2). It is an integrated system that offers complete 3D software with tools that will help to design, carry out a simulation of the resulting products, also manage the technical documentation of the product. It is relatively easy to use and simple program. He became very helpful in creating advanced 3D design machinery, allowed the creation of the whole design of mechanical milling machines, without using other software [2].
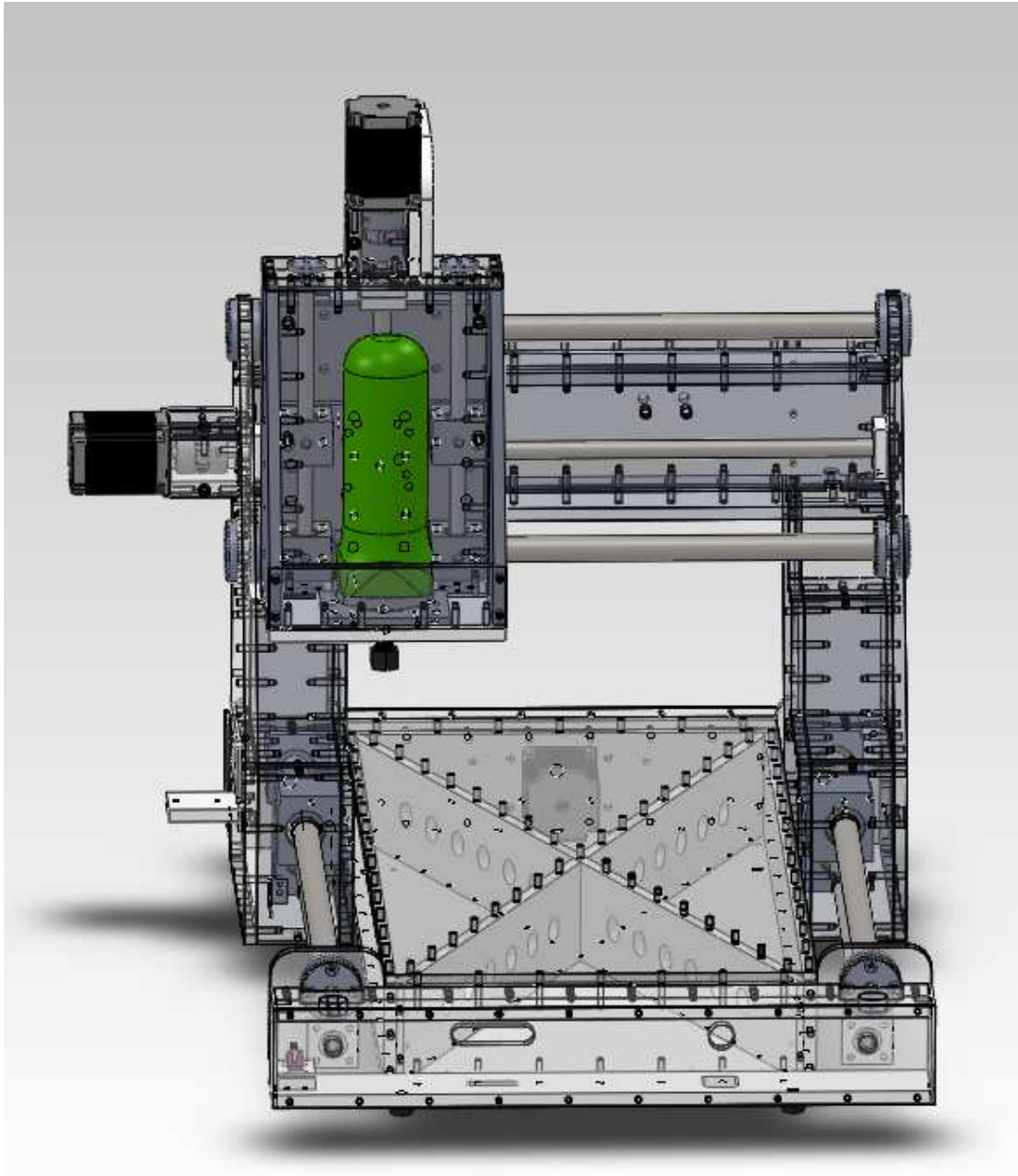

Fig. 2. Spatial view of a virtual project.

To perform milling machines were used as ready-made components and standard parts are described below. The spindle due to a similar distribution of forces during machining grinding machine used GS 500 VS DWT with a capacity of 500 W and the maximum speed 27,000 rpm.

To drive the X and Z axis was used stepper motor for 0.8 Nm moments due to the presence of small forces of inertia. To drive the gates of milling machine moving in the Y axis was used a larger 1.4 Nm stepper motor which, through a toothed belt drives the two trapezoidal screws. Stepping motors were used, because it made it possible to in open loop control and a wide speed range, accurate positioning and repeatability of movement and high reliability. Open linear bearings KB12OP, KB20OP were used for bearing parts of all the axles on the rolls of the special precision

WV12 and WV16. Power screws of all axes are supported by conventional ball bearings 608RS. Axes X, Y and Z are driven through trapezoidal steel screws with symmetrical thread Tr14x4 made in tolerance e7.

These bolts work with nuts BA1032 made of aluminum bronze. To all components such as spindle motors, guides, screws, couplings and bearings have been developed their spatial drawings.

Other elements of the construction have been designed from the basics. Machine base, gate, spindle clamping system has been designed and constructed of transparent plexiglass panels in the box-system. This solution achieved a very high rigidity of the construction and low weight.

A stepper motor has been mounted by the construction consists of an open cuboid fixed on at the top of gates of moving in the y-axis machines. Claw clutch was mounted on the shaft of the stepper motor and trapezoidal screw pivot.

Box-like structure of the gate moves relative to the milling machine Y axis along a fixed base, because it was supported on linear bearings moving on the shaft leading embedded in the base. Gate is driven by the stepper motor centrally located, then through the toothed belt with pretensioners on the pulleys trapezoidal screw on the nut attached to the walls of the gates.

To control the milling machine was used Mach 3 Artsoft program. This is a program for numerical control machines built up to six axes. The program is based on control by the G-codes. In the window, you can keep track of the route that moves the tool and to control the depth, spindle speed, size and other processing parameters. The program is used to control stepper motors, servo drives and gives it possibility the error correction performance power screws. Makes it possible to erase slack during relapse milling machine table. Control is from a PC via the parallel port. Mach 3 Software can import files in DXF, HPGL, JPG and BMP and recognize text files that the G-code.

3. Conclusion

The paper presents the design gantry milling machine. Using the CAD program has been designed and made between all elements of the machine, making it possible to eliminate errors and optimize the construction. It has satisfied all the design intent. The machine is fully functional, is used for learning the fundamentals of programming and cutting machine is used for teaching purposes. This is an example of the creation of the project and its implementation in accordance with the technical documentation.

References

[1] http://www.machsupport.com

[2] http://www.solidworks.com

[3] TOMZIK R. *Projekt i wykonanie lekkiej frezarki sterowanej numerycznie*. Praca magisterska, Instytut Technologii Maszyn i Automatyzacji Produkcji Politechniki Częstochowskiej, Częstochowa 2010.

Application of the Turning Lathe Simulator

[*]Piotr Paszta, Rafał Gołębski

[*]Częstochowa University of Technology, Institute of Machines Technology and Production Automation, 42-200 Częstochowa, Al. Armii Krajowej 21, Poland, {paszta, rafal}@itm.pcz.pl

Abstract. Lathe claw OSA 200 gives the opportunity to making such technological operations as turning, boring, drilling, threading, turning cones and spherical surface. The lathe is applied in the industry, small manufacturing plants, and education. OSA 200 is equipped with Mitsubishi control system. Operation of the lathe can be simulated by software Swansoft. The simulator makes it possible to check the machine-generated NC programs, their optimization and the calculation of the time of manufacture. Because the simulator imitates the real turning lathe, allows you to test the NC program for specific manufacturing tasks.

Keywords: Lathe OSA 200, Swansoft

1. Introduction

Lathe claw OSA 200 (Fig. 1) is equipped with Mitsubishi control system. It is used for machining as disc and shaft class. Gives the opportunity to making such technological operations as turning, boring, drilling, threading, turning cones and spherical surface. The lathe is apply in the industry, small manufacturing plants, and education. It is designed for individual and mass production. Using it can be machined steel, cast iron, non-ferrous metals and plastics. Cutting tools can be mounted with carbide inserts and sintered ceramic metal. The lathe is built on the bed, it has a rectangular cross-section, bottom bracket moves along the longitudinal bed, it is placed on the cross slide, mounted on the carriage head tool. The main drive consists of the headstock and the motor with variable speed regulation. The headstock is screwed in to the bed. In the headstock is the spindle. The spindle is supported on precision bearings. The bed is made of cast iron and has a rectangular form. Are bolted to the bed slides. At the slides moves suport. Tailstock is moved by hydraulic cylinder. Tailstock has a claw rotation. To drive the feed used ballscrews.

Cross slide comes standard with eight positional turret's Pragati. The head has a blade utility knife with a direct attachment to the external turning tool. Coolant is supplied to the machining area by the blade tool. For the control was used Mitsubishi Meldas system.

2. Numerical control

Numerical control puts more and more demands modern lathe, which determines their construction. Machining spaces are increasingly optimized and characterized by automatic tool change. In contrast to the conventional machines with all the tools are placed in the tool head, this allows significantly shorter downtimes. Tool set in tool head according to the plan resulting from the technological process and timely machining moves in the workspace by entering to work.

Machining technology program is written in such a way that its achievement can be on any lathe, regardless of the kinematic system, so you must write a program in the system from the base point is located at the zero point of the workpiece. Information about the origin location are determined in any manner, according to the criteria of practical skills and the technologist-programmer and stored machine control system. Usually it is easiest to fix in such a way that can be easily read the data dimension. t is necessary for accurate measurement and adjustment of the tool tip against the base point at the stage of preparation of the lathe to work. Tools should be set with

accuracy greater than the desired accuracy of the item worked. Due to the length and radius compensation equivalent reference tools, tool base point is possible to write part programs without regard to the specific dimensions of tools. The dimensions of the tools will be taken and converted by the control system of the lathe. This allows the application program can be written in a universal way.

Fig. 1. View of lathe WASP 200

3. Swansoft simulator

Swansoft CNC Simulation includes 17 sorts, 67 systems, and 126 control panels. It has programming and processing function of FANUC, SIEMENS(SINUMERIK), MITSUBISHI (Fig. 2), FAGOR, HAAS, PA, Romi, GSK, HNC, KND, DASEN, WA, GREAT, SANYING, RENHE, SKY. By using the software in PC, students can master operation of all kinds of NC lathe, NC milling and machining center in short time [1].

The simulator makes it possible to check the machine-generated NC programs, their optimization and the calculation of the time of manufacture. Because the simulator imitates the real turning lathe, allows you to test the NC program for specific manufacturing tasks It also allows to determine the dimensions of the workpiece surface roughness after machining. Using the capacities of the simulator can effectively support industrial production. With its capabilities can be corrected downtimes and eliminate errors in the NC program.

Work on the simulator Swansoft is like working on a real machine tool CBKO WASP 200. The simulation program takes account of the working space and all the preparations. We can determine the size of the workpiece, the type of clamping, set the coordinate origins the workpiece, cutting tool to select. Been applied a realistic visualization of three-dimensional space.
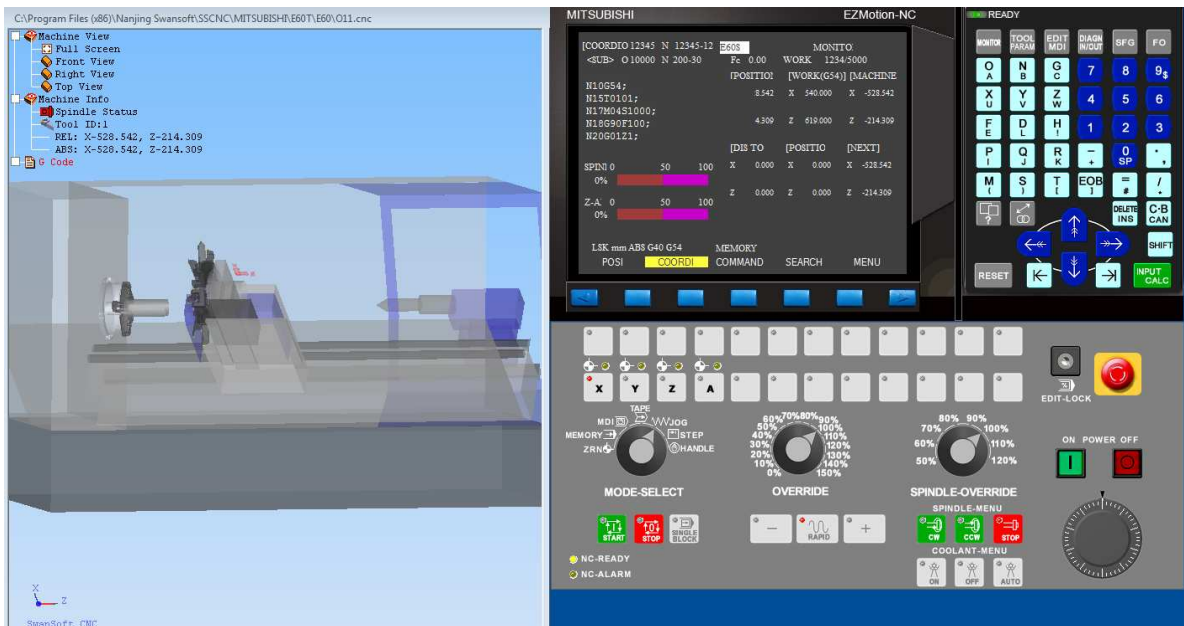
Fig. 2. View of the virtual lathe with the controls Mitsubishi.

In a preparatory mode to prepare the simulator as a real machine tool (Fig. 3). The first step is to attach the power, turn off the emergency stop button, and attach the key editing. To perform any maintenance operations on a lathe, use the following reference. It involves moving carriage to the reference point in the directions Z and X. The location of this point has been determined by the manufacturer, is used to determine the position of the tool in relation to the spindle, it occurs only in the lathe with the incremental position measurement systems. Thus, it is determined that a specific distance from the zero point of the machine it is possible to build an absolute coordinate system.

The lathe can be run in manual mode JOG, STEP, or HANDLE. To start the terminal grip chuck, we must first determine whether grab the sleeve or shaft. Short programs can make or edit mode using the MDI. Each program can be run step by step, or stop in progress. In both simulation and real, we can turn a graphic tool trajectory. The simulator and the real lathe should be mounted and set the cutting tools. Can be do this either directly. The advantage of this method is the elimination of measuring tools, it is easy to do. The disadvantage is the extra time to set the tool.

This method is good at not too frequent exchange of tools in the tool head. In order to determine the dimension of the tool turn longitudinally cylindrical surface of any size who need to know. The length of the tool in the X axis is the ratio of the size of the correction in the axis of the monitor reading and pre-measured turning radius of the cylinder. In order to determine the length of the tool in the Z axis must turn the front face. Tool length is the ratio of the size of the correction in the Z-axis and zero offset from the planned front the shaft piece.
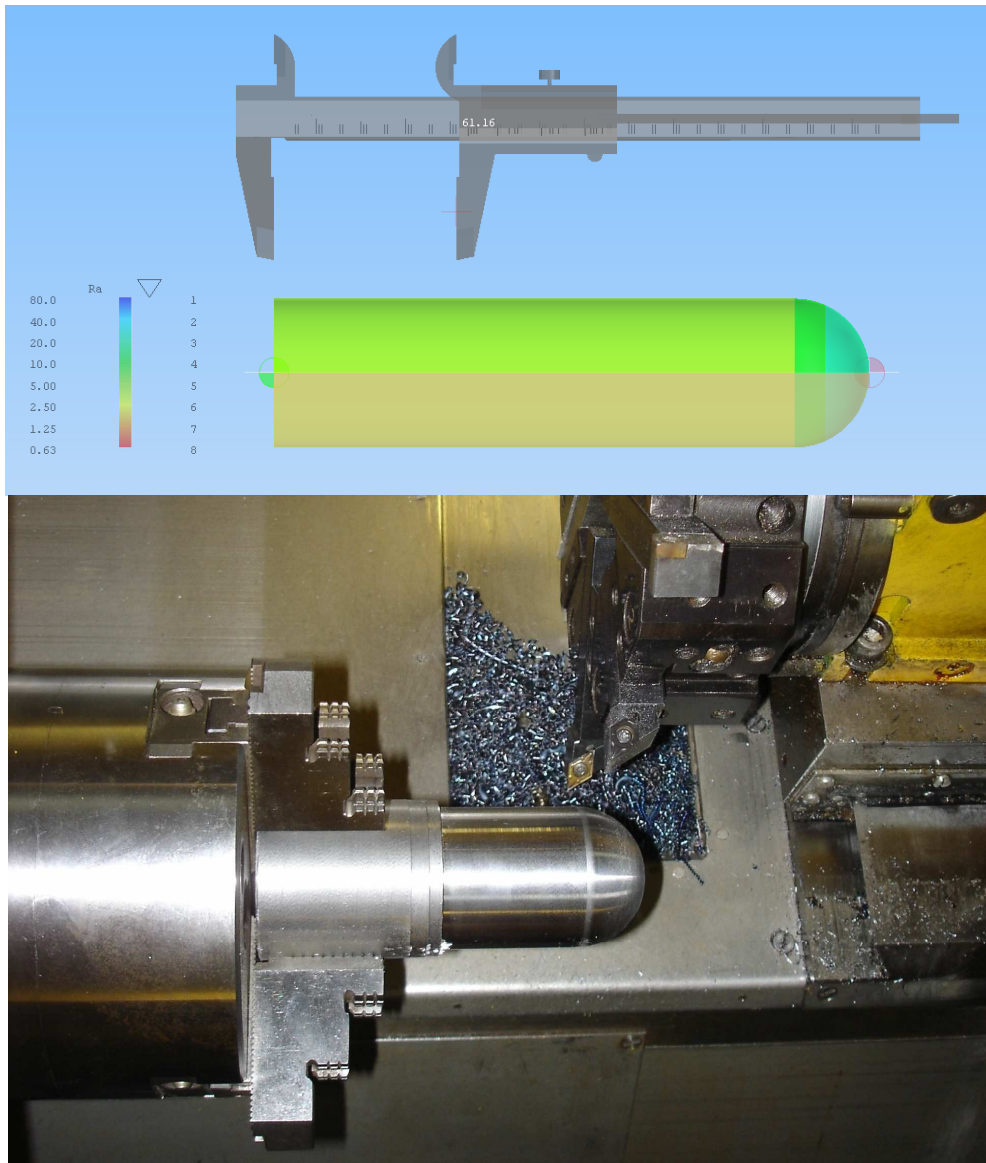
Fig. 3. The measurement of the virtual object and his a real views.

4. Conclusion

The paper presents the possibility of turning WASP 200 with controls Mitsubishi and with virtual counterpart. To control lathes have been used CNC systems made in Japan. They cooperate with digital propulsion systems with high reliability. Program processing technology is a standard G-codes according to ISO. In order to provide comfort, operating all operations can be similarly being done with the simulator. Before operating the machine can reproduce virtually her work and earn education in operating and CNC programming.

References

[1] http://www.swansc.com/index_en.htm

[2] Instrukcja Użytkowania tokarki kłowej TPS20N1-OSA 200. Centrum Badawczo Konstrukcyjne Pruszków. 1997.

[3] Mitsubishi CNC Meldas 50. Podręcznik Użytkownika. 1999.

Glycerin Combustion

[*]Marek Patsch, Ján Lábaj, Peter Pilát

[*]University of Žilina, Faculty of Mechanical Engineering, Department of Power Engineering, Univerzitna 1, 01026 Žilina, Slovakia, {marek.patsch, jan.labaj, peter.pilat}@fstroj.uniza.sk

Abstract. The aim of the article is comparison and setting of computing combustion model for CFD simulation and empirical calculation of glycerin combustion. The comparison was made based on calculation of adiabatic combustion temperature.

Keywords: glycerin, combustion, adiabatic combustion temperature, CFD simulation

1. Introduction

The combustion from chemical aspect is fuel oxidation which can perform in any temperature. Glycerin combustion is very problematic and complicated due to its high viscosity, low pressure of vapor, high temperature of auto-ignition, and fears from production of dangerous emissions. Antecedent attempts showed that the most suitable means for glycerin combustion was burner usage. The burner has to be modified to be able to effective work with this type of fuel. Before practical construction of experimental burner it is necessary to verify theoretical conditions by CFD simulation. The simulations were made with computational program Fluent. For CFD simulation of glycerin combustion in experimental two-fuel burner it is important to right set up computational model of combustion. As a computational model it was chosen model of stoichiometric mixture combustion, and model of chemical equilibrium. For verification of chosen model of glycerin combustion with theoretic glycerin combustion we use calculation of adiabatic combustion temperature. This temperature is most important fuel characteristics.

2. Statics of glycerin combustion

For theoretic computation we will reflect with pure glycerin using whose heating capacity gets from thermodynamic table is *16658 kJ.kg^{-1}*. Experimental burner has performance 20 kW. We can define theoretical glycerin consumption from burner performance and heating capacity. Theoretical fuel consumption will be *4,35 kg.h^{-1}*.

Glycerin $C_3H_8O_3$			
Relative molecular weight		92,09	g.mol^{-1}
Mass ratio C		39,14	%
Mass ratio H		8,69	%
Mass ratio O		52,17	%
Density (20°C)		1260	kg.m^{-3}
Kinematic viscosity (20°C)		$1,2.10^{-3}$	m^2.s^{-1}
Dynamic viscosity (20°C)		1,48	Pa.s
Thaw point		17,8	°C
Boiling point		290	°C
Self-ignition temperature		370	°C
Heating capacity		16558	kJ.kg^{-1}
Specific heat capacity	(0°C)	2,261	kJ.kg^{-1}.K^{-1}
Specific heat capacity	(20°C)	2,428	kJ.kg^{-1}.K^{-1}

Tab. 1. Main properties of pure glycerin

Perfect combustion requires correct quantity of combustion air. This quantity we compute by using of mass ratios of fuel components (obtained from table 1.) and by excess-air coefficient λ. By using of empirical equations we obtain total air quantity which is $L_t = 46,1 \ kg.h^{-1}$.

2.1. Amount of exhaust gases and their composition

For adiabatic temperature calculation we have to know amount of exhaust gases which rise by combustion of given fuel. The calculation assumes with perfect fuel combustion without water content (fuel has chemical composition by tab. 1). The calculation assumes with excess dry air content λ.

Minimal amount of exhaust gases $V_{sp,min}$, which are caused by combustion of stoichiometric mixture (with excess-air content, $\lambda=1$) for given case will be present on base of chemical fuel composition, and on base of chemical reactions during combustion. The production of exhaust gases describes following equation

$$V_{sp,min} = 1,867 \frac{C}{100} + 11,2 \frac{H}{100} + \frac{79}{100} L_t \ \ [m^3.kg^{-1}] \tag{1}$$

Real amount of exhaust gases is minimal amount of exhaust gases which is increased in the consequence of excess-air content and we calculate it by using equation (2)

$$V_{sp} = V_{sp,min} + (\lambda - 1)L_t \ \ [m^3.kg^{-1}] \tag{2}$$

We can calculate the composition of exhaust gases on the assumption that equation (1) determines count of particular components of exhaust gases. Volumes of particular components are following

$$V_{CO_2} = 1,867 \frac{C}{100} \ \ [m^3.kg^{-1}] \tag{3}$$

$$V_{H_2O} = 11,2 \frac{H}{100} \ \ [m^3.kg^{-1}] \tag{4}$$

$$V_{N_2} = \frac{79}{100} \lambda L_t + 0,8 \frac{N}{100} \ \ [m^3.kg^{-1}] \tag{5}$$

$$V_{O_2} = \frac{21}{100} (\lambda - 1)L_t \ \ [m^3.kg^{-1}] \tag{6}$$

Then for real amount of exhaust gases V_{sp} results on base of antecedent equations

$$V_{sp} = V_{CO_2} + V_{H_2O} + V_{N_2} + V_{O_2} \ \ [m^3.kg^{-1}] \tag{7}$$

3. Combustion temperatures

Heat rises during fuel combustion, this heat skips into exhaust gases, which in this regard reach certain combustion temperature. We use following combustion temperatures in the calculations:
- adiabatic combustion temperature
- theoretical combustion temperature
- theoretical combustion temperature with dissociation
- real combustion temperature

3.1. Adiabatic combustion temperature

Adiabatic temperature is theoretical temperature. It is important fuel characterization which suggests possible available temperatures during combustion, and presents chances to compare different fuel types from this aspect. Fundamental premises for calculation are:
- fuel and combustion air enter into combustion chamber of burner with temperature $t = 0°C$, fuel has given heating capacity
- excess-air coefficient is $\lambda = 1$ and combustion is ideal
- arose heat is transferred only into exhaust gases, heat non-takes away into environment (it is adiabatic action, $dq = 0$)

We can calculate adiabatic combustion temperature as:

$$t_a = \frac{Hu}{V_{sp,min} \cdot c_{p,sp}} \quad [K] \qquad (8)$$

where particular members of equation are:

Hu – fuel heating capacity, [kJ.kg^{-1}]

$V_{sp,min}$ – theoretical minimal amount of exhaust gases, [m^3.kg-1]

$c_{p,sp}$ – middle specific heat capacity of exhaust gases with composition for $V_{sp,min}$, [kJ.m^{-3}.K^{-1}]

As we can see in equation (8), for calculation we require know middle specific heat capacity of exhaust gases with given composition. But it depends on temperature, which is also unknown. Therefore, calculation of adiabatic combustion temperature and middle specific heat capacity of exhaust gases is possible do by iterative method. We use graphs of dependencies between specific heat capacities and temperature. Dependencies are shown in the figure 1.
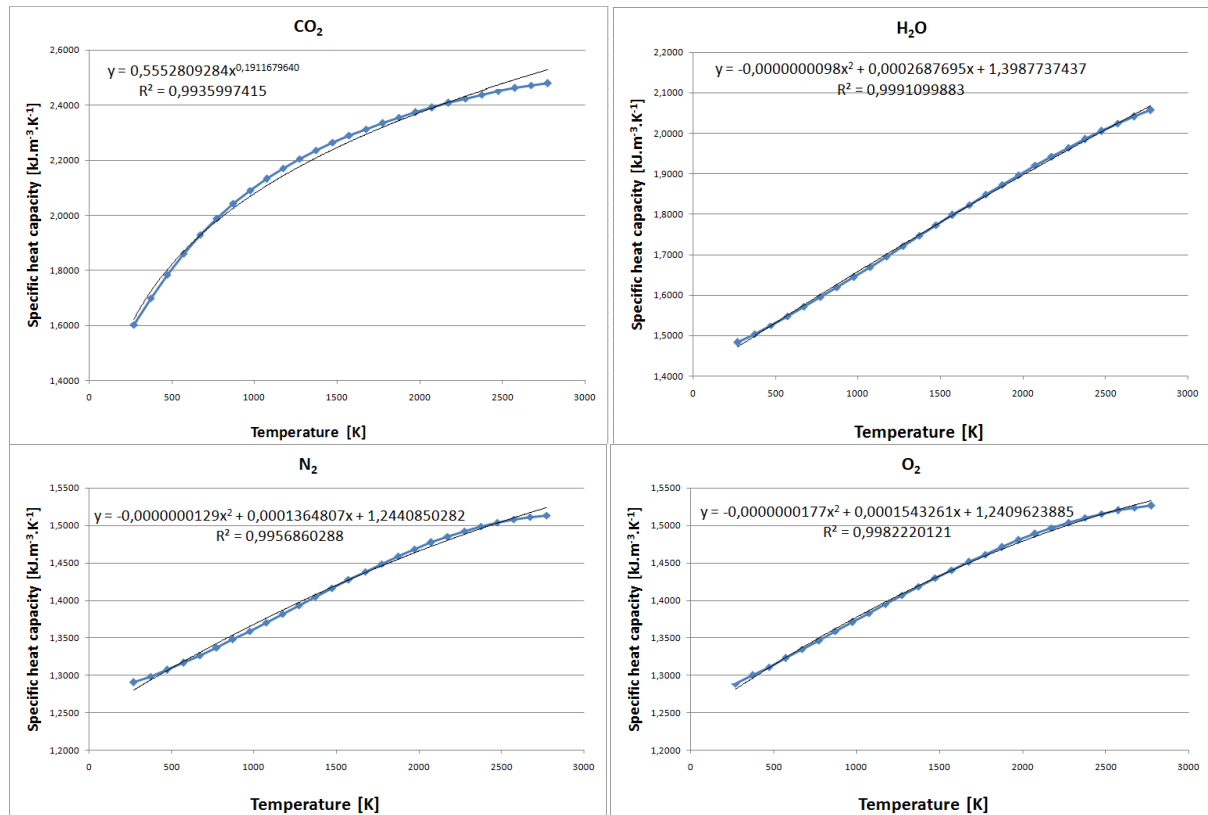

Fig. 1. Dependencies between specific heat capacity of CO_2, H_2O, N_2, O_2 [kJ.m^{-3}.K^{-1}] and temperature [K]

The final value of middle heat capacity of exhaust gases is calculated as middle heat capacity of gas mixture by equation

$$c_{mixture} = \sum_{i=1}^{n} r_i c_i \quad [kJ.m^{-3}.K^{-1}] \qquad (9)$$

where:

r_i – percentage of component i (computed by equations (3) to (6))

c_i – specific heat capacity of component i

We have to choose expected glycerin adiabatic temperature for calculation by iterative method. We suppose $t_a = 2100$ K. By using of graphs (Fig. 1) and equation (9) we compute resultant value of middle heat capacity of exhaust gases. This value we subsequently institute to equation (8) for adiabatic temperature calculation. We again use computed adiabatic temperature for new calculation of middle value of heat capacity of exhaust gases. We repeat calculation while value of adiabatic temperature isn't constant. The resultant value of adiabatic combustion temperature obtained by this method is $t_a = 2022$ K.

The calculation of adiabatic combustion temperature by CFD method uses combustion model of stoichiometric mixture of fuel and air. The course of combustion temperature depending on mixture richness is shown in the figure 2. Maximum value of temperature is equal adiabatic temperature when excess-air coefficient is $\lambda = 1$. Computed adiabatic temperature by CFD method using is $t_a = 2030$ K.
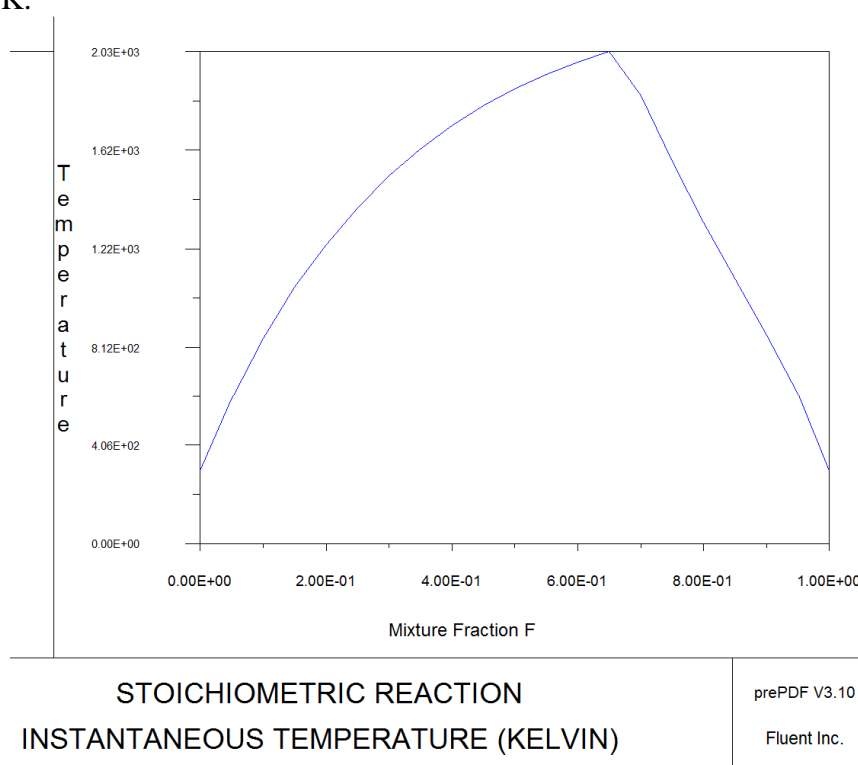

Fig. 2. Dependencies between combustion temperature [K] and mixture richness [-]

4. Conclusion

The adiabatic temperature computed by empirical equations is **2020 K** and adiabatic temperature computed by CFD model of stoichiometric mixture combustion is **2030 K**. The comparison of these two temperatures we can establish that the CFD model was chosen correct and we can use it for next complex CFD simulations of glycerin combustion in two – fuel experimental burner.

Acknowledgement

References

[1] LÁBAJ, J., KALINČÁK, D., KUKUČA P., GAJDOŠ J., GERLICI J., LACK T. *Výpočtové metódy* v dopravnej a manipulačnej technike, ES ŽU v Žiline, 1997

[2] PATSCH, M., LÁBAJ, J. *Possibilities of glycerine combustion in energy facilities*, Košice: TU Košice, Acta Metallurgica Slovaca, 1/2009

[3] LÁBAJ, J., PATSCH, M. *Proposal of dual-fuel burner for glycerin combustion*, Bojnice 2010, Aplikácia experimentálnych a numerických metód v mechanike tekutín a energetike

[4] PATSCH, M., LÁBAJ, J. *CFD simulation of glycerin combustion in experimental dual-fuel burner*. Rožnov pod Radhoštěm 2010, XXIX setkání kateder mechaniky tekutin a termomechaniky

[5] WARNATZ, J., MAAS, U., DIBBLE R.W. *Combustion, Physical and Chemical Fundamentals, Modeling and Simulation, Experiments, Pollutant Formation*, Springer-Verlag Berlin Heidelberg 1996, 1999, 2001, and 2006

Experimental Adsorption Cooling Device with Sun Collector

[*]Peter Pilát, Marek Patsch

[*]University of Zilina, Faculty of Mechanical Engineering, Department of Power Engineering, Univerzitná 1, 01026 Žilina, tel./ fax: +421 41 5252 541, e-mail: {peter.pilat, marek.patsch}@fstroj.uniza.sk

Abstract. This article describes project of adsorption cooling device, which utilize the solar energy from the solar collector for its work, with working pair adsorbent/ coolant zeolit/ methanol or zeolit/water. Prototype device we will use for parameters measuring of this device types. Result of measurings will be calculating of COP and ratio of energy supplied from the public electricity network and energy reached from the sun.

Keywords: adsorption, cooling, desorption

1. Introduction

Humanity still don't utilize some energetic sources, which don't charge environment or sources, which utilize, doesn't utilize them effectively. Adsorption cooling system with utilization of sun energy can be one of example, how is possible simply make a cool in the summer time, when is most necessary. Part of energy, what needs the device for work it takes from sun collector and part from the electric power net.

2. Utilization of sorption effect in cooling devices

Adsorbents are high porous material with very large inside space, on which can bind molecules of coolants with very big power. This effect we utilize in cooling Technologies for non compressor devices. Adsorbent sharply soak vapours of coolant (system is discharging) like a compressor in under pressure part of device. Pressure in system is going down and boiling point of coolant is moving down. Evaporative heat need on boiling of coolant is from air conditioning system or inside space of refrigerator, etc. But when the capacity of adsorbent is full, we have to coolant reach from the asorbent (desorption) by heat from the heat source –charge the system. This heat will be in our case from the sun collector or electric heat exchanger. Its means that this devices work discontinually. If is necessary, to have cool non-stop, system must to have minimally two absorbers, first one will be discharged and second one charged and upside down.

Coolant we choose according the temperature, we need. Every coolant has other freezing point and other evaporating heat. Where we need temperatures under 0°C, we can not use water like a coolant. Other coolant has, in comparison with water, lower evaporating heat.

Adsorbents we choose according the coolant, because not all coolants work with combination with all adsorbents. Next factor in association with adsorbent is desorption temperature. Every adsorbent has other desorption temperature. If is desorption temperature not so high (lower than 100°C), we can use for desorption low-potential heat sources, for example flat sun collectors.

3. Composition of system and how does adsorption system work

Adsorption cooling device are simple construction systems. It is assembled from heat source (in our case sun collector or electric heat exchanger) heat exchanger, evaporator-condenser and absorber-generator. Because the adsorption device is not continually working, in 1st phase absorber (dry adsorbent is charged by water vapour) absorb the vapour from the evaporator is cooling and we can utilize the cool for example to air conditioning system. System is discharged. In the 2nd phase we need the wet adsorbent to dry – charge the system. In this case absorber become to generator and evaporator become to condenser in our case we have condenser like separate device (because measuring of condensing heat and faster working). Discharge the adsorbent is possible by the heat and in our case by the solar thermal energy from collector. By heating of generator is the adsorbent agent charged and water vapour is condensed in condenser.
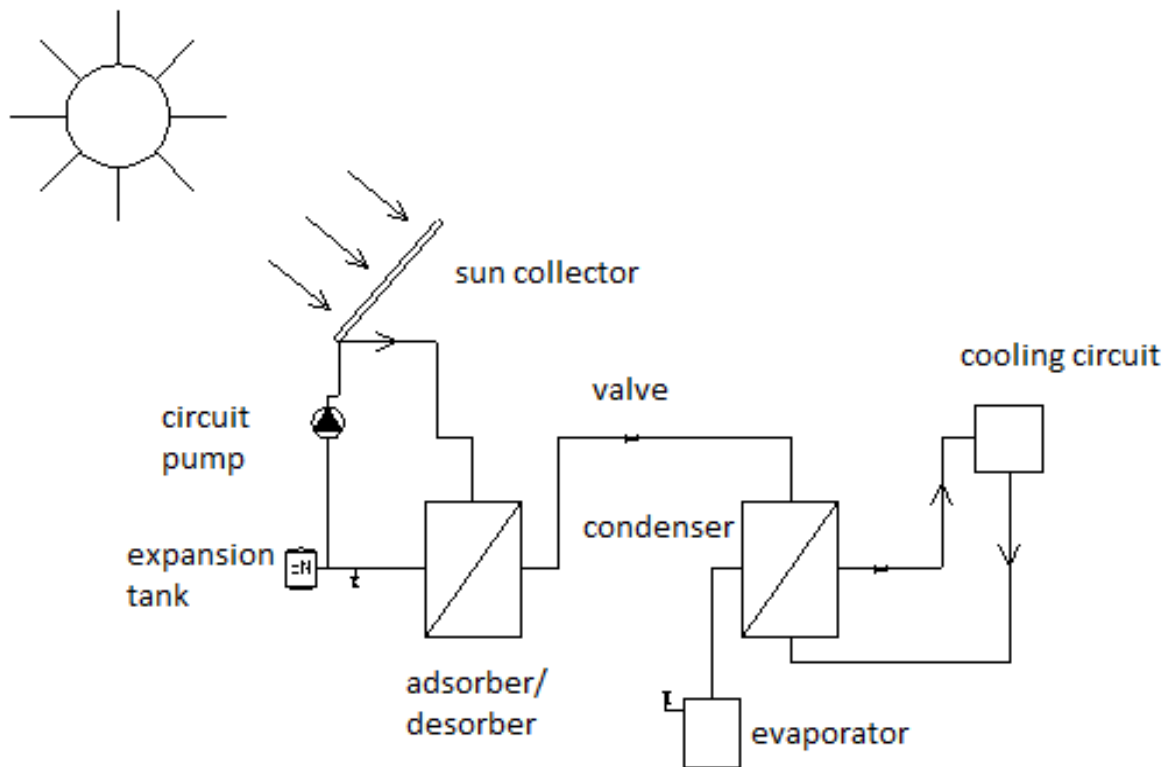

Fig. 1.   Scheme of experimental adsorption cooling device.

4. Experimental adsorption cooling device with utilization of sun energy with working pair zeolit/water, zeolit/methanol.

This device we designed for working pair zeolit/water or methanol. Watre has high evaporating heat, methanol has evaporating heat approx. half of water evaporating heat. But with methanol we can achieve lower temperatures (under °C), higher condensation temperatures, than with water and we suppose lower desorption temperatures. Water is very good, ecological and very cheap coolant. Methanol is for human poison but we will fill the device in liquid form – not so dangerose. Methanol occurs in nature and originate by germs anaerobic process.

For desorption we use heat from vacuum sun collector from company Viessmann, because has better power parameters, than flate collectors with the same surface and achieves higher temperatures, what is necessary for desorption process. Collector has active surface 3 m2. Like a

heat transport medium we use Alycol Thermo from company Slovnaft. For circulation of medium serve solar circuit pump Grundfoss.

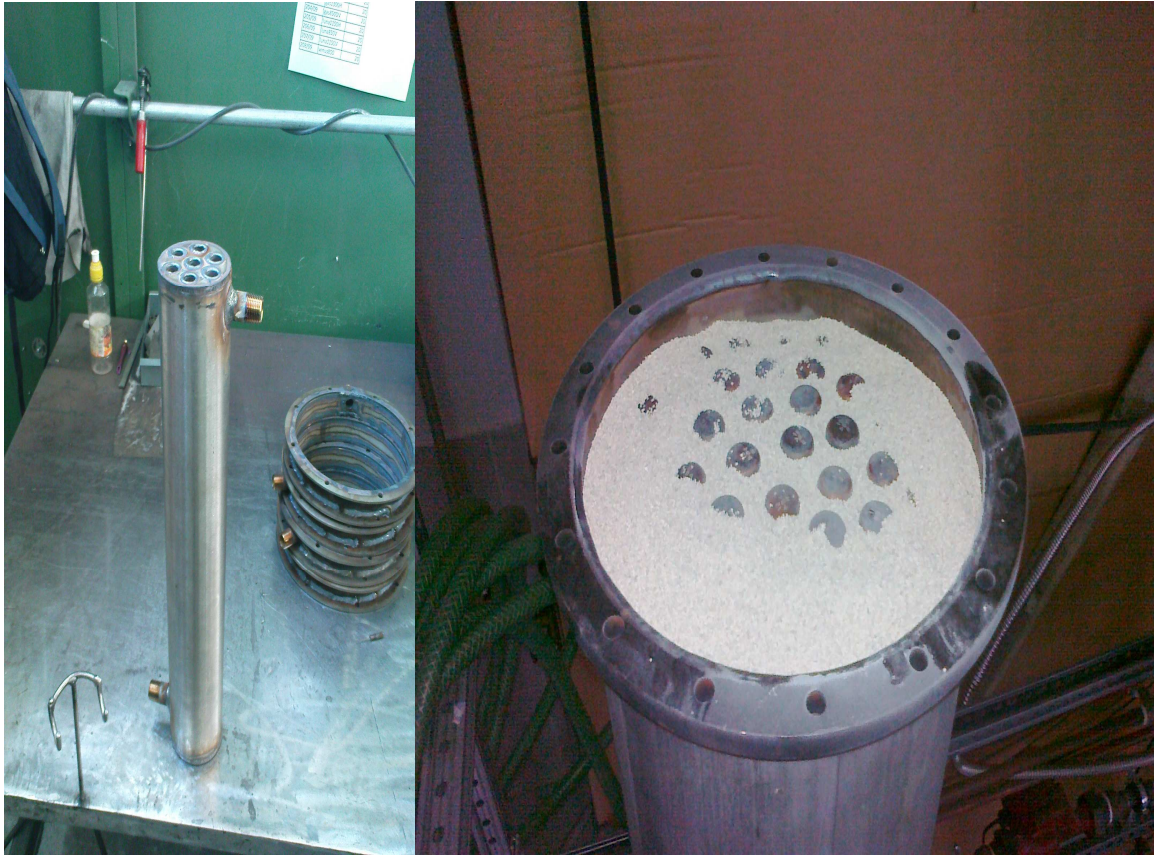System needs the others components like a expansion tank, system of valves safety system, etc.

Fig. 2. Condenser and adsorber with zeolit

5. Problems with construction of adsorption cooling system

The main problem with construction of this system is assuring vacuum tightness. If is not assured this parameter, boiling point temperature of coolant is moving up, or don't boil neither. System needs special material, which can work with temperatures to 250°C and can work in aggressive ambience, it hold for gaskets, fittings and constructions materials. Additional problem is dilatation of material, because device works with big temperature differences – in device have to be used high stiff screws.

Fig. 3. Construction of adsorber

6. Conclusion

The aim of project is relate coefficient of performance, desorption temperature with various coolants, lowest temperatures, which we can achieve with this device and exactly describe problems with construction, describe advantages and disadvantages of this system and possibility of utilization in practice.

References

[1] MASARYK, M. *Využitie zeolitových technológií v klimatizačnej technike,* Zpravodaj českého zväzu chladiacej techniky 6/97 (ČR), str. 14-18

[2] JANDAČKA, J. – MALCHO, M. – SMATANOVÁ, H. *Vplyv niektorých parametrov na chladiaci výkon absorbčných chladiacich jednotiek pracujúcich s roztokom voda – lítium bromid.* Acta Mechanica Slovaca 3-A/2004, Košice str. 581, ISSN 1335-2393

[3] JANDAČKA, J. – MALCHO, M. *Vplyv prevádzkových parametrov absorbčných klimatizačných systémov na zabezpečenie chladiaceho výkonu;* Zborník prednášok; 9.konferencia so zahraničnou účasťou; Vetranie a klimatizácia 2004, Liptovský Ján; jún 2004; str.103, ISBN 80-969030-4-7

[4] ULLRICH, H. J. *Chladící technika* II, Svaz CHKT, Praha, ISBN 80-238-5889-0

[5] LADISLAV N. *Solární kolektory, jejich účinnost a využití solárních systémů,* Chlazení / klimatizace 4/2006, ISSN 1211-1171

Thermodynamics of a Jet Engine in Experiment

[*]Peter Rajčan, Vladimír Hlavňa

[*]University of Žilina, Faculty of Mechanical Engineering, Department of automotive technology,
Univerzitna 2, 01026 Žilina, Slovakia, {rajcanp, vladimir.hlavna}@fstroj.uniza.sk

Abstract. Thermodynamics of Jet engines working on the principle of Brayton cycle is theoretically well described. Verification this knowledge by experiment will increase the opportunities to further examine this issue on the level of study and scientific level as well. It motivates students to a deeper examination of the problem. Allows you to compare theoretical and actual values of parameters and allows investigating the behavior of a jet engine in various modes includes standard and nonstandard. Such experiments will use small aircraft engines. For our experiment will be used engine Jet-Cat P200. It's single spool, single flow, jet engine with centrifugal compressor and axial turbine.

Keywords: Jet engine, test bench, measurement, thermodynamic, Brayton cycle, experiment

1. Introduction

A small jet engine Jet-Cat P200 was bought as a Support for teaching the subject of aircraft engines on Department of aviation, Faculty of Operation and Economics of Transport and Communications.

It will be used for a simple experiments focused on [1]:

- familiarize students with the operation of jet engine
- thermodynamics of jet engines
- energy balance of jet engine
- comparison of theoretical and real values of thrust and efficiencies of the engine
- comparison of specific parameters of this engine and commercial engines

Similar engines, for example. SR 30 from Turbinetechnologies are used in many laboratories around the world. Their arrangement is generally as follows: inlet diffuser radial compressor, annular combustor, axial turbine and fixed nozzle. Fig. 1. shows a simplified diagram of a jet engine operating on the Brayton cycle.
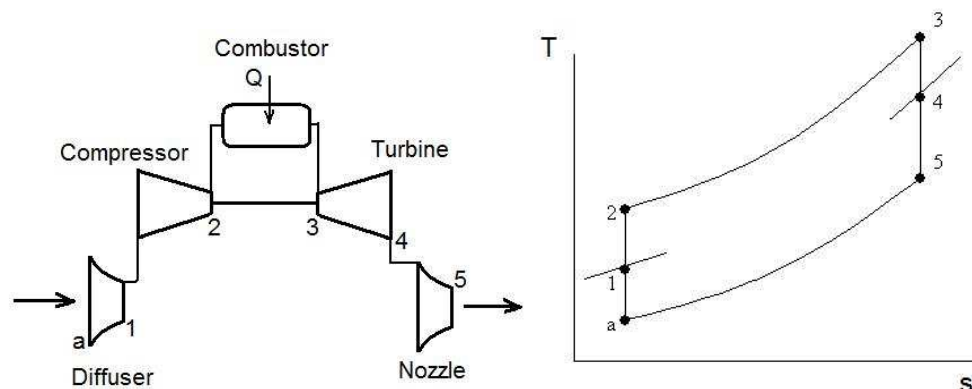

Fig. 1. Scheme of jet engine and his T-S diagram

But for this purpose are necessary changes so that it was possible to measure the basic operating parameters. In cooperation with Department of Automotive Technology of Faculty of Mechanical Engineering the engine test bench is being designed so that it is possible to record these parameters.

2. Design of test bench

Based on knowledge of similar experimental devices and set of requirements has been designed measuring scheme and itself the structure of the bench.

2.1. Measuring scheme

For experiments on a test bench is necessary to measure, record and evaluate these parameters:

Inlet air flow, fuel consumption, RPM's and temperatures and pressures on each section of the engine.

The measuring scheme for these measurements was created as on Fig.2 It contained two sections: control section and measuring section.
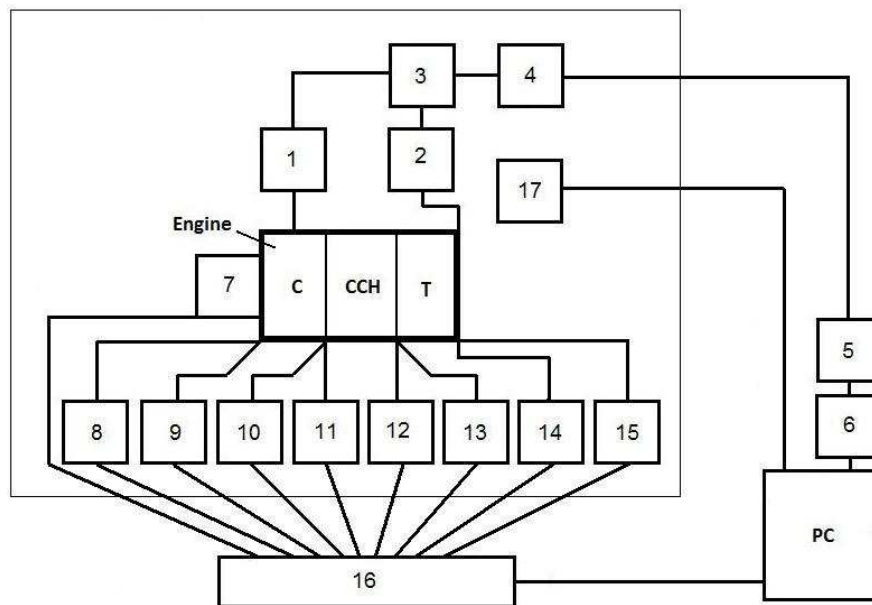

Fig. 2.   Measuring scheme

C – compressor, CCH – combustion chamber, T – turbine
Control section:
1.   RPM sensor
2.   Temperature sensor – exhaust
3.   ECU
4.   LED board
5.   GSU
6.   RS 232 interface
Measuring section:
7.   Inlet Air Flowmeter
8.   sensor EMS 20 – thrust
9.   RPM sensor
10. Sensor PTTJ-183 – compressor exit temprerature
11. Sensor of compressor exit pressure
12. Sensor PTTK-1 – turbine inlet temperature
13. Sensor of turbine inlet pressure
14. Sensor PTTK-1 – exit temperature
15. Sensor of exit pressure
16. Measuring card
17. Sensor T7510 – Atmospheric parameters

2.2. Test bench

The design of the bench must provide the ability to measure the required parameters and to provide user protection in case of destruction of the engine. According to these requirements was designed the test bench and engine mount as on Fig. 3.
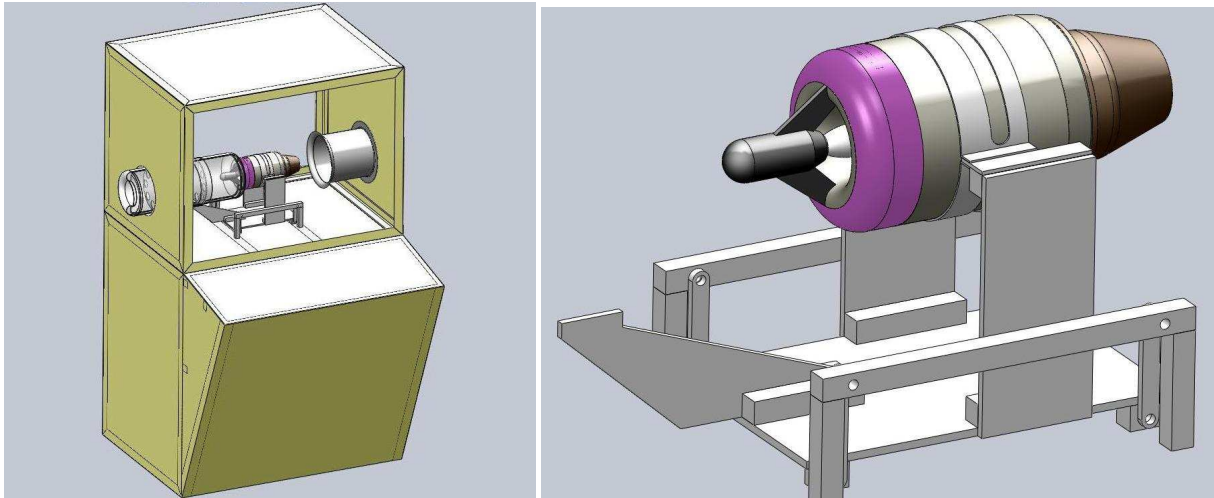

Fig. 3. Design of test bench and engine mount

3. Basic role of experiment

One of the main objectives of the experiment is to verify the theoretical parameters obtained by numerical methods with the actual values and observation of behavior of Jet engine in different modes. Fig. 4 shows the theoretical parameters of the engine on the output of the simulation software GasTurb11.
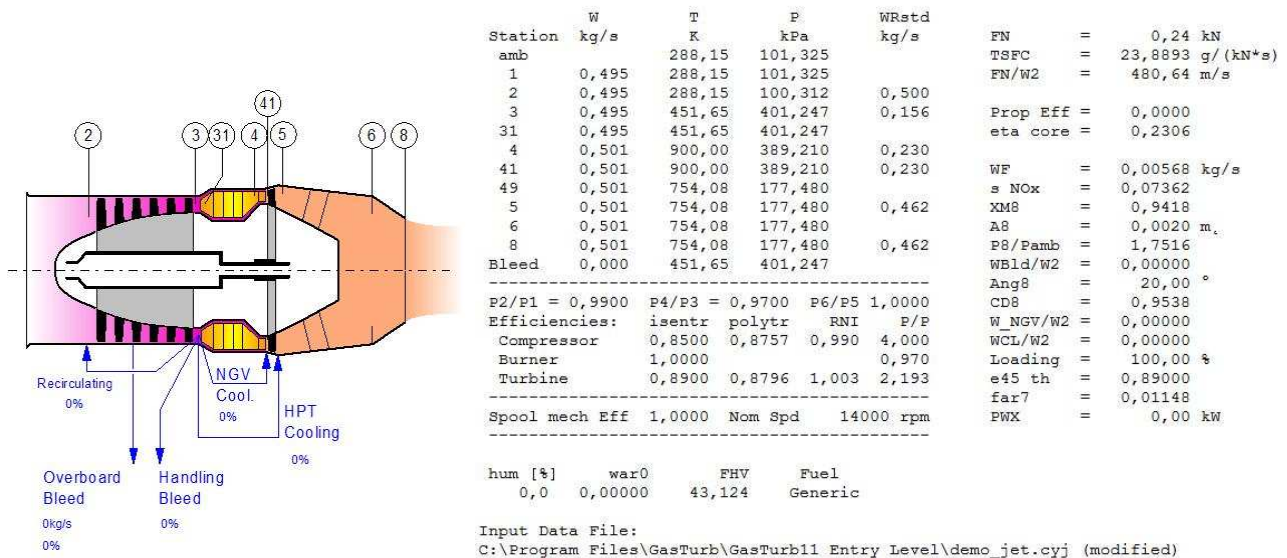

Fig. 4. Sections of engine and output parameters of GasTurb11

4. Conclusion

The test bench of small aircraft engine Jet-Cat P200 allows us to verify theoretical knowledge of jet engines, to transfer simple thermodynamic experiments in order to compare parameters with commercial jet engines and the investigation of energy flows in the engine. Read in to teaching students it will enrich their practical knowledge and motivate them to a deeper study of this issue.

References

[1] POURMOVAHED, A., JERUZAL, C. M., BRINKER, K. D. *Development of a Jet Engine Experiment for the Energy Systems Laboratory*. Washington, D.C.: ASME, 2003.

[2] KURZKE, J. *Gasturb 11*.

[3] www.turbinetechnologies.com

Selecting Flexible Manufacturing System Configuration Using CRISP-DM Methodology

[*]Marcin Rak, Jerzy Stamirowski
[*]Kielce University of Technology, Faculty of Mechatronics and Machine Building, Al. Tysiąclecia Państwa Polskiego 7, 25-314 Kielce, Poland

Abstract. This paper deal with CRISP-DM (Cross-Industry Standard Process for Data Mining) process model which can be utilized to develop model for selecting physical resources for flexible manufacturing system. Following sections describe main step for CRISP-DM process model as well as data structure model for machining system.

Keywords: CRISP-DM, flexible manufacturing system, system design.

1. Introduction

Nowadays, manufacturing companies have to cope with unpredictable changes in market demand. Manufacturing systems have to have adequate level of flexibility in order to react to market fluctuations immediately and cost-effectively. A system that is able to accomplish these goals have to consist with modules (hardware and software) that can be removed, added, replaced or upgraded so that a new process technology can be quickly adjusted to cope with the unstable environment. The level of system flexibility strictly depends on modules determined at the system design stage. Therefore, it is necessary to develop an integrated methodology that allow system designers easily and quickly choose most appropriate modules for new or existing manufacturing systems. This article deals with methodology that can be applied to determined hardware system modules (machine, conveyors, auxiliary equipment) for flexible manufacturing systems. This methodology based on CRISP-DM (Cross Industry Standard Process for Data Mining) reference model using relational databases. Section 2 briefly describes main step in CRISP-DM model, while section 3 shows proposed data structure model for machining systems.

2. The CRISP-DM reference model

The CRISP-DM is the industry standard methodology for data mining and predictive analytics that was developed by a consortium funded by the European Commission. The CRISP-DM methodology was invented for data mining projects with large dataset, but can be also applied for projects with smaller dataset.

The CRISP-DM reference model for data mining projects is shown on Fig. 1. This model depicts overall life-cycle of a data mining projects. In the CRISP-DM model, six major phases were distinguished:

1) Business understanding – this phase was divided into four tasks: determine business objectives, assess situation, determine data mining goals, produce project plan. It focuses on understanding data mining project objectives and requirements from a business point of view.

2) Data understanding – this phase was divided into four tasks: collect initial data, describe data, explore data, verify data quality. It focuses on collecting and understanding initial data as well as identification data quality problems and detection subset to form some hypotheses for hidden information.

3) Data preparation – this phase was divided into five tasks: select data, clean data, construct data, integrate data, format data. It focuses on creating the dataset that will be next introduced into the modeling tools. It also includes cleaning and transformation (normalization, standardization or even assignment some coefficients for qualitative data if it is necessary for modeling tools). In most cases this step will be performed several times before data reach the final state.

4) Modeling – this phase was divided into four tasks: select modeling technique, generate test design, build model, assess model. It focuses on selecting the best modeling technique and determining optimal values for his parameters. Some modeling technique require special preparation of input data, so it is common to move back to data preparation phase.

5) Evaluation – this phase was divided into three tasks: evaluate results, review process, determine next steps. It focuses on assessing selected model in order to verify if all business objectives and requirements were reached.

6) Deployment – this phase was divided into four tasks: plan deployment, plan monitoring and maintenance, produce final report, review project. It focuses on developing and improving obtained model.
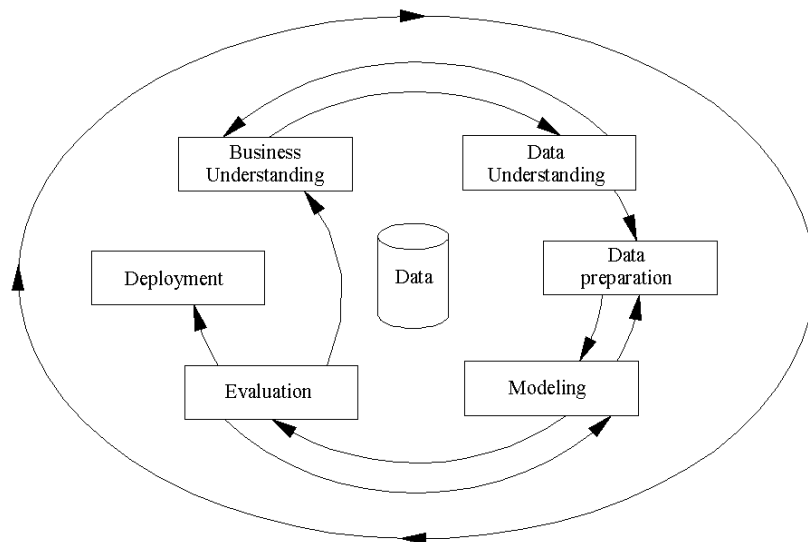

Fig. 1. The CRISP-DM reference model [1]

Relationships, that were shown in Fig. 1, are the most important dependencies between defined phases. However, relationships could be determined between each phases depending on users requirements. Data mining is a cyclic process, it is depicted as a outside circular loop. All results, information and experiences gained from one data mining cycle should be utilized for next one in order to find the best solution.

CRISP-DM reference model can be applied for selecting modules for manufacturing systems. Methodology presented in this section was outlined briefly, for more details see [1].

3. Database model of flexible manufacturing system

Colledani, Terkaj and Tolio in their work proposed process-product-system information formalization for production system. In flexible manufacturing systems, three main areas, as shown in Fig. 2, were distinguished: System, Product, Process.

An UML (Unified Modeling Language) object-oriented model of production system for decision support methods was presented in [2]. Each main area was divided into several classes (some of this classes are derived from STEP-NC standard), and each class is characterized by several attributes.

Production System area was divided into ten classes as shown on Fig. 3. All of those classes describe physical resources and structural characteristics of the manufacturing system. More detailed information about classes and their attributes can be found in [2]. Machine class, for example characterized by following attributes: number of controlling axes, work cube dimensions, maximum spindle speed, precision level, number of slots in the tool magazine, machine efficiency, time to change a tool on machine etc.
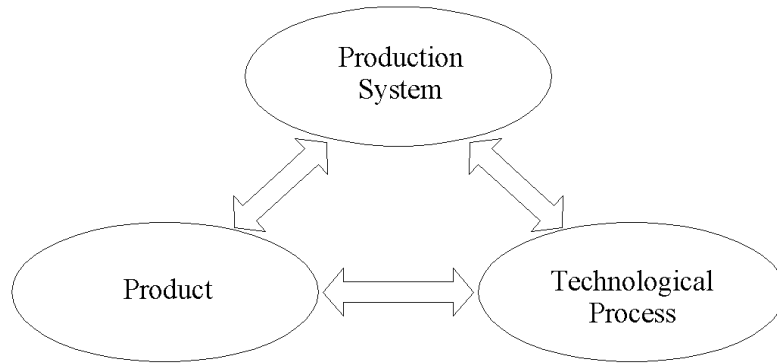

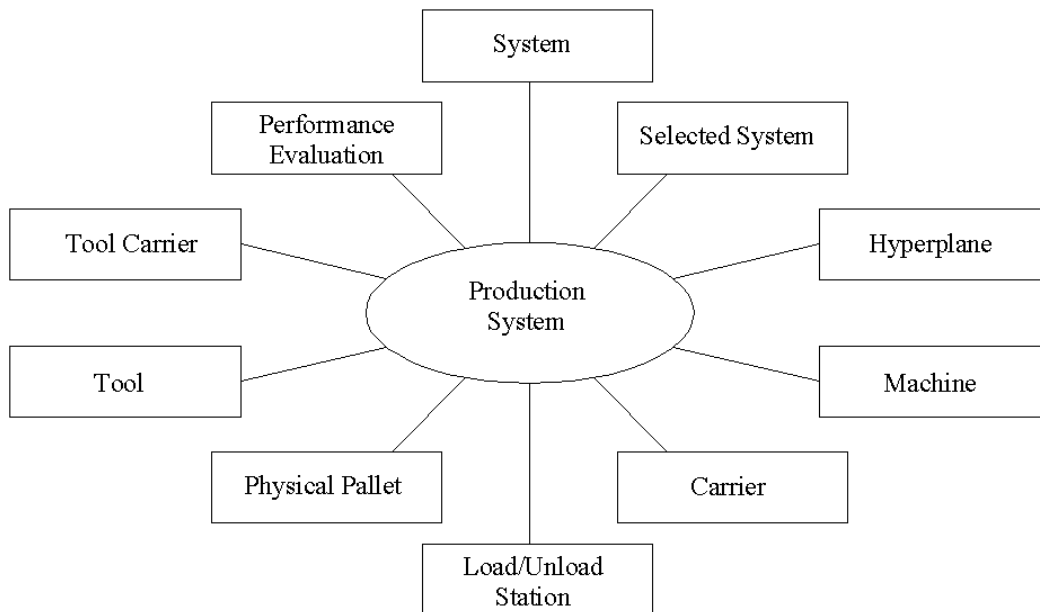**Fig. 2.** Three main areas in manufacturing systems [2]

Fig. 3. Production system classes [2]

Product area was divided into four classes (Fig. 4). All of those classes describe the workpiece, his geometrical complexity and possible evolution of the workpiece according to predicted scenarios.
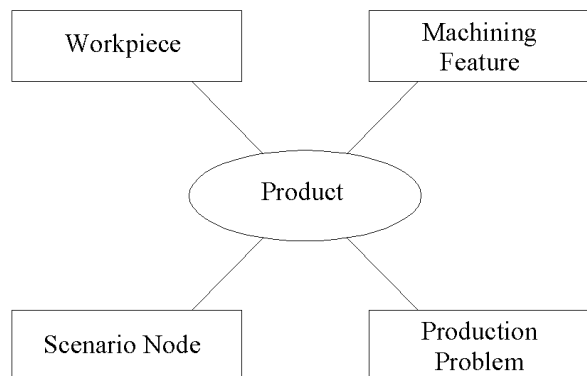

Fig. 4. Product classes [2]

161

Technological Process area was divide into six classes as shown on Fig. 5. All of those classes describe machining process, tools, technological parameters, operation sequence, location and orientation workpiece on the pallet, time needed to machine particular feature on the workpiece.
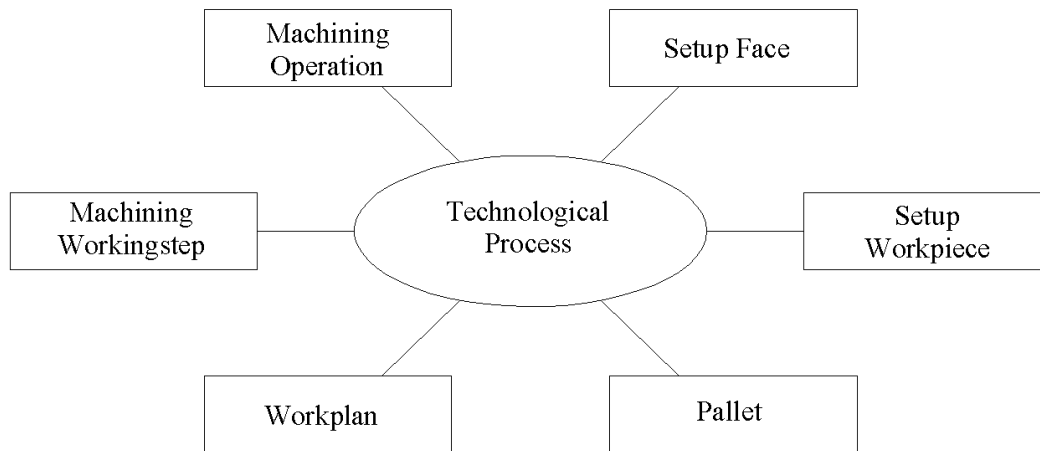

Fig. 5. Technological process classes [2]

Model of flexible production system presented in this section is a framework that can be utilized for developing methodologies and tools in manufacturing system design domain. In peculiarity, it can be used to determine physical resources (machines, carriers, pallets) for flexible manufacturing systems. The proposed data structure model can be use to define new production system, starting from the green field, as well as, to define new configuration of existing system (reconfiguration task). Methodology presented in this paper can also be used for design a new type of system, namely, Reconfigurable Manufacturing System (RMS). This type of system, from its definition, has full modular structure, consist with hardware and software modules. Therefore this methodology can also be used for determining physical resources (modules) for reconfigurable systems.

4. Conclusion

Nowadays companies must struggle with aggressive competition and rapid changes in market demand. Developing methodologies and tools for manufacturing system designers is a main issue for researchers in this domain. Methodology presented in this work can be used for selecting physical resources for flexible manufacturing systems as well as for determining physical modules for reconfigurable manufacturing systems.

Acknowledgement

References

[1] CHAPMAN, P. – CLINTON, J. – KERBER, R. – KHABAZA, T. – REINARTZ, T. – SHEARER, C. – WIRTH, R. *CRISP-DM 1.0 Step-by-step data mining guide.* 2000.

[2] TOLIO, T. *Design of flexible production system: methodologies and tools.* Springer-Verlag Berlin Heidelberg, 2009.

[3] STAMIROWSKI, J. – RAK, M. *An integrated methodology for selecting physical resources for flexible manufacturing systems.* XVII International Science and Engineering Conference: Machine-Building and Technosphere of the XXI Century, Sevastopol 2010.

[4] LAROSE, D. T. *Odkrywanie wiedzy z danych.* PWN, Warsaw 2006.

The Algorithm of the New Method for Mechanical Structures Adaptive Identification and its Software Support

*Ján Raždík, Bohuš Leitner

*University of Žilina, Faculty of Special Engineering, Department of Technical Sciences and Informatics, 1.mája 32, 01026 Žilina, Slovakia, {Jan.Razdik, Bohus.Leitner}@fsi.uniza.sk

Abstract. The paper deals with one of possible ways of an identification of stochastically loaded mechanically structures. The purpose of this approach is to find an algorithm of a forecasting control of their working in real working conditions. It deals with a proposal of an application of vector time series moving average models (VARMA). The paper contains a theoretical principle of problems solved and a description of a real testing methodize.

Keywords: Mechanically structure, stochastic loads, identification, vector autoregressive models VARMA, virtual model of crane jib, software support - ArmaGet, ARMASA Package.

1. Introduction

It is well known that working of majority of machines is significantly influenced by different kinds of stochastic loads. There is possible to respect the tendency a limitation of energetically and material consumption to oversize their dimensions. But it is necessary to look for some more ingenious methods to deal with this problem`s. Some of them are the ways to control (influence) the working of a mechanical system in respect to their proposed behaviour. But it needs to follow of the system behaviour in the real time and to make some necessary controlling interventions.

2. VARMA models in Stochastically Loaded Parts Identification Process

There is necessary to identify such a system at first. It means to get its statistically adequate mathematical model. There is possible by using this model and by developing sufficient fast and correct machine control system and suitable software to forecast behaviour of system in the near future. We can get in such a way the possibility of making some controlling corrections before the system reaches an unstable region.

2.1. Vector Autoregressive Moving Average Models (VARMA)

It was found the as a suitable solution for a stochastically loaded mechanical structure identification can be used the ARMA (autoregressive moving average) models or their vector modification VARMA (Vector Autoregressive Moving Average) models [3], [4].

A stochastically loaded part of structure and its behaviour during time can be described by using of scalar autoregressive moving average model ARMA. Its identification (stochastically adequate model) but gives just an information about its own behaviour without a relationship to the whole structure during acting of different working regimes.

We have found as one of possible ways the use of vector autoregressive moving average models VARMA to improve accuracy of stochastically loaded mechanical structures identification.

These models are suitable for stochastically loaded mechanical structures identification which outputs are reflections on stochastically loads in more number of points – vector time series (Fig.1).
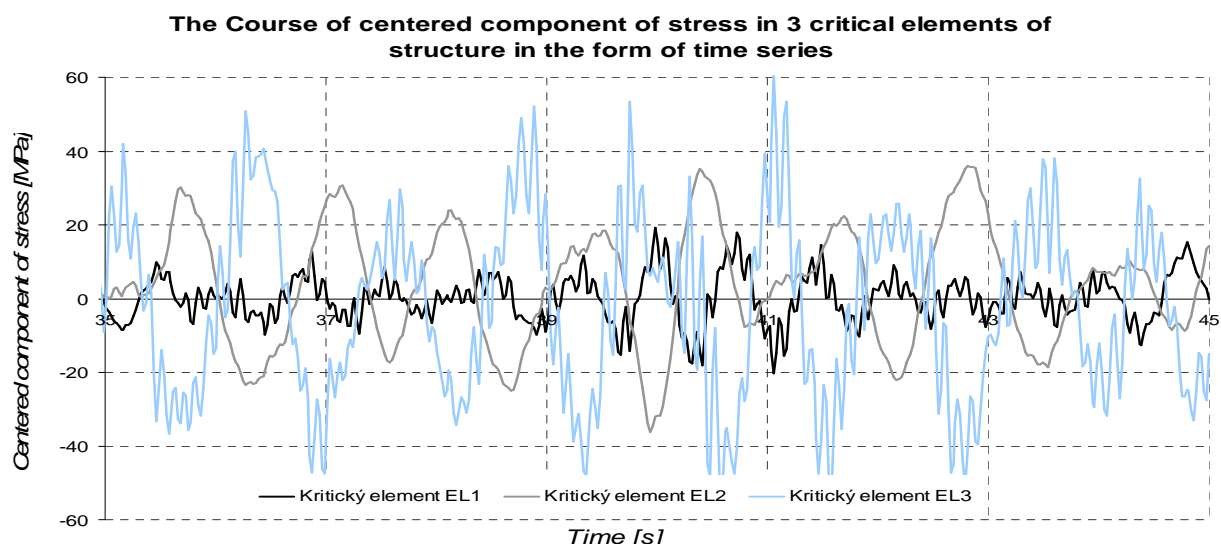
The Course of centered component of stress in 3 critical elements of structure in the form of time series

Fig. 1. A Vector Time Series of Stress in elements of structure.

A searched vector model VARMA (m,n) can be expressed as a matrix equation in form [3]

$$\mathbf{x_t} - \mathbf{A_1} . \mathbf{x_{t-1}} - \mathbf{A_2} . \mathbf{x_{t-2}} - ... - \mathbf{A_m} . \mathbf{x_{t-m}} = \boldsymbol{\varepsilon_t} - \mathbf{B_1} . \boldsymbol{\varepsilon_{t-1}} - \mathbf{B_2} . \boldsymbol{\varepsilon_{t-2}} - ... - \mathbf{B_n} . \boldsymbol{\varepsilon_{t-n}} \quad (1)$$

or in written out form [3]

$$
\begin{bmatrix} x_{1t} \\ x_{2t} \\ ... \\ x_{kt} \end{bmatrix} - \begin{bmatrix} a_{111} & a_{121} & ... & a_{1k1} \\ a_{211} & a_{221} & ... & a_{2k1} \\ ... & & & \\ a_{k11} & a_{k21} & ... & a_{kk1} \end{bmatrix} . \begin{bmatrix} x_{1t-1} \\ x_{2t-1} \\ ... \\ x_{kt-1} \end{bmatrix} - ... - \begin{bmatrix} a_{11m} & a_{12m} & ... & a_{1km} \\ a_{21m} & a_{22m} & ... & a_{2km} \\ ... & & & \\ a_{k1m} & a_{k2m} & ... & a_{kkm} \end{bmatrix} . \begin{bmatrix} x_{1t-m} \\ x_{2t-m} \\ ... \\ x_{kt-m} \end{bmatrix} =
$$
$$
\begin{bmatrix} \varepsilon_{1t} \\ \varepsilon_{2t} \\ ... \\ \varepsilon_{kt} \end{bmatrix} - \begin{bmatrix} b_{111} & 0 & ... & 0 \\ 0 & b_{221} & ... & 0 \\ ... & & & \\ 0 & 0 & ... & b_{kk1} \end{bmatrix} . \begin{bmatrix} \varepsilon_{1t-1} \\ \varepsilon_{2t-1} \\ ... \\ \varepsilon_{kt-1} \end{bmatrix} - ... - \begin{bmatrix} b_{11n} & 0 & ... & 0 \\ 0 & b_{22n} & ... & 0 \\ ... & & & \\ 0 & 0 & ... & b_{kkn} \end{bmatrix} . \begin{bmatrix} \varepsilon_{1t-n} \\ \varepsilon_{2t-n} \\ ... \\ \varepsilon_{kt-n} \end{bmatrix}
$$
$$(2)$$

this can be transformed in the system of k linearly independent equations. The symbol of "k" means number of points of the structure in which the output on dynamic loads are recorded. The left hand side of matrix equation (1) expresses the dependence of vector time series values on former values of the series and the right hand side shows the relationship of stochastically random deviations.

2.2. The Possibilities and Advantages of VARMA Models

The application of VARMA models as an alternative to the systems of differentials equations for stochastically loaded structures identification is suitable from different point of view too. If we can express the system of differential equations in a simplified form [4] as

$$\mathbf{M}\ddot{\mathbf{x}} + \mathbf{K}\dot{\mathbf{x}} + \mathbf{C}\mathbf{x} = \mathbf{F}(\mathbf{t}) \quad (3)$$

where **M**, **B** and **K** are *n x n* mass, damping and stiffness matrices, $\ddot{\mathbf{x}}, \dot{\mathbf{x}}, \mathbf{x}$ and $\mathbf{F}(t)$ are n–dimensional column vectors of accelerations, velocities, displacements and force respectively. Its matrix formulation is in form (4). We can judge the matrix of damping **K** and the matrix of stiffness **C** as a mathematical expression of the relationship among the individual parts of structure.

164

The matrix coefficients as $\mathbf{a_1, a_2, \ldots, a_m}$ of a vector model VARMA are the mathematical expressions of individual parts interaction.

$$\begin{bmatrix} m_1 & 0 & \ldots & 0 \\ 0 & m_2 & \ldots & 0 \\ \ldots & & & \\ 0 & 0 & \ldots & m_n \end{bmatrix} \cdot \begin{bmatrix} \ddot{x}_1 \\ \ddot{x}_2 \\ \ldots \\ \ddot{x}_n \end{bmatrix} + \begin{bmatrix} k_{11} & k_{12} & \ldots & k_{1n} \\ k_{21} & k_{22} & \ldots & k_{n2} \\ \ldots & & & \\ k_{n1} & k_{n2} & \ldots & k_{nn} \end{bmatrix} \cdot \begin{bmatrix} \dot{x}_1 \\ \dot{x}_2 \\ \ldots \\ \dot{x}_n \end{bmatrix} + \begin{bmatrix} c_{11} & c_{12} & \ldots & c_{1n} \\ c_{21} & c_{22} & \ldots & c_{n2} \\ \ldots & & & \\ c_{n1} & c_{n2} & \ldots & c_{nn} \end{bmatrix} \cdot \begin{bmatrix} x_1 \\ x_2 \\ \ldots \\ x_n \end{bmatrix} = \begin{bmatrix} f_1(t) \\ f_2(t) \\ \ldots \\ f_n(t) \end{bmatrix} \quad (4)$$

The advantages of VARMA models:
- they can show the physically base of problem studied (this means that they to obtain the natural frequencies and natural modes of vibrations) [4],
- they can describe a wanted accuracy of real system [2], [3],
- the mathematical apparatus of methods is relative simple (use for "real time" control [3], [4]).

3. The Software Support of a Proposed Method of Identification

The scalar models of a simple description of dynamic system can not express statistically adequate description of complex systems. For this reason there was developed an effective software system which enables to create the statistically models of dynamic stochastic system by using VARMA models. The accuracy and the reliability of the developed methods and algorithms were verified by use of commercial software packages.

The creation of a software support which is able to identify some stochastic loaded parts of structures is just the firs step for applying of the adaptive control of mechanical system activity. The result of a proposed application of this methodology is software product ArmaGet. This developed software is able to create an adequate mathematical model for describing a matrix model of a tested stochastic loaded mechanical system. There was developed a FEM (Finite Element Method) model of a crane jib (Fig.2) and in MATLAB environment was realized simulation of its loading. The acting loads were described as a stochastic excitation in form of a stochastic time series.
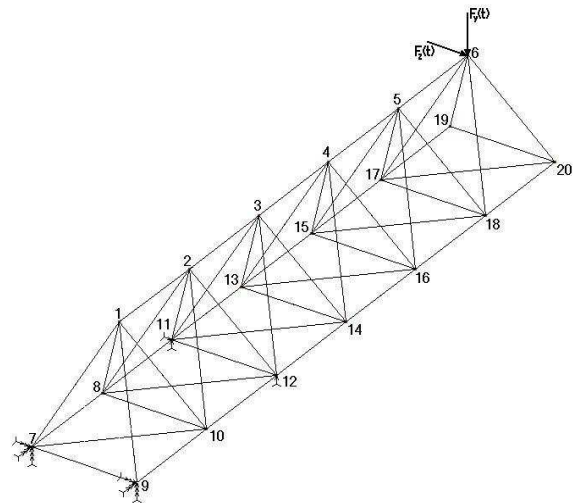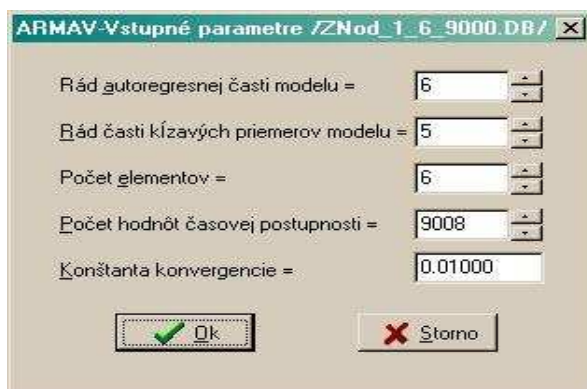

Fig. 2. FEM model of a crane jib
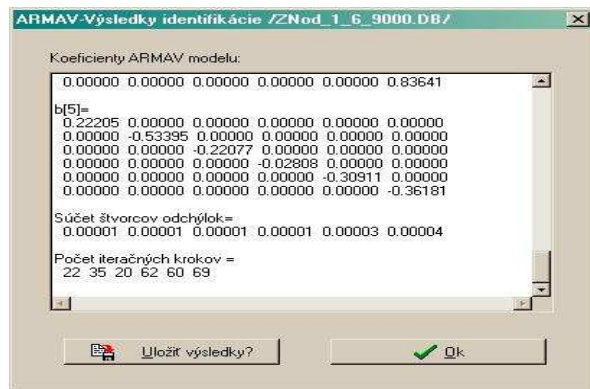

Fig. 3. Settings of input parameters.

Fig. 4. Results of a jib upper boom identification –
an optimal model VARMA (6,5).

165

There were used as an application of a numeric Crank-Nicolson method [5] of direct integration the deformation of all nodes of FEM model (20 nodes). The time intervals were selected as Δt vz = 0.01 s. Resulting outputs for deformation were organized in corresponding vector time series. There was selected in a testing example a vector time series of deflection in "z" axe direction. The determination of vector time series in direction of "z" axe is introduced on Fig.3 and results of identification are introduced on fig.4 (an optimal order of model is VARMA (6,5)). The verification of developed software support (ArmaGet) was realized by two different ways.

At first it was the simulation of time series with determined parameters and their "back way" identification (this option is available by menu item *Simulation→Model VARMA*). The second way was a comparison with results of software Package ARMASA [2]. There are showed in Tab.1 the results of an application of ArmaGet software and their comparison with results obtained using available product - ARMASA Package.

	VARMA(6,5)		VARMA(8,7)		VARMA(10,9)	
	ArmaGet	*ARMASA*	*ArmaGet*	*ARMASA*	*ArmaGet*	*ARMASA*
Node 1	$7{,}9591.10^{-6}$	$7{,}9606.10^{-6}$	$7{,}9251.10^{-6}$	$7{,}8991.10^{-6}$	$7{,}8985.10^{-6}$	$7{,}8398.10^{-6}$
Node 2	$1{,}0659.10^{-5}$	$1{,}1381.10^{-5}$	$1{,}0493.10^{-5}$	$1{,}1243.10^{-5}$	$1{,}0365.10^{-5}$	$1{,}1953.10^{-5}$
Node 3	$1{,}1204.10^{-5}$	$1{,}2789.10^{-5}$	$1{,}0689.10^{-5}$	$1{,}1868.10^{-5}$	$1{,}0424.10^{-5}$	$1{,}1307.10^{-5}$
Node 4	$1{,}4823.10^{-5}$	$2{,}4128.10^{-5}$	$1{,}4327.10^{-5}$	$2{,}1467.10^{-5}$	$1{,}4028.10^{-5}$	$2{,}0833.10^{-5}$
Node 5	$2{,}5955.10^{-5}$	$4{,}3874.10^{-5}$	$2{,}3396.10^{-5}$	$4{,}2690.10^{-5}$	$2{,}2255.10^{-5}$	$3{,}5906.10^{-5}$
Node 6	$4{,}1240.10^{-5}$	$8{,}4167.10^{-5}$	$3{,}8608.10^{-5}$	$6{,}4402.10^{-5}$	$3{,}7822.10^{-5}$	$6{,}2980.10^{-5}$

Tab. 1. The verification of the identification results (ArmaGet and Excel).

4. Conclusion

It was shown that by using of a suitable mathematical apparatus can forecast the future behaviour of a mechanical structure. The vector time series and its models (VARMA) were chosen as a suitable mathematical apparatus and the suitability of this choice were proven by use of computer simulation of stochastically excited mechanical systems parameters.

Acknowledgement

References

[1] BROERSEN, P.M.T. *ARMASA Package.* http://www.mathworks.com/matlabcentral/fileexchange/loadFile.do? objectId =1330&objectType=file .

[2] BROERSEN, P.M.T. – BOS, R. *Time-series analysis if data are randomly missing*. TU Delft digital repository, IEEE, 2006, Netherlands. http://repository.tudelft.nl/file/379514/370833.

[3] LEITNER, B. – BEŇO, B. *Identification of stochastic systems exposed to lifting and transport machinery through vector autoregressive models*. In: Electronical magazine „Zdvíhací zařízení v teorii a praxi", 1/2007, 8 p., VŠB-TU, Ostrava 2007, Czech Republic. http://www.342.vsb.cz/zdvihacizarizeni/zz-2007-1.pdf (in Slovak).

[4] LEITNER, B. – MÁCA, J. *Theoretical Principles of Mechanical Structures Identification and Their Use For selected Modal Characteristics Determination*. In: Proceedings of International Conference "TRANSPORT 2005", VTU of Todor Kableshkov, Sofia 2005, Bulgaria, pp. IX.44 – IX.50. ISBN 954-12-0115-6.

[5] SÁGA, M. et al. *Computer analysis and synthesis of mechanical systems*. ZUSI, Žilina 2002, 267 p. (in Slovak)

Transient Dynamic Analysis of Rectangular Orthotropic Composite Plates

*Daniel Riecky, Milan Žmindák, Pavol Novák
*University of Žilina, Faculty of Mechanical Engineering, Department of Applied Mechanics, Univerzitna 1, 01026 Žilina, Slovakia {daniel.riecky, milan.zmindak, pavol.novak}@fstroj.uniza.sk

Abstract. This contribution deals with transient dynamic analysis of composite plates. The finite element method (FEM) and meshless local Petrov-Galerkin method (MLPG) are applied. First, the FEM solves the problem of a simple supported rectangular plate reinforced with carbon fiber and compressive loading, and then the MLPG method solves a three-layer orthotropic plate loaded with a single force.

Keywords: Finite element method, Meshless local Petrov- Galerkin method, transient analysis, orthotropic composite plate.

1. Introduction

In recent years are the demands on planar and space structures increasing. The objective is to minimize their weight and increase strength and resistance. One possibility is to use layered structures composed of composite materials. Thin laminated plate structures are commonly used in engineering practice for designing aircraft, ships and civil engineering. The most significant advances in the analysis of shell structures were made using the finite element method (FEM) and boundary element method (BEM). Apart from some problems of bending of thin plates with simple transverse loads or simple boundary conditions, it is very difficult to obtain general analytical solutions. Therefore are the numerical studies of their behavior for different loads necessary. The idea of numerical simulations of plates is to transform complex problems into real simple discrete mathematical forms. Then it is necessary to solve the problem in the computer and thus create a model approaching the requirements of analysts. If properly used, numerical methods can be effectively obtain numerical or approximate solution to a complex problem.

In this paper we applied FEM and MLPG method to solve simple supported orthotropic plates. Numerical examples are presented and discussed to show the accuracy and the efficiency of the present MLPG method.

2. Theoretical background

Shells and plates are structures in which the thickness h is at least one order of magnitude smaller than the representative planar dimension L (Fig. 1). This fact allows use Reissner-Mindlin theory [1] to reduce the 3D problem to a 2D problem (Fig. 2). This reduction transforms the problem, which is defined at each point in the 3D continuum to a problem defined in each point of the reference surface of the plate. Elimination of the coordinate in the thickness direction h is usually performed during the integration of equilibrium equations. This elimination can be done by several methods [2].

So far known formulations for monocoque plates and shells are divided into three groups:
1. Continuum based or stress resultants based models.
2. Asymptotic type approaches.
3. Axiomatic type approaches.

There exist a number of plate and shell theories, and they differ from each other in two principal ways: (1) the choice of the assumed field (i.e. displacement or stress), (2) the choice of terms in expansion (i.e. number of terms and powers of thickness coordinate z in displacement expansion.
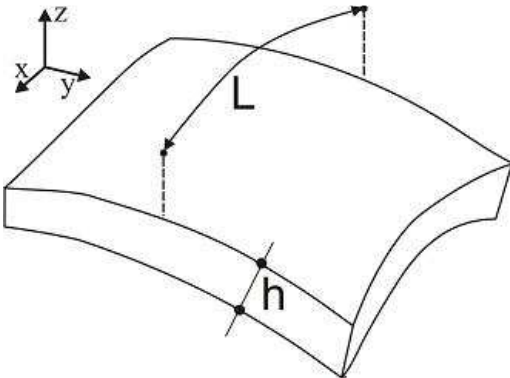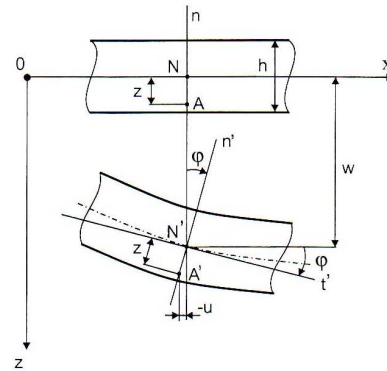

Fig. 1. Geometric parameters

Fig. 2. Bending of the plate

The number of theories further multiplies if different order expansions are used for different components of a field variable and types of nonlinear terms included in the strain-displacement relations.

3. Numerical solution

There is a growing interest to develop new advanced numerical methods despite the great success of the FEM and the BEM. Meshless approaches to problems of continuum mechanics have attracted more attention during the last decade, particularly due to their low requirements and high adaptivity on preparation of input data for numerical analysis. Many meshless methods are derived from the weak formulation on the global domain or a set of local subdomains [3]. Cells are required in the global formulation for the integration of the weak form [4]. Cells are not required in the methods based on local weak formulation and therefore are often referred to as real meshless methods. The MLPG method is the basis for the derivation of many meshless formulations. Test functions for the MLPG are selected from different functional areas. The method was successfully applied to problems of plates and shells with homogeneous and orthotropic material properties.

4. Solved problems

Example 1 – simple supported plate under pressure loading
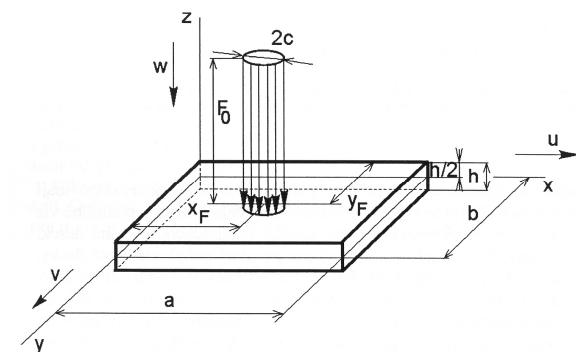

Fig. 3. Plate under pressure loading

The first problem solved is a rectangular plate of dimensions 250 x 250 x 0.89 (fig. 3). It's made of unidirectional composite, carbon fibers in epoxy matrix. Fibers are parallel to one edge of the plate, labeled as the direction "11". Other directions are "22" and "33". Density of this material is 1 540 kg.m^{-3}. Material constants are: $E_{11} = 1.299.10^{11}$ Pa, $E_{22} = 1.39.10^{10}$ Pa , $E_{33} = E_{22}$, $\mu_{12} = 0.28$, $\mu_{23} = 0.741$, $\mu_{31} = 0.03$, $G_{12} = 4.5.10^9$ Pa, $G_{23} = 3,992.10^9$ Pa, $G_{31} = 4.5.10^9$ Pa. Relaxation time is $t = 3.68932.10^{-5}$.

Given the symmetry of the plate, we modeled only a quarter of the plate. The plate is supported and its degrees of freedom are restrained on its edges and in the middle. The area loaded with pressure has a circular shape and a radius of c, $F = \pi.c^2 p_z$. The time course of the load is determined by Heaviside function $F(t) = F_0.H(t)$. The main task in this problem was to obtain values of displacement components $u_x(x, y, z, t)$, $u_y(x, y, z, t)$, $u_z(x, y, z, t)$ and velocity and acceleration components.

Fig. 4a shows the time course of the displacement and fig. 4b shows the time course of velocity in the middle of the plate and center lines which cross the plane of symmetry. Fig. 5a shows the course of the acceleration and fig. 5b shows the displacement field u_x at time 0.025 s. Its maximum value is 0.001892 mm.
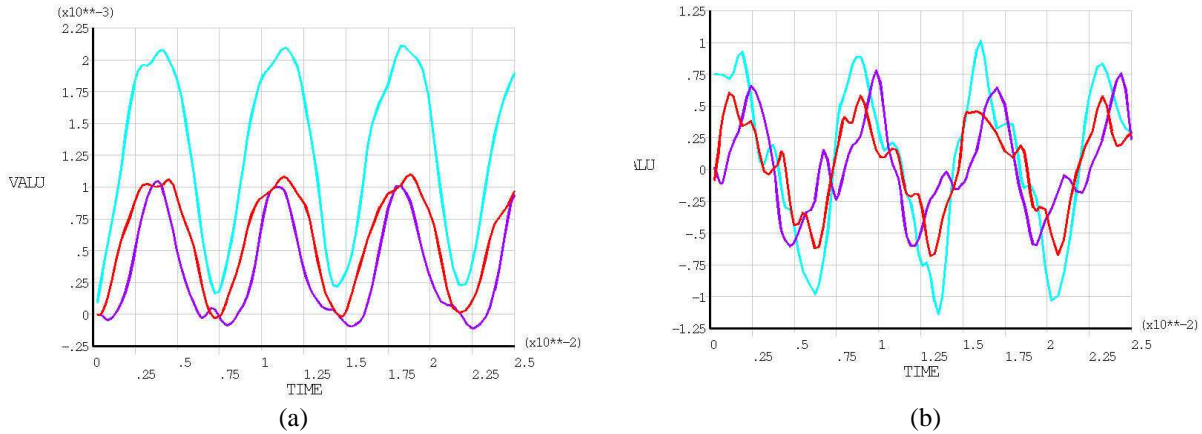

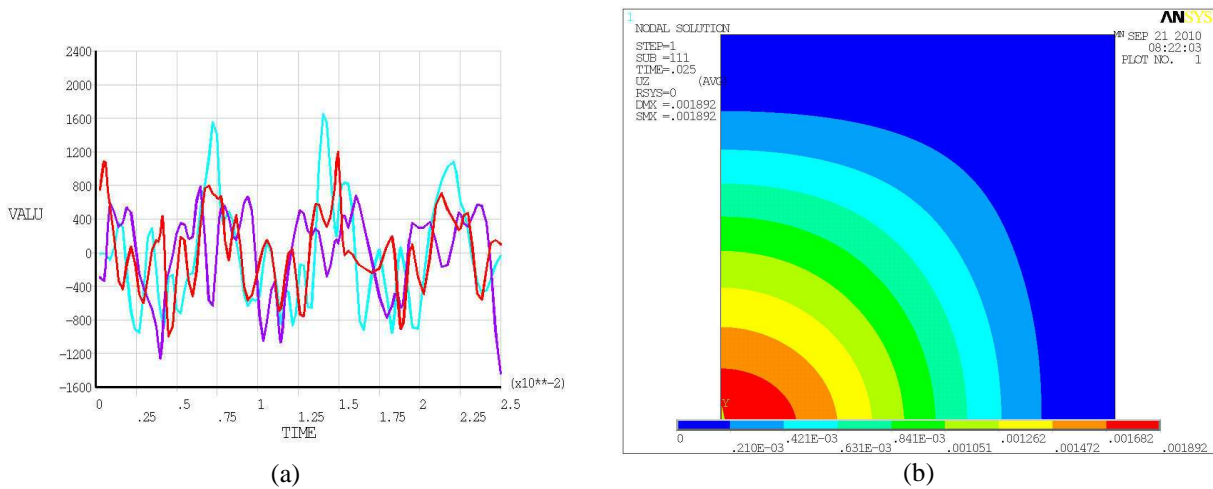**Fig. 4.** Time course of displacements and velocities

Fig. 5. Time course of accelerations and displacement field

Example 2

In this example a clamped square plate with a side-length a = 0,254 m and the plate thicknesses h/a = 0.05 considered. The plate is subjected to a uniformly distributed static load. Homogeneous material properties are considered firstly to test the accuracy of the present computational method. The following material parameters are used in our numerical analysis: Young's modulus E2 = 0,6895.1010 Pa and E1 = 2E2, Poisson's ratios µ21 = 0.15 and µ12 = 0.3 and density of 5 000 kgm-3. The modulus of elasticity corresponds to Young's modulus E2, so G12 = G13 = G23 = E2/[2(1+ µ12)]. The model was created out of 441 nodes with equidistantly distributed nodes.

In our numerical calculations, 441 nodes with a regular distribution were used for the approximation of the rotations and the deflection. The origin of the coordinate system is located at

the center of the plate. The variation of the deflection with the x_1-coordinate at $x_2 = 0$ of the plate is presented in Fig. 6. The deflection value is normalized by the corresponding central deflection of an isotropic plate with material constants given above but $E_1 = E_2$. For a uniformly distributed load $q_0 = 2,07.10^6$ Pa we have $w_3^{iso}(0) = 8.842.10^{-3}$ m. The numerical results are compared with the results obtained by the FEM-ANSYS code with a very fine mesh of 900 quadrilateral eight-node shell elements for a quarter of the plate. Our numerical results are in a very good agreement with those obtained by the FEM for an orthotropic plate. One can observe that the deflection value is reduced for an orthotropic plate if one of the Young's modulus is increased. This is due to the increase of the plate stiffness for the orthotropic plate.
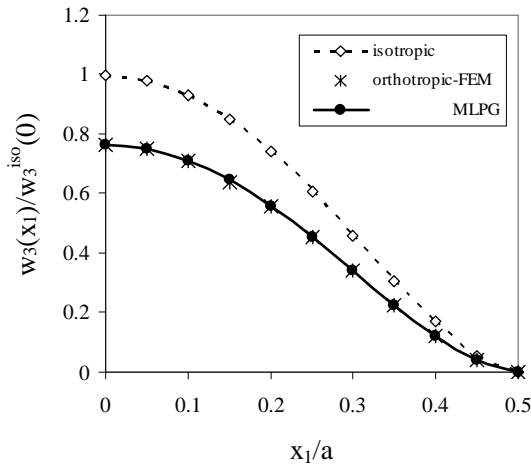

Fig. 6. Variation of the deflection with the x_1 – coordinate for a clamped homogenous square plate
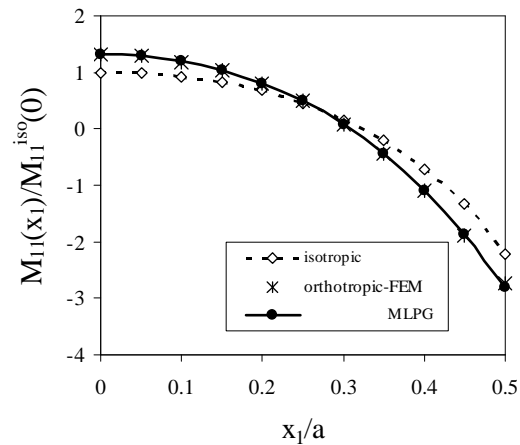

Fig. 7. Variation of the deflection with the x_1 – coordinate for a clamped homogenous square plate

The variation of the bending moment M_{11} is presented in Fig. 7. Here, the bending moment is normalized by the central bending moment value corresponding to an isotropic plate $M_{11}^{iso}(0) = 3064 Nm$. The absolute values of the bending moment at the plate center (0,0) and the center of the clamped side (0.5a; 0) are higher than in the isotropic case.

Next, a clamped orthotropic thick square plate under an impact load with Heaviside time variation is analyzed. The used geometrical and material parameters are the same as in the static case. For the numerical modeling we have used again 441 nodes with a regular distribution. Numerical calculations are carried out for a time-step $t = 0,357.10^{-4}$s.
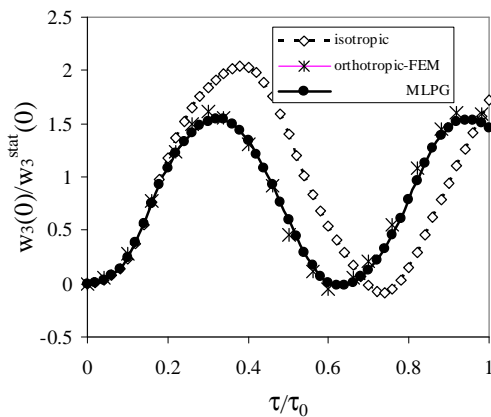

Fig. 8. Time variation of the deflection at the center of a clamped square plate subjected to a suddenly applied load
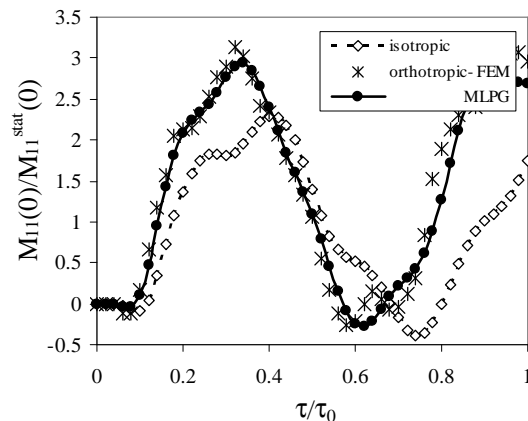

Fig. 9. Time variation of the bending moment at the center of a clamped square plate subjected to a suddenly applied load

170

The MLPG results are compared with those obtained by FEM-ANSYS computer code, where 900 quadrilateral eight-node shell elements with 1000 time increments have been used. The time variations of the central deflection and the bending moment M_{11} are given in Fig. 8 and Fig. 9, respectively. Both quantities are normalized by their corresponding static values at the center of the isotropic plate. The static central deflection is $w_3^{stat}(0) = 8,842.10^{-3}$ m for the considered load $q_0 = 2.07.10^6$ Pa. The static bending moment is $M_{11}^{stat}(0) = 3064$ Nm. The time is normalized by $\tau_0 = 0.3574.10^{-2}$ s. A good agreement of the present results for the deflection and the bending moment at the plate center and the FEM results is observed in both figures.

The peaks of the moment amplitudes are shifted to shorter time instants for the orthotropic plate with a larger flexural rigidity. Since the mass density is the same for both isotropic and orthotropic plates, the wave velocity is higher for the orthotropic plate with higher Young`s modulus. The amplifications of the bending moments due to the dynamic impact load for both isotropic and orthotropic plates are almost the same if they are normalized with respect to the corresponding static values. The static bending moment for the orthotropic plate is slightly higher at the center of the plate (see Fig. 7). Then, the peak value for the orthotropic plate under an impact load in Fig. 9 has to be higher since that value is normalized by the isotropic bending moment.

Example 3 – supported orthotropic plate loaded with a force

In this example we are considering simply supported square plate with three orthotropic layers. The plate is loaded with impact load in the form of the Heaviside functions. The following material properties are used: Young's modulus $E_2 = 0.6895.10^{10}$ Pa and $E_1 = 2 E_2$, Poisson's ratios $\mu_{21} = 0,15$ and $\mu_{12} = 0,3$ and density of $5\,000$ kg.m^{-3}. The modulus of elasticity corresponds to Young's modulus E_2, so $G_{12} = G_{13} = G_{23} = E_2/[2(1+ \mu_{12})]$. The model was created out of 441 nodes with equidistantly distributed nodes. The time step size was $t = 0.357 .10^{-4} s$.

Fig. 8 and 9 show the course of displacement in the middle of the plate and the bending moment M_{11} dependant on time. Both values are normalized with respect to their static values in the middle of isotropic homogenous plate. Static values of displacement is $w_3^{stat} = 0.02829$ m for the considered load of $q_0 = 2.07.10^6$ Pa. The value of the static bending moment is $M_{11}^{stat}(0) = 6482$ Nm. Time is normalized with the value $\tau_0 = 0.3574 .10^{-2} s$.
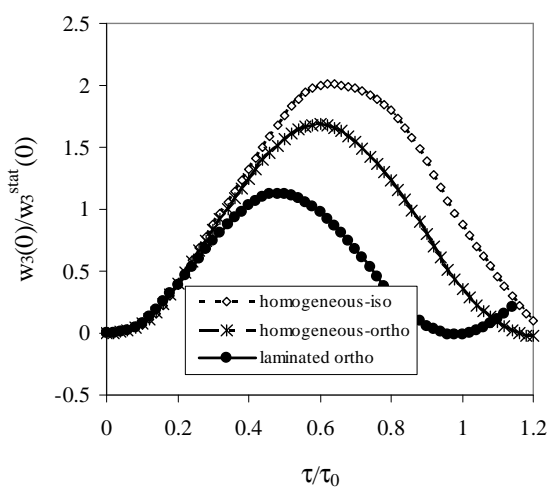
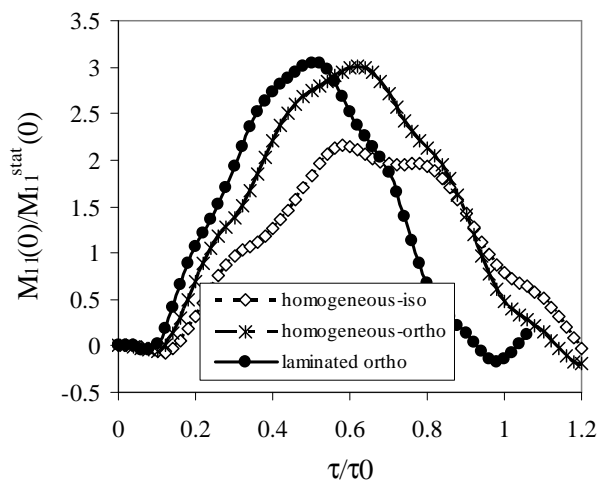

Fig. 10. Displacement time course   **Fig. 11.** Bending moment time course

From the shown results we can see, that for the homogeneous orthotropic and laminated plates the maximum displacement amplitude and bending moment amplitude are shifted at shorter time intervals. This is caused by the higher Young modulus. The highest values are obtained for the

laminate orthotropic plate. The elastic wave speed is highest for the laminate plate, because the density is the same for all plates. The maximum decrease in displacement is achieved for the laminate plate, which has the highest stiffness. The lamination has practically no influence on the bending moment. Therefore, the maximum values of bending moments in the laminate plates have almost the same values.

5. Conclusion

In this article we applied classical FEM and meshless MLPG method for vibration of plates loaded with mechanical shock loads. Reissner-Mindlin theory reduces the original 3-D thick plate problem to a 2-D problem. The numerical FEM results are presented for a square plate with a compressive load.

The proposed MLPG method is a truly meshless method, which requires neither domain elements nor background cells in either the interpolation or the integration. The MLPG method has no limitation on the number of laminate layers or on their material properties. Nodes can be distributed randomly or equidistantly on the surface of the considered plate. The MLPG method is applied on the vibration of the plate loaded with impact force with Heaviside time variation. It is demonstrated numerically that the quality of the results obtained by the proposed method is very good. The degree of the agreement of our numerical results with those obtained by the FEM-ANSYS computer code ranges from good to excellent.

Since in our illustrative examples only simple problems are analysed, only a regular node distribution has been used. However, a random location of nodes should be considered for general boundary value problems. To this end, an efficient random node generator is required, which has to be developed for further progress of the method.

Acknowledgement

References

[1] REDDY, J.N. *Energy Principles and Variational Methods in Applied Mechanics*, Revision version, John Wiley and Sons, 2002.

[2] CARRERA, E. *Developments, ideas and evaluations based upon Reissner's Mixed Variational Theorem in the Modeling of Multilayered Plates and Shells*, Applied Mechanics Review. Vol. 54, 2001, s. 301–329.

[3] SLADEK, J. – SLADEK, V. – MANG, H.A. *Meshless LBIE formulations for simply supported and clamped plates under dynamic load*. Computers and Structures, 81, 2003, pp. 1643-1651.

[4] ŽMINDÁK, M., DANIŠOVIČ, S., NOVÁK, P. *Meshless dynamic analysis of composite plate structures* (in Slovak). In: Dynamics of rigid and deformable bodies 2010, Ústí nad Labem, 2010, CD ROM.

Simulation of Misfire in Vehicles with SI Engine

[*]Marcin Rychter

[*]Motor Transport Institute, Diagnostic and Servicing Proccess Department, PL-03-301 Warsaw, 80 Jagiellońska St., Poland, rychter@poczta.fm

Abstract. OBD system is assembly diagnostic test, analytical and decision procedures realization in actual time for the purpose improvement emission efficiency and efficiency of components responsible for passive and active safety of vehicles. OBD system is integral components of vehicles with connecting with control module of engine. One of the basic problem connected with OBD technology is test of on board diagnostic efficiency in different application. Self-diagnostic is to minimize the volume of substances generated by the combustion engines polluting the natural environment. Self-diagnostic is the basis for creating the best conditions for the most effective operation of the engine. Those paper include same results of testing and possibilities monitoring of catalytically converter in SI engine and simulating of signal from oxygen sensor. There are results of simulation of misfire in these engine.

Keywords: sensor, monitor, OBD II, catalytic converter.

1. Introduction

The purpose of the examinations was to develop and to check under the laboratory conditions the operation of devices simulating the failure of selected engine components covered by the OBD II system monitoring. The obtained results are to be applied for improving their design and implemented to the laboratory procedures. The scope of the examinations assumed performing the determination of the influence of the simulated failures on the emission of the limited gas pollutions, fuel consumption, and the driving performance of the tested vehicle. The tests were performed for the following vehicles: Fiat Panda brand new and Opel Astra. Fiat Panda was equipped by its maker with the OBD II system, whereas Opel Astra was subject to some complementary examinations.

2. Running of investigation

The measurements of the total vehicle friction loss on the road were carried out by a cast down test method according to the Regulation no.83 UN/ECE (Supplement 3 to Annex 4). The harmful components emissions from the exhaust system after a cold start at normal ambient temperature of (20–30ºC) and the fuel consumption were measured in the Type I test (Regulation no.83 UN/ECE, series 5 of Supplements) for different percentages of "misfire" events. The "misfire" defect was generating by the AMX 700, version II, device.

The results of the pollutant emissions and fuel consumptions measurements are shown in figures 1–3. The "misfire" defect was set on the cylinder no. 2 at synchronization with the cylinder no. 1. For every one per cent of the "misfire" events it was checked whether any expectation error had appeared or MIL lamp (Malfunction Indicator Light) had lighted. Three driving cycles were realised at the percentage of 15% of "misfire" events and ten cycles at 25%. At the percentage of 35% of "misfire" events and after realisation of three driving cycles the expectation error occurred, however, the MIL lamp did not light. Next the driving test was performed consisting in driving under the urban traffic conditions. The MIL lamp started lighting after three driving cycles and travelling the distance of 70 km (error nos. P0300 and P0302 – multiple "misfire" events).
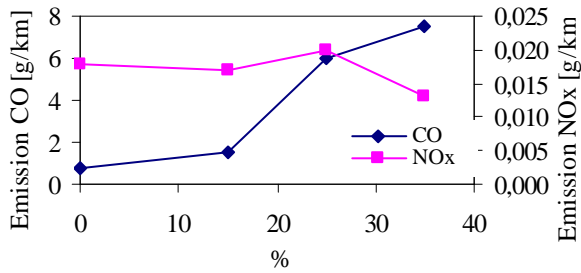
Fig. 1. The modification of the CO and NOx emission in function of positioning misfire in the test type I Regulations 83 EKG UNO, the 05 series correction – the weighted average (the test after a cold start)
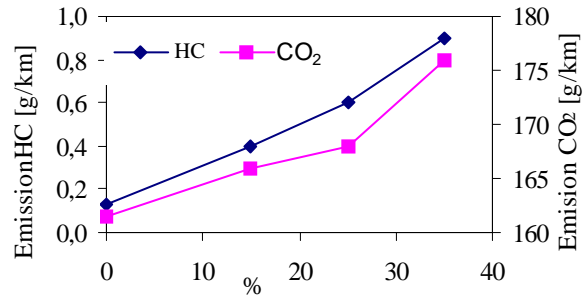
Fig. 2. The modification of the HC and CO_2 emission in function of positioning misfire in the test type I Regulations 83 EKG UNO, the 05 series correction – the weighted average (the test after a cold start)

During the exhaust emission measurements, after cold starting at the ambient temperature of (–7ºC), the "misfire" event was set on the cylinder no.2 at synchronization with the cylinder no.1. After each test it was checked whether the OBD system had detected the "misfire" events. The errors P0300 and P0302 occurred only at the percentage of the "misfire" events of 35%, however, the MIL lamp did not light. The measuring results are presented in figures 4–6.
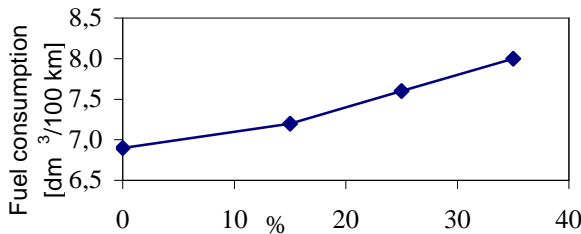
Fig. 3. The modification of a fuel consumption in function of positioning misfire in the test type I Regulations 83 EKG UNO, the 05 series correction – the weighted average (the test after a cold start)
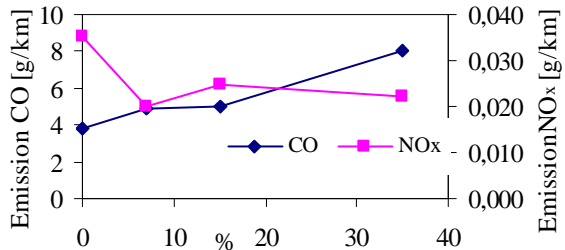
Fig. 4. The modification of the CO and NO_x emission in function of positioning misfire in the test type I Regulations 83 EKG UNO, the 05 series correction – the weighted average (the test after a cold start in the temperature –7ºC)
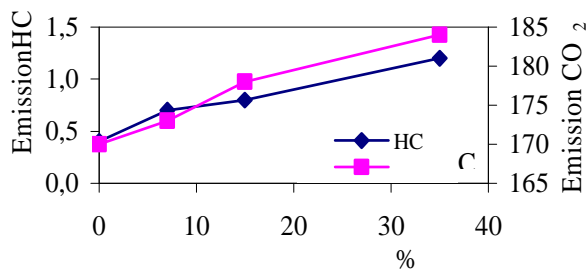
Fig. 5. The modification of the HC and CO_2 emission in function of positioning misfire in the test type I Regulations 83 EKG UNO, the 05 series correction – the weighted average (the test after a cold start in the temperature –7ºC)
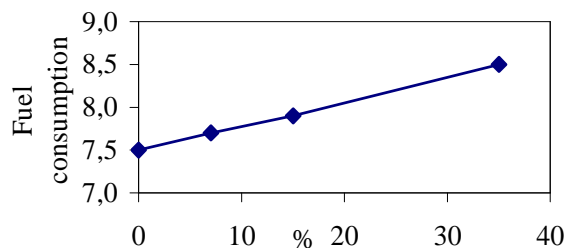
Fig. 6. The modification of the fuel consumption in function of positioning misfire in the test type I Regulations 83 EKG UNO, the 05 series correction – the weighted average (the test after a cold start in the temperature –7ºC)

The traction characteristics of the vehicle was also examined by measuring the changes in the net output at wheels for different percentages of the "misfire" events. The measurements were taken for the fifth gear at driving velocities ranging from 60 to 150 km/h. Figure 7 shows the results of the decrease in the net output at wheels measurements taken for different percentages of "misfire" events in relation to the output power measured with no "misfire" events recorded.
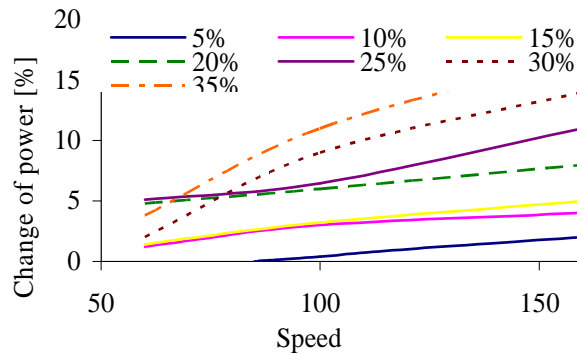
Fig. 7. The relative modification of the net power on wheels during different settings of a misfire in relation to measurement value without a misfire

As the percentage of "misfire" events increases the value of the net output decrease at wheels of the tested vehicle increases as well. At small values of the engine crankshaft speed the effect of the changes in the "misfire" events percentage was smaller in comparison with the one noted at the rated engine output speed. To perform the comparative tests of the exhaust emissions from the exhaust system of a car equipped with a spark-ignition system, SI, with a multi-points fuel injection, the AMX 700 device was installed. That device was used for forcing an incorrect operation of the ignition system by preventing the conditions essential for forming a spark between the spark plug electrodes. The "misfire" event failure was simulated on the cylinder no.2 of the engine.

During the examinations the following actions were carried out, namely:
- the measurements of the concentrations of the harmful exhaust emission from the engine exhaust system were taken according to the provisions of the Regulation no.83 UN/ECE, series 04 of Amendments, at the "misfire" events percentage for one of the cylinders increasing from 0 to 30% (table 1);
- the measurements of the concentrations of the harmful exhaust gas components in the engine exhaust system were carried out with the use of the diagnostics analyser at a percentage of the "misfire" events for one of the cylinder increasing from 0 to 40%;
- the characteristics of a voltage signal from the lambda probe at the idle running speed and its increased value as well, without " misfiring" and for the percentage of the "misfire" events of 35 % for one of the cylinders.

% "misfire"		0%	10%	15%	20%	30%
Emission		[g/km]	[g/km]	[g/km]	[g/km]	[g/km]
UDC	CO	5,479	7,889	7,807	7,920	15,24
	NO_x	0,126	0,251	0,295	0,193	0,463
	HC	0,301	0,711	0,772	0,847	2,525
	CO_2	252,0	261,9	275,0	271,2	251,0
EUDC	CO	0,656	0,841	0,950	2,341	1,861
	NO_x	0,059	0,065	0,091	0,113	0,076
	HC	0,045	0,075	0,095	0,253	0,233
	CO_2	150,6	148,9	156,2	153,9	159,8
Average	CO	2,422	3,436	3,459	4,394	6,776
	NO_x	0,084	0,134	0,166	0,142	0,218
	HC	0,139	0,309	0,343	0,471	1,075
	CO_2	187,7	190,5	199,7	197,1	193,3

Tab. 1. Results of the emission measurement in driving cycles

In order to evaluate the changes in the concentrations of the harmful exhaust gas components and composition of the air-fuel mixture against the "misfire" events percentage under the

measurement conditions corresponding to the ones of technical examinations some additional tests were performed which consisted of (table 2):

- the measurements of the CO, HC, CO_2 and O_2 concentrations and the mixture composition taking into account the excess air number for the engine operating point under the idle running conditions;
- the measurements of the CO, HC, CO_2 and O_2 concentrations and the mixture composition taking into account the excess air number for the engine operation under the increased idle running speed conditions (~3000 rpm).

The performed investigations show that there are some significant differences between the characteristics of the concentrations of the harmful exhaust gas components obtained for the engine operating without and with "misfire" events. In the first case the concentrations were adjusted in a variable way from the values corresponding to n = 3000 rpm to the ones of the idle running. The stabilization state was obtained after 30 seconds. In the second case a decrease of concentrations to the very small ones was recorded after 30 seconds, and after 80 seconds a significant increase in their values was noted. The stabilization was obtained after 150 s, however, some oscillations near the average value were still occurring, what was likely caused by a fan switching on in the cooling system. At the speed value of 3000 rpm an increase in the preset percentage of the "misfire" events resulted in:

- an increase in the CO and HC concentrations,
- a decrease in the CO_2 concentration,
- a decrease in the excess air number,

whereas after the stabilization of indications at speed corresponding the idle running conditions it resulted in:

- an increase in the CO and HC concentrations,
- a decrease in the CO_2 concentration,
- an increase in the excess air number.

Palace of "misfire"	n = 3000 obr/min				Idle			
	CO	HC	CO_2	λ	CO	HC	CO_2	λ
cylinder 2	0,63	439	14,7	0,972	0,16	273	11,3	1,277
cylinder 3	0,12	68	15,1	1,001	0,34	199	11,2	1,294
cylinder 2 & 3	0,68	573	14,8	0,967	0,43	200	9,2	1,536
cylinder 1	0,14	59	15,2	0,999	0,38	298	11,5	1,259
cylinder 4	0,70	574	14,8	0,965	0,24	476	11,4	1,263
Cylinder 1 & 4	0,76	615	14,8	0,968	0,47	189	8,5	1,626

Tab. 2. The measurements results of the CO, HC, CO_2 concentration and the air factor in different settings of the 35% misfire in a different configuration of the AMX 790 device

During the performed measurements it was observed that the CO, HC and CO_2 concentrations and the mixture composition depend not only on the percentage of the "misfire" events but also on settings on the AMX 790 device for a cylinder, which the synchronization comes from and a cylinder/cylinders in which the "misfire" events occur.

Some tests verifying the correctness of operation of the AMX 790 device were carried out in the aspect of a possibility of its software improvement. The operation of the Version II of AMX 790 device was subject to an evaluation. Special emphasis was put on checking whether there was a conformity of a programmed percentage of ignitions in which the "misfire" events were expected with a real percentage recorded under the engine operating conditions.

For comparing the programmed and real percentages of "misfired" ignitions a certain research method was developed. That method allowed for:

- evaluation of the engine operation with and without forcing the "misfire" events;
- developing the method for measuring the real percentage of "misfired" ignitions;

- checking whether the defects detected for the version I of the device can be also detected for the version II;
- measuring the real percentage of "misfired" ignitions against the engine speed.

The device's task is to force the "misfired" ignitions in the spark-ignition engines. It can be realized by changing the voltage characteristics in a low voltage circuit of the ignition installation by shorting it to frame or to the battery positive electrode. It prevents from generating the pulse in a high voltage circuit of the ignition unit which is necessary to force a spark between the ignition plug electrodes. The device is expected to be provided in cars for which the ignition installation is equipped with more than one high voltage coils. The device's design calls for taking a synchronizing signal from one of the low voltage circuits and calculating on its base a time in which the individual low voltage circuits interfere in the circuits of other high voltage coils. The device's software provided a possibility for determining what a percentage of ignitions was to be "cut out", and in what cycle, and on which cylinder it was to be done. Programming any sequence of the "misfired" ignitions consisting of (up to) 1000 items was possible.

During all performed tests the device was synchronized by a signal from the ignition coil for the cylinders 1-4 forcing the "misfired" ignitions for the cylinders 2 and 3 at one programmed speed range (600-4000 rpm). The subject of tests was a passenger car of Opel make. Two testing methods were used. In the first part a method of checking the real percentage of "misfired" ignitions based on a signal from the lambda probe was used. In the adaptive engine operation managing systems the mixture composition is monitored by a lambda probe monitored (installed) in the engine exhaust system. The presence in the exhaust system the exhaust gases coming from a combustion of a very rich mixture, thus containing insignificant amounts of oxygen, forces the generation of a voltage signal of 1 V, whereas, in case of exhaust gases from the very poor mixture combustion, thus containing significant amounts of oxygen – a voltage signal of 0 V is generated.

The method assumptions are as follows:
- the misfired ignition results in a lack of combustion in a cylinder; the unburnt mixture with a high oxygen content flows into the exhaust manifold; a high amount of oxygen causes a momentary drop in the lambda probe voltage;
- a signal from the lambda probe can be a basis for determining the number of engine operating cycles in which the "misfired" ignitions occurred:
- a proper operation of the AMX 790 device is confirmed if a voltage signal frequency from the lambda probe corresponds to the its programmed frequency of the "misfired" ignitions;
- the "misfired" ignitions are forced by the device operation.

The used method shows that the engine "misfire" results in the irregularity of the engine operation which is accompanied by a characteristic noise. The evaluation of the engine operation consisted in watching a control diode on the AMX device casing, which was (lighted) on while the device was forcing the "misfired" ignitions, and observing whether the mentioned disturbances (had) occurred. Such evaluation was possible at low engine speed for idle running. It was found out that usually after the diode had lighted some irregularity of the engine operation and the characteristic noise accompanying the "misfired" ignitions occurred. However, there were some cases when the engine was running with no disturbances even after the diode had lighted. It can be supposed that not in every case a real engine "misfire" occurs and a certain nonconformity of the programmed percentages of the "misfired" ignitions with the real one can appear. It was also found that some short brakes in the diode lighting had been occurred from time to time suggesting that during those brakes the ''misfired" ignitions had not been realised.

During the tests eight lambda probe voltage characteristics were recorded for the unloaded engine running at the following engine speeds: idle running, 2000, 3000, 3500 rpm at different settings of the "misfired" ignitions frequency. An increase in the "misfired" ignitions frequency of the AMX 790 device caused an increase in the frequency of the lambda probe signal changes. However, in case of all settings there was no conformity of the frequency of the lambda probe signal changes with the programmed "misfired" ignitions frequency.

If a frequency of the "misfired" ignitions is lower than a frequency of changes in the mixture composition adjusted by an engine controller it is difficult to distinguish a drop in the lambda probe voltage resulting from a typical mixture composition regulation process from the one caused by the engine "misfired" ignitions. The works [?] suggested that under some engine operating conditions an occurrence of certain nonconformities of the percentage of "misfired" ignitions programmed in the AMX 790 device with the real one would be possible. The performed tests verify such a possibility. The evaluation of the correctness of operation of the device in respect of conformity of the programmed percentage of the "misfired" ignitions with the real one on the basis of an analysis of the lambda probe voltage characteristics gave a positive result at the idle running speed.

However, at speeds of 2000, 3000 and 3500 rpm a frequency of changes of the lambda probe voltage is different by 33 % from the "misfired" ignitions frequency programmed in the device. The difference is approximately constant, independent on the engine crankshaft speed and the device's settings. The obtained results of tests do not confirm the correct operation of the device, however, they cannot be regarded as an unambiguous evidence of a wrong measurement of the "misfired" ignitions number. Such situation made a modification of the applied research programme necessary. A new research programme consisted in measuring the voltage characteristics in the ignition unit on the primary winding of an ignition plug. The number of the "cut out" ignitions and sequences of their occurrence were subject to evaluation. The lambda probe voltage was also measured.

The tests showed, in most cases, the conformity of "cutting out" ignitions characteristics at the idling running speed with the characteristics programmed in the AMX 790 device. However, some cases were noted in which the pulses for the ignition "cutting out" were omitted or mistaken. Despite the detected errors the frequencies of the real "cutting out" pulses were slightly different than the programmed ones.

3. Conclusion

The operation of the AMX 790 device consists in modifying the voltage characteristics in a low voltage circuit of the ignition plug. The investigations showed that the voltage is induced in the secondary circuit. A connection between the voltage "cutting out" in the primary circuit and the lambda probe voltage characteristics allows to state that a decrease in voltage acts on the engine operation. This action confirms the expectations. Some additional engine examinations should be performed in order to confirm unambiguously that despite of the voltage drop in the primary circuit there is a spark-over in an ignition plug, and its reduced energy lowers the combustion rate. This fact intensifies irregularities in the engine operation and the HC emission.

There is no conformity of the programmed percentage of the "misfired" ignitions with the real one. Moreover, it was found that at the engine speed of 2000 rpm an increase in the percentage of the "cut out" ignitions programmed in the AMX 790 device results in, neglecting the pulses "losing", an increase in the real percentage of their "cutting out".

The performed tests show that at the engine speeds higher than the idle running speed there is some nonconformity of the percentage of "misfired" ignitions programmed in the device with the real one observed during the engine running.

References

[1] Commission Directive 1999/100/EC of 15 December 1999 adapting to technical progress Council Directive 80/1268/EEC relating to the carbon dioxide emissions and the fuel consumption of motor vehicles. Official Journal of the European Communities, L 334, 28/12/1999.

[2] Directive 1999/96/EC of the European Parliament and of the Council, 1.12.1999.

[3] Directive 98/69/EC of the European Parliament and of the Council of 13 October 1998 Relating to Measures to be Taken Against Air Pollution by Emissions from Motor Vehicles and Amending Council Directive 70/220/EEC, Official Journal L 350, 28.12.1998.

Influence of Throttleless Load Control of Petrol Engine on Its Effectiveness

[*]Juraj Saniga, Pavol Kukuča
[*]University of Žilina, Faculty of Mechanical Engineering, Department of automobile technology, Univerzitná 1, 01026 Žilina, Slovakia, {juraj.saniga, pavol.kukuca}@fstroj.uniza.sk

Abstract. This paper describes impact of use valve train without camshaft and its benefits. Chapter valve trains deals with a brief overview, short description of the advantages of variable timing of valve trains. The next section describes the valve train VARROZ. The main task of this work is to assess the impact of throttleless load control of petrol engine on its effectiveness. The result of modeling of flow in the intake manifold is presented in the last chapter.

Keywords: petrol combustion engine, throttle, valve trains, mixture, valve timing.

1. Introduction

Reciprocating internal combustion engines to power vehicles is subject of continuous improvement. In concerns the improvement of its thermodynamic processes, reducing the negative environmental impact, in terms of design, using modern materials for its production and in terms of its management.

2. Valve trains

One of the sub-combustion engine is valve train, which has a significant impact on the quality of exchanges of fuel mixture. Quality exchange of fuel mixture affects the conversion of thermal energy contained in fuel to mechanical work. Practically, shortly before the end of the last century began to receive increased attention, mainly valve train, looking for ways to improve their impact on the quality of the exchange of fuel mixture. Until then, more attention was given to their kinematic and dynamic properties and related self definition gap in the mechanism, which is necessary for trouble-free distribution function of valve train.

Result of quite quickly proceeding research and development was the introduction of variable timing valve train into mass production, especially in cars. In principle, it concerns a change of valve opening angle and its stroke, adapted to the requirements of the engine in the working mode. Its effect helped to achieve a significant improvement in parameters of internal combustion engines especially in partial load. Initially it was a variable timing for the two discrete modes – lower engine speed and load (urban cycle) and higher engine speed and load (highway cycle), which later developed into a proportional variable timing across the range of engine operating modes. The proportional timing valve train has a significant interest in improving the thermal efficiency of gasoline internal combustion engines at part load. It allows the valve train by an early intake valve closing to take over control of the amount of fuel mixture rather than classically used throttle. The consequence of this fact is to minimize the negative work related to the exchange fuel mixture (Fig.1.), which positively affects the efficiency of the engine.
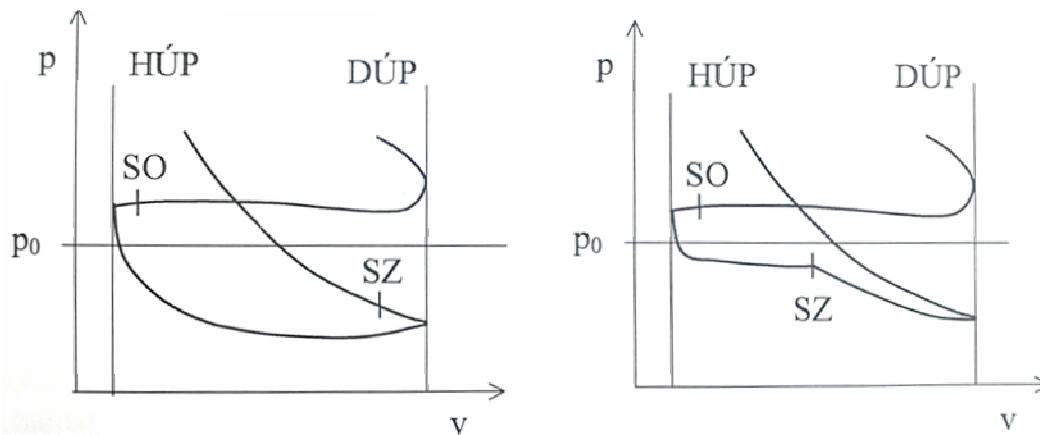
Fig. 1. Negative area of work diagram of engine – on left – with throttle, on right – engine management with intake valve timing

VVT naturally led to a need of using different non-conventional valve trains solutions and alternative methods of propulsion, which resulted in a number of non-conventional mechanisms, used in internal combustion engines. It can be powered by mechanical, hydraulic, pneumatic, electric, or their possible combination. In any case, control of valve train is in an electronic engine control unit. Moreover, these mechanisms can have a positive effect on the mechanical efficiency of internal combustion engine.

3. Variably timed electrohydraulic valve train VARROZ

On the department KDMT, later KAT of University of Zilina, model without camshaft hydraulically operated and proportional control valve train with variable timing VARROZ was designed and constructed. One of the reasons of this proposal is the ongoing development of intelligent hydraulic and pneumatic elements, components of which have the ability to provide very fast and accurate operation systems. The proposed system not only provides continuous valve timing of the internal combustion engine, but also continuous change of valve stroke, independently from each other, which is one of the advantages of this system.
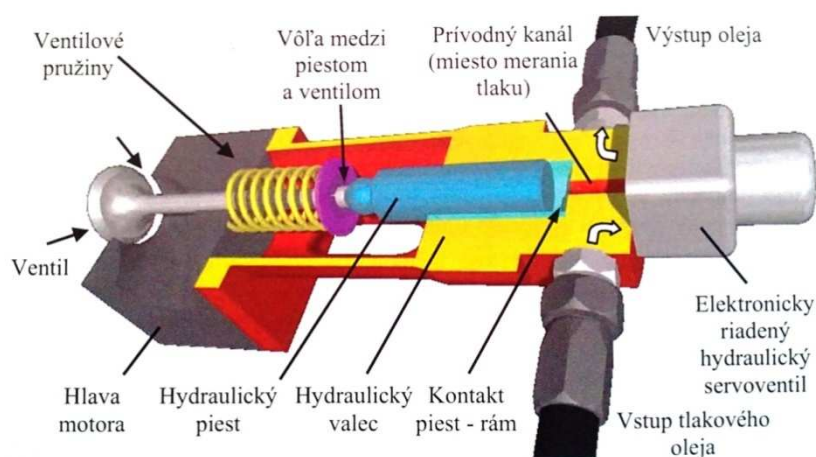

Fig. 2. Valve train VARROZ

The big advantage of variable valve timing is the possibility of removing the throttle of the intake tract, resulting in the increase of engine torque by its better performance and lower fuel consumption.

4. Modeling pressure drop in the intake manifold of internal combustion engine

The biggest problem of spark ignition engines is their inferior efficacy in partial and limited load. This relates to power control in a quantitative way, by throttle. (Fig. 3.) In case of partial load of the petrol engine, with throttle occurs throttling with a significant decrease in effective efficiency, because of the growing losses associated with the Exchange fuel mixture, the negative area of work diagram. Ideal situation would be if throttle was not at all in the intake tract. You can see turbulence around the throttle in the Fig. 3.
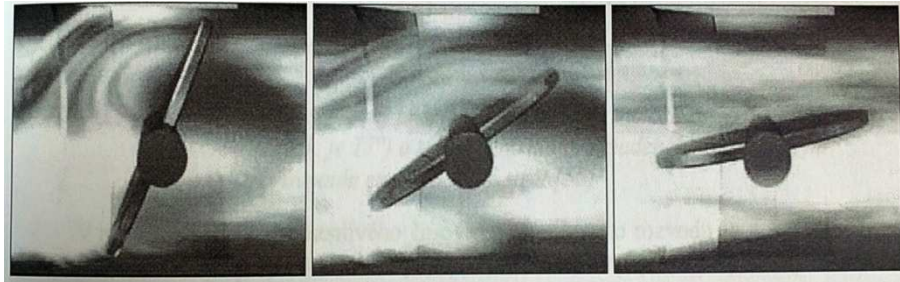

Fig. 3. Turbulence around the throttle

The Fig. 4. shows the calculated course of manifold pressure, the piston considered speed is 10 m/s, the throttle opening angle is 40 degrees and fully open the inlet valve. Pressure at the intake manifold was intended by the atmospheric, it is 101325 Pa. Calculated pressure behind the throttle is 76800 Pa, a pressure drop is approximately 24%. The pressure in the cylinder space, behind the intake valve is 72000 Pa, which represents the pressure drop about 29% compared to atmospheric pressure before the suction line.

Fig. 4. Pressure in intake manifold
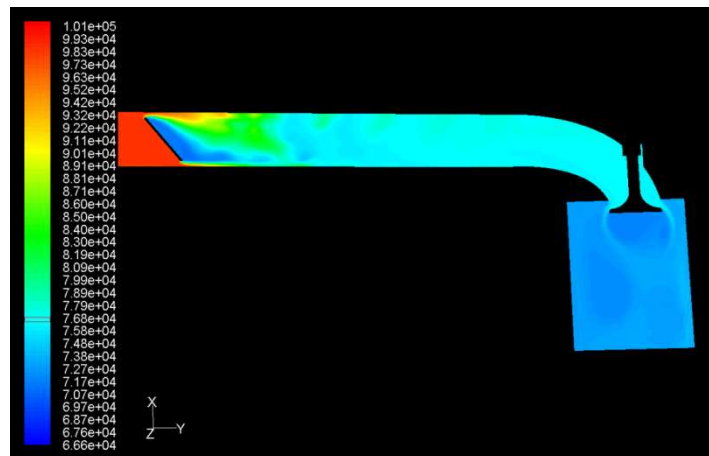
The Fig. 5. shows when the turbulence intensity in the same conditions as in the course of pressure. From the results obtained by the modeling of flow in the intake manifold can be assumed that after removal of the throttle from manifold of petrol engine the negative labor associated with the exchange of fuel mixture will be reduce, which positively affects the efficiency of the engine.
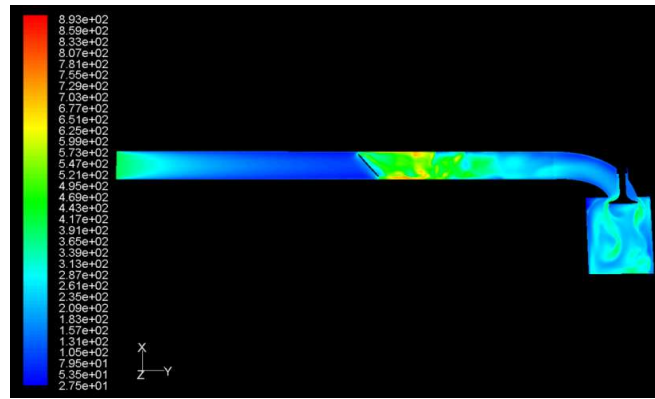
Fig. 5. Intensity of turbulence in intake manifold

The Fig. 6. shows course of manifold pressure without the throttle, calculated under the same conditions as before. The difference in pressure before the inlet valve and behind it is approximately 4,4 %.
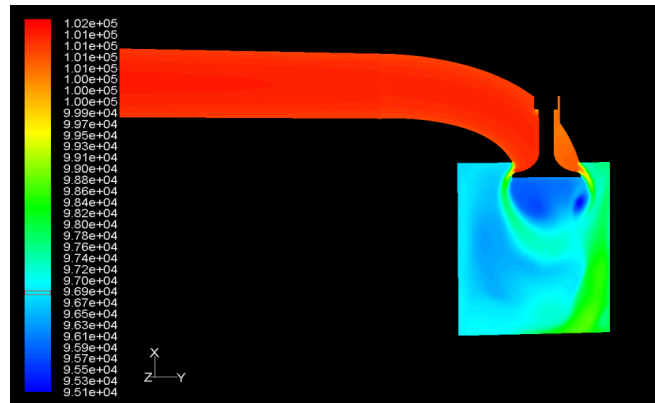
Fig. 6. Pressure in intake manifold and valve without throttle

5. Conclusion

For a full investigation of the impact of the removal of the throttle from intake manifold of a petrol engine it is necessary to make more model situations that involve the dynamic processes of opening and closing intake valve. The obtained results will be use for comparison with results of the experiment, which will simulate real work of combustion engine. In measurements it is necessary to measure the mass or volume air flow at the conventional valve train, as well as the management of hydraulic VVT VARROZ without throttle.

Acknowledgement

References

[1] ISTENÍK, R., & KUKUČA, P. (2008). *Rozvody a nekonvenčné mechanizmy spaľovacích motorov*. Georg, Žilina, Slovakia, ISBN 978-80-89401-00-0.

[2] MUCHA, W. (2005). *Modelovanie vybraných parametrov ventilového rozvodu s variabilným časovaním*. Doktorandská dizertačná práca.

[3] LÁBAJ, J., & BARTA, D., (2006). *Unsteady flow simulation and combustion of the ethanol in diesel engines*. Communications - scientific letters of the University of Žilina, EDIS, Žilina, ISSN 1335-4205.

Assessment of Possibility of Diagnosing Rail Vehicle's Disc Brake System

[*]Wojciech Sawczuk
*Poznan University of Technology, Faculty of Working Machines and Transportation, Institute of Combustion Engines and Transport, Division of Railway Vehicles, Piotrowo 3, 60-965 Poznan, Poland, wojciech.sawczuk@put.poznan.pl

Abstract. Attempt to raise train speed involves application of greater braking power i.e. braking systems rapidly absorbing and dispersing stored heat energy. To maintain high efficiency of braking system in the whole operational process, it is necessary to control the friction set: brake and pad before reaching limitary wear particularly of friction pads. This article presents assessment of possibility of diagnosing rail vehicle's disc brake system. In this article usability of parameters and symptoms to diagnose the wear of friction pads was analyzed.

Keywords: disc brake, wear of friction pad, diagnostic disc brake system, vibration signal, braking distance.

1. Introduction

After carrying out stationary friction tests it was found out that certain parameters of braking process can be used to diagnose the wear of friction pads. Dependencies of friction parameters of braking process on pad's thickness determined by their wear during the measurement in the whole braking process or its part are defined for average coefficient of friction μ_m, maximum temperature of the brake disc T_m, braking time t and braking distance s.

Diagnostic stationary tests proved possibility of obtaining dependencies of pad's thickness on selected diagnostic parameters (vibration). To diagnose the wear of friction pads it is possible to use the following diagnostic values determined in time domain and amplitude domain: RMS value of vibration accelerations a_{RMS} and average value of vibration accelerations $a_{AVERAGE}$.

2. Selection of assessment criteria and their evaluation

Usability of suggested friction and vibration parameters to diagnose the wear of brakes pads was evaluated by using the following assessment criteria: sensitivity, repeatability, uniqueness, availability and the cost of diagnosis.

Diagnostic sensitivity of a certain parameter is defined on the basis of dynamics of changes described with dependency (1).

$$D = 20 \lg\left(\frac{s_2}{s_1}\right).$$

(1)

where: s_1 –   value of point parameter determined for pad G_3 or G_2,
                   s_2 –   value of point parameter determined for pad G_1.

Then it is possible to conclude if a certain diagnostic parameter shows changeability to change of state stemming from the wear of friction pad. A certain diagnostic parameter shows satisfactory sensitivity to change of state if dynamics of changes of received symptoms is over 6dB [1]. Then double change of values of measured diagnostic parameters is concluded.

The condition of repeatability of the process of diagnosing the wear of friction pads is connected with statistical assessment of symptoms received during braking. With assumed

confidence interval amounting to 95% and assumed significance level α=0,05, changes of symptom values into decrease of pad's thickness in the process of its wear were observed. Repeatability of diagnostic process was assessed on the basis of calculating coefficient of changeability described with dependency (2) for a certain number of repetitions of measurements.

$$W = \frac{S}{\bar{x}} \cdot 100\%. \tag{2}$$

where: S –   standard deviation,
          $\bar{x}$ –   arithmetic average.

Assessment of uniqueness of diagnosis, as one of criterion of assessing suggested diagnostic parameters with defining pad's thickness, was carried out by determining diagnosis error (dependence 3).

$$B_{Diag} = \frac{g_D - g_R}{g_R} \cdot 100\%. \tag{3}$$

where: g_D –   pads thickness calculated on the basis of measuring braking time t and dependencies in [4],
          g_R –   pads thickness measured with measuring instrument.

Assessment of uniqueness of diagnosis was verified with representation of implemented regression diagnostic models from paper [4] against pad's thicknesses measured before verification research. Already at the stage of evaluation of suggested assessment criteria of diagnostic process of the wear of friction pads, it was concluded that the following parameters: average coefficient of friction, RMS value and average value of vibration accelerations as a point parameter of vibrations in their analysis in amplitude domain, are inadequate because of lack of possibility to verify received values during operational research.

Diagnostic availability was connected with easiness of carrying out diagnosis and inference about the condition of friction pads. Availability criterion was evaluated on the basis of the following items, significant from diagnostics perspective: direct or indirect measurement, measurement with and without disassembly of parts or sets of braking system, measurement with and without modification of parts or sets of braking system, measurement using additional measuring instruments.

Assessment of availability of carrying out diagnostics of the condition of friction pads was carried out on the basis of experience from stationary and operational research. Preparation for research and registration of diagnostic symptoms enabled to classify analyzed parameters for diagnosing the wear of friction pads of disc brake. For a parameter characterized with the best availability 1 point was assumed in 6-point assessment scale (measurement of braking time) and for a parameter characterized with the worst availability 6 points were assumed, which was concluded by analyzing preparation of the station for measurement of instantaneous coefficient of friction.

Cost of diagnosis is connected with assessment of usability of a certain diagnostic parameter in the aspect of expenses incurred for purchase of appliances (measuring instrument) together with equipment. To assess the cost of carrying out diagnostics, a non-dimensional coefficient of cost of diagnosis calculated in dependency (4) was suggested:

$$K_{Diag.ij} = \frac{k_{diag,par.ij}}{\min k_{diag,par.i}}. \tag{4}$$

where: $k_{diag,par.ij}$ –   cost of carrying out diagnostics by using diagnostic parameter ij,
          $\min k_{diag,par.i}$ –   the lowest cost of carrying out diagnostics by using diagnostic parameter i.

Cost of carrying out diagnosis from non-dimensional perspective was determined for all considered parameters against the lowest diagnosis cost basing on braking time.

3. Analysis of usability of parameters and symptoms of the condition of disc brake

Assessment criteria of diagnostic parameters collected and analyzed in point 2 of this article possible to use in diagnostics of the wear of brake's friction pads, are presented together with suggested evaluation in Table 1.

	DIAGNOSTIC PARAMETER		sensitivity	repeatability	uniqueness	availability	Cost of diagnosis
			Dynamics of changes, [dB]	Coefficient of changeability, [%]	Diagnosis error, [%]	Scale	Coefficient of cost.
1	Average coefficient of friction	μ_m	0,35	0,73	98*	6	60
2	Maximum temperature of disc	T_m	0,34	11,32	16	5	25
3	Braking time	t	0,45	0,5	12,2	1	1
4	Braking distance	s	0,38	0,68	12,2	2	12
5	RMS value of vibration accelerations	a_{RMS}	5,3	0,74	98*	4	30
6	Average value of vibration accelerations	$a_{AVE.}$	4,5	0,6	98*	4	30
	* rough assessment of pad's thickness						

Tab. 1. Assessment criteria and evaluation of diagnostic parameters

Indicating the best diagnostic parameters to assess the wear of friction pads is connected with solving decision-making problems basing on selected selection criteria. For this purpose usage of special multi-criteria programming method including plurality of goal function [5]. Aggregation of decision criteria was carried by using one of the methods enabling normalization of diagnostic variables through study of the range of a value called Metoda Unitaryzacji Zerowanej (*MUZ*) [3]. Six different variants of diagnosing the wear of friction were assumed. Variants were characterized by five features (diagnostic variables).

Normalization of diagnostic variable (feature) was calculated on the basis of dependencies (5) and (6) [4].

For maximalization value:

$$z_{ij,S} = \frac{x_{ij} - \min \cdot x_{ij}}{\max \cdot x_{ij} - \min \cdot x_{ij}} \tag{5}$$

For minimalization :

$$z_{ij,D} = \frac{\max \cdot x_{ij} - x_{ij}}{\max \cdot x_{ij} - \min \cdot x_{ij}} \tag{6}$$

where: z_{ij} –   i-th normalized value of j-th diagnostic variable,
         x_{ij} –   value of a certain feature (diagnostic variable).

The last stage of MUZ was to calculate the value of the aggregated variable, which characterizes diagnostic parameters (variants) regarding assessed effect. Calculating the value of aggregated variable for each variant and diagnostic variable value was carried out by using dependency (7) [3]:

$$Q_i = \sum_j z_{ij} \tag{7}$$

where: Q_i –   value of aggregated variable assigned to i-th object.

Table 2 presents a collation of results of normalization for considered variants, whereas Table 3 presents ranking and selection of best variants for diagnosing the wear of friction pads.

Variants	Normalized diagnostic variables					Q_i
	Z1	Z2	Z3	Z4	Z5	
W1	0,009	0,979	0	0	0	0,987
W2	0,008	0	0,904	0,2	0,593	1,705
W3	0,017	1	0,945	1	1	3,962
W4	0,011	0,983	0,945	0,8	0,814	3,553
W5	0,430	0,978	0	0,4	0,508	2,316
W6	0,362	0,991	0	0,4	0,508	2,261

Tab. 2. Collation of normalization results for considered diagnostic variants

Parameter	Variant	Q_i	Assessment
Braking time	W3	3,962	Max[*]
Braking distance	W4	3,553	
RMS value of vibration accelerations	W5	2,316	Max[**]
Average value of vibration accelerations	W6	2,261	
Maximum temperature of the disc	W2	1,705	
Average coefficient of friction	W1	0,987	
[*] the best variant concluded on the basis of stationary friction research, [**] the best variant concluded on the basis of operational vibration reserach.			

Tab. 3. Ranking and selection of the best diagnostic parameters (variants)

After carrying out multi-criteria analysis by using *MUZ,* it was found out that for the purpose of diagnosing the wear of friction pads, out of friction parameters, braking time should be selected. From vibration parameters, after stationary diagnostics research, it is justified to use RMS value of vibration accelerations. In both considered cases the highest values of aggregated variables were concluded.

4. Conclusion

Multi–criteria analysis carried out with the method called Metoda Unitaryzacji Zerowanej (*MUZ)* showed that for all considered braking parameters (variants) assessed on the basis of diagnostic variables (features) it is preferable to use braking time and RMS value of vibration accelerations. In both cases the highest values of aggregated variables of analyzed diagnostic variants were found out. Basing on measurement of braking time, carrying out assessment of the wear of pads, errors connected with dispersion of results of braking time should be considered as well as error stemming from approximation of the function of the wear of friction pads against barking time. Overall diagnosis error, not considering the speed at the beginning of braking v=50 and 200km/h, does not exceed 12%.

References

[1] GRYBOŚ, R. *Drgania maszyn*, Wydawnictwo Politechniki Śląskiej, Gliwice 2009, s. 214.

[2] KARTA UIC 541-3*, Hamulec: hamulec tarczowy i okładziny hamulcowe, warunki ogólne dla prób na stanowisku badawczym,* Wydanie 6-te listopad 2006.

[3] KUKUŁA, K., *Metoda unitaryzacji zerowej.* WNT, Warszawa 2000.

[4] SAWCZUK, W. *Badanie tarczowego układu hamulcowego pojazdu szynowego w aspekcie możliwości jego diagnozowania*, Rozprawa doktorska Politechnika Poznańska, Poznań 2010.

[5] SZWABOWSKI, J. – DESZCZ, J. *Metody wielokryterialnej analizy porównawczej. Podstawy teoretyczne i przykłady zastosowań w budownictwie*, Wydawnictwo Politechniki Śląskiej, 2001.

Testing a Prototype for an Innovative Water Turbine

[*]Mariola Starzomska, Jerzy Zbigniew Piotrowski
[*]Kielce University of Technology, Faculty of Civil and Environmental Engineering,
Kielce, Poland, rav4ms@wp.pl, piotrowski@tu.kielce.pl

Abstract. The possibility of using rivers with small depths and dips to produce electricity requires building innovative turbines. Prototype of a new turbine is tested on a natural watercourse, and is designed to determine the hydrodynamic characteristics. Water turbines installed on the rivers with small dips and depths without the need for building any extra bottlenecks may contribute the development of micro power plants using rivers.

Keywords: Water turbine, micro power plant

1. Introduction

Poland has small water resources. Theoretical water resources in Poland were calculated during the 1960s, based upon the methodology of the World Energy Council. The amount of electricity was about 23 TWh per year (1TWh = 109kWh). The theoretical energy resources using all flowing waters determined by A. Hoffman and M. Hoffman [1] were about 12 TWh per year and the technical NEW resources (water objects less than 5MW) were about 2 TWh per year. However, only 10-12% of the technical potential of Polish rivers was being used and operating hydropower plants were producing an average of about 1.8 TWh per year.

There are no natural conditions in the Świętokrzyski region sufficient for the construction of typical hydro power stations, which is why scientific research being carried out at the Technical University in Kielce is mainly focusing on the usage of kinetic energy contained in flowing water, regardless of the watercourse conditions.

2. Research of turbine prototype

The studied turbine is a prototype. The properties such as its dependence on the parameters of the turbine power, i.e. the number of combined sections and the distance between them, or the dependence of rotational speed and the speed of the flowing water are not known yet. Tested turbine will allow using shallow rivers. It is constructed from the combined section and guiding system which is increasing the water flow velocity directed on the turbine. It works without having to build expensive bottlenecks and passes almost without interfering with the natural environment.

A model of the turbine which will be tested on natural conditions is currently being built. Tests are designed to determine the hydrodynamic characteristics of the turbine - power and torque in function of water flow rate. Shaft speed and torque will be directly measured (net power of the turbine will be determined by the product of velocity and torque without considering transmission efficiency). Due to the sectional construction of the turbine performed tests will allow to define number of sections and a distance between them to achieve necessary optimal amount of power. The study will also be used to determine blade angle.

Absence of windings and rotating electrical parts will result in a higher efficiency and reliability compared to conventional generators. Due to the low rotation speed the turbine will cooperate with an innovative synchronous generator induced by permanent magnets, which will also reduce noise and increase structural reliability.

3. Power of water turbine

Kielce University of Technology tested the water turbine with an innovative solution which uses the flow of water without a need to build expensive bottlenecks. Other important advantages of this device are its relatively low cost and minimal impact on the environment.

The kinetic energy of flowing water stream is determined by the following formula:

$$E = \frac{m\vartheta^2}{2} \ [\text{J}] \tag{1}$$

where:

$$m = \rho A \vartheta t \tag{2}$$

A – area through which water flows $[m^2]$,
ϑ – speed of the flowing water $\left[\frac{m}{s}\right]$
ρ – water density $\left[\frac{kg}{m^3}\right]$
Hydraulic power of the flowing water:

$$P_h = \frac{E}{t} = \frac{\rho A \vartheta^3}{2} \ [\text{W}] \tag{3}$$

By adding the water density ($\rho = 1000 \frac{kg}{m^3}$), we get:

$$P_h = 500 A \vartheta^3 \ [\text{W}] \tag{4}$$

The amount of power calculated from the formula (4) is only theoretical because the recovery of the entire kinetic energy of the water would cause it to stop flowing. Available capacity is due to the slowing of the water as it passes through the turbine (the difference between average speed of the water before and beyond the turbine).

$$P_t = \frac{1}{2} P_h \left(1 + \frac{\vartheta_2}{\vartheta_1}\right)\left(1 - \left(\frac{\vartheta_2}{\vartheta_1}\right)^2\right) \tag{5}$$

Assuming a minimum average speed of the water behind the turbine:

$$\vartheta_{2min} = 0.75\vartheta_1 \tag{6}$$

we get a maximum power of the turbine:

$$P_t = 0{,}38 P_h \tag{7}$$

Actual hydraulic power of flowing water is weaker and it depends on the physical conditions of the riverbed through which water flows, hydraulic loss, depth of the river, etc., and the cube of the flow speed, which is not very large for the majority of the rivers and remains between 1-2 m/s. In spite of its rivers great potential, flowing water cannot obtain large amounts of energy from a single device. Therefore, the appropriate use of multiple components would be for them to work on a single receiver.

4. Economical efficiency

Energetic and economical calculations:

$$\mu_t = \frac{P_1}{P_t} \tag{8}$$

where:
μ_t – turbine efficiency,
P_1 – power on the shaft of the turbine,
P_t – hydraulic power calculated using the formula (7).

Tab. 1. shows the calculations for the following principles: efficiency of the turbine $\mu_t = 0,8$, the efficiency of the generator $\mu_p = 0,8$, and the efficiency of the turbine complex $\mu_h = \mu_t\mu_h = 0,64$. The income from energy produced during one year S / year. Calculations were performed for the diameter of a turbine 0.4 m with a single rotor, a complex of 5, 10 and 15 sections, and the current energy price – 0.13 EUR/kWh.

No. of sections [/]	$\vartheta \left[\frac{m}{s}\right]$	P_h [W]	P_t [W]	P [W]	Produced energy [kWh]	S/year [EUR]
1	1	62.8	23.9	15.3	134	17.42
	2	502.4	190.9	122.2	1070	139.1
	3	1841.4	699.7	447.8	3923	510
5	1	314	119.5	76.5	670	87.1
	2	2512	945.5	611	5350	695.5
	3	9207	2498.5	2239	19615	2549.95
10	1	628	239	153	1340	174.2
	2	5024	1909	1222	10700	1391
	3	18414	6997	4478	39230	5100
15	1	942	358.5	230	2010	261.3
	2	7536	2863.5	1833	16050	2086.5
	3	27621	10495.5	6717	58845	17653.5

Tab. 1. Turbine power, amount of the produced energy and the income from its sale

The calculations above indicate that it is very important to use multiple subunits working for a single collector to get suitably economical results, especially at low speeds of flowing water.

5. Conclusion

Water turbines installed on the rivers with small dips and depths without the need for building any extra bottlenecks may contribute the development of micro power plants using rivers.

Turbines built on rivers with small dips should maximize the kinetic energy of flowing water. Using several subunits working on a single collector would increase efficiency of the turbine.

Reference

[1] HOFFMAN, M. Prognozy rozwoju energetyki wodnej w Europie i Polsce, IV Konferencja Naukowo-Techniczna „Mała Energetyka-97" Zakopane Kościelisko

[2] Praca zbiorowa: Kierunki rozwoju energetyki kompleksowej w Polsce do 2010 r. Ekspertyza PAN, Komitet Problemów Energetyki, Warszawa listopad 1994

[3] ZAWADA, T. Prądnice asynchroniczne. Materiały informacyjne dotyczące stosowania seryjnie produkowanych silników indukcyjnych jako generatorów asynchronicznych. Centralny Program Badawczo-Rozwojowy pn. „Kompleksowy Rozwój Energetyki . Informator, seria „Mała energetyka wodna"

[4] HOFFMAN, M. (red.) Małe elektrownie wodne-poradnik, Nabba sp. z o.o., Warszawa 1991

[5] KRZYŻANOWSKI, W. Turbiny wodne, konstrukcja i zasady regulacji, Wydawnictwo Naukowo-Techniczne, Warszawa 1971 r.

Measuring Method of Thermophysical Parameters of Grounds

[*]Jana Stránska, Milan Malcho

[*]University of Žilina, Faculty of Mechanical Engineering, Department of Power Engineering, Univerzitná 1, 010 26 Žilina, Slovakia, {jana.stranska, milan.malcho}@fstroj.uniza.sk

Abstract. In this article is described a mechanism of heat transfer, the way of measurement of thermal conductivity, specific heat capacity and thermal conductivity of rocks. It is very important to know about thermo-technical properties of grounds, which are describing transport of heat.

Keywords: heat conduction, thermal conductivity, thermal diffusivity, specific thermal capacity, temperature and ground.

1. Heat conduction

The heat is transferred by conduction in the solid bud also liquid and gaseous substances. For heterogeneous structures, which include ground, is primarily a mechanism of heat transfer conduction. In addition to conduction, heat can be transmitted by the convection of groundwater flow. Among the information needed to assess the effect of temperature on the transport of heat from the ground mass is important to know the temperature field and thermophysical parameters of grounds, such as temperature, geothermal gradient, thermal conductivity, coefficient of thermal diffusivity of grounds and heat flow.

Based on knowledge of temperature distribution is possible to determine the temperature gradient and heat flow. The quantification of the thermal field is based on a differential equation of heat conduction.

Temperature field is a set of temperature values of all the points considered space at each time point. Distinguish between *stationary* and *non-stationary* temperature field. *Stationary heat conduction* is thermally stable thermokinetic story mode characterized at the time of constant temperature at all points of the point or point system. Heat, which passes heat conduction area at the time, expresses Fourier law. Expressed in the form

$$\dot{Q} = -\lambda \, grad \, T . S \;\; [W], \tag{1}$$

where λ is thermal conductivity [$\mathrm{W.m^{-1}.K^{-1}}$], T is temperature [K] a S is area [$\mathrm{m^2}$].

Non-stationary heat conduction involves going where the temperature field in the body of function space and time. The solution of the conservation of energy for heating or cooling of a homogeneous and isotropic body without a heat source we get *the Fourier heat conduction differential equation* for non-stationary temperature field without internal source in the form:

$$\frac{\partial T}{\partial \tau} = \frac{\partial^2 T}{\partial x^2} + \frac{\partial^2 T}{\partial y^2} + \frac{\partial^2 T}{\partial z^2}, \tag{2}$$

where T is temperature [K] and x, y, z are Cartesian coordinates[$-$].

By modifying equation (2) we get the Fourier differential equation of the form:

$$\frac{\partial T}{\partial \tau} = \nabla . a^2 . T, \tag{3}$$

where coefficient of thermal diffusivity is given by:

$$a = \frac{\lambda}{c_p . \rho} \;\; [\mathrm{m^2 . s^{-1}}], \tag{4}$$

where λ is thermal conductivity [$\mathrm{W.m^{-1}.K^{-1}}$], c_p is specific thermal capacity [$\mathrm{J.K^{-1}.kg^{-1}}$] and ϱ is density [$\mathrm{kg.m^{-3}}$].

Substances such as thermal conductivity, specific heat capacity and density, which act in the definition of thermal conductivity are dependent on mechanical parameters such as rock (non heterogeneous structure) and some grounds and the water content in rock. The amount of water in the rock significantly affect the thermal conductivity of grounds at the phase transition of water ice. Therefore relevant for modeling transport processes in the deep borehole temperature working media below 0 ° C is necessary to know the dependence of thermal conductivity of grounds, specific heat capacity and density of the water content and temperature.

2. Measurement of thermal conductivity

Thermal conductivity reflects the ability of agents to keep warm. Value of the coefficient of thermal conductivity of rocks can be measured in the laboratory to test samples of several methods, such as methods relying on stationary heat flow, or methods of unsteady heat flow.

Currently, the most common for measuring thermal conductivity by employing the stationary flow apparatus according to Bock as "Fig.1", or a plate Poensgenov device.
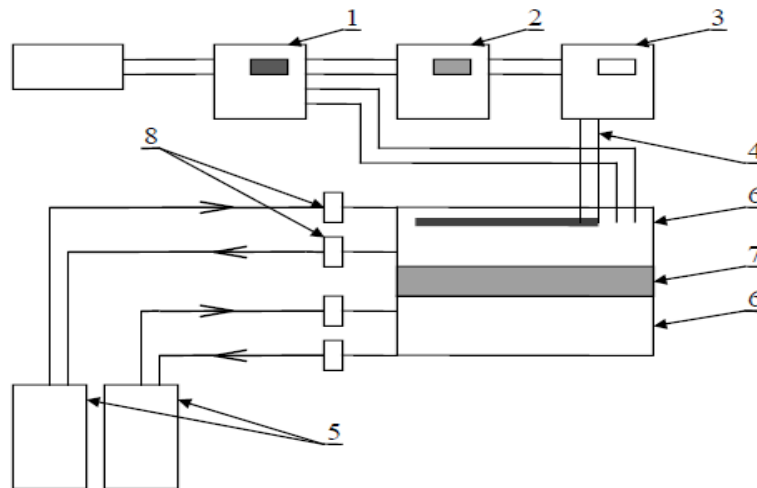
Fig. 1. Principle of measuring thermal conductivity.

1 - compensator, 2 - meter, 3- switch heater, 4 - heating, 5 – thermostats, 6 - heated plates, 7 - tested board, 8 - resistance thermometers.

Principle of measurement using Bock´s method device is that the test sample (rock) is placed between two thermally tempered plate device. Under constant temperatures of both state boards, which has a maximum temperature of 5 ° C to 10 ° C warmer than the lower plate, measured perpendicular to the flow of heat tested material of known thickness.

Subsequently in the laboratory on a similar device for measuring thermal conductivity measurements will be made of rock samples. By making a deep hole and thermal conductivity measurements obtained values necessary for establishing a mathematical model of heat transport in the ground.

In practice, the measurement of thermal conductivity is often used hand-held device ISOMET is controlled by a microprocessor. Used to measure the coefficient of thermal conductivity, specific heat capacity, density, coefficient of thermal conductivity and temperature of the compact, loose and liquid materials using the needle exchange and surface probes. The principle of measurement of thermophysical quantities using said device, which corresponds to the hot wire method. Hot wire method is one of the methods of measurement with non - stationary heat flux. In the test sample are transmitted heat pulses is measured and the subsequent time-dependent thermal response of the material. Heat flow creates a scattered electric power in the probe resistance, which is thermally bonded to the laboratory detection of material.

Fig. 2. Measuring equipment ISOMET

3. Measurement of specific thermal capacity

The heat capacity as a basic input parameter for heat conductivity factor calculation is a determinate for each sample. The heat capacity is measured on the base of physical definition „equation (5)". The transmitted heat is determined by calorimetric method, which assumes the heat – isolated calorimeter with sample and medium. The specific heat capacity is determines by calorimetric equation after achievement of temperatures´ balance.

$$c = \frac{1}{m} \cdot \frac{\Delta q}{\Delta T} \ [\text{J.K}^{-1}.\text{kg}^{-1}], \tag{5}$$

where m is mass of the sample [kg], Δq is transmitted heat to sample [J] and ΔT is change of temperature for transmitted heat [K].

To measure specific heat capacity is most commonly used mixing calorimeter. It is a thermally insulated container in which the substance under review by the mass m delivering and collecting the amount of heat and its temperature measured by the change. Mixing calorimeter consists of a cylindrical container (a) filled with liquid (b) (usually distilled water) of known thermal capacity, which does not react chemically with the substance under investigation (body), thermometer (c) and mixers (d).

This container is placed into another, larger container.
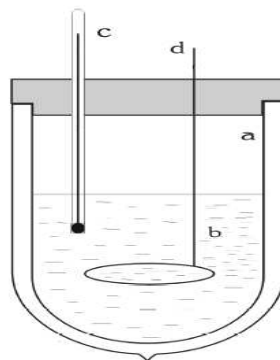
Fig. 3. Mixing calorimeter.

3.1. Determination of specific thermal capacity of ground

Calorimeter for heat capacity K of partially fills with water for specific thermal capacity c_1 and weight m_1. Wait until the water and heat exchange calorimeter, t. j. until the temperature stabilizes t_1, at the value they will measure. Then warm up the body mass (rock mass thermal capacity, which we provide) to the temperature t_2 , which should be at least 40-50 degrees higher than the

temperature t_1 a and put it into the calorimeter. There will be an exchange of heat and temperature of the water body in the calorimeter and the calorimeter to stabilize the temperature. t.

Based on the law of conservation of heat energy given to the sample, the sum of the heat taken by water and heat it takes calorimeter with accessories we can express the relationship for calculating the heat capacity of the sample examined.

$$c = \frac{(m_1.c_1+K)(t-t_1)}{m_2(t_2-t)} \ [\text{J}. \text{K}^{-1}. \text{kg}^{-1}], \tag{6}$$

4. Conclusion

To assess the effect of temperature of the rock mass is necessary to know the temperature field and thermophysical parameters of grounds, such as thermal conductivity, thermal conductivity, specific heat capacity. Rock properties also depend on various factors, namely the structure of rocks, porosity, humidity, pressure and temperature geostatical. Contribution to this research is to obtain a database of thermophysical properties of different types of rocks and their application in solving transport phenomena in grounds.

Acknowledgement

References

[1] ESKILSON, P. 1987. *Thermal analysis of heat extraction boreholes*. Doctoral thesis. Department of Mathematical Physics. University of Lund. Sweden.

[2] CARSLAW, H.S., – J.C. JEAGER. 1959. *Conduction of Heat in Solids*, 2d ed.. Oxford: Oxford Press.

[3] KREMPASKÝ, J. 1969. *Meranie termofyzikálnych veličín*, Veda, Bratislava.

[4] SAZIMA, M. a kol. 1989. *Sdílení tepla*, STNL – Nakladatelství technické literatúry, Praha, 1989, 592s. ISBN 80 – 03 – 00675 – 9

[5] http://www.appliedp.com/en/isomet.htm

Application of Two – Dimensional Digital Image Correlation for Measurement of Plastic Deformations

*Michaela Štamborská

*Technical University of Kosice, Faculty of Mechanical Engineering, Department of Applied Mechanics and Mechatronics, Letna 9, 042 00 Kosice, Slovakia, {michaela.stamborska}@tuke.sk

Abstract. The paper is aimed at the presentation of the choice applications of experimental methods of the mechanics. The main attention is focused on using of modern optical method – digital image correlation method (DIC). This method allows to perform a contactless measuring of deformation fields on a surface of tested objects. As a practical and effective tool for quantitative in-plane deformation measurement of a planar object surface, two-dimensional digital image correlation (2D DIC) is now widely accepted and commonly used in the field of experimental mechanics. There are presented procedures and results obtained under the determination of plastic strains of thin-walled elements in the domain of stress concentration.

Keywords: digital image correlation, plastic deformation.

1. Introduction

The digital image correlation is an advanced method, which provides recording of data and evaluate spatial deformations of the whole surface of object. Characteristic properties which result from its conception we can consider flexible area of measurement (mm^2 to m^2), material and geometry independence and spatial visualization of measured parameters. This is the reason why digital image correlation has been successful applied for many areas of science and survey. It has been applied for testing of components in engineering and microelectronic, determination of material properties and so on.

The principle of digital image correlation is based on application of stochastic pattern the surface of the test object. This pattern can be sprayed with a white base color and spattering a black color on top. Observed area is divided into smaller areas called facets (Fig. 1).
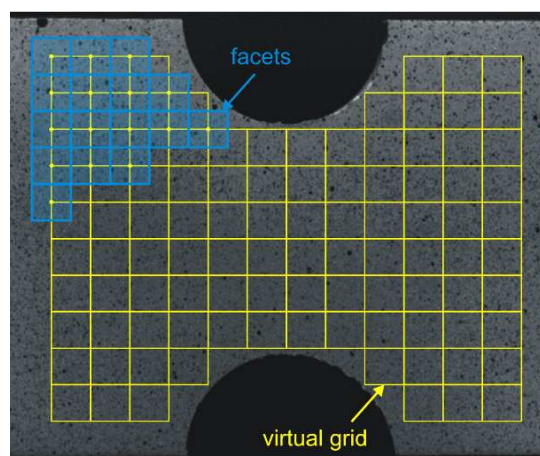

Fig. 1. Stochastic speckle pattern on examined surface

These speckles on the top of surface represent material points of body. The speckles copy deformations of surface and they move together with surface. Displacement and strains of points are calculated through correlation of corresponding facets on digital snapshots in state before and after deformation [1]. In case of plane digital image correlation object deformations are determine by

observation with camera vertically aimed at surface which provides to determine displacements in parallel plane with imagine plane. Figure 2 shows the schematic illustration of a typical experimental setup using an optical imaging device for the 2D DIC method [2].
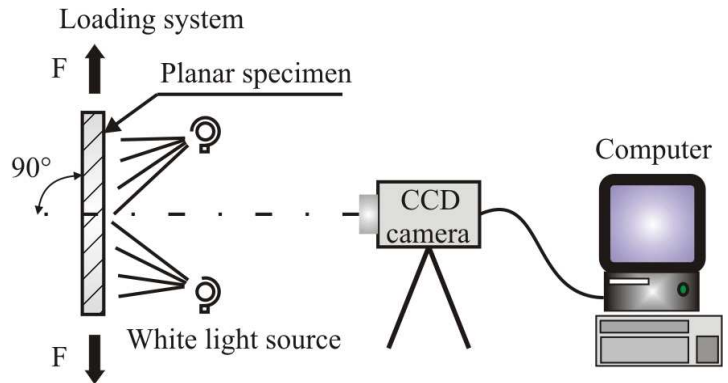

Fig. 2. Typical optical image acquisition system for the 2D DIC method

2. Determination of plastic deformation of thin-walled members

The experimental analysis of plastic deformation [3] is applied for every area, where material is stressed above yield stress. Knowledge of plastic characteristics of material has great deal especially in areas of compression molding of components, cold pressing, as well as loading supporting members in yield stress area. In these cases it is useful to apply DIC method, because it provides to plot field of full-field deformations on the surface and evaluate deformation at every point. In next part there is described experimental evaluation of plastic properties of pressing steel plate.
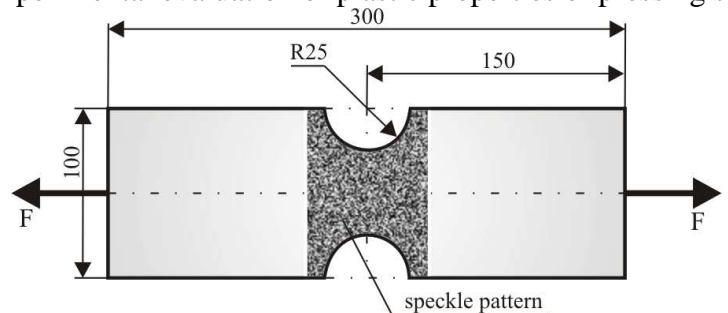
Fig. 3. Specimen with speckle pattern

Specimen (Fig. 3) is created by DCO3 cold pressing steel plate (tractile, suitable for indoor parts of care frame and other pressings). Mechanic properties of specimen are shown in Tab. 1.

Name	Thickness [mm]	R_e [MPa]	R_m [MPa]	A80 [%]	r_{90}
DCO3	0,8	236	335	37	1,90

Tab. 1. Mechanic properties of specimen material

Measurements were realized by shredder FPZ 100/1 (Fig. 4) [4], while plastic deformation was measured around area of dent of specimen by high-speed correlation measure system Q-450. As it was plane analyze, the measurement was realized by only one camera [5]. The specimen was tension in longitudinal direction to the total break.
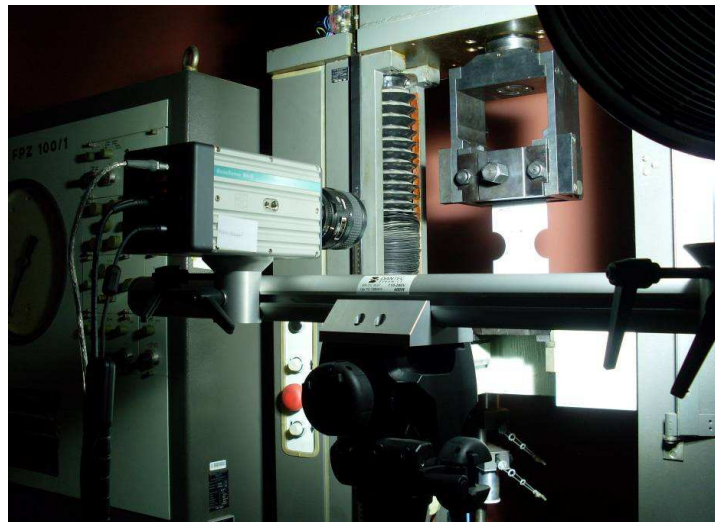
Fig. 4. Position of the camera during specimen loading

Velocity of motion girder was $v_T = 0{,}1$ mm/s, while approximate time of break of sample was 100s. Plastic deformation of the whole cramped section was achieved by force $F_{Re} = 9\,400$ N. Break of sample was caused by force $F_{max} = 13\,400$ N. In the Fig. 5 are shown fields of strains ε_y (Fig. 5a) and fields of shear strains γ_{xy} (Fig. 5b) (mm/m) of specimen, which were obtained by system Q-450.
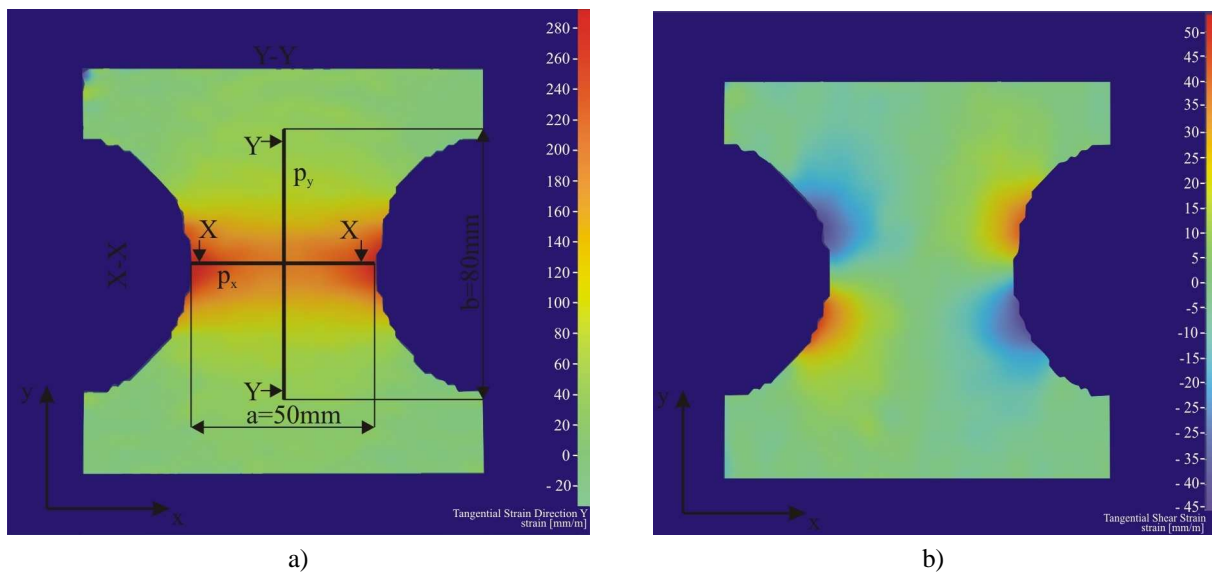

a)   b)

Fig. 5. a) The fields of strains εy [mm/m] and b) the fields of shear strains γxy [mm/m]

Results of measurement, which were obtained by system Q-450 were exported into HDF5 files and then they were numerically calculated by program Matlab in order to plot strains at sections X-X and Y-Y (Fig. 5) as a dependence of measurement step. Dimensional coordinate with respect of length of lines p_x and p_y is expressed non-dimensional coordinates of position $\xi_x=x/a$ a $\xi_y=y/b$, where "a" is width of measured area in "x" direction and "b" is width of measured area in "y" direction (Fig. 5). Strain diagram ε_y with respect of lines p_x and p_y at 100th step is shown in the Fig. 6.
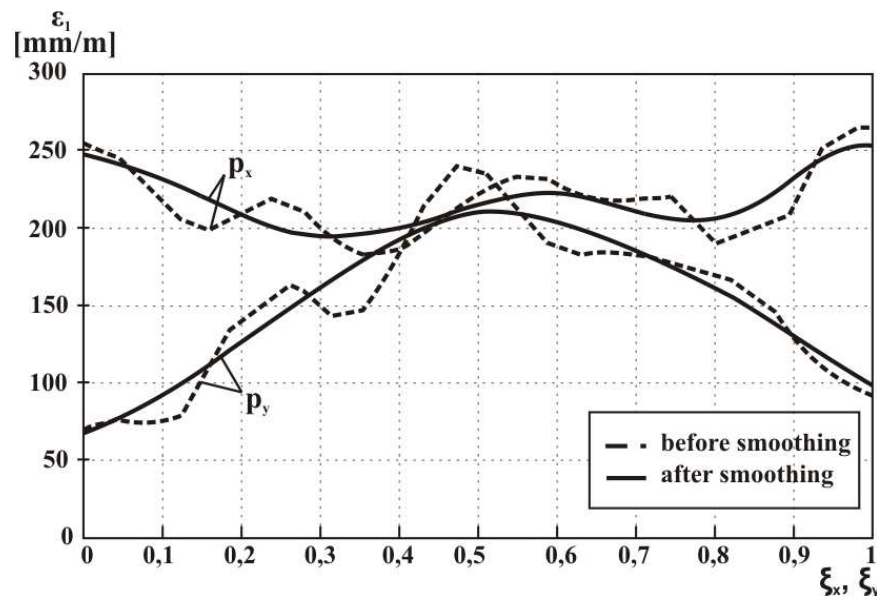
Fig. 6. Strains εy measured at lines px and py before smoothing and after smoothing

As a result of diagrams obtained by Matlab (Fig. 6) by smoothing were obtained more continuously strain diagrams ε_y, however process of smoothing caused reductions in size of results at points with maximum values. Except for this choosing sample frequency was occurring like map line sample with steps after processing by Matlab.

3. Conclusion

In this paper there is introduced 2D example of using digital image correlation method. As it was shown this modern method provides to observe different events during deformation of object. Recall that 2D DIC can only be used for in-plane deformation of a planar object. Even if optical methods with white light are preferred in technical field, DIC method has been expanded on electronic microscopy field. Nowadays it covers areas of mechanical engineering, car and air industry.

Acknowledgement

References

[1] TREBUŇA, F. – ŠIMČÁK, F. *Príručka experimentálnej mechaniky*. TypoPress, Košice, 2007.

[2] BING, P. – KEMAO, Q. – HUIMIN, X. – ANAND, A. *Two-dimensional digital image correlation for in-plane displacement and strain measurement*. Measurement Science and Technology. 20th (17pp), 2009.

[3] ŠIMČÁK, F. – TREBUŇA, F. – BERINŠTET, V. – ŠTAMBORSKÁ, M. *Application of numerical and experimental modelling for analysis of plastic deformation of steel sheets*. Metalurgija. Vol. 49, No. 2 (2010), p. 545-549.

[4] FILČÍK, P. *Možnosti využitia skúšobného stroja FPZ 100/1 pre skúšky nízkocyklovej únavy*. Diplomová práca, KAMaM/SjF, 2007.

[5] WATTRISSE, B. C. – MURACCIOLE, A. – NEMOZ-GAILLARD, J. M. *Analysis of strain localization during tensile tests by digital image correlation*. Exp. Mech. 41, pp. 29–39, 2001.

Experimental Studies of Fatigue Life of Aluminum Alloy under Uniaxial and Biaxial Loading

[*]Ondrej Števka, Peter Kopas, Milan Uhríčik
[*]University of Žilina, Faculty of Mechanical Engineering, Department of Applied Mechanics, Univerzitná 1, 010 26 Žilina, Slovakia, {ondrej.stevka, peter.kopas, milan.uhricik}@fstroj.uniza.sk

Abstract. This article deals with experimental verification of fatigue life prediction of aluminum alloy under biaxial fatigue loading. The theoretical part describes a physical process of fatigue material in regime of low cycle loading. There is also discussed an influence of various factors to fatigue characteristics and multiaxial fatigue of loading. The experimental part of this article deals with evaluation of biaxial fatigue failure to aluminum alloy EN AW 6063.T66 from fatigue lifetime point of view. The fatigue test was realized on multiaxial fatigue device with these conditions: a sinusoidal wave type of loading was used for bending and torsion experimental testing; frequency of loading was f = 30 Hz and temperature was 20 ± 5 °C.

Keywords: Experimental verification, fatigue resistance, biaxial fatigue, aluminum alloy.

1. Introduction

Fatigue failure of materials is still statistically the most common cause of serious accidents of mechanical structures in the world despite of extensive research and studies over last 5 decades. This situation is caused by complexity of fatigue process and large number of impacting factors. Nowadays the Material Science and Engineering define fatigue failure as tendency of material to fracture under repeated alternating or cyclic loading [1]. The nominal maximum stress values are considerably below the ultimate tensile stress limit and may be below the yield stress limit of material. If the loads are above a certain threshold, microscopic cracks will begin to form at the surface. Repeated cyclic deformation even changes other mechanical properties therefore serious theoretical life time prediction is strongly influenced by experimental testing especially for new materials. The aim of these studies is to increase endurance, safety and reliability of components and structures, to protect human life and contribute in economical point of view. Current trend in technology and manufacturing has led companies to design optimized products in recent few years. There is not usually requirement for unlimited life of devices and used materials. For this purpose fundamental knowledge about behavior of materials in low-cycle area of loading started to be really important for designers. This is the reason why many research teams perform experiments in regime of low-cycle loading to determine exact characteristics of material and component life for special types of loading and verified boundary conditions. For most of mechanical structure is typical bi/multiaxial character of loading and better estimated lifetime value can be obtained and whereupon used for practical purposes only from multiaxial fatigue life diagrams [2,3].

2. Low cycle fatigue

Low-cycle fatigue as a phenomenon has received much attention since the early work of Coffin and Manson in the fifties and the sixties. It became clear that low-cycle fatigue is a problem which is different from high-cycle fatigue. As pointed out before, the high-cycle fatigue mechanism on a macro scale occurs as an elastic phenomenon. However, in low-cycle fatigue, macroscopic plastic deformation occurs in every cycle. Low-cycle fatigue can be relevant to structures that are subjected to small numbers of load cycles in their economic life. If it would be required to keep all stress

levels below a fatigue limit, the structure may become very heavy without this being necessary. Under low-cycle fatigue, failure can occur in a small number of cycles, say 1000 cycles or less. Small cracks are usually nucleated immediately. In view of the high stress level, final failure will occur when the cracks are still small. Periods of visible crack growth are hardly present. It is known that low-cycle fatigue under constant amplitude loading leads to a high plastic deformation in the first cycle followed by much smaller strain amplitudes in subsequent cycles. For that reason, it is instructive to study the low-cycle fatigue process in the laboratory by imposing constant strain cycles on a specimen. In general, this loading condition is also representative for the low-cycle conditions in structures [4, 5, 6].

Coffin and Manson independently observed that the fatigue life under low-cycle fatigue conditions plotted as a function of the strain amplitude, ε_a, indicates linear relations if plotted on a double logarithmic scale, see Fig. 1. The relation can be written as:

$$\varepsilon_a = \varepsilon_{ae} + \varepsilon_{ap} = \frac{\sigma_f}{E} \cdot \left(2N_f\right)^b + \varepsilon_f \cdot \left(2N_f\right)^c .$$

(1)

where E is Young modulus, ε_f is the fatigue ductility coefficient, c represents the fatigue ductility exponent.
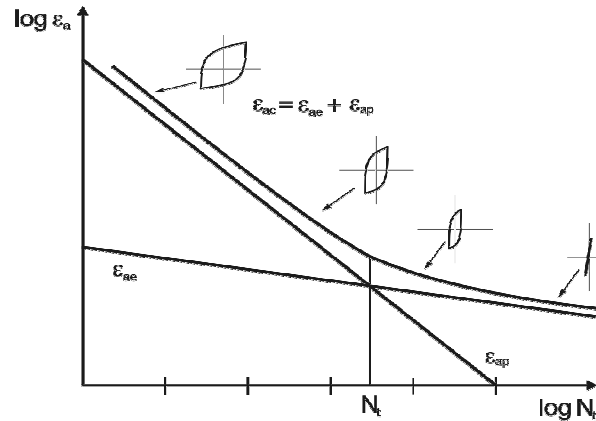

Fig. 1. Manson-Coffin curve.

3. Material and experimental procedures

Experimental material used for fatigue tests was an aluminum alloy EN AW 6063.T66. It is a medium strength alloy, with magnesium and silicon as the alloying elements suitable for application where no special strength properties are required. Ultimate stress limit was $R_a = 247$ MPa. It is commonly referred as architectural alloy with good surface quality characteristics, high corrosion resistance and suitable to welding. Low-frequency fatigue tests were carried out with using a multiaxial testing apparatus for low-frequency sinusoidal cyclic bending and torsion loading (working frequency f ≈50 Hz, temperature T = 20 ±5 °C, load ratio R = –1). Smooth 4 mm-dia round bar specimens polished in the working area were used for fatigue test program (see Fig. 2).
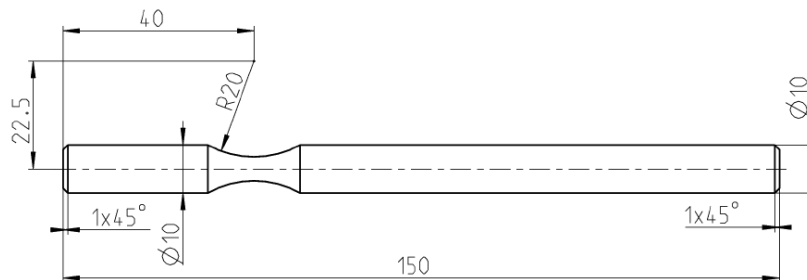

Fig. 2. Shape and dimension of the specimen for multiaxial fatigue test.

The final shape of experimental specimen has been designed by the standard to support easy manufacturing and connection with testing machine. The fatigue lifetime, strain amplitude vs. number of cycles to failure, was investigated in the region from N ≈ 103 cycles to N ≈ 106 cycles of loading.

Mechanical fatigue test equipment used for experiments has been developed on Department of applied mechanics at University of Žilina. Figure 3 show two independent parts of fatigue test machine. Both types of loading – bending and torsion can be synchronized and controlled by computer.
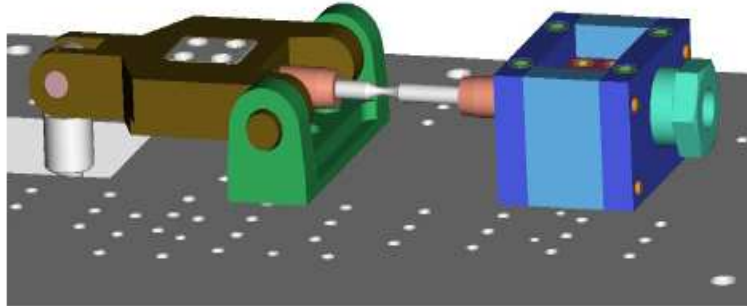
Fig. 3. Work area of the multiaxial fatigue test machine.

4. Experimental results

The results, fatigue resistance (strain amplitude vs. number of cycles to failure) of tested structural material EN AW 6063.T66 in the low cycle regime are presented in Fig. 4 and Fig. 5. In the low cycle regime of loading the strain amplitude decreases with increasing of cycles number to failure.

The first series of performed experiments were to verify fatigue behavior of aluminum alloy EN AW 6063.T66 under low-cycle bending loading to obtain relation between strain magnitudes versus number of cycles to failure. The Fig. 4 had shown the results of fatigue tests with the symmetrical pure bending loading. The specimen failure criterion during the testing was a creation of fracture area more than 90% in the measured cross section of the testing rod.

The second series of performed experiments were to verify fatigue behavior of aluminum alloy EN AW 6063.T66 under low-cycle bending-torsion loading to obtain relation between strain magnitudes versus number of cycles to failure. The Fig. 5 had shown the results of biaxial fatigue testing. There were seventeen different combinations with low amplitude (constant torsion value $\gamma_{ac}= 2,4 . 10^{-3}$) of the torsion loading combined with gradually scale up amplitude of the bending loading. The loading sequences were constant torsion followed by bending (torsion/bending) loading combination.
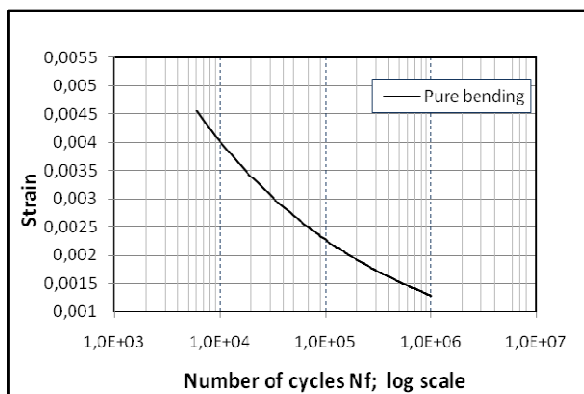

Fig. 4. Fatigue resistance, low–frequency fatigue testing, pure bending, EN AW 6063.T66
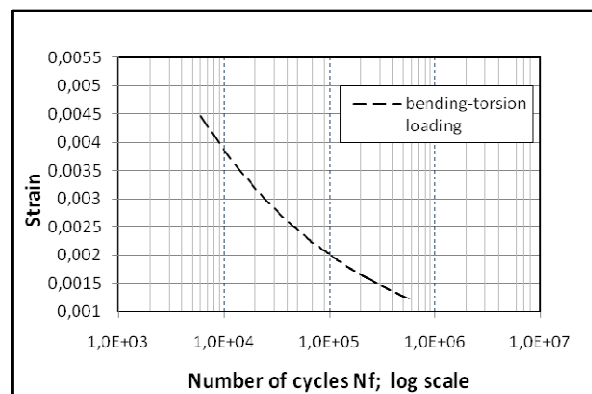

Fig. 5. Fatigue resistance, low–frequency fatigue testing, bending and torsion loading, EN AW 6063.T66

Generally we can say, that results are in good agreement with published results of other authors [1,4,6]. The differences in fatigue resistance of aluminum alloy of specimens are caused by different history of loading. Unless fatigue under cyclic tension and under cyclic bending are not that much different during by torsion loading there are some differences. The critical stress of a specimen in bending case is cyclic tension in the surface layer of the material. The stress gradient perpendicular to the material surface is different for tension and bending, but the more important stress gradients occur along the material surface. Classical examples of fatigue under cyclic torsion are associated with axles and spiral springs. Nucleation of the first microcrack again occurs in slip bands carrying the maximum shear stress. This shear stress amplitude in a specimen loaded in tension is equal to half the tensile stress, or $\tau_a = \delta_a/2$. For a specimen, loaded under cyclic torsion, the maximum shear stress is equal to the shear stress on the specimen. As a first estimate, one might expect that the fatigue limit under cyclic torsion, τ_f, is half the fatigue limit δ_f under cyclic tension in agreement with the Tresca yield criterion. However, as was before indicated, such slip bands under cyclic tension are also loaded by a tensile stress perpendicular to the slip bands, whereas this tensile stress is absent for cyclic torsion. As a result, the conversion of cyclic slip into a microcrack may be more difficult under cyclic torsion, and τ_f may be larger than $S_f/2$.

5. Conclusion

The results of experimental observations about fatigue resistance of EN AW 6063.T66 in the low cycle number of loading shows:

- The fatigue resistance of aluminium alloy increases with decreasing stress amplitude continuously in the cycles of number region.
- The fatigue properties of aluminium alloy strongly depends on type of loading (combination of loading).
- According to this fact it is necessary to verify the fatigue resistance in respect to working reliability and safety of the components and devices.

Acknowledgement

References

[1] STEPHENS, R.I – FATEMI, A. – STEPHENS, R.R. – FUCHS, H.O. *Metal fatigue in engineering,* 2nd ed. John Wiley and Sons, Inc; 2000.

[2] BULLEN, W.P. – HEAD, A.K. – WOOD, W.A. *Structural changes during the fatigue of metals.* Proc. Roy.Soc., Vol. A216, 1953.

[3] FORSYTH, P.J.E. *The Physical Basis of Metal Fatigue.* Blackie and Son, London, 1969.

[4] SURESH, S. *Fatigue of Materials.* 2nd ed. Cambridge University Press, Cambridge, 1998.

[5] BOKŮVKA, O. – NICOLETTO, G. – KUNZ, L. – PALČEK, P. – CHALUPOVÁ, M. *Low & high frequency fatigue testing.* CETRA and Univerzity of Žilina, Žilina, 2002.

[6] SIGLER, D. – MONTPETIT, M.C. – HAWORTH, W.L. *Metallography of fatigue crack initiation in an overaged highstrength aluminium alloy.* Metall. Trans. A, Vol. 14A, 1983.

Flow Modeling in Intercoolers

[*]Peter Tučník, Emil Toporcer, Vladimír Hlavňa
[*]University of Žilina in Žilina, Faculty of Mechanical Engineering, Department of Automotive Technology, Univerzitná 1, 01026 Žilina, Slovakia, {peter.tucnik, emil.toporcer, vladimir.hlavna}@fstroj.uniza.sk

Abstract. The paper deals with the numerical simulation of the flow in the charge air intercoolers of the turbocharged internal combustion engine. First the 3D virtual model of the intercoolers space is created within the 3D parametric modeler CATIA V5. Then the flow simulation is performed through the computational fluid dynamics software Fluent.

Keywords: numerical simulation, flow modeling, velocity, intercooler, charge air.

1. Introduction

Both boosted air intercoolers are designed for the four stroke compression ignition engine with the engine displacement of 7.6 l. The first intercooler is liquid/air type and the second intercooler is the air/air type. The simulations are the part of the simulations performed with the aim to acquire the information about the influence of the extremely low temperatures of charging air on the exhaust emissions production.

2. First Intercooler Design and Flow Simulation

As mentioned above the intercooler is liquid/air type. The charging air flow is perpendicular to the coolant flow. The intercooler has 5 pipes for each of the 3 drafts. The pipes have the outer diameter of 10 mm and the thick of the wall of 1 mm. The pipes has the active length of 760 mm. The cooling fins have these parameters: height 150 mm, width 50 mm, thickness 0.2 mm. The design of the intercooler can be seen in Fig. 1. The distance between the cooling fins is 1.4 mm.
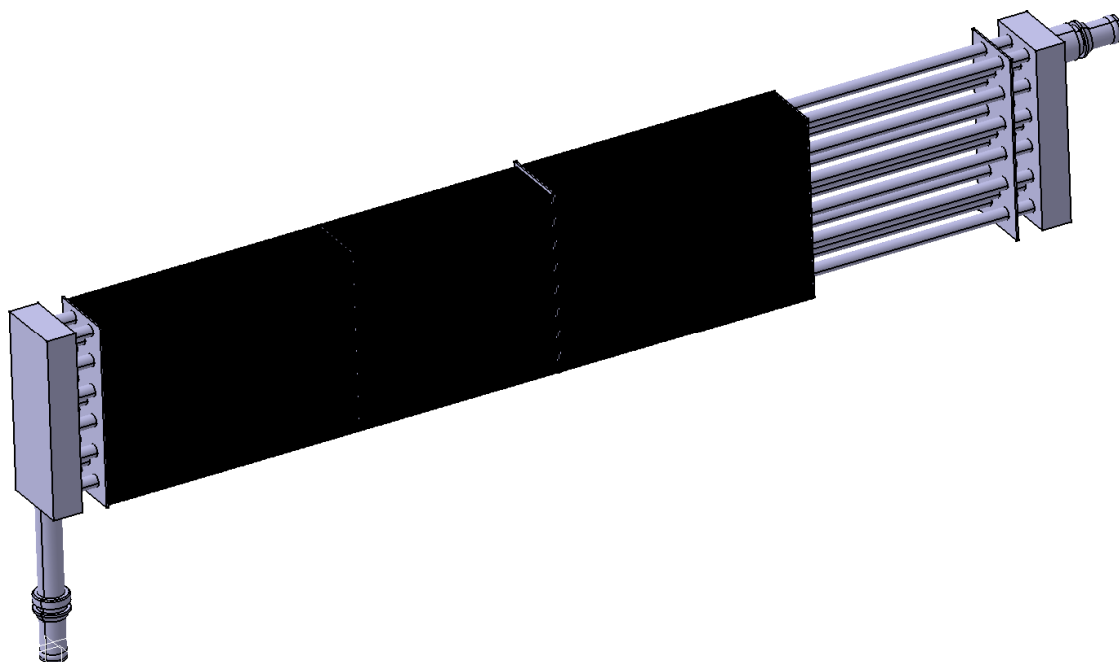

Fig. 1. The design of the first intecooler

First the coolant flow simulation is performed. The CAD model is created through the CATIA V5 – 3D parametric modeler. Then the part of the model needed for the flow simulation is prepared (see Fig. 2). This CAD model is then imported into the preprocessor Gambit and the computational mesh is created. The mesh consists of 1 399 065 tetrahedral cells. Then the mesh is imported into the Fluent – CFD (Computational Fluid Dynamics) software. The values for the boundary conditions are set. The velocity at the coolant inlet has the value of 1.26 m.s^{-1}.
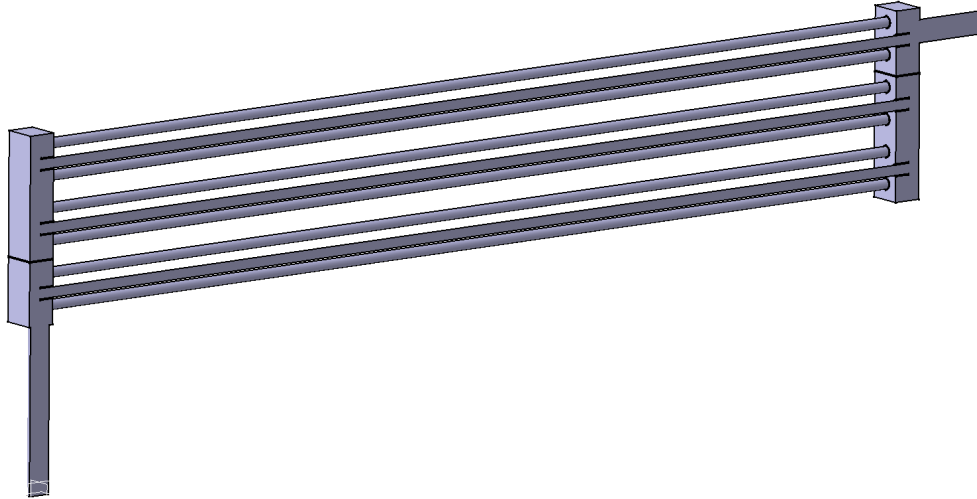
Fig. 2. The CAD model for the simulation preparation

Fig. 3 shows the distribution of the velocity vectors in the pipe. The maximum value of the velocity is about 2.6 m.s^{-1}.
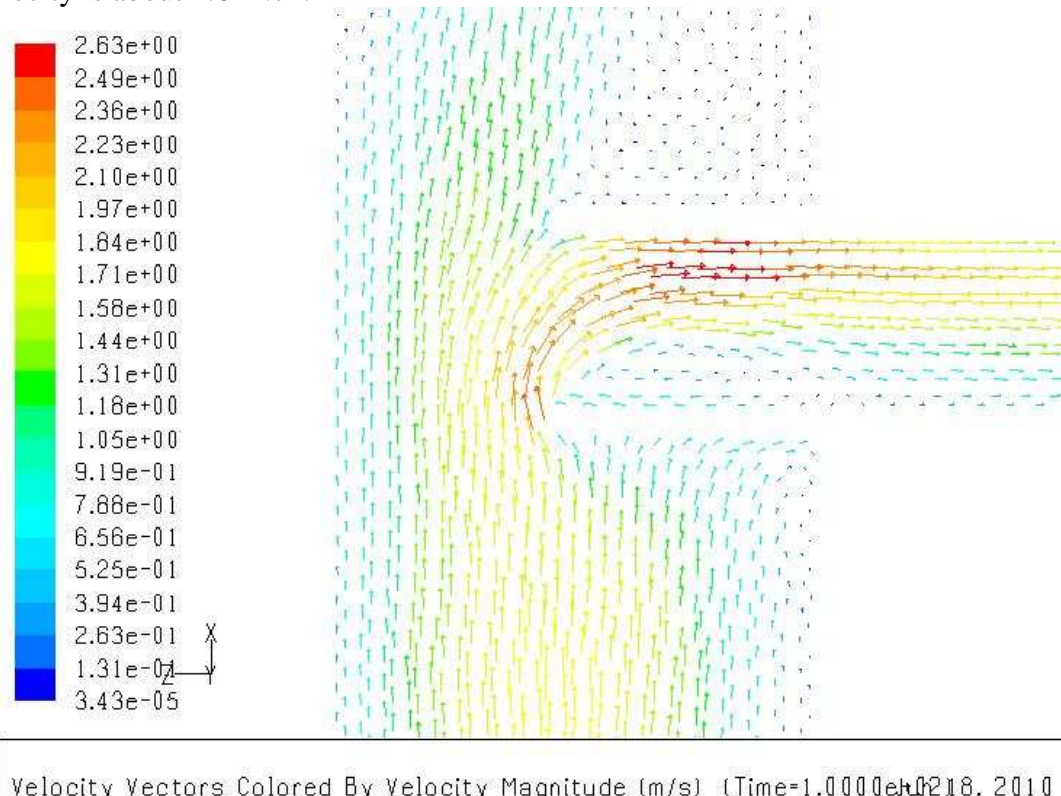

Fig. 3. Velocity vectors distribution in the inlet of the pipe

The second simulation is the simulation of the charging air flow between the cooling fins. The CAD model is again created within CATIA, the mesh is prepared in the Gambit and the simulation is performed in the Fluent. The velocity of charging air at velocity inlet boundary conditions is 5.6 m.s^{-1}. The result can be seen in Fig. 4. The maximum values of velocity occur in the proximity of pipes and achieve 13.3 m.s^{-1}.
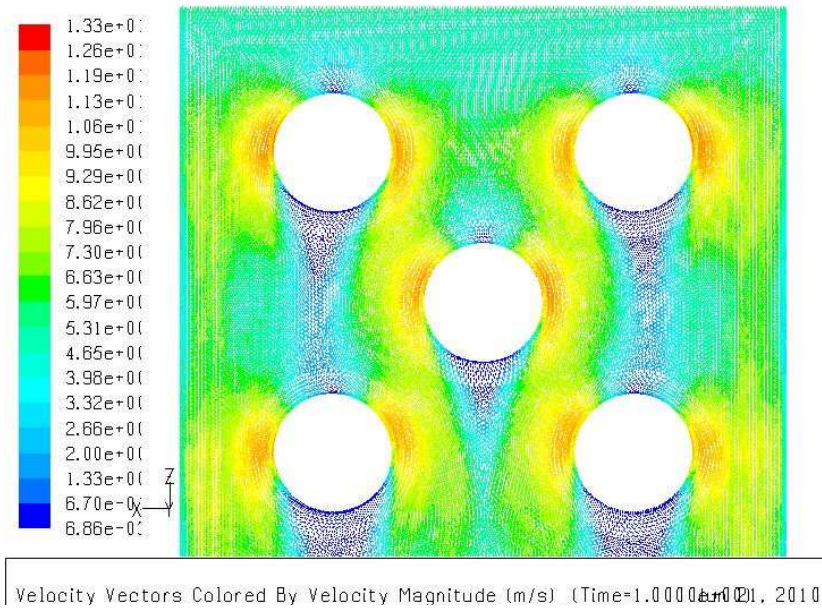
Fig. 4. Velocity vectors distribution between the cooling fins

3. Second Intercooler Design and Flow Simulation

As mentioned above the intercooler is air/air type. The charging air flows perpendicular to the cooling air. The intercooler consists of 54 pipes in one draft. The pipes have the same outer diameter of 10 mm and the same thick of the wall of 1 mm. The distance between the axis of the pipes is 25 mm. The active length of the pipes is 410 mm. Fig. 5 shows the arrangement of the pipes and the cooling fins and the complete design of the intercooler. The parameters of the cooling fins are: height 462 mm, width 64 mm, thickness 0.2 mm. There are 165 cooling fins and the distance between each two fins is 2.3 mm.
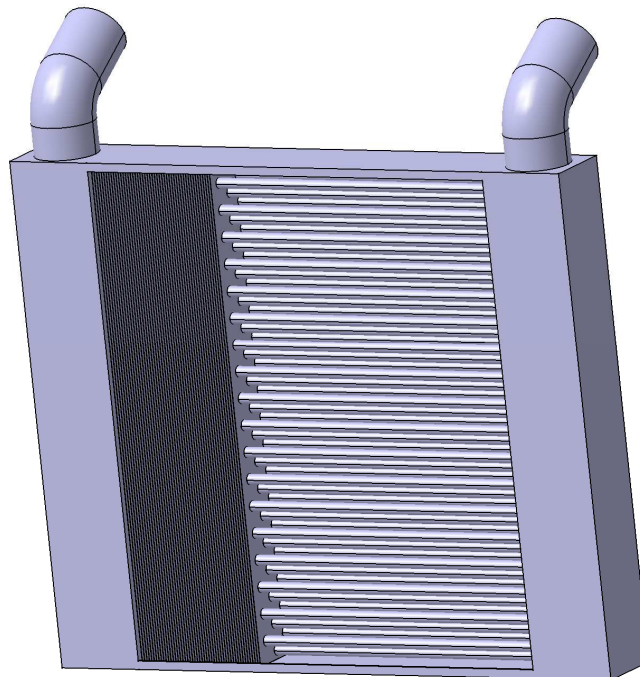

Fig. 5. The design of the second intercooler

The same means are used for the preparation of simulation – CATIA, Gambit and the simulation is again performed in the Fluent. In this case the mesh consists of 1 323 792

tetrahedral cells. The charging air inlet velocity has the value of 6.7 m.s^{-1}. Fig. 6 shows the simulation result. As we can see the maximum velocity magnitude is about 91 m.s^{-1}.
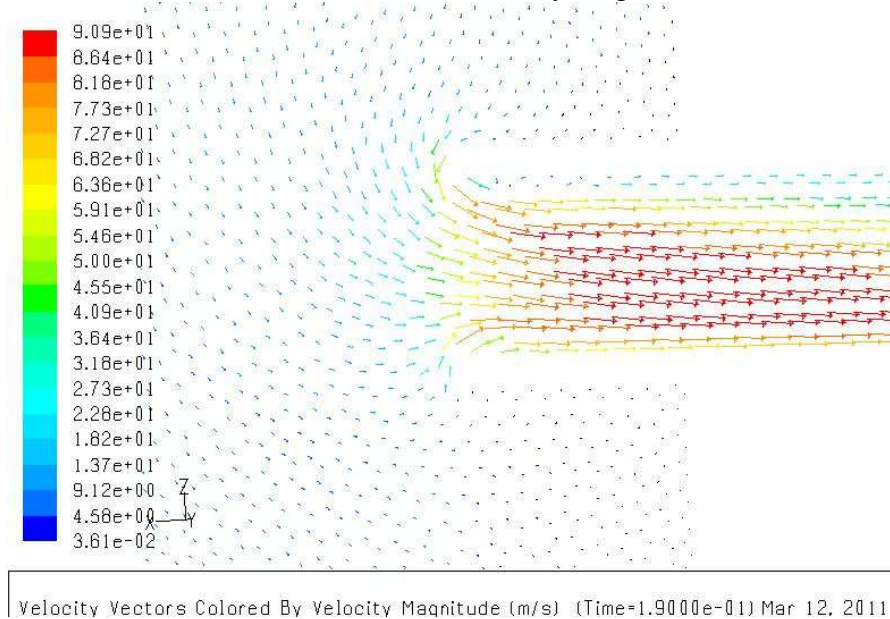

Fig. 6. Velocity vectors distribution in the area of inlet into the pipe

4. Conclusion

The coolant flow simulation for the first intercooler shows that the maximum values of velocity magnitude is about 2.6 m.s^{-1} in the area of pipe inlet. The charging air flow simulation shows that the maximum values of velocity magnitude for the first intercooler reach 13.3 m.s^{-1} which is lower compared to the value of 91 m.s^{-1} in the case of the second intercooler.

Acknowledgement

References

[1] HUDÁK, A. – BARTA, D. *Analýza prúdenia chladiaceho media v okolí valca motora Z8004C.* In: Hydraulika a pneumatika: časopis pre hydrauliku, pneumatiku a automatizačnú techniku, ISSN 1335-5171, vol. 7, No. 1-2, 2005, p.52-54.

[2] KONDEPUD, D. *Modern Thermodynamic.* John Wiley and Sons, 1998.

[3] KOVALČÍK, A. *Pressure and flow measurement in a nonconventional energetic system.* In proceedings of the international conference TRANSCOM 2009, ISBN 978-80-554-0031-0, section 6, EDIS – University of Žilina, Žilina, 2009.

[4] KOVALČÍK, A. – SOJČÁK, D. – ZVARKOVÁ, D. *Combined cycle plants for cogeneration in industrial power station.* In proceedings of the international conference TRANSCOM 2009, ISBN 978-80-554-0031-0, section 6, EDIS – University of Žilina, Žilina, 2009.

[5] LABUDA, R. – ISTENÍK, R. *Vplyv dynamiky zmeny režimu spaľovacieho motora na jeho prevádzkové veličiny.* In proceedings of the international conference KOKA 2005, ISBN 80-01-03293-0, CTU Prague, Prague, 2005, p.173-178.

[6] LÁBAJ, J. – BARTA, D. *Unsteady flow simulation and combustion of the ethanol in diesel engines.* In: Communications, ISSN 1335-4205, Vol. 8, No. 2, 2006, pp. 27-37.

Impact of Cogeneration Units on the Environment

[*]Peter Tučník, Emil Toporcer, Vladimír Hlavňa
*University of Žilina, Faculty of Mechanical Engineering, Department of automobile technology,
Univerzitná 2, 01026 Žilina, Slovakia, {peter.tucnik, emil.toporcer, vladimir.hlavna}@fstroj.uniza.sk

Abstract. Emissions reduction and the impact of technological equipment on the environment is a very important issue at the moment. One of possibilities for reduction of this impact is the use of cogeneration for production of heat and electricity. Using this combined production of energy, significant part of primary fuel can be saved and operating costs may be reduced. The paper discusses the measurement of emissions of cogeneration units. There are results of measurement of CO, CO_2, HC, NO_x in graphical form for several monitored types of cogeneration units. These units are deployed to variable technological processes of production. Engine running of cogeneration units have to adapt this process. Therefore, emissions have been measured in transient modes of combustion engine as well.

Keywords: cogeneration, emissions, engine, transient modes of engine.

1. Cogeneration

When traditional production of electricity is used, waste heat generated during production is emitted to the atmosphere without future use. The efficiency of this equipment is 35 – 40%. Use of waste heat generated as a secondary product of combustion for hot water heating or household heating may increase the efficiency of technological unit up to 80 – 90%. Combined production of electricity and heat – cogeneration, represents an effective and highly ecological way of using the primary energy contained in fuel. The fuel is usually natural gas, but also biogas, propane and other fuels have been successfully used. This technology is currently widely used in industry.

1.1. Advantages of cogeneration:

- Significant saving of primary fuel compared to separate production of electricity in condensing power plants.
- Significant reduction of emissions of technological entities using combined production energy which use natural gas as a fuel compared to technological entities which use coal as a fuel.
- High energy-use efficiency, fast start up into operation (in case of technological entities with internal combustion engines or combustion turbines).
- Possibility of an independent operation in case of failure of public electricity power network for technologies with a synchronous electric generator.

Cogeneration eliminates ineffective processes of separate energy production because this technology enables a combined production of heat and electricity in a single device and in one place. This way, we can get up to 40% saving of fuel consumption. Currently, this technology represents a significant proportion of heat and electricity production in the market.

1.2. Disadvantages of cogeneration

Benefits of this technology are accompanied by some problems. The main one is the initial investment, which is today the largest energy problem. We have to calculate between inputs and outputs, but often in these unstable conditions these calculations only turn into estimates. In order to

use all benefits that cogeneration offers, a demand of heat energy for at least 4500 hours per year must be ensured.

2. Gas emissions of cogeneration units

Department of automobile technology participated in the development of cogeneration units for the private sector. It provided also tests of three cogeneration units in normal operation and evaluation of measured results. The tests were carried according to customer's requirements.

Earlier measurement detected that the combustion engine, despite expected steady mode, often worked in transient modes. This is a result of adaptation of the engine to the requirements of technological process. The results of some measurements, which were carried out in order to determine the burden of cogeneration units in transient modes on the environment, are listed below. Monitored gas emissions produced by three different cogeneration units have been measured.

First cogeneration unit

Cogeneration unit consists of three-phase generator and spark ignited gas engine. It is in-line, six cylinders, four stroke, liquid cooled, turbocharged engine of stoichiometric conception without three-way catalyst.
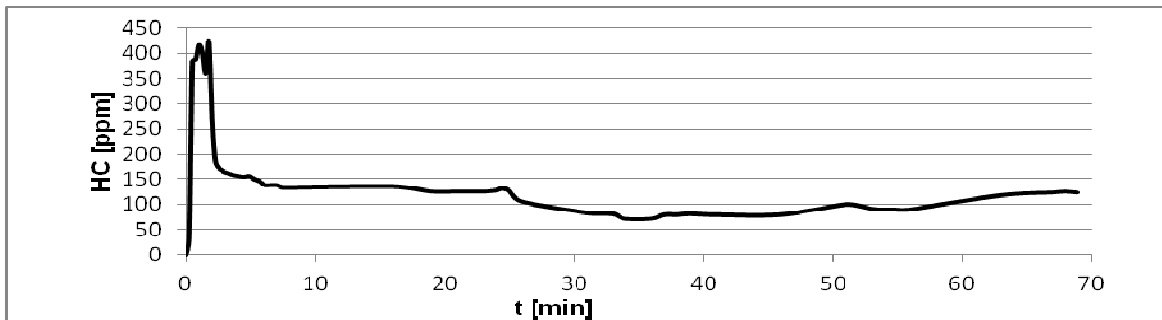

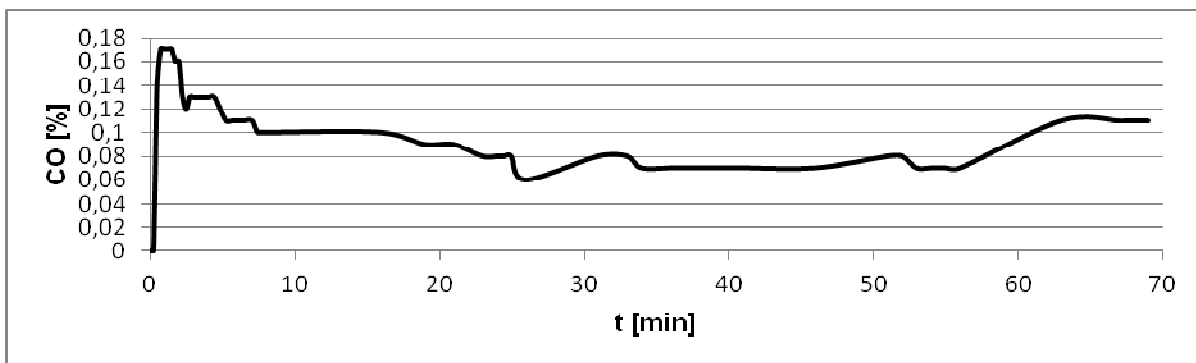**Fig. 1.**   Produced HC after hot start engine

Fig. 2.   Produced CO after hot start engine

Gas emissions have been measured behind exhaust heat exchanger after hot start of engine during the first 70 minutes of operation. In Fig. 1. the course of the emissions of unburned hydrocarbons is shown. The highest amount of emissions were recorded during the first minutes after startup. Fig. 2. shows the course of the emissions of CO. As we can clearly see in the figure, greatest values were recorded during the first minutes after startup in this case as well.

Second cogeneration unit

Cogeneration unit consists of three-phase generator and spark ignited gas engine. In this case, it is V-engine, eight cylinders, liquid cooled, four stroke engine of stoichiometric conception with three-way catalyst of exhaust.

In this case, emissions behind the three-way catalyst of engine have been measured. Measurement was carried out at the constant engine speed of 1500 rpm. The course of emissions depending on the active power of generator of cogeneration unit was monitored. Fig. 3. shows the course of emissions of CO, CO_2, HC and NO_x.
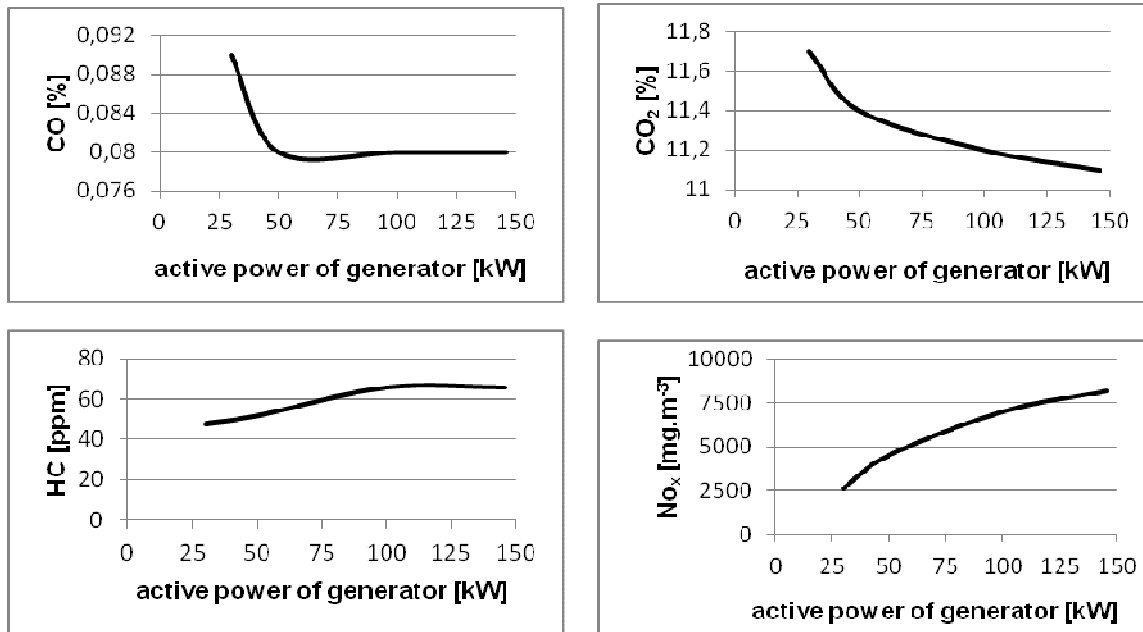

Fig. 3. Produced CO, CO_2, HC, NO_x second cogeneration unit behind catalyst

Third cogeneration unit

Third cogeneration is a combined cogeneration unit consisting of three-phase generator with electronic control allowing electric engine mode, heat pump and spark ignited gas engine. It is in-line, six cylinders, four stroke, liquid cooled, turbocharged engine without three-way catalyst.
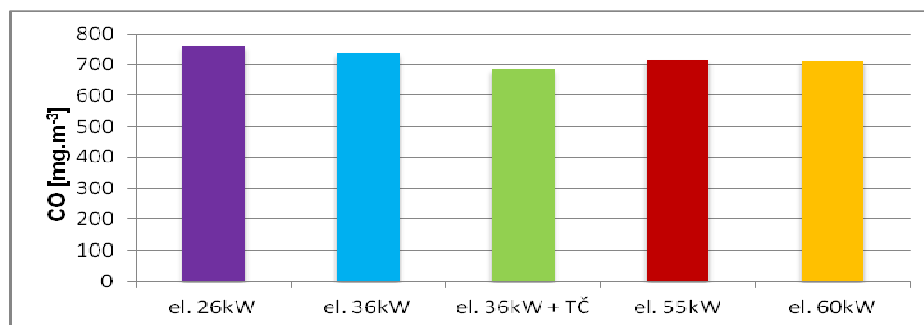

Fig. 4. Emissions CO produced at various operating modes

Gas emissions behind exhaust heat exchanger of combined cogeneration unit at constant engine speed have been measured. Fig. 4., Fig.5. and Fig. 6. in successive steps show a comparison of the emissions of CO, NO_x and CO_2 at various operating modes. They are characterized by the value of active power of electric generator and connection or disconnection of the heat pump. The heat pump was connected only in the third case.
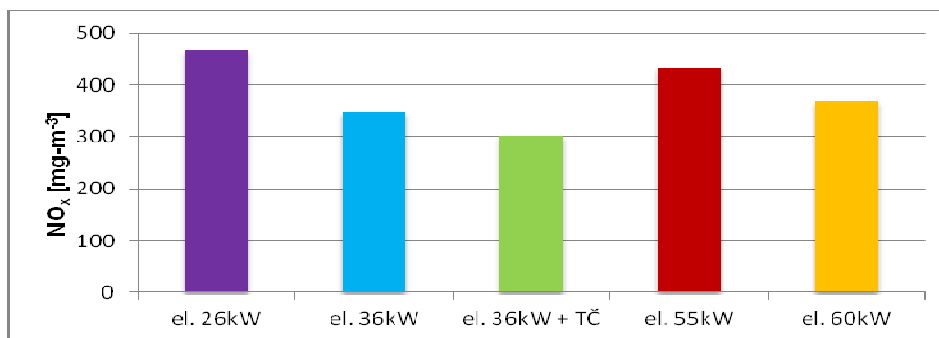
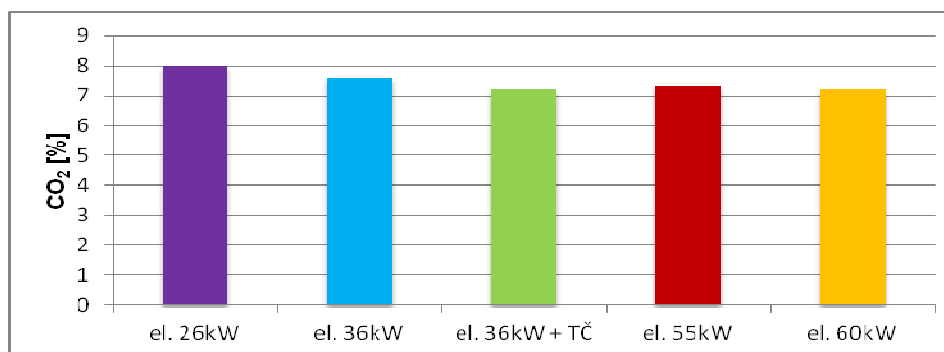**Fig. 5.** Emissions NO_x produced at various operating modes

Fig. 6. Emissions CO_2 produced at various operating modes

3. Conclusion

The use of gas combustion engines has both economic and environmental benefits. Installation of gas combustion engines into cogeneration units deployed in the technological process will increase significantly the use of primary energy contained in the fuel. However, adaptation of the engine to the technological process results in the engine working in the transient mode. This has the effect of increasing the burden on the environment because the engine does not work in steady mode.

Acknowledgement

References

[1] HLAVŇA, V. – KADÁK, M. – MRUK, A. *NOx and extremely low temperatures of charging*. In: Journal of KONES -Powertrain and transport, Vol.17, No. 3, Warsaw 2010, ISSN 1231-4005.

[2] KOVALČÍK, A. – TOPORCER, E. *Optimization of a nonconventional engine evaporator*. In: Journal of KONES - Powertrain and Transport – 2010 Vol.17, No. 2 2010, Warsaw 2010, ISSN 1231-4005.

[3] HLAVŇA, V. – LABUDA, R. *A non-conventional energetic circuit - measurement and control*, Advances in automotive engineering, ISBN 978-80-552-0255-6.

Implementiation new Technologies in Process of Wheelsets Repair in the ŽOS Trnava, a.s. Workshop

[*]Marek Tylka, Peter Zvolenský
[*]University of Žilina, Mechanical Engineering Faculty , Department of Transport and Handling Technology, Univerzitna 2, 01026 Žilina, Slovakia, marek.tylka@zos.sk, peter.zvolensky@fstroj.uniza.sk

Abstract. This report is repair of wheelsets in ZOS Trnava, a.s. and implementation new technologies in process of wheelsets repair in the company (replacement parts wheelset, nondestructive testing, running profile). They say of new devices for wheelset.

Keywords: wheelsets, repair, control, nondestructive testing, devices

1. Repair of wheelsets in ŽOS Trnava, a.s.

ŽOS Trnava, a.s. as one of the leading repairer of rail cars in Central Europe is trying to keep pace in technological equipment. This also applies to the repair of wheelsets. Illustrated by the fact that in 2010 were in this company repaired through 24.000 pieces wheelsets. Because wheelsets in ŽOS are repaired for several railways in the EU, high quality of repair is required. The company presently owns licenses of wheelsets repair for railways:

➢ Railway Company Slovakia, (ZSSK),
➢ Cargo Slovakia, as (ZS Cargo),
➢ Czech Railways (CD),
➢ Deutsche Bahn (DB),
➢ The Austrian Federal Railways (ÖBB),
➢ Association of private owners – VPI,
➢ Swiss Railways (AAE).

1.1. A technology wheelset repair

A technology wheelset repair provides:
➢ entry control of wheelset
➢ removal of bearings boxes, bearings and bearing rings
➢ destructive inspection
➢ exchange of worn or damaged parts
➢ mounting of bearing boxes, bearings and bearing rings
➢ output control

Entry control – control of the wheelset at the entrance is done according to valid regulations:

    a) tread area (running profile), monitors the height, width and slope of the flange, damage on the tread area, the overall shape of the tread, or cracks

    b) measures, each type of wheelset has its own wed measures (diameters). If the diameter of the wheels is not suitable, monoblocs must be replaced

    c) Brake discs, monitoring its overall thickness, worn, cracks on active area.

Removing of the bearing boxes – after an entry inspection, the wheelset is moved to repair line, where the greasy is cleaned. As the first bearing boxes are dismounted together with the bearings. After their removal and the greasy cleaning a visual inspection is done. Damaged parts are removed.

Destructive inspection, so. NDT (nondestructive testing) – after removing the bearing rings starts prescribed wheelset–destructive testing. Each railway has its own rules concerning repair of wheelsets, and therefore the scope of these tests is set according to the railway company to the wheelset belongs.

On the basis of the increasing levels requirements of NDT inspections for wheelsets ŽOS Trnava, as bought device that automatically performs non-destructive inspection of the whole wheelset axle (Fig. 1).
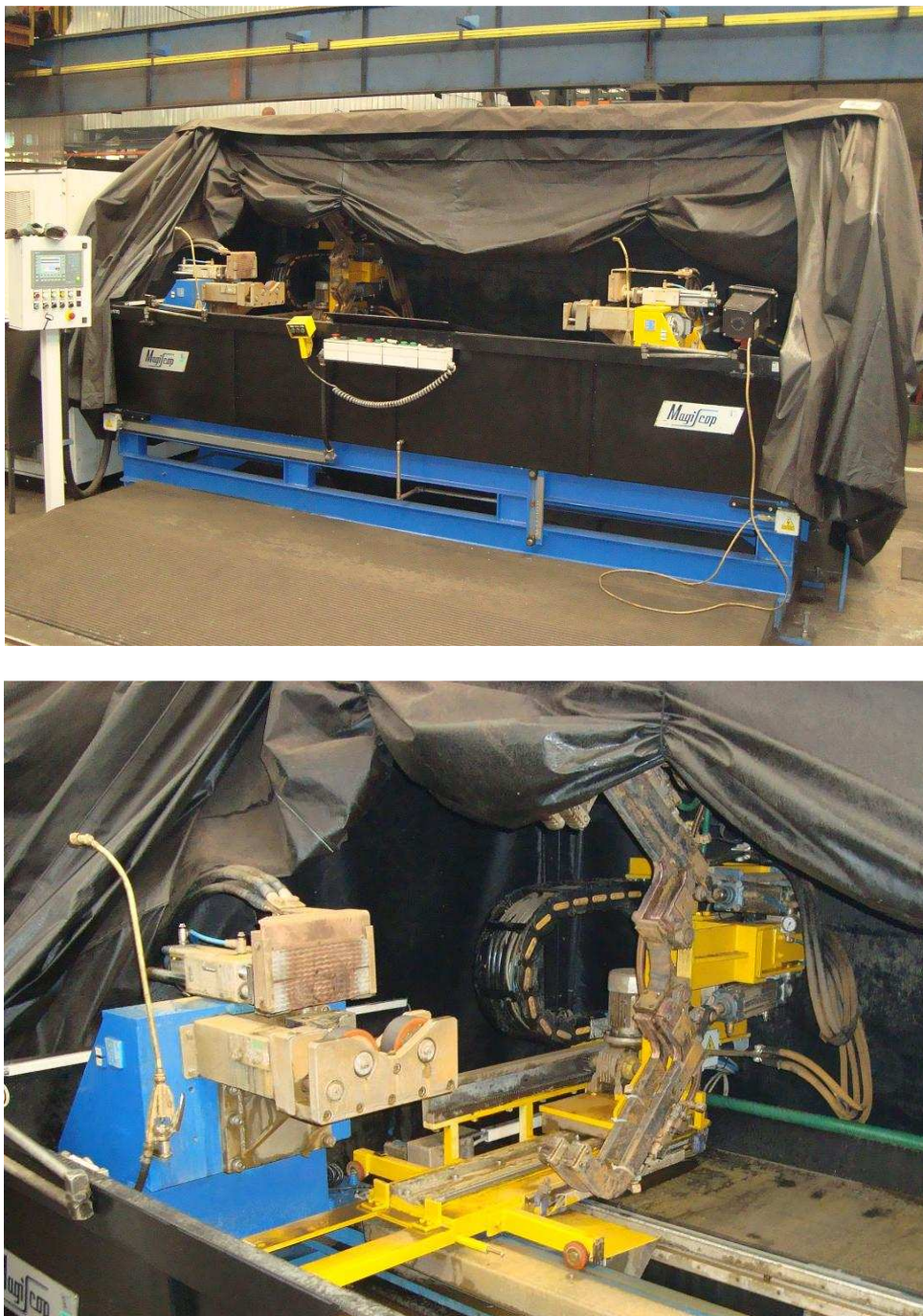

Fig. 1. The device for defectoscopy of the wheelset axle

Exchange of worn, or damaged parts – the extent of replacement parts wheelset is found during an entry inspection, as well as the results of NDT testing. If the measurements and tests revealed not any needs to replace any part of the wheelset, the wheelset is repaired mostly just turning the running profile on a wheel lathe (Fig. 2). It may also occur in case that the measurements found only over "sharpness" wheel flanges. In this case, some railways allow surfacing the flange (Fig. 3) and then turning the running profile.

If parts are necessary to replace, wheelset moves to the pressing machine (Fig. 4), which is carried out removing the wheels, if necessary brake discs. After this removal is definitely set, if the axle will be replaced. All appropriate parts are exchanged for new ones (are pressed) and wheelset moves to the wheel lathe, which makes turning the driving wheel profile.

Fig. 2. Device for turning of the driving profile and the brake discs

Fig. 3. Device for surfacing of wheelset wheel flanges

Installation of bearing boxes, bearings and bearing rings – the first are the bearings heat pressed on the axle, then also the bearings are heat pressed in the bearing box and finally the bearing box is mounted on the axle. In some cases, after the installation the boxes welded joints are checked on the bearing box for crack detection (especially in bearing boxes, where the mangan plates are welded).

Output control – after mounting the bearing boxes the exit control of the wheelset is done where are measures the important dimensions of wheelset (distance between monoblocs, shape and thickness of danges, the diameter of monoblocs and others). If everything is in permissible tolerance, the wheelset is assigned an identify tape and is transported to the workplace, where is mounted into the bogie.

Device for cracks defectoscopy axle wheelsets. It is a device type from MAGISKOP CEM 2500/350x350 from CGM company (Italy). That device was developed specifically for the company ŽOS Trnava, a.s as a prototype. It has the following parameters:
- ➢ capable of detecting surface and subsurface cracks to a deep of 2 mm
- ➢ works on the principle of magnetic watering methods
- ➢ used fluorescent powder is diluted with water (recommended type PAD 31-73/50)
- ➢ device allows the detection of cracks in horizontal and in vertical direction.
- ➢ allows defectoscopy axle in three modes:

  1. only axle (without monoblocs, brake discs, and bearing boxes and rings),
  2. axle with disk brakes (no bearings boxes and rings),
  3. axle with monobloc and brake discs (no bearings boxes and circles).

1.2. New devices for wheelset

Other new devices for wheelset are:
1. pressing machine for pressing the brake discs and monobloc (Fig. 4),
2. lathe for turning axle (Fig. 5),
3. lathe for turning the hub of monobloc "Carousel" (Fig. 6).

A hydraulic press CDRA 500 (Fig. 4) is a device for pressing and unpressing brake discs and monobloc. Its technical parameters are:
- ➢ nominal force – 5.000 kN,
- ➢ maximum stroke - 700 mm,
- ➢ working pressure - 320/80 bar,
- ➢ working speed – 0,5-3 mm/s,
- ➢ maximum length wheelset – 2.650 mm,
- ➢ maximum diameter tread wheelset – 1.250 mm,
- ➢ max. wheelset weight – 3.500 kg,
- ➢ working liquid - mineral hydraulic oil VG46 class.

Peak lathe SUA 80 NUMERIC / 3500 (Fig. 5) is used for turning axle wheelset, namely turning "seats" for the pressing brake discs and monobloc. The parameters are as follows:
- ➢ distance between centers – 3.500 mm,
- ➢ max. turning path length – 3.350 mm,
- ➢ max. workpiece weight (without support / with support) - 6.000/8.000 kg,
- ➢ max. torque – 8,0 kN,
- ➢ spindle speed - 5 to 1250 min^{-1},
- ➢ max. feed rate - 4 m / min^{-1}.

Lathe VL 200 ATC + C (Fig. 6) allows turning hubs (holes) monoblocks or brake discs before they are pressed on the axle. Technical parameters are as follows:
- ➢ max. outer diameter turning – 1.350 mm,

- ➢ max. diameter of workpiece – 1.600 mm,
- ➢ max. workpiece weight – 5.000 kg,
- ➢ working feed 1-2000 mm.min^{-1}.

Fig. 4. The pressing maschine for brake discs and monoblocks pressing

Fig. 5. An axle lathe

Fig. 6. The Lathe for turning hubs (holes) of monoblocks

2. Conclusion

All described procedures and machinery equipments contribute, that the repair of wheelsets in ŽOS Trnava, a.s. is on high level, thereby offering customers in the future a required quality.

References

[1] details of ZOS Trnava, a.s.
[2] Photos of author

Modeling of Multiaxial State of Stress to Determine the Fatigue Lifetime of Structural Materials during Cyclic Loading

[*]Milan Uhríčik, Peter Kopas, Ondrej Števka

[*]University of Žilina, Faculty of Mechanical Engineering, Department of Applied Mechanics, Univerzitná 1, 010 26 Žilina, Slovakia, {milan.uhricik, peter.kopas, ondrej.stevka}@fstroj.uniza.sk

Abstract. This article deals with determining of fatigue lifetime of structural materials during by multiaxial cyclic loading. The theoretical part deals with the fatigue and with the criterions for evaluation of multiaxial fatigue lifetime. The experimental part deals with modeling of combined bending - torsion loading and determining the number of cycles to fracture in region low-cycle and high-cycle fatigue and also during of loading with the sinusoidal wave form under in phase $\varphi = 0°$.

Keywords: Multiaxial fatigue, stress and strain, sinusoidal cyclic loading, structural material.

1. Introduction

Fatigue failures in metallic structures are a well-known technical problem. In a specimen subjected to a cyclic load, a fatigue crack nucleus can be initiated on a microscopically small scale, followed by crack grows to a macroscopic size, and finally to specimen failure in the last cycle of the fatigue life. Understanding of the fatigue mechanism is essential for considering various technical conditions which affect fatigue life and fatigue crack growth, such as the material surface quality, residual stress, and environmental influence. This knowledge is essential for the analysis of fatigue properties of an engineering structure [1, 2].

Fatigue under combined loading is a complex problem. A rational approach might be considered again for fatigue crack nucleation at the material surface [3]. The state of stress at the surface is two-dimensional because the third principal stress perpendicular to the material surface is zero [4]. Another relatively simple combination of different loads is offered by an axle loaded under combined bending and torsion. This loading combination was tested in our and also in many others experiments [5, 6, 7]. In spite of this fact, fatigue mechanisms are still not fully understood. This is partly due to the complex geometrical shapes and also complex loadings of engineering components and structures which result in multiaxial cyclic stress-strain states rather than uniaxial.

2. Criteria

Criteria valid for the fatigue lifetime calculation can be classified in three different categories: strain based methods, strain-stress based methods and energy based approaches.

Brown and Miller [8] observed that the fatigue life prediction could be performed by considering the strain components normal and tangential to the crack initiation plane. Moreover, the multiaxial fatigue damage depends on the crack growth direction. Different criteria are required if the crack grows on the component surface or inside the material. In the first case they proposed a relationship based on a combined use of a critical plane approach and a modified Manson-Coffin equation, where the critical plane is the one of maximum shear strain amplitude. Criterion, which was created, has the following form:

$$\frac{\Delta\gamma_{\max}}{2} + S \times \Delta\varepsilon_n = A \times \frac{\sigma'_f - 2\sigma_{n,mean}}{E} \times \left(2 \times N_f\right)^b + B \times \varepsilon'_f \times \left(2 \times N_f\right)^c \tag{1}$$

Fatemi and Socie [9] observed that the Brown and Miller's idea could be successfully employed even by using the maximum stress normal to the critical plane, because the growth rate mainly depends on the stress component normal to the fatigue crack. Starting from this assumption, he proposed two different formulations according to the crack growth mechanism: when the crack propagation is mainly MODE I dominated, then the critical plane is the one that experiences the maximum normal stress amplitude and the fatigue lifetime can be calculated by means of the uniaxial Manson-Coffin curve; on the other hand, when the growth is mainly MODE II governed, the critical plane is that of maximum shear stress amplitude and the fatigue life can be estimated by using the torsion Manson-Coffin curve [9]. Criterion has the following form:

$$\frac{\Delta\gamma}{2}\times\left(1+k\times\frac{\sigma_{n,mean}}{\sigma_y}\right)=\frac{\tau'_f}{G}\times\left(2\times N_f\right)^{b_\gamma}+\gamma'_f\times\left(2\times N_f\right)^{c_\gamma} \qquad (2)$$

Liu created a virtual model of the deformation energy, which is a generalization of the axial energy on the basis of prediction of fatigue life. Criterion has the following form:

$$\Delta W = 4\times\sigma'_f\times\varepsilon'_f\times\left(2\times N_f\right)^{b+c}+\frac{4\times\sigma'^2_f}{E}\times\left(2\times N_f\right)^{2b} \qquad (3)$$

Smith, Watson and Topper (SWT) created a parameter for multiaxial load, which is based on the main deformation range $\Delta\varepsilon_1$ and maximum stress $\sigma_{n,max}$ to the main plane. Criterion has the following form:

$$\sigma_{n,mean}\times\frac{\Delta\varepsilon_1}{2}=\frac{\sigma'^2_f}{E}\times\left(2\times N_f\right)^{2b}+\sigma'_f\times\varepsilon'_f\times\left(2\times N_f\right)^{b+c} \qquad (4)$$

Goodman used main stresses for evaluating the fatigue under multiaxial loading. Normal stresses are calculated for each plane and their ranges are used for calculation of fatigue lifetime. This is a less conservative criteria based on the material ultimate strength yield point Sut. To establish the factor of safety relative to the Goodman´s criteria can be written as:

$$\frac{K_f\times\sigma_{amp}}{S_e}+\frac{\sigma mean}{S_{ut}}=\frac{1}{f_f} \qquad (5)$$

Findley criterion is the first critical plane criterion. He suggested that the normal stress σ_n, acting on a shear plane might have a different linear influence on the allowable alternating shear stress, $\Delta\tau/2$. Criterion has the following form:

$$\frac{\Delta\tau}{2}+k\times\sigma_n=\tau'_f\times\left(N_f\right)^b \qquad (6)$$

Sines's criteria are very much alike, utilizing the amplitude of second invariant of stress tensor deviator (which corresponds to the von Mises stress) as the basis. His resulting failure criterion can be expressed as:

$$\frac{\Delta\tau_{oct}}{2}+\alpha\times\left(+\times\sigma_h^{mean}\right)=\tau'_f\times\left(N_f\right)^b \qquad (7)$$

Minimum circumscribed ellipse (MCE) – The origin of this method goes out from minimum circumscribed circle method (MCCM). This method was first presented by Papadopoulos. Its major feature is its explicitness in determination of mean shear stress. The contrast in comparison with MCCM is clear – it should offer a better solution of phase shift effect problems. Nevertheless, as regards the definition of mean shear stress, it does not offer any new approach. For proportional loading this will always be a straight line and for non-proportional loading histories will have some complex shape.

$$\tau_a=\sqrt{R_A^2+R_B^2} \qquad (8)$$

Where γ_f' is the fatigue ductility coefficient in torsion; ε_f' is the fatigue ductility coefficient; σ_f' is the fatigue strength coefficient; σ_h^{mean} is the mean hydrostatic stress; σ_n is the normal stress; $\sigma_{n,max}$

is the maximum stress; $\sigma_{n,mean}$ is the mean stress; σ_y is the stress in the direction of the axis y; τ_a is the equivalent shear stress; τ_f' is the fatigue strength coefficient in torsion; Δy_{max} is the maximum shear strain range; $\Delta\varepsilon_1$ is the principal strain range; $\Delta\varepsilon_n$ is the normal strain range; $\Delta\tau/2$ is the alternating shear stress; $\Delta\tau_{oct}$ is the octahedral shear stress; ΔW is the virtual strain energy; N_f is the number of cycles to fracture; S_e is the modified fatigue strength; S_{ut} is the ultimate tensile strength; f_f is the factor of safety applicable the fatigue; E is the elasticity modulus in tension; G is the elasticity modulus in torsion; R_A is the major axis of the ellipse; R_B is the maximum distance of stress point; b is the fatigue strength exponent; b_γ is the fatigue strength exponent in torsion; c is the fatigue ductility exponent; c_γ is the fatigue ductility exponent in torsion; A, B, S, k, α are material parameters.

3. Numerical calculations and results

In ANSYS software was created the model of the test bar. The real geometry of this component is shown in Fig. 1. The rod bar had a circular shape with a defined section, in which was expected an increased concentration of stress and creation a fatigue fracture. The ends of this model were loaded by reversed bending moment on the one side and by reversed torsion moment on the opposite site. The values of presented stresses and strains in the middle of the rod radius were taken from computational analysis using finite element method. We used the following parameters in finite element model: used material was aluminum alloy EN AW 2007.T3 (AlCu4PbMg) with Young's modulus $E = 0,817.10^{11}$ Pa, Poisson number $\mu = 0,3$ and with the strength limit $R_m = 491$ MPa.

Obtained values of the stresses from finite element analysis were next computational analyzed using Fatigue Calculator software. This is a program which can quickly calculate fatigue lifetime of selected material. After starting the calculation, Fatigue Calculator displayed the number of cycles to failure for different models of damage. In our calculation we considered with all multiaxial criteria described above which can be applied to low-cycle and also to high-cycle fatigue region. The computational fatigue tests were performed under in-phase cyclic loading with the zero mean value. All the tests were performed under controlled bending and torsion moments. Frequency of each analysis was equal to 50 Hz.
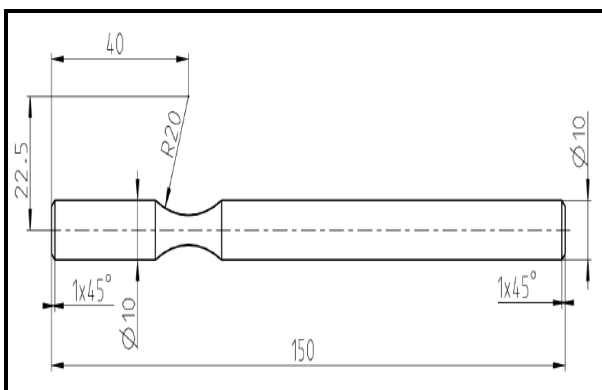
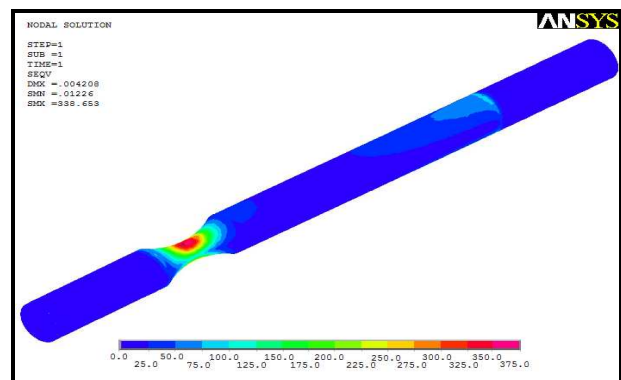

Fig. 1. Geometry of the test bar

Fig. 2. Result of FEM analysis

From computational analysis can be seen that the area with greatest concentration of stresses or eventually the place with the higher deformation was localized in the middle of the rod radius (see Fig. 2).

The obtained results can be discussed i.e. from the point of view of multiaxial criteria applied on low-cycle and high-cycle region of fatigue loading. Generally, we can say, that stress amplitude continually decreasing with number of cycles to failure increasing after conventional limit of cycles number ($N_C = 2.10^6$ cycles to $N_C = 1.10^7$ cycles) used to fatigue limit σ_C determination.
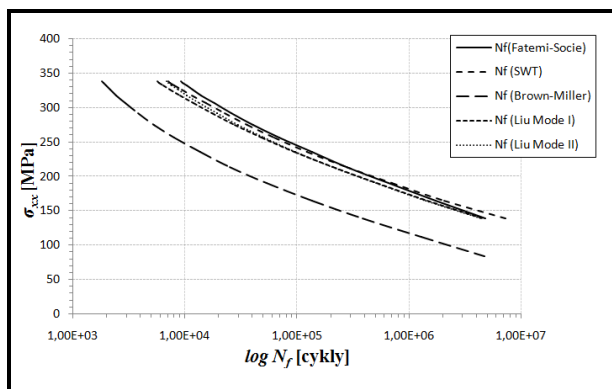
Fig. 3. Wöhler curves for multiaxial low-cycle fatigue with phase shift 0°, AW 2007.T3
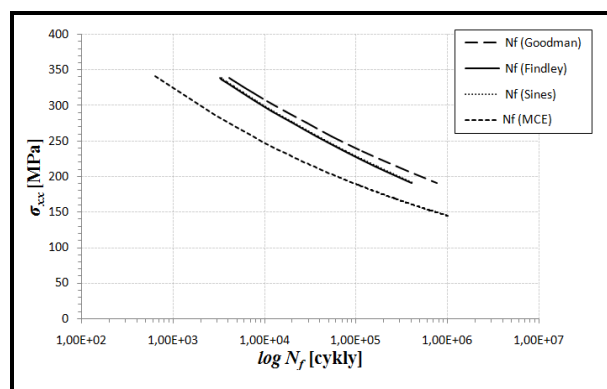
Fig. 4. Wöhler curves for multiaxial high-cycle fatigue with phase shift 0°, AW 2007.T3

4. Conclusion

All multiaxial models applied to fatigue lifetime calculation of aluminum alloy EN AW 2007.T3 increases with decreasing stress amplitude continuously in the cycles of number region. In the region low-cycle fatigue, Wöhler curves have shown a good agreement of progress line with Fatemi-Socie, SWT and Liu damage models. For Brown-Miller model, it was also observed significant decrease of stress amplitude with increasing number of cycles to failure but the fatigue endurance values in comparison with reference number of cycles were markedly lower as for Fatemi-Socie, SWT and Liu damage multiaxial models.

In the region high-cycles fatigue, Wöhler curves have shown a good agreement of progress line with Goodman, Findley and Sines damage models too. For MCE model, it was also observed significant decrease of stress amplitude with increasing number of cycles to failure. Fatigue endurance values in comparison with reference number of cycles were lower too.

Acknowledgement

References

[1] BATHIAS, C. *Fatigue in the very high cycle regime*. Vienna, Austria 2001.

[2] BOKŮVKA, O. – NICOLETTO, G. – KUNZ, L. – PALČEK, P. – CHALUPOVÁ, M. *Low & high frequency fatigue testing*. CETRA and Univerzity of Žilina, Žilina 2002.

[3] NOVÝ, F. – KOPAS, P. – BOKŮVKA, O. – CHALUPOVÁ, M. *Vplyv zlievarenských chýb na únavovú životnosť perliticko – feritickej LGG*. Materiálové inžinierstvo, 3, 10, SK, 2003.

[4] BANNANTINE, J. A. – SOCIE, D. F. *A multiaxial fatigue life estimation technique*. In: Advances in Fatigue Lifetime Predictive Techniques, ASTM STP 1122. Eds: M. R. Mitchell a R. W. Landgraf. Philadelphia, American Society for Testing and Materials 1992, pp. 249-275.

[5] LEGER, J., *Fatigue life testing of crane drive shafts under crane-typical torsional and rotary bending loads*. Schenck Hydropuls Mag., Issue 1/89 (1989), pp. 8–11.

[6] GOUGH, H.J. – POLLARD, H.V. *The strength of metals under combined alternating stresses*. Proc. Inst. Mech. Engrs, Vol. 131 (1935), pp. 3–103.

[7] GOUGH, H.J. – POLLARD, H.V. *Some experiments of the resistance of metals to fatigue under combined stresses*. Min. of Supply, Aero Res. Council, RSM 2522, Part I (1951).

[8] BROWN, M. W. – MILLER, K. J. *A theory for fatigue under multiaxial stress-strain conditions*. In: Proc. Inst. Mech. Engrs, Vol. 187 (1973), pp. 745-755.

[9] FATEMI, A. – SOCIE, D. F. *A critical plane approach to multiaxial fatigue damage including out-of-phase loading*. Fatigue Fract. Engng. Mater. Struct. 11 3 (1988), pp. 149-166.

Proposal and Realization the System for Retrieving Low-potential Ground Heat with the Heat Pipe System

[*]Martin Vantúch, Michael Jakubský, Milan Malcho
* University of Žilina, Faculty of Mechanical Engineering, Department of Power Engineering,
Univerzitná 2, 01026 Žilina, Slovakia, {Martin.Vantuch, Michal.Jakubsky, Milan.Malcho}@fstroj.uniza.sk

Abstract. This paper describes execution of a project for retrieving low - potential ground heat with heat pipe system and his comparison to conventionally being exploited methods retrieving heat off the ground. Be along described general procedure deepening borehole and feeding earth probes. Further paper induct preparation entire devices for measuring thermodynamic process of connection with transport low - potential heat. A part of single systems design is too analysis by and selection convenient working substance of heat pipes waste going temperature potential.

Keywords: low potential heat, heat exchanger, geothermal heat, heat pipe.

1. Introduction

Development and introduction of new energic technology is very important for safeness delivery, tenability and competitiveness energic sectors. Research pertinent to energetics considerably contribute for energic effectiveness (e.g . in the engine cars) and to diversification of energy through piggybacking on revivable source of power. Balk renewable energy sources range too low - potentially heat contained in the surface, which is situated more deeply how neutral zone (10 – 20 m away from the levels of surface earth). Heat is possible gaining several in ways. One of them is the system vertical heat exchangers (earth probe). System with vertical heat - exchanger does not require big jerked - in - fillings soil and independent away from the intensity sunny radiation, which impinges topsides earth. Vertical heat - exchangers effectively work virtually in all the geological environs, besides soils with low thermic conductivity (for example they are in dry sand or dry gravel).

In the surrounding ZU was deepening two borehole 150m depths for retrieving low - potential heat on principle vertical exchangers through the medium:

- forced circulation heat carrier substance (with brine circulations),
- circulation heat carrier substance (heat pipes technology) on thermosyphon principle.

2. Simulation measuring for realization

Outside the single realization devices for retrieving heat in the laboratory condition was simulating given project in the reduced dimensions. There was considered machined simulation bore pro forced circulation working media and for informal circulation (heat pipe). Both of them bore simulate effective strength conditions in the earth and all of thermodynamic processes. For transport heat has been waste heat pump type of earth/water in like manner, how be those by the real condition.

3. Implementation borehole for low-potencial heat transport

Laboratory results from measuring on simulation furnished, who has been machined for laboratory measurement, was supply information for the next progress realization given devices in the real condition.

Two bore by over 150 meters depth were they concave drilling furnished for digging geothermal caprice at distance approximately 25 meters apart, that to avoid mutual thermic influenced. By the realization propeller with forced circulation with brine media was treated the same way as is used to heat the pump type of ground-water. This means U-type pipe PE 100 RC is embedded in the soil massif with special sensors temperature. Sensors were attached to the pipe axis grouting duct designated for supply of bentonite to bottom of the borehole. Liquid bentonite is then filled free space and air bubbles in the borehole from the bottom up to the surface of the tubes. Contact surface of the tubes will provide more efficient heat transfer to vertical heat exchangers. Temperature sensors were positioned to detect high temperatures accelerate changes in four different depth of the borehole and in the range 150, 100, 50 meters and 2 m close to the ground surface. There were used the thermo couples type K (NiCr-Ni) series TFAU. There being it is an thermocouple wires, it should provide safe berth of the measurement ends so as not to damage when applied pipes set into the ground. For this reason, these thermocouples were attached to removal ribbons of short sections of pipe for injection, which is held in the middle of the piping system of PE 100 RC geothermal probes (Fig. 1).
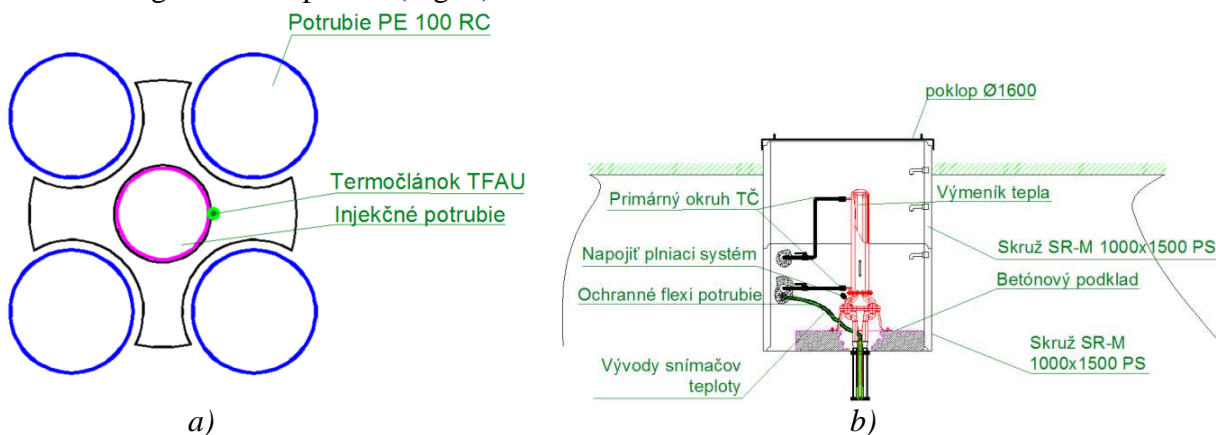

Fig. 1. a) - The cut of the earth's probe and the mounting of temperature sensor (thermocouple), b) - the location of the condensing heat exchanger of the HP into a concrete pit.

Thermocouples are so protected pipe to collect heat. Heat pipe of the second hole is made in the same way, but on the surface of the borehole will be equipped with specially designed heat exchanger for heat pipes of this type. Gravitational heat pipe working on the principle of phase transition working substance of CO_2 will work under high pressure because, at $0\,°$ C is saturated vapor pressure of this substance around 35 bar. It is 5 times more than in ammonia NH_3 (R717), which is also part of the experiment using heat pipe. It is therefore necessary to ensure greater emphasis in terms of tightness and pressure resistance. Thermocouple sensors are located just to the injection pipe but in smaller distances, it is every 25 meters.

This method of obtaining low-potential heat by HP is a method in the research stage. It is therefore necessary to have a detailed overview of all the thermodynamic processes in its operation. Stainless steel heat exchanger for HP will be planted about 1.5 meters in the ground in sewage shaft on the concrete surface.
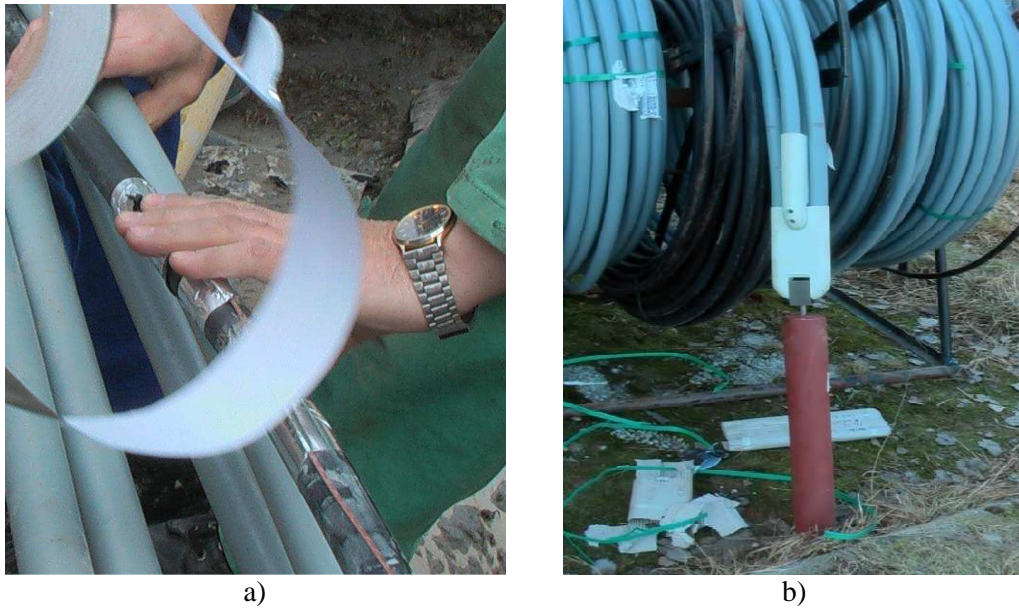
Fig. 2. a) - Strengthening of thermocouples to injection pipe, b) - Earth Probe PE 100 RC.

Piping system from individual borehole will be conducted underground to laboratory, where heat dissipation will be realized by two heat pump ground-water on performance 2x8kW. Parallel connection of individual probe will allow us to measure individually. Primary brine heat pump circuit is connected to the borehole with forced circulation and heat exchanger with heat pipe. On this and the secondary circuit will be measured thermal power measuring set, which will be installed in the premises of laboratory. Excess heat will be fed into the cooling circuit. If necessary, heat will be used as a supportive source of heat to heating system of the University of Žilina and into storage tanks for further measurements associated with accumulation of heat.

The aim of the device will draw heat from the soil massif conventionally employed method of forced circulation and its comparison with the experimental method without forced circulation of the working substance. This method has advantage self-activity circulation without additional energy. Costs associated with the operation of this system, which uses additional energy for pumping circulating working substance in the pipe is that fall on power circulator.

4. Filling system

Heat exchanger, which will be mounted on the condensing heat pipe has two holes designed for the implementation of working substance. Here is accompanied by filling furnished consisting of pumps, cylinder with working substance and fittings designed for high pressure systems. Since the use of CO_2 and NH_3 medium is necessary to ensure a perfect tightness and security of the bottling plant and process performance. Before the actual performance the heat pipe will be subjected to vacuum the desired pressure (Pa). Then opens the supply performance of CO_2 (NH_3) and working medium is pressurized to the desired pressure. Because of the high pressure in the pipe will be used in carrying out (discharge) special valves. Media will vary according to the needs of measurement because of the comparison features of each. When using the working media will go after CO_2 pressure to 40 bar, so it will be necessary to ensure the tightness of connections and the resilience of the system to applied pressure. The whole system goes into operation before relevant safety and environmental protection.

Fig. 3. Sinking geothermal borehole.

5. Conclusion

After done of all realization act will realize measuring, whose aim will be comparison methods retrieving low - potential heat through the medium thermic tube with method of forced circulation working substance thermic pump earth/water type. Measurements give us information about the effectiveness and reliability of such system and energy balance compared with commonly used methods of obtaining heat. The results can be very useful for the further use of low-potential heat of the earth for the purpose of heating and hot water.

Acknowledgement

References

[1] PETRÁŠ, D. *Low temperature heating and renewable energy*. Bratislava: Jaga, 2009. 216 s. ISBN 80-07-00031-5.

[2] LENHARD R. – JAKUBSKÝ, M. *Device for simulation of transfer low potential geothermal heat in laboratory conditions*, Experimental fluid mechanics 2010, Technical Univerzity in Liberec 2010, ISBN *978-80-7372-670-6*.

[3] ČAJA, A. – NEMEC, P. – MALCHO, M. *The dependence of quantum and filling type to heat transport of gravity heat pipe*, Experimental fluid mechanics 2010, year 4, rok 2010, Technical Univerzity in Liberec 2010, str.98, ISBN 978-80-7372-670-6.

Virtual Prototyping of Mechatronic Systems

[*]Grzegorz Witkowski, Leszek Płonecki
[*]Kielce University of Technology, Department of Mechatronics and Machine Building,
Tysiąclecia Państwa Polskiego 7, 25-314 Kielce, Poland, witkow.grzeg@gmail.com, plonecki@tu.kielce.pl

Abstract. The paper discusses modern methods of rapid prototyping of mechatronic systems. Article raises the possibility of integration of modern engineering package for a comprehensive synthesis and analysis of the system. Paper also illustrates the concept and the real implementation of selected methods of hydraulic equipment excavator bucket.

Keywords: automation, robotics, prototyping, control, excavator.

1. Introduction

Engineers and scientists use virtual prototyping to design, optimize, validate, and visualize their products digitally and evaluate different design concepts before incurring the cost of physical prototypes. Mechanical and control engineers can collaborate and assess the operation of moving parts. Virtual prototyping allows to visualize realistic machine operations, estimate the cycle time throughput, determine whether the product will fail, and glean important information about the dynamic behavior of the system. Rapid and virtual prototyping are fundamental tools in the design, development and manufacturing of a different products. It involves using CAD systems and some simulation software to validate a design before making a physical mechatronic system [1]. This is done by creating 3D computer generated geometrical parts and either combining them into an assembly and testing different mechanical motions, fit and function or just aesthetic appeal. The assembly or individual parts could be opened in CAE software to simulate the behavior of the product in the real world. Virtual prototyping entails integration of multi-domain dynamic simulation in the design process, in order to reproduce and analyze the effects of design choices on the overall performance.

Main areas of virtual prototyping and simulation of control can be divided into following domains:
- mechanical prototyping,
- motion analysis,
- control system simulation,
- CAE analysis.

Some techniques for virtual prototyping can also be used to determine the behavior of existing mechatronic systems. Motion analysis can help to explore, how the system will works without the physical movement of any part of the system. It is possible to simulate any equipment like drives or sensors. Control engineers can predict behavior of mechanic system by applying virtual drives, actuators [1] and virtual drivers same as in reality.

The remainder of the paper presents a virtual prototyping of existing hydraulic equipment excavator bucket [2]. The method includes mechanical prototyping and control system prototyping, by creating CAD models, motion analysis and applying virtual control equipment.

2. Mechanical prototyping

Geometrical model was created in the SolidWorks environment. SolidWorks is a Parasolid-based solid modeler [3], and utilizes a parametric feature- based approach to create models and assemblies. This software integrates with each of the mechanical characteristics of the CAD system, project controls, management, technical documentation, design communication in one, easy to use package. Enables the creation of an entire project from the initial assumptions for its advanced visualization, without having to use other software. Particularly useful was a motion module to examine the dynamic volumes, such as displacement, velocity and acceleration, while controlling collision of object elements.

Work usually starts with a two dimensional sketch. The sketch consists of geometry such as points, lines, arcs, conics and splines [3]. Dimensions are added to the sketch to define the size and location of the geometry. Relations are used to define attributes such as tangency, parallelism, perpendicularity, and concentricity. Then dimensions are applied to define the size and location. SolidWorks allows users to do all the testing and simulating virtually. The virtual prototype behaves as it would in the real world because users input all the characteristic of the real thing. Software offers another tremendously beneficial feature allowing users to put together components – creating a virtual assembly. Each piece is individually designed and then one can see how parts interact together. Tests can be run to make sure components assembly properly and don't interfere with each other as they move.
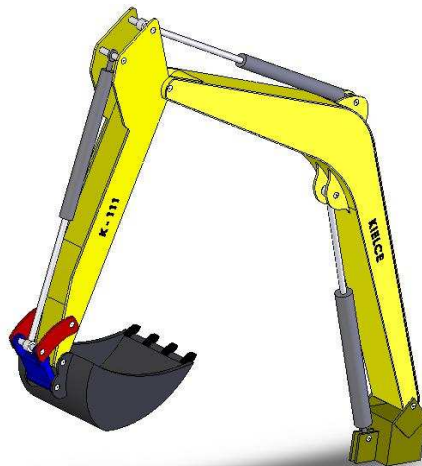

Fig. 1. Geometric model of a hydraulic excavator bucket

3. Motion analysis

Motion simulation was performed in SolidWorks environment using the Motion module. Each of the three actuators have been given a linear movement along their axis. It was found lower and upper markers defining the minimum and maximum hanging of rod. As a result of analysis of linear motion of actuators, it is possible to set minimum and maximum rotation angles between the various constituents. Motion study also allowed the determination of the critical position of the object and possible configurations giving rise to a conflict of accessories.
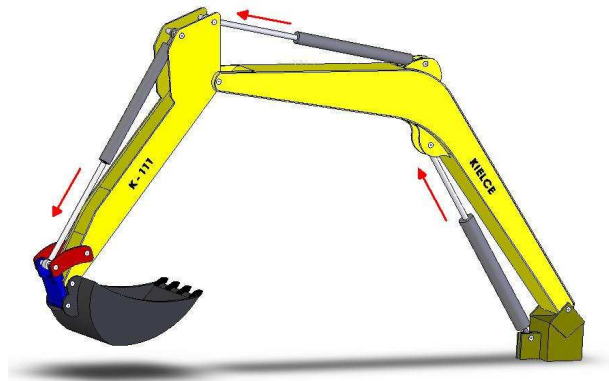
Fig. 2. Ggeometric model of a hydraulic excavator bucket during motion analysis

4. Control system simulation

LabVIEW is a graphical programming environment used by millions of engineers and scientists to develop sophisticated measurement, test, and control systems using intuitive graphical icons and wires that resemble a flowchart. It offers unrivaled integration with thousands of hardware devices and provides hundreds of built-in libraries for advanced analysis and data visualization – all for creating virtual instrumentation. LabVIEW programs are called virtual instruments [4]. Each program has three components: a block diagram, a front panel and a connector panel. The last is used to represent the program in the block diagrams of other. Controls and indicators on the front panel allow an operator to input data into or extract data from a running virtual instrument. However, the front panel can also serve as a programmatic interface. Thus a virtual instrument can either be run as a program, with the front panel serving as a user interface or when dropped as a node onto the block diagram, the front panel defines the inputs and outputs for the given node through the connector pane. This implies each program can be easily tested before being embedded as a subroutine into a larger program. By integrating engineering environments LabVIEW and SolidWorks, a procedure for a virtual model of the positioning actuators was developed.
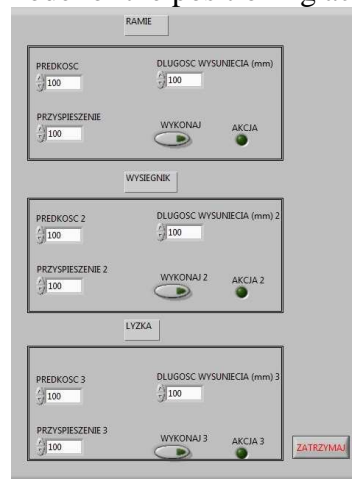

Fig. 3. Control system front panel.

Designed application, gives a possibility to control each cylinder individually or all simultaneously. The action consists of choosing the parameters such as the distance, velocity and acceleration. Motion parameters are transmitted to the SolidWorks package, where the motion simulation takes place. Depending on the motion parameters, the complexity of the object and computing power, the simulation can be run in real time mode or close enough. The advantage of this method is possibility to check displacement, velocity and acceleration of any specified point on the object.
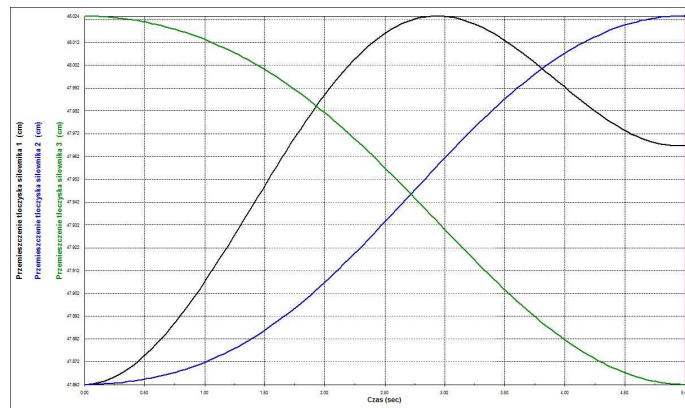
Fig. 4. Hydraulic actuators displacement chart.

Interesting is also the possibility of drafting trajectory [5] and displacement of any specified point while control process.
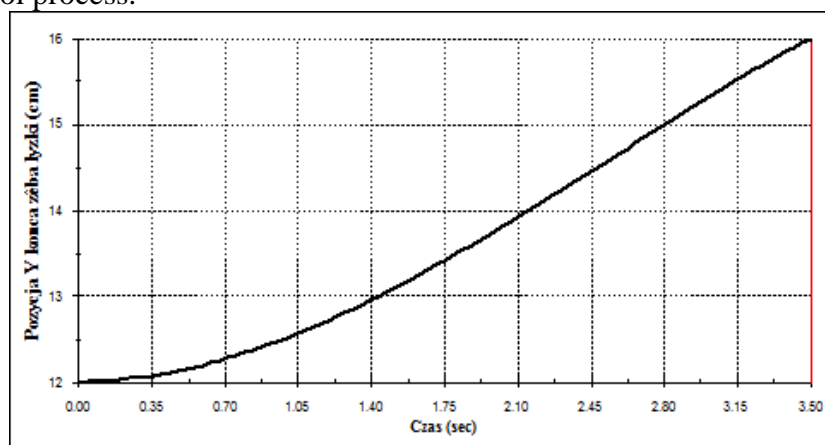

Fig. 5. Bucket tooth displacement chart.

5. Conclusion

Virtual prototyping methods allows to rapid synthesis of mechatronic systems [1]. Also gives possibility to virtual examine existing systems. Mechanical prototyping allows to get realistic looking parts and assemblies. By applying motion analysis it is possible to determine the critical position of the object and possible configurations giving rise to a conflict of accessories. It gives also important information about the dynamic behavior of the system. Motion analysis can help to explore, how the system will works without the physical movement of any part of the system. Control system simulation allows to simulate any equipment like drives or sensors. Control engineers can predict behavior of mechanic system by applying virtual drives, actuators and virtual drivers same as in reality. Article raises the possibility of integrating modern engineering package for a comprehensive synthesis and analysis system. Also discusses the two most powerful development environments. for the virtual prototyping. By integration of SolidWorks with Motion module and LabVIEW with Soft Motion module it is possible to simulate any mechatronic system.

References

[1] OLESZWSKI, M. *Mechatronika*. Warszawa., REA, 2009.

[2] TRĄPCZYŃSKI, W. – PŁONECKI, L. – CENDROWICZ, J. *Problemy sterowania osprzętem zautomatyzowanych maszyn do robot ziemnych*. Transport przemysłowy i Maszyny Robocze, 2009.

[3] LOMBARD, M. *SolidWorks 2010 Bible*. Warszawa., John Wiley & Sons, 2010.

[4] CHRUŚCIEL, M. *LabVIEW w praktyce*. Legionowo., BTC, 2008.

[5] SPONG, M. – VIDAYASAGAR, M. *Dynamika I – Sterowanie robotów*. WNT, 1997.

TRANSCOM 2011

Proceedings, Section 6